

USAAMRDL-TR-77-41

12

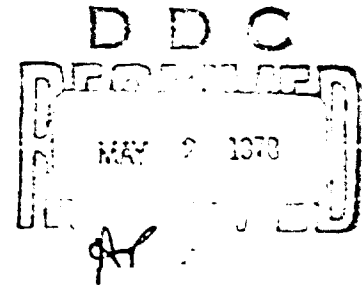


**HEAVY LIFT HELICOPTER - ADVANCED TECHNOLOGY
COMPONENT PROGRAM - ROTOR BLADE**

Reproduced From
Best Available Copy

AD A 053423

Boeing Vertol Company
P.O. Box 16858
Philadelphia, Pa. 19142



September 1977

Final Report for Period July 1971 - July 1975

Approved for public release;
distribution unlimited.

Prepared for

U. S. ARMY AVIATION RESEARCH AND DEVELOPMENT COMMAND
P.O. Box 209
St. Louis, Mo. 63166

APPLIED TECHNOLOGY LABORATORY
U. S. ARMY RESEARCH AND TECHNOLOGY LABORATORIES (AVRADCOM)
Fort Eustis, Va. 23604

DDC FILE COPY

APPLIED TECHNOLOGY LABORATORY POSITION STATEMENT

Due to the termination of the HLH program, reports summarizing the strides made in many of the supporting technology programs were never published. In an effort to make as much of this information available as possible, selected draft reports prepared under contract prior to termination have been edited and converted to the DOD format by the Applied Technology Laboratory. The reader will find many instances of poor legibility in drawings and charts which could not, due to the funding and manpower constraints, be redone. It is felt, however, that some benefit will be derived from their inclusion and that where essential details are missing, sufficient information exists to allow the direction of specific questions to the contractor and/or the U.S. Army.

DISCLAIMERS

The findings in this report are not to be construed as an official Department of the Army position unless so designated by other authorized documents.

When Government drawings, specifications, or other data are used for any purpose other than in connection with a definitely related Government procurement operation, the United States Government thereby incurs no responsibility nor any obligation whatsoever; and the fact that the Government may have formulated, furnished, or in any way supplied the said drawings, specifications, or other data is not to be regarded by implication or otherwise as in any manner licensing the holder or any other person or corporation, or conveying any rights or permission, to manufacture, use, or sell any patented invention that may in any way be related thereto.

Trade names cited in this report do not constitute an official endorsement or approval of the use of such commercial hardware or software.

DISPOSITION INSTRUCTIONS

Destroy this report when no longer needed. Do not return it to the originator.

TABLE OF CONTENTS

	<u>Page</u>
LIST OF ILLUSTRATIONS	5
LIST OF TABLES.	10
1.0 INTRODUCTION	11
2.0 SUMMARY.	15
3.0 DESIGN DEVELOPMENT	21
3.1 Design Goals and Objectives	21
3.2 Rotor Blade Geometry and Sizing	24
3.3 Rotor Blade Structural Concept.	33
3.4 Preliminary Design Studies and Support Tests.	36
3.5 Detail Design of the ATC Blade Configuration.	45
3.6 Detail Design of the Prototype Blade Configuration	85
4.0 STRUCTURAL AND AEROELASTIC ANALYSIS.	119
4.1 Criteria and Requirements	119
4.2 Limit and Ultimate Loads.	119
4.3 Design Fatigue Flight Loads	120
4.4 Material Properties	120
4.5 Blade Physical Properties	121
4.6 Ultimate Strength Analysis.	121
4.7 Safe Life Fatigue Analysis.	133
4.8 Fail Safe Analyses.	133
4.9 Natural Frequency Analysis.	134
4.10 Classical Flutter	135
4.11 Rotor Blade Torsional Divergence.	135
4.12 Pitch Lag Stability	136
5.0 MANUFACTURING DEVELOPMENT.	140
5.1 Spar Fabrication.	140
5.2 Tooling	142
5.3 Forming of Titanium Cap	142
5.4 Quality Assurance	143
6.0 DEMONSTRATION TESTS.	163
6.1 Full-Scale Component Structural Tests	163
6.2 Natural Frequency and Stiffness Test	175
6.3 Lightning Tolerance Evaluation.	177
6.4 Wind Tunnel Demonstration Test.	179
6.5 Rotor Whirl Demonstration Test.	193

REFERENCES 199
LIST OF SYMBOLS. 201

ACCESSION No	
DTIC	White Section <input checked="" type="checkbox"/>
DDI	Diff Section <input type="checkbox"/>
UNANNOUNCED	<input type="checkbox"/>
JUSTIFICATION.....	
BY.....	
DISTRIBUTION/AVAILABILITY CODES	
Dist. AVAIL. and/or SPECIAL	
A	

LIST OF ILLUSTRATIONS

<u>Figure</u>		<u>Page</u>
1	General Arrangement - Model 301 HLH.	13
2	Completed Blade Number 1	17
3	Root End View of Completed Blade	18
4	HLH Rotor Blade.	19
5	Rotor Airfoils	26
6	Maximum Lift Boundaries and Zero Lift Pitching Moment Levels.	27
7	Maximum Lift Boundaries and Pitching Moment Levels	28
8	Drag Comparison, Wake Probe Data (HLH Reynolds Number).	29
9	HLH Rotor Blade Geometry	30
10	Chord Trade Study.	31
11	Rotor Flying Qualities Boundary - Steady Flight Condition	32
12	HLH Rotor Blade.	34
13	HLH Spar Assembly.	35
14	Trade Study - Rotor Blade Concepts	40
15	Tension Fatigue Failure of Graphite Composite (Room Temperature)	41
16	Tension Fatigue Failure of Graphite Composite (160°F).	42
17	Shear Fatigue Failure of Graphite Composite.	43
18	Impact Test - 1 Lb Ball on +45° Graphite and Nomex Core	44
19	Impact Test - 1 Lb Ball on +45° Glass and Nomex Core	44

<u>Figure</u>		<u>Page</u>
20	Design Support Tests	54
21	Coupon Fatigue Tests of 6AL4V Titanium Alloy Sheet.	56
22	Wraparound Root End.	57
23	HLH Rotor Blade Aft Fairing.	58
24	Fiberglass Composite Does Not Lose Strength After Operating in Service Environment	59
25	Comparison of Fatigue Strength of 1002S and SP250 Unidirectional Fiberglass Epoxy Composites	60
26	Location of Chordwise Center of Gravity.	61
27	HLH/ATC Rotor Blade Assembly Drawing Tree.	62
28	HLH Rotor Blade Assembly	63
29	Geometry Two-Pin, Fittingless HLH Rotor Blade.	69
30	Bonded Assembly - Rotary Wing - HLH.	71
31	Spar Assembly - Two-Pin, Fittingless HLH Rotor Blade.	73
32	Prototype Blade Modifications.	91
33	Lightning Protection.	92
34	Typical Crossply Wrinkles in Spar Heel Area.	93
35	1-Inch Section of HLH Prototype Spar Precure Heel, Fiberglass and Graphite.	94
36	Comparison of HLH Spar Heels Before and After Modifications.	95
37	Aft Fairing Core	96
38	Aft Fairing Skin	97
39	HLH/Prototype Rotor Blade Assembly Drawing Tree	98

<u>Figure</u>	<u>Page</u>
40	Blade Assembly Prototype HLH Rotor Blade 99
41	Bonded Assembly - Rotary Wing - HLH. 105
42	Spar Assembly Two-Pin, Fittingless HLH Rotor Blade. 107
43	Basic Design Requirements. 122
44	Rotor Blade Moments for Design Limit Maneuver Condition. 125
45	Rotor Blade Design Moments for High-Speed Level Flight 126
46	Rotor Blade Centrifugal Force. 127
47	Spanwise Distribution of Mass and Stiffness. . . 130
48	Spanwise Distribution of Blade Axes. 131
49	Rotor Blade Frequency Spectrum 137
50	Demonstration of Blade Torsional Aeroelastic Stability at High Speed With 14-Foot-Diameter Model Rotor. 138
51	Comparison of Analytical Pitch Link Load With 14-Foot-Diameter Rotor Wind Tunnel Test Load for Limit Design Dive Speed. 139
52	HLH Rotor Blade Fabrication Sequence 145
53	HLH Blade Fabrication Flow Diagram 146
54	Leading-Edge Assembly Flow Chart 147
55	Spar Assembly Flow Chart 148
56	Root End Fitting Fabrication Flow Chart. 149
57	Tip Fitting Assembly Flow Chart. 150
58	Fitting Installation Flow Chart. 151
59	Fairing Fabrication Flow Chart 152
60	Blade Bonding Flow Chart 153

<u>Figure</u>	<u>Page</u>
61 Damper Arm Assembly Flow Chart	154
62 Final Assembly Flow Chart.	155
63 Main Bond Tool Being Closed.	156
64 Spar Bonding Fixture Ready for Use	158
65 Spar Curing Operation Heating Cycle.	159
66 Titanium Cap Forming Tool.	160
67 Tooling Improvements for Titanium Nose Cap . . .	161
68 Quality Assurance Flow Chart	162
69 HLH Rotor Blade Structural Test Specimens. . . .	168
70 Full-Size Root End Tests Verified Design Allowables for Unidirectional Fiberglass	169
71 Fiberglass Damage Tolerance and Survivability Demonstrated by HLH Root-End Test.	170
72 Intermediate Section Fatigue Test Fixture. . . .	171
73 Titanium Nose Cap Fatigue Failure.	172
74 Fatigue Strength of Highly Directional 6AL4V Titanium Alloy Sheet With Effect of Molten Deposits	173
75 Nomex Honeycomb Prototype Configuration.	174
76 14-Foot-Diameter Model HLH Rotor Blade Installed in Wind Tunnel	183
77 Hover Figure of Merit HLH/ATC 14-Foot-Diameter Rotor Wind Tunnel Test	184
78 Cruise Efficiency HLH/ATC 14-Foot-Diameter Rotor Wind Tunnel Test	185
79 Flying Qualities Boundary HLH/ATC 14-Foot- Diameter Rotor Wind Tunnel Test.	186
80 Rotational Noise of 14-Foot-Diameter Model Rotor.	187

<u>Figure</u>	<u>Page</u>
81 Comparison of Analytical Blade Bending Moments With Scale 14-Foot-Diameter Rotor Wind Tunnel Test Data.	188
82 Comparison of Design Pitch Link Load With Scaled 14-Foot-Diameter Rotor Wind Tunnel Test Data . .	189
83 Comparison of Analytical Pitch Link Load With 14-Foot-Diameter Rotor Wind Tunnel Test Load for Level Flight Design Condition.	190
84 Fixed System Control Load Reduction With Damping, 14-Foot-Diameter Model Rotor Test.	191
85 Blade Torsional Load Growth Fixed Load Criteria From 14-Foot-Diameter Model Rotor Test	192
86 Rotor Whirl Test	194
87 Dynamic System Test Rig.	195
88 Rotor Hover Efficiency From Whirl Test	196
89 Blade Bending Moments From Whirl Tower and DSTR Tests.	197
90 Blade Natural Frequencies Determined From Test .	198

LIST OF TABLES

<u>Table</u>		<u>Page</u>
1	Rotor System Description.	20
2	Rotor Blade Design Goals and Objectives	23
3	Comparative Properties of Blade Materials . . .	55
4	Basic Fatigue Loading Schedule.	123
5	Maneuver Airspeed Distribution.	124
6	Material Properties and Design Allowables Summary	128
7	Calculated Weight and Centrifugal Force	129
8	Minimum Margins of Safety	132
9	Nondimensional Natural Frequency.	134
10	Coefficient of Thermal Expansion Comparisons. .	157
11	Comparison of Theoretical and Experimentally Determined Blade Bending Stiffnesses.	176
12	Comparison of Theoretical and Measured Natural Frequency	176

1.0 INTRODUCTION

The initial HLH preliminary design concept was formulated and submitted to meet the mission requirements and broad design criteria for the Advanced Technology Component (ATC) Program. This preliminary design concept included an initial estimate of the aircraft size and weight, a definition of the major subsystem interfaces, an identification of potential risk areas and, most importantly, an identification and definition of those components considered to be of advanced technology and requiring advanced development.

BACKGROUND

The purpose of the ATC Program was to seek maximum reduction of technical and cost risk associated with the Engineering Development of an HLH system through the design, fabrication, demonstration and test of selected critical HLH components. Engineering Development or full-flight qualification of any component or concept was not the purpose of this program.

The critical components of the HLH were determined to be the rotor blades, hub and upper controls, drive system, flight control system and cargo handling system. The scope of the HLH ATC program was limited to these components, plus the interface analytical activities necessary to assume the ATC components would be suitable for subsequent integration with the complete aircraft. The general arrangement of the HLH is shown in Figure 1.

ROTOR BLADE ATC PROGRAM

The rotor blade was an obvious selection as one of the components of the HLH Advanced Technology Component (ATC) program. It is a high-cost, long-lead item requiring high reliability and offering a potential reduction in maintenance hours.

The blade program was conducted during the period from July 1971 through July 1975. The phases of the program included:

- | | |
|--------------------|--|
| Preliminary Design | - trade studies and selection of concept |
| Detail Design | - preparation of complete drawings |
| Fabrication | - development of manufacturing concept
full-scale blade fabrication |

Demonstration

- Structural Test
- Wind Tunnel Test
- Whirl Tower
- Dynamic System Test Rig

This report presents a summary or review of each of these phases which have been reported in detail in the documents reference herein. Descriptions of the several improvement modifications which were incorporated into the blade design for the prototype helicopter are included.

MAJOR CHARACTERISTICS

ROTOR

DIAMETER (FT)	92.0
TIP SPEED (H.P.S)	750.0
DISC LOADING (H.P.F) AT DGW	8.9
BLADE AREA (3 AT 155 SQ. FT)	1224.0
GEOMETRIC SOLIDITY RATIO	.09226
GEOMETRIC DISC AREA (2 AT 6647.6 SQ. FT)	13,295.0

PROPULSION

NUMBER OF ENGINES / TYPE	T701-AD-700(3) TURBOSHAFT
TRANSMISSION RATING (H.P.)	17,700
MAX. SINGLE ENGINE RATING	8,079
INTEGRAL FUEL CAPACITY (GAL.)	2,938
INTEGRAL FUEL CAPACITY (LBS.)	19,100

WEIGHT (LB)

	<u>BASELINE</u>
DESIGN GROSS WEIGHT, LF * 1.5	8,000
DESIGN PAYLOAD	45,000
DESIGN MISSION FUEL	11,080
FIXED USEFUL LOAD (INCLUDES 5 MAN CREW)	7,340
EMPTY WEIGHT	59,580
MAX. ALTERNATE GROSS WEIGHT	148,000
MISSION GROSS WEIGHT	18,000

GROUND ANGLES (DEGREES)

TURNOVER (WT. EMPTY)	GROUND LINE	34.0° @ 93,000 LBS
TIP BACK (WT. EMPTY)	GROUND LINE	31.0° FROM HOVER REF @ DESIGN GROSS WEIGHT

CONTROL MOVEMENTS

	FORWARD	AFT
COLLECTIVE PITCH	-1.0° TO 14.7°	-2.0° TO 16.0°
DIFFERENTIAL COLLECTIVE PITCH	15.0°	15.5°
PROGRAMMED LONGITUDINAL CYCLIC PITCH	-5.2° TO 12.0°	-5.4° TO 10.0°
SIDE ARM CONTROL CYCLIC PITCH	15.5°	15.0°
DIFFERENTIAL LATERAL CYCLIC PITCH	117.0°	111.0°
LATERAL CYCLIC PITCH	14.0°	14.2°

LANDING GEAR

NOSE - WHEEL / TIRE SIZE	14 PLY	NOSE	MAX.
MAIN - WHEEL / TIRE SIZE	RATING	5.00 - 6	15.50 - 20
		TYPE III	TYPE III

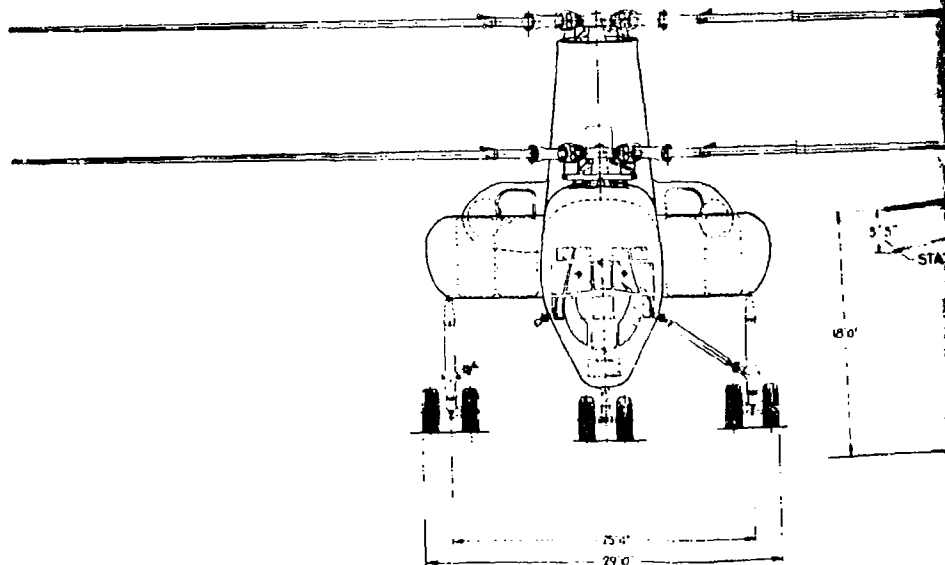
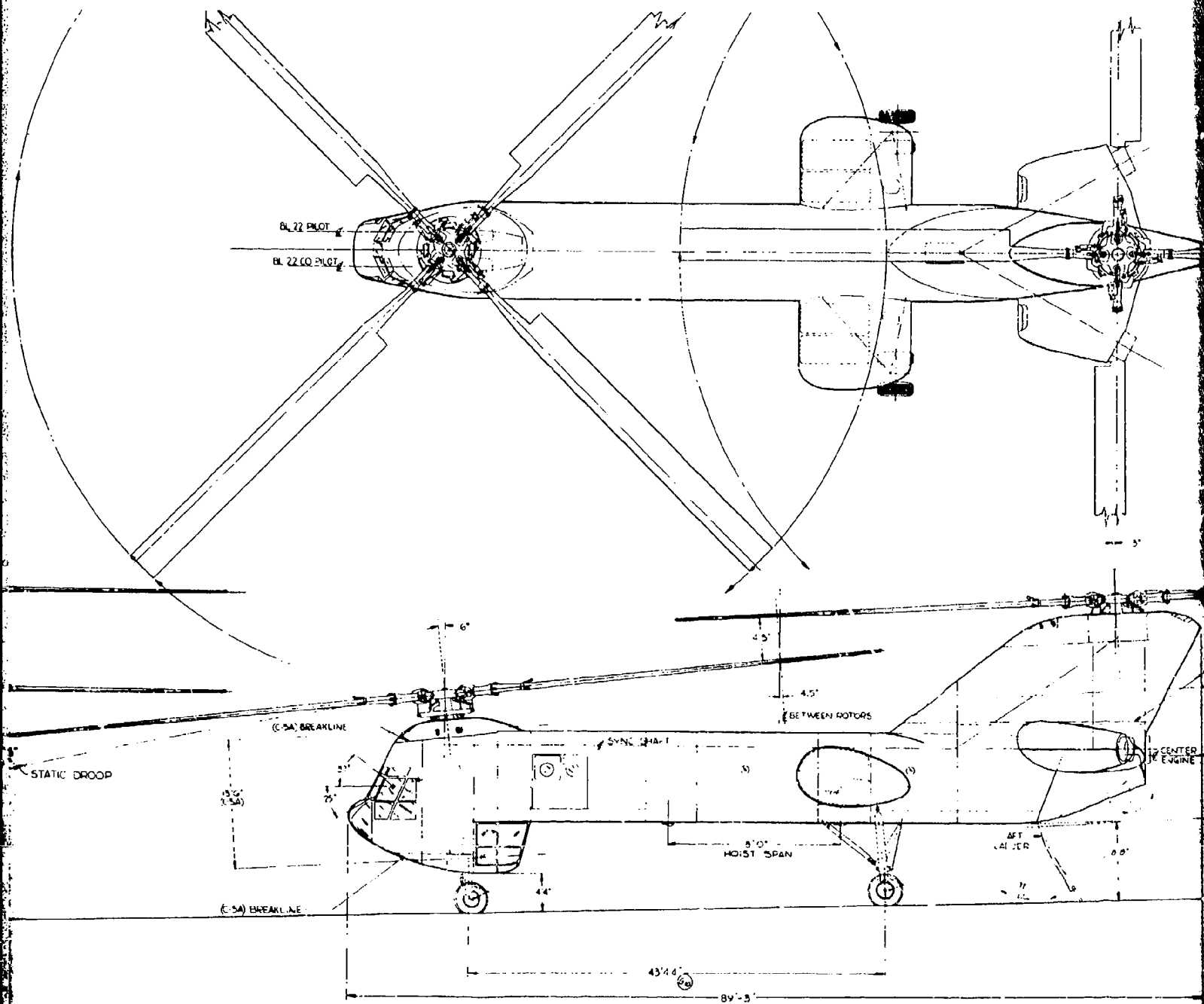
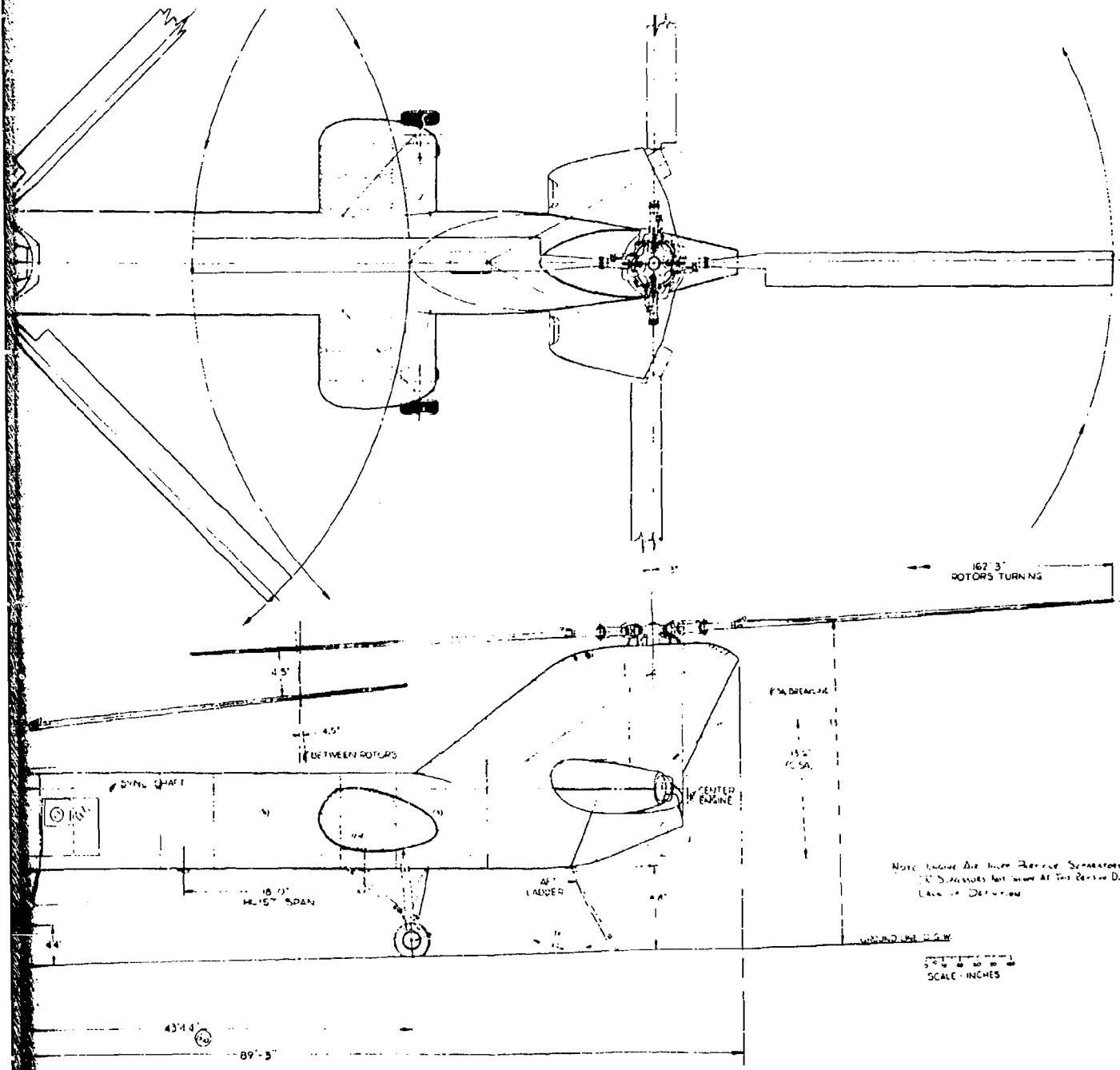


Figure 1. General Arrangement - Model 301 HLH



P
↓



2.0 SUMMARY

The Boeing Heavy Lift Helicopter rotor blade is an application of advanced technology encompassing improved airfoil and twist distribution and composite materials.

The fiberglass rotor blade represents a major advance in rotor system fail safety and reliability. The achievements of the design are:

- Improved rotor performance using advanced airfoils and optimized thickness and twist distribution.
- Fail safety of the fiberglass construction and an inherently redundant root end attachment.
- Improved maintainability and reliability with a pneumatic delta pressure failure system.
- Controlled cost with a production oriented tooling and fabrication concept.

A photograph of the complete blade is shown in Figure 2. Details of the root end are shown in Figure 3.

The rotor blade structural concept consists of a closed fiberglass "D" spar terminating in a multiple wraparound root end retention system. The aft fairing uses fiberglass over a Nomex honeycomb core. Erosion protection is provided by a titanium nose cap with a nickel leading edge at the blade tip. A pneumatic delta pressure failure detection system is employed within the "D" spar. This, and the inherently slow crack propagation of fiberglass and the multiple load path design, provides for long-term detection capability and over 200 hours of safe operation after detection.

The radius of the blade is 46 feet; the chord is 40 inches. The airfoil sections start with the V43015-2.48 at the root cutout (.25R) which transitions to the V43012-1.58 at 0.4R. This transitions to the new VR-7, which extends from 0.5R to 0.85R. The VR-7 transitions again to the VR-8 at the tip.

The rotor characteristics are described in Figure 4 and Table 1 for the ATC and the Prototype blade configurations. Manufacturing development and structural testing performed during the ATC program led to modifications improving the

design and structural capability of the Prototype blade. The most important of these were a precured spar heel to improve layup operations and to eliminate wrinkling of the fiberglass stiffening of the heel web to increase the aft fairing honeycomb core strength, and a titanium nose cap using highly directional material with reduced cost and improved fatigue properties. The weight of the ATC blade is 760 pounds and the prototype blade is 774 pounds.

Demonstration tests verified the design predictions and met the design objectives.

- A rotor hover efficiency with a figure of merit (FM) of .767 was demonstrated by wind tunnel and whirl tower tests compared to the design objective FM of .751.
- Structural tests demonstrated essentially an unlimited life for the blade fiberglass spar and root attachment.
- Absolute fail safety of the blade was demonstrated by structural tests. The root end is capable of sustaining at least 172 hours of high-speed level flight loads with one of four attachment lugs failed. An outboard airfoil section with the titanium nose cap failed was subjected to 427 hours at level flight loads, and 109 hours at maneuver loads without degradation to the remaining fiberglass spar.
- The fatigue strength of the titanium nose caps tested was lower than the design objectives due to defective material and processing. However, the fatigue strength was still greater than level flight stresses, and a fatigue life in excess of 1000 hours is predicted for the prototype helicopter mission. Because of the demonstrated fail-safe characteristics of the composite rotor blade, cracking of the titanium nose cap is not considered to be a flight safety issue.

Airworthiness of the blade for flight on the HLH Prototype aircraft was proven in this HLH/ATC program.

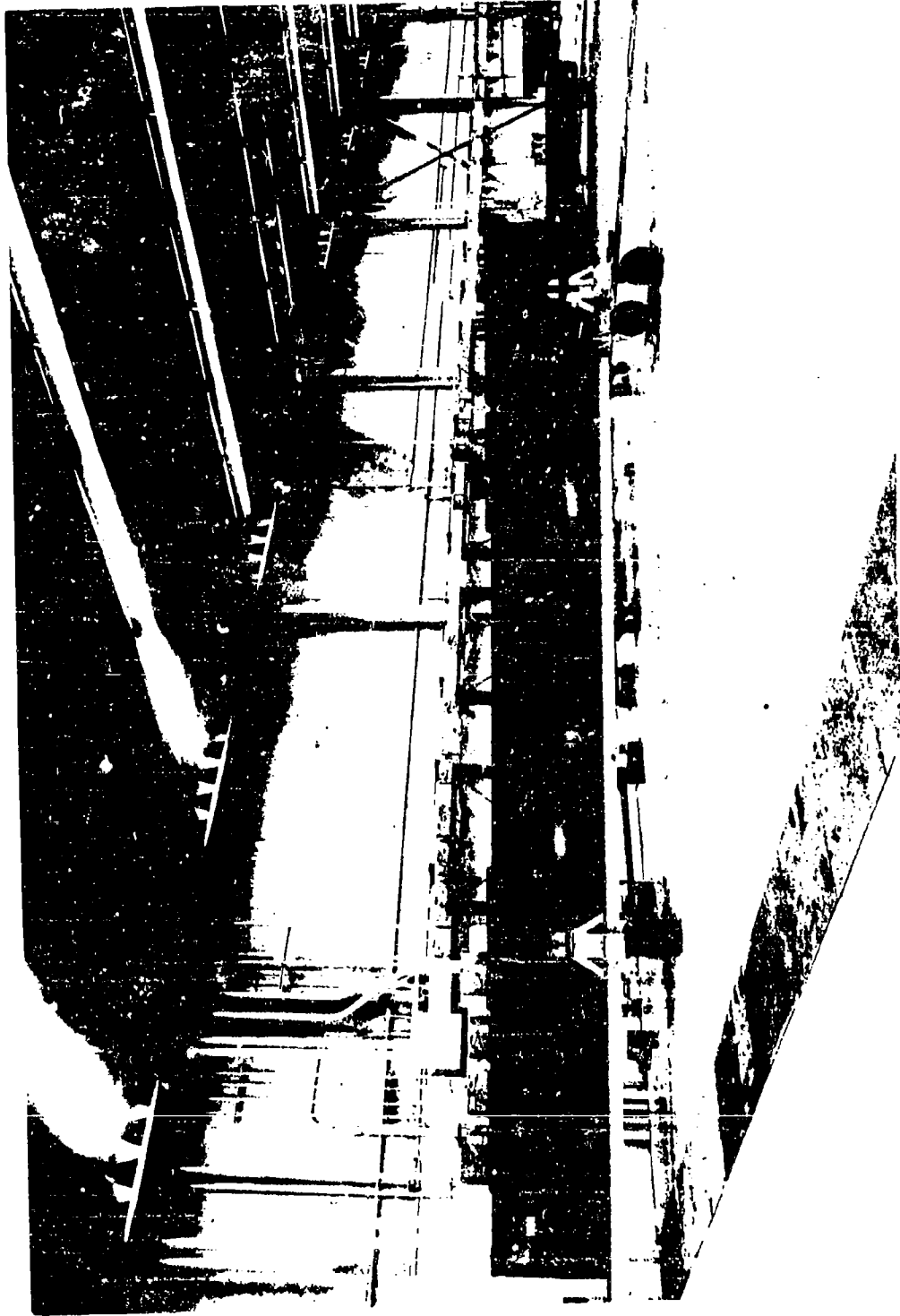


Figure 2. Completed Blade Number 1

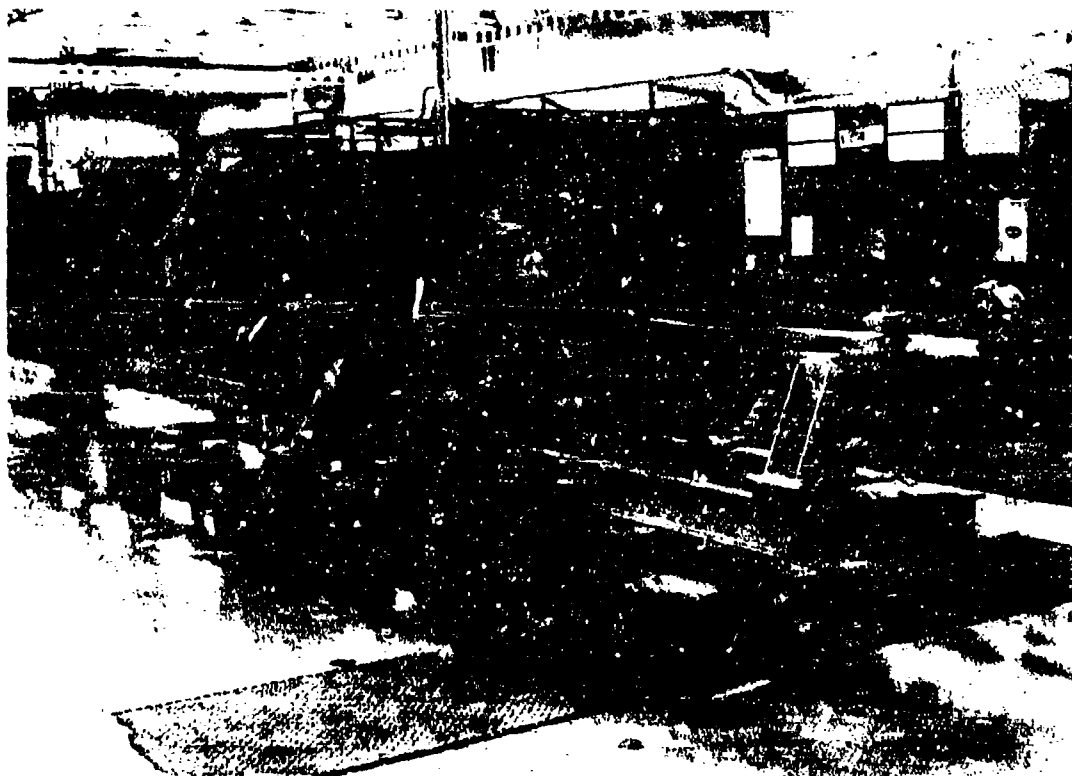


Figure 3. Root End View of Completed Blade

TABLE 1. ROTOR SYSTEM DESCRIPTION

Rotor Diameter	92	Ft.
Blade Chord	40.0	In.
Blade Twist (Aerodynamic)	-12°	
Normal RPM	156	
Torque Offset (Lead)	4.5	In.
Articulation Hinge Radial Location	26	In.
Blade Attachment Radial Location	66	In.
Damper Arm at Station 66	10	In.
Pitch Axis	25%	Chord

	<u>ATC</u>	<u>Prototype</u>
Rotor Blade Weight:		
Outboard of Fold Pins Sta.66	760	774 Lb
Outboard of Elastomeric Bearing	1,131	1,180 Lb
Rotor Blade Static Moment about Hinge (Including Pitch Housing and Loop)	17,325	17,960 Ft Lb
Rotor Blade Inertia about Hinge (Including Pitch Housing and Loop)	15,640	16,141 Slug-Ft ²
Centrifugal Force:		
At Blade Attachment Sta. 66	153,139	158,324 Lb
At Hinge Sta. 26	155,299	162,094 Lb

3.0 DESIGN DEVELOPMENT

3.1 DESIGN GOALS AND OBJECTIVES

The major design goals and objectives for the rotor blade compared to the blade concept achievements are summarized in Table 2.

- Fail Safety

The multiple load path spar results in inherent fail safety since no single failure of a component will cause a catastrophic condition. The fiberglass spar fail safety is due to its high damage tolerance, insensitivity to defects and stress raisers, and soft failure modes. The pneumatic failure detection system, which consists of evacuating pressure in the enclosed "D" spar, provides additional assurance.

- On-condition Operation

The design objective to provide a blade which is field repairable and maintainable and capable of "on-condition" retirement is satisfied by the failure detection system, a damage tolerant structure, repairable fairing, and a replaceable leading edge erosion protection at the blade tip.

- Reduced Maintainability Rates

Maintenance man-hours will be reduced by the detection system which eliminates the need for special inspections.

- Improved Reliability Rates

A major reduction in blade malfunctions will be achieved by the use of the sealed Nomex honeycomb fairing core which eliminates the extensive metal core-to-spar corrosion problem.

- Reduced Blade Weight

The blade weight is minimized by the composite fiberglass and titanium spar and the performance benefits from advanced airfoil profiles.

- Improved Rotor Performance

Improved performance is accomplished by tailoring the blade airfoil section, thickness ratio and twist at each spanwise radial section. Variation of these parameters is facilitated by the composite spar manufacturing approach. The increased fatigue strength of fiberglass compensates for the higher strains associated with increased airfoil thickness and twist.

TABLE 2. ROTOR BLADE DESIGN GOALS AND OBJECTIVES

GOAL/OBJECTIVE	BLADE CONCEPT
Improved Safety Survivability	<ul style="list-style-type: none"> ● Composite fiberglass/titanium structure ● Multiple load paths ● Failure detection system
On-Condition Operation	<ul style="list-style-type: none"> ● Failure detection system ● Multiple load paths ● Composite damage tolerance ● Replaceable tip nose cap
Reduced Maintainability Rates	<ul style="list-style-type: none"> ● Failure detection system
Improved Reliability Rates	<ul style="list-style-type: none"> ● Composites ● Sealed Nomex honeycomb fairing cor₂
Reduced Blade Weight	<ul style="list-style-type: none"> ● Composite fiberglass/titanium spar ● Advanced airfoil
Improved Rotor Performance	<ul style="list-style-type: none"> ● Advanced airfoil profile ● Tailored sections permitted by composite blade

3.2 ROTOR BLADE GEOMETRY AND SIZING

The use of fiberglass as the primary structural material in the HLH/ATC blade permits the optimization of blade geometry to an extent not possible with extruded metal spar blade construction. Blade airfoil section, thickness, and twist can be tailored along the span to provide the optimum aerodynamic and structural blade configuration. This tailoring of geometry was first accomplished in the U. S. Army/Boeing Advanced Geometry Blade (AGB) program. In the AGB, existing airfoil sections were employed along the span to provide an optimum aerodynamic configuration. Figure 5 shows the AGB compared to Chinook rotors. Planform taper and a low twist oriented to high-speed flight were also employed in the AGB. In the HLH program, advanced airfoils suitable to the particular blade spanwise aerodynamic environment were developed and blended along the span to provide maximum lift and minimum drag. The HLH blade, also shown in Figure 5, has a 12° twist reflecting the desire for optimum hover performance and no requirement for very high-speed flight. The 12° twist provides a 1.5 percent improvement in hover figure of merit over the Chinook 9° twist while increasing the blade bending moment in forward flight by 10 percent at the 150-knot V_H design condition.

The HLH/ATC airfoil development program included two-dimensional airfoil development, as well as 6-foot and 14-foot diameter model rotors. Two-dimensional wind tunnel data is shown in Figures 6, 7, and 8. Figure 6 is a composite plot of airfoils which existed and either were already used on rotors or showed potential for rotor usage. Examination of this plot shows that no one airfoil provides maximum lift over the entire Mach number ranges (blade span) leading to the conclusion that the optimization of rotor lift capability requires a family of airfoils suitable for the range of Mach numbers encountered in the rotor environment. This led to the establishment of the HLH objective shown in Figure 6, and an 11% improvement in $C_{L \max}$ over the Chinook airfoil V23010-1.58 at Mach number = .5, which represents the lifting areas of the rotor on the forward and aft portions of the rotor disk. Figure 7 shows the results of the HLH/ATC airfoil development, the VR-7 and VR-8 airfoils for working section and tip section, respectively, and the V43012-1.58 in the inboard section. Actually, a V43015-1.58 was ultimately employed inboard for the best structural, as well as aerodynamic configuration.

A maximum airfoil pitching moment objective was also established in order to assure that $C_{L \max}$ would not be achieved at the expense of increased control loads. Figures 6 and 7 show that the HLH/ATC developed airfoils satisfy the objective and have lower pitching moments than existing high lift airfoils.

Measured drag data for the HLH/ATC airfoils in Figure 8 show a significant reduction in drag at all Mach numbers compared to the Chinook V23010-1.58.

The HLH/ATC rotor blade geometry is shown in Figure 9. The rectangular planform and squared-off tip were selected because they represented the simplest manufacturing approach and because a review of existing data showed that little further improvement in blade performance could be achieved over that possible with optimum airfoil section, thickness taper, and twist.

A 40-inch chord was selected on the basis of chord/weight trade studies and the $C_{T/\sigma}$ requirement for the basic HLH design gross weight and alternate gross weight configurations. The chord trade study results are shown in Figure 10 and indicate that a 40-inch blade chord could be provided with no weight penalty and with no significant effect on other blade parameters over a 38-inch chord considered initially as the minimal requirement. The 40-inch chord results in an average $C_{T/\sigma}$ of .077 at the SL/95°F design condition. This point is shown in Figure 11 relative to the $C_{T/\sigma}$ limits which were estimated for the HLH on the basis of 11% increased lift capability over the Chinook. The over-load gross weight condition is also shown to have adequate bank angle capability.

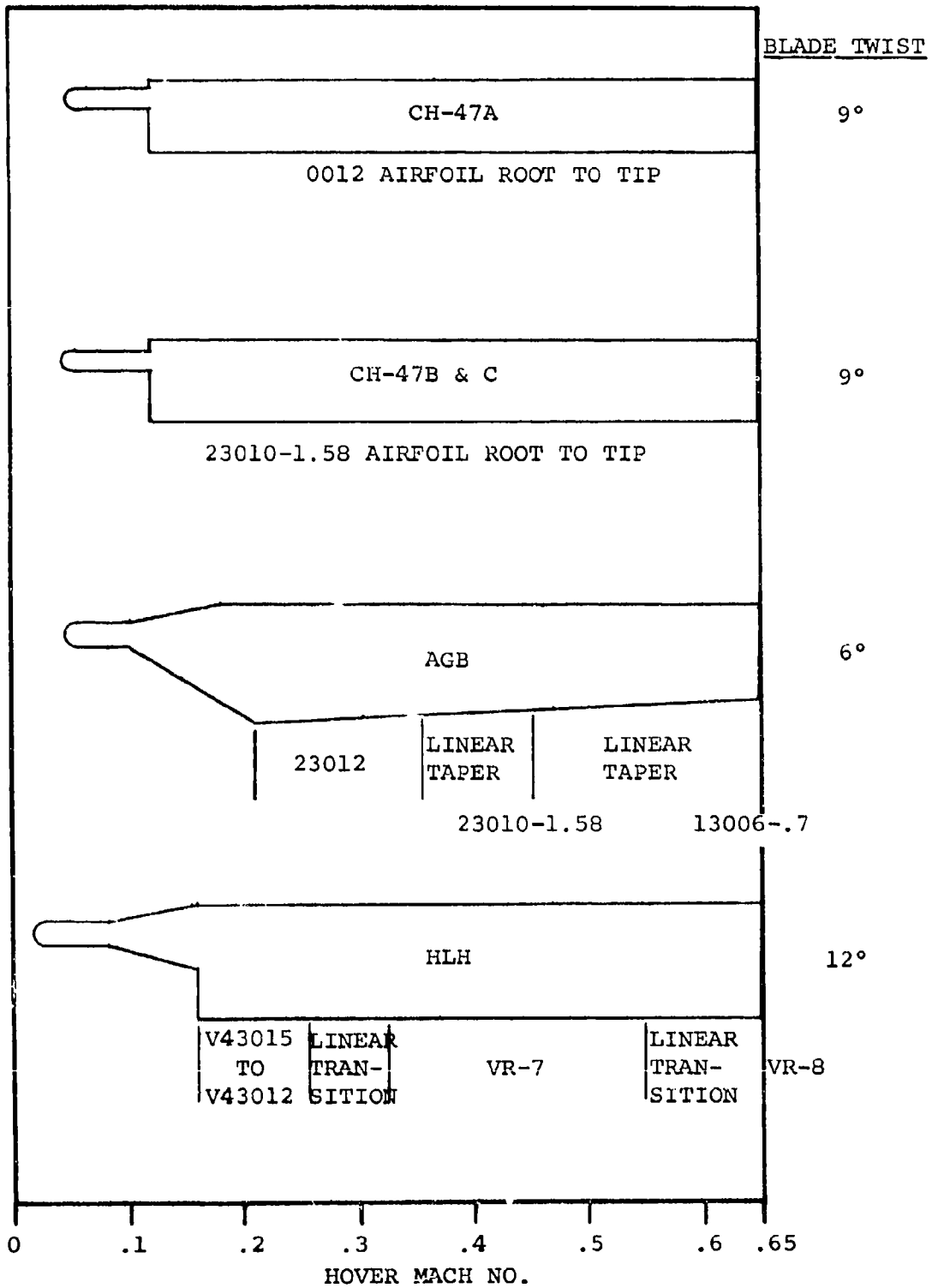


Figure 5. Rotor Airfoils

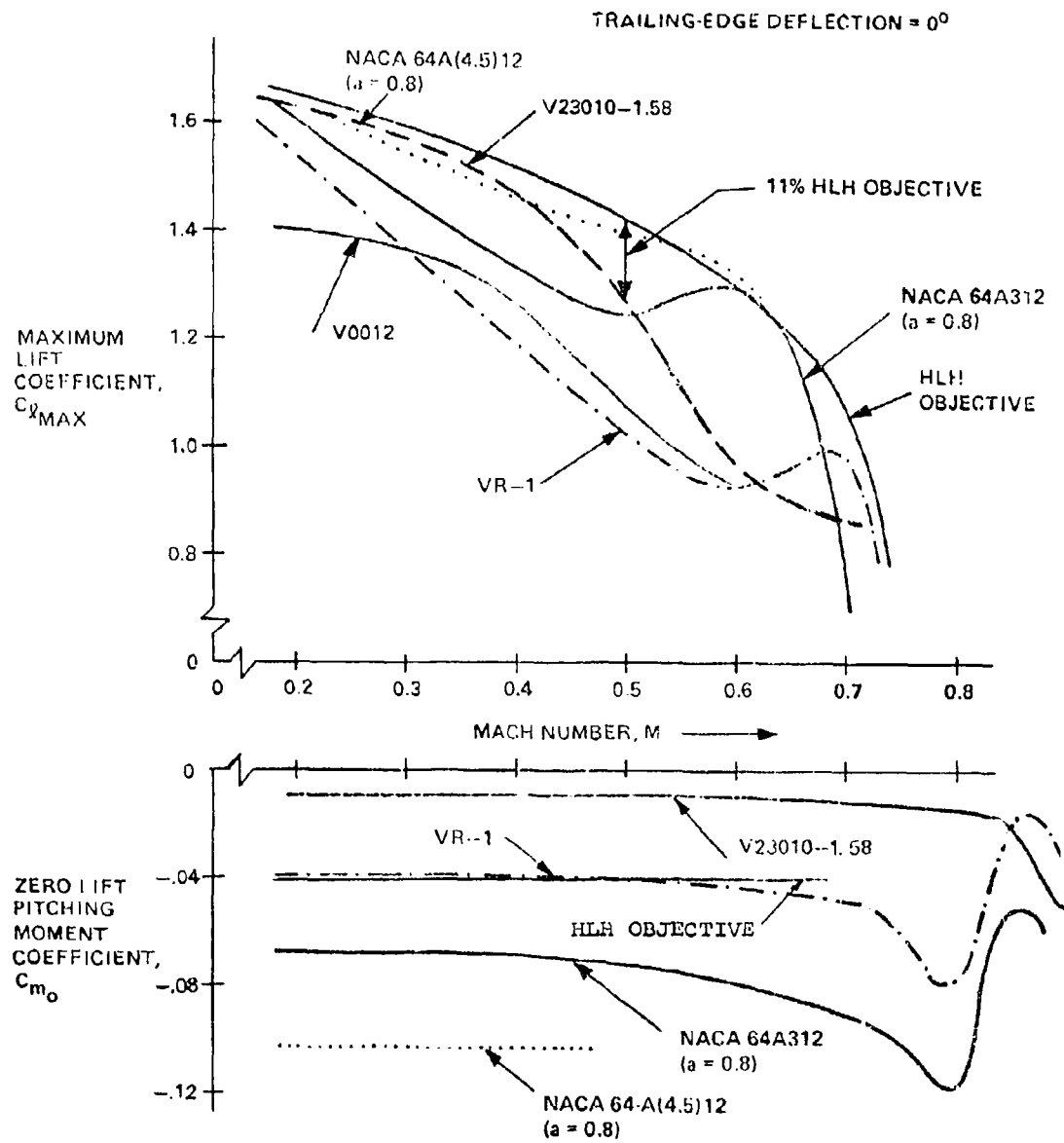


Figure 6. Maximum Lift Boundaries and Zero Lift Pitching Moment Levels

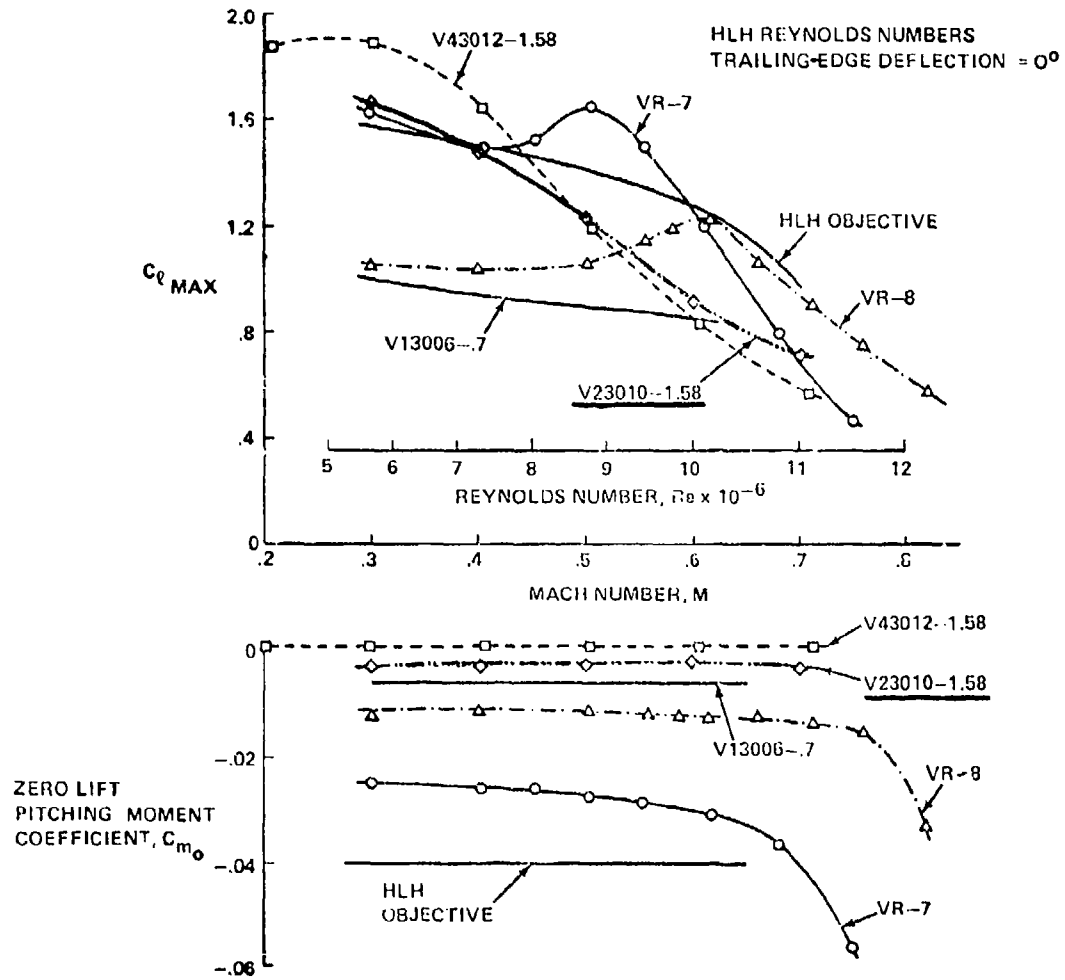


Figure 7. Maximum Lift Boundaries and Pitching Moment Levels

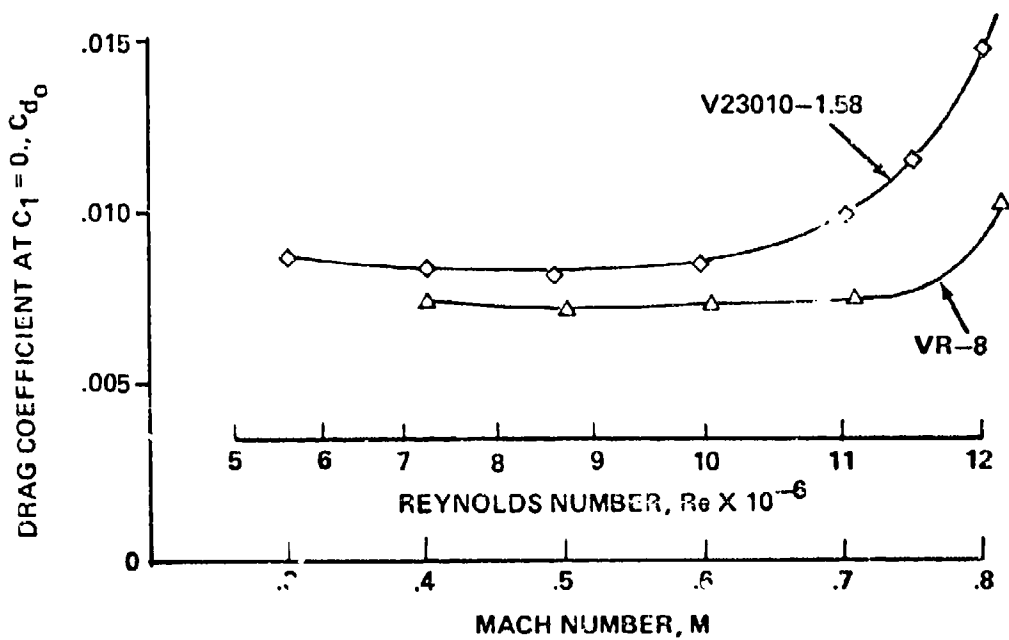
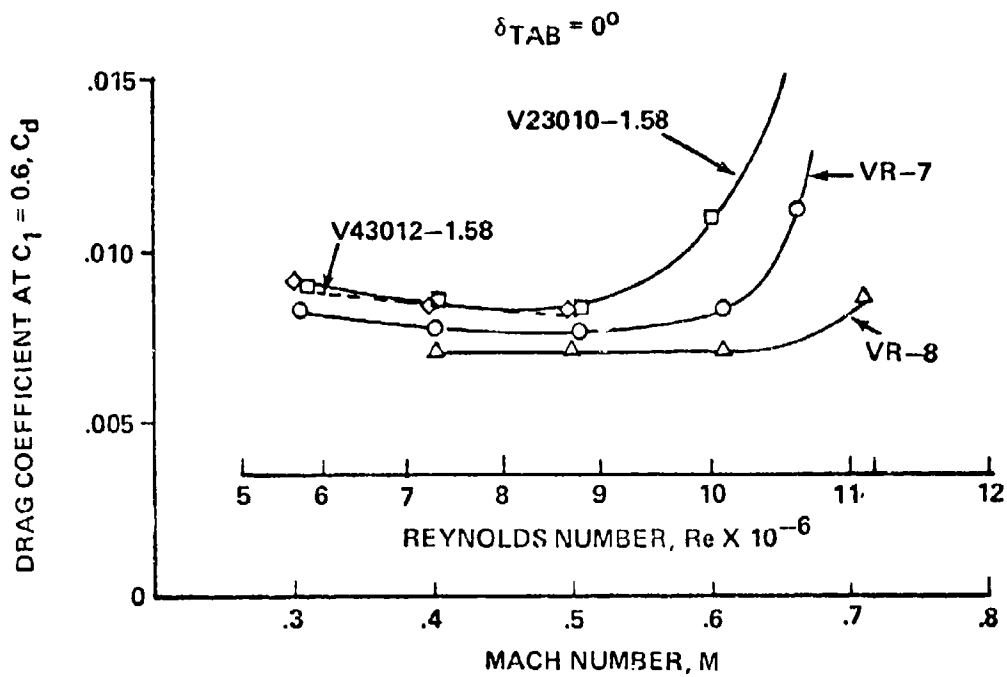


Figure 8. Drag Comparison, Wake Probe Data (HLH Reynolds Number)

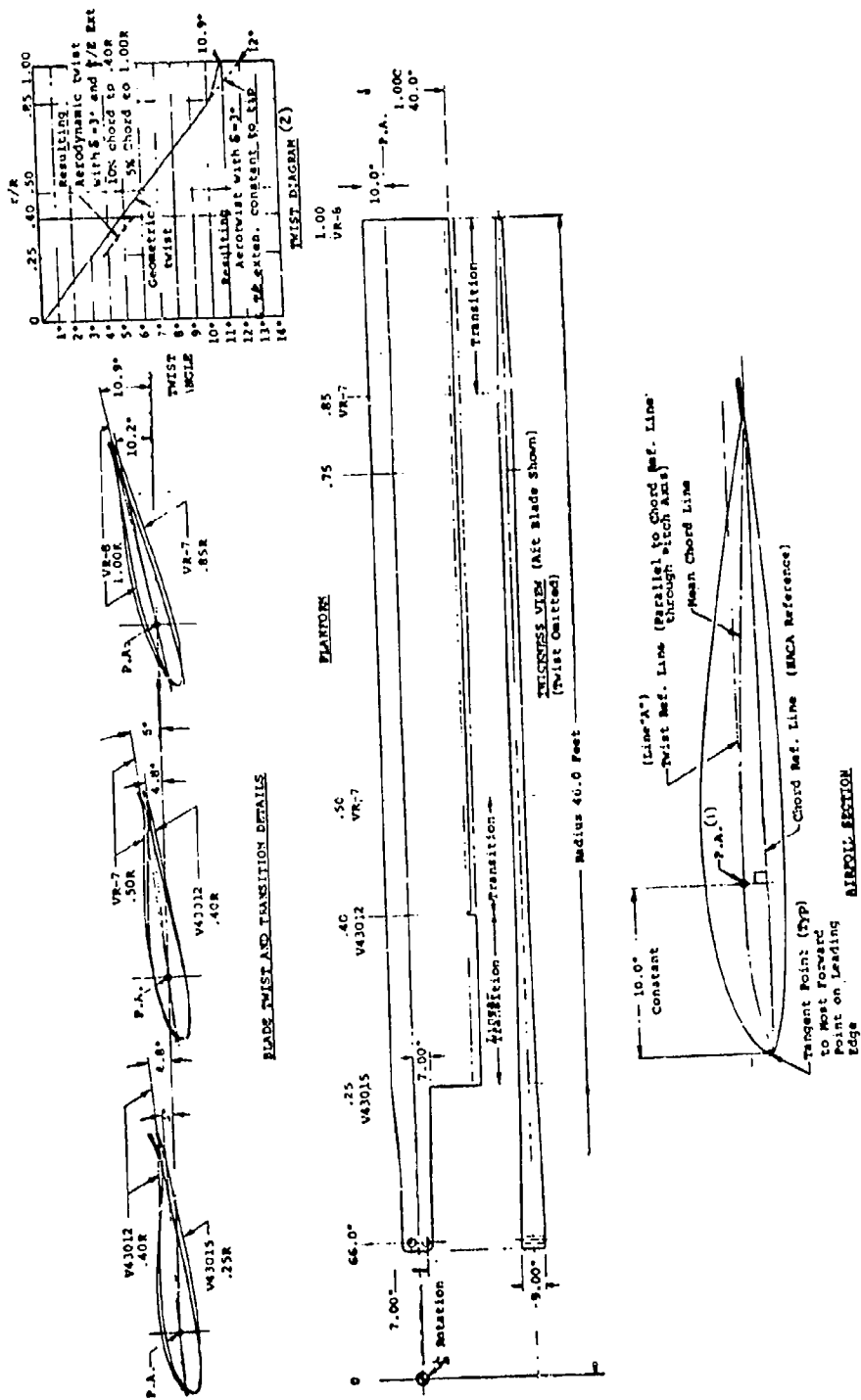


Figure 9. HLH Rotor Blade Geometry

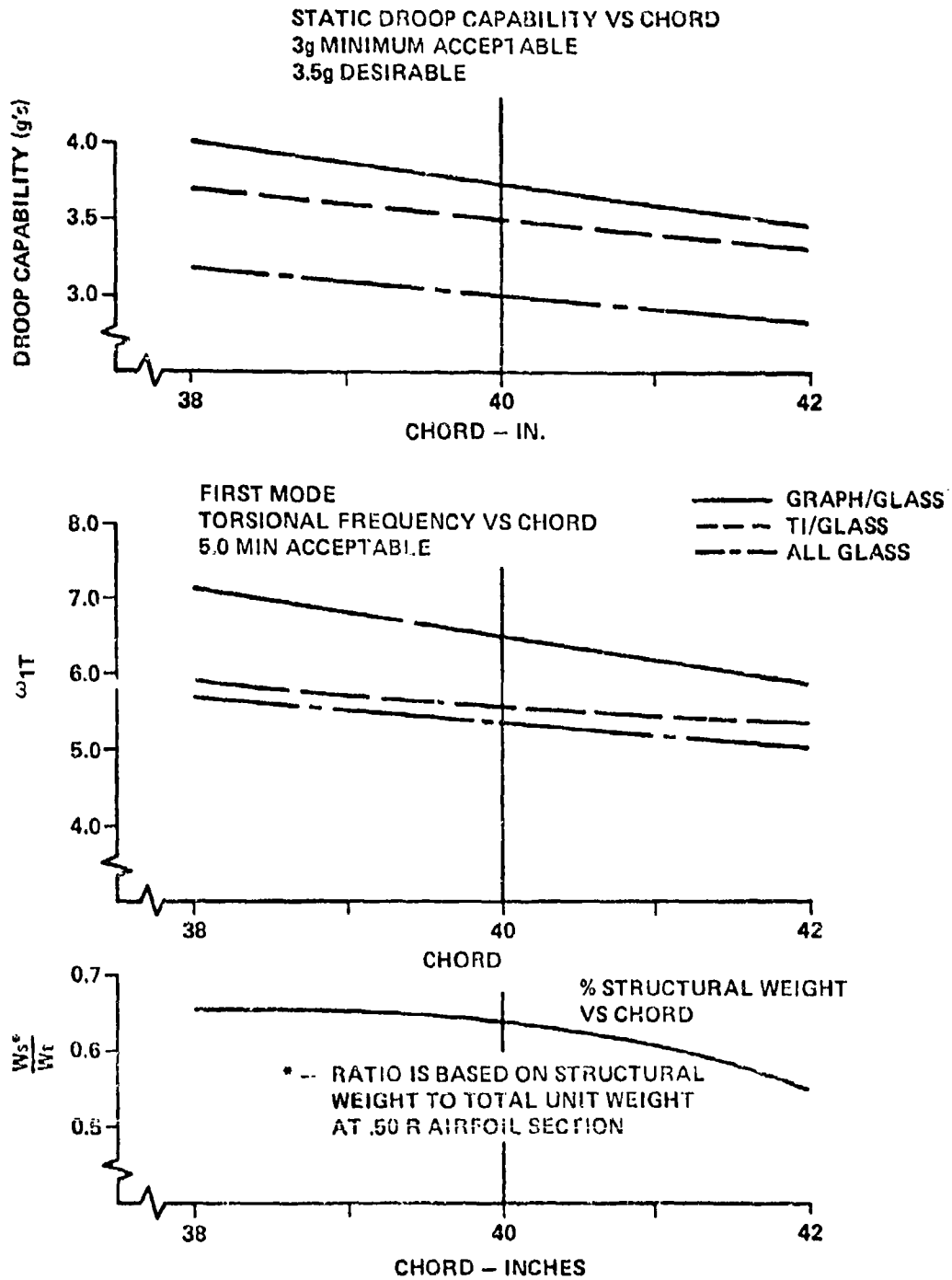


Figure 10. Chord Trade Study

*LEVEL FLIGHT AVERAGE C_T/σ

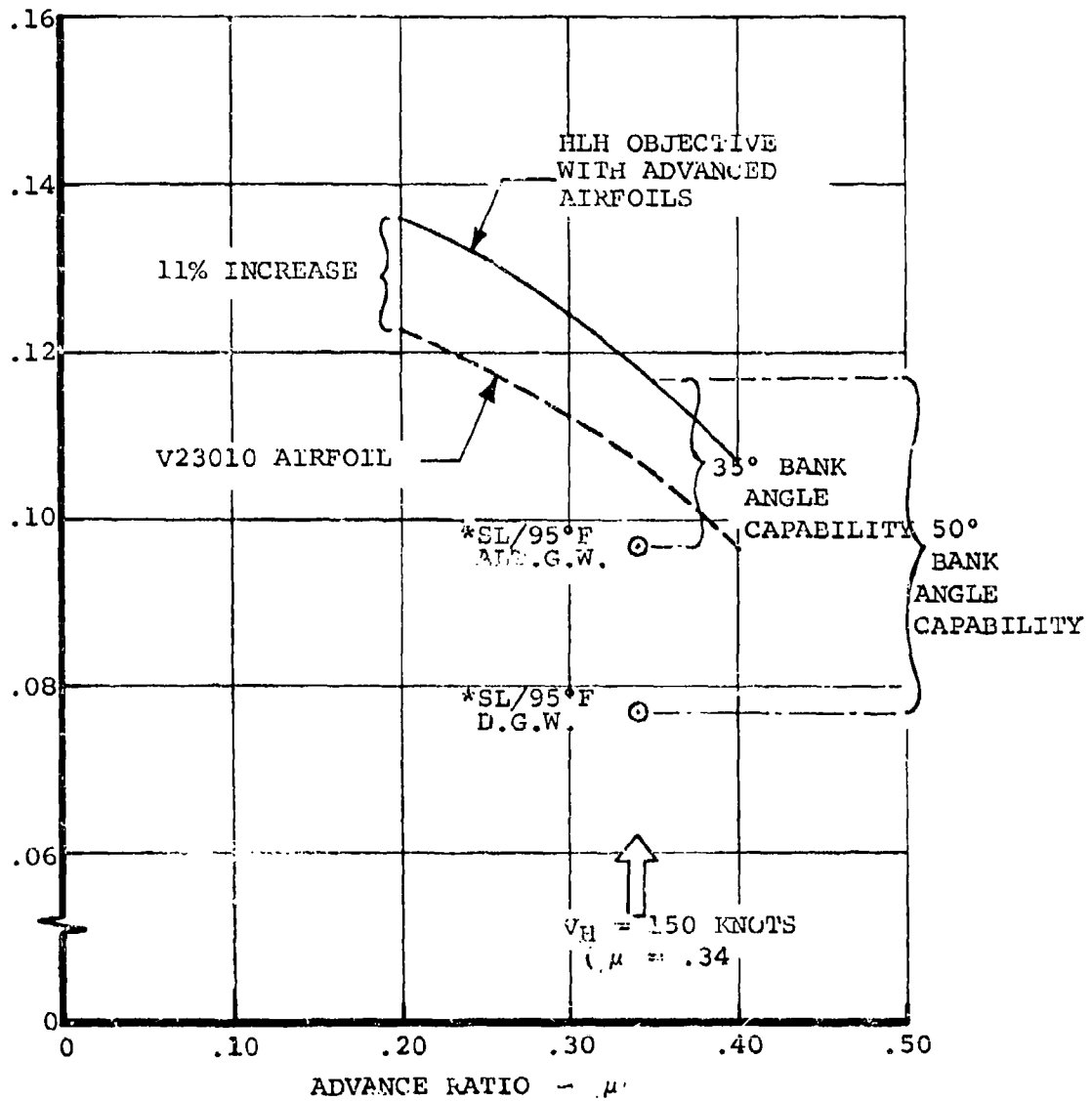


Figure 11. Rotor Flying Qualities Boundary - Steady Flight Condition

3.3 ROTOR BLADE STRUCTURAL CONCEPT

The HLH composite rotor blade shown in Figure 12 uses a unidirectional and crossply fiberglass closed "D" spar as the primary structural element. The external surface of the spar is covered by a titanium nose cap bonded to the fiberglass. The nose cap provides erosion protection and torsional and bending stiffness. Replaceable erosion protection in the high-wear area at the tip of the blade is given by nickel covering the leading edge of the blade.

The root end attachment features an all-fiberglass wraparound construction in which the spar unidirectional fiberglass material is layed in equal packs from the tip to the root and symmetrically back to the tip. This feature is illustrated in Figure 13.

The aft fairing is a single box with fiberglass skins and a Nomex-honeycomb core. A pneumatic failure detection is installed for fail safety. The blade concept described evolved from initial design studies and support testing, and is the design fabricated for structural, whirl tower and Dynamic System Test Rig demonstration tests and that planned for the Prototype HLH.

The above concept was selected as a result of the preliminary design studies and supporting tests discussed in the following paragraphs.

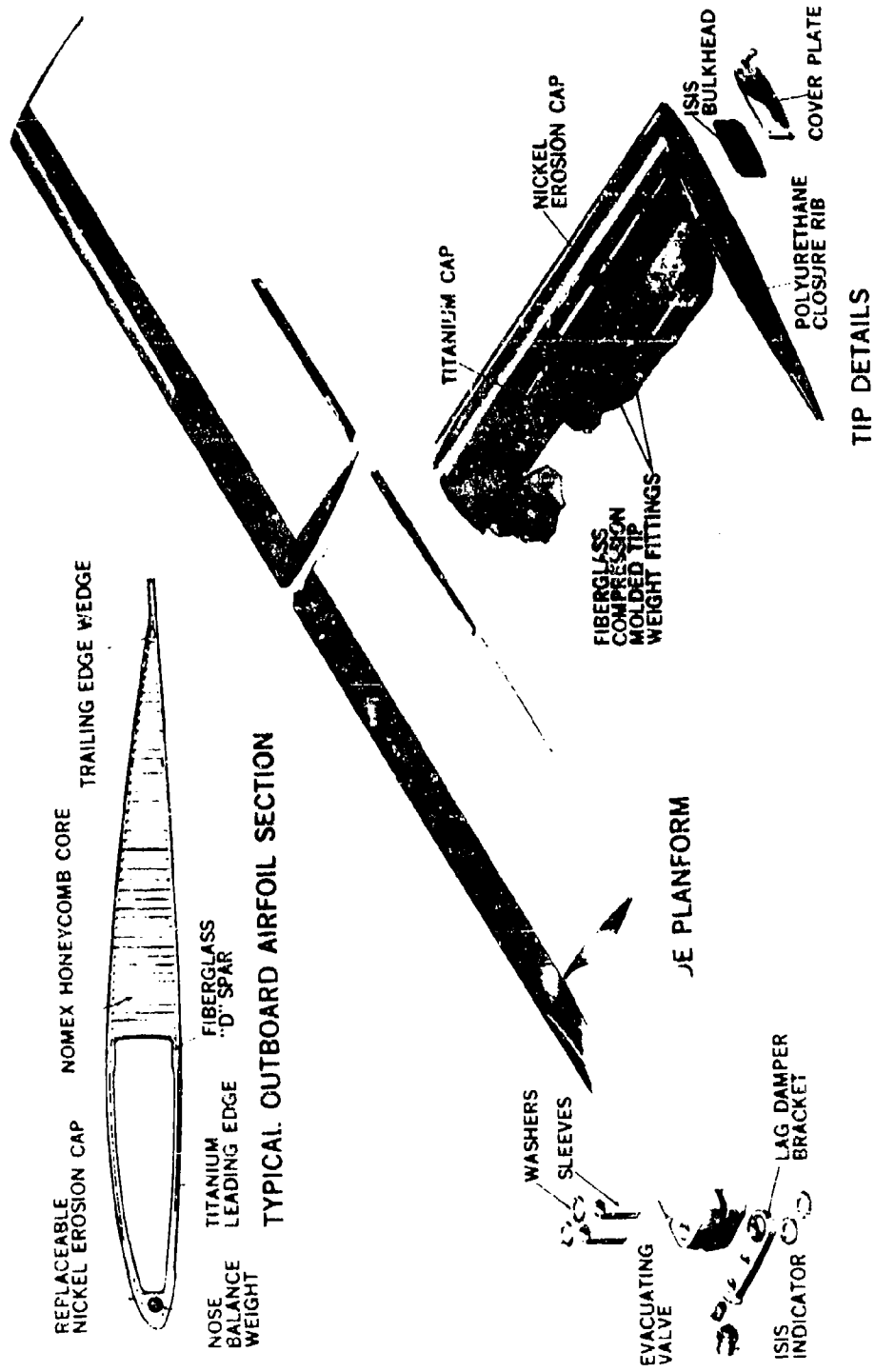


Figure 12. HLH Rotor Blade

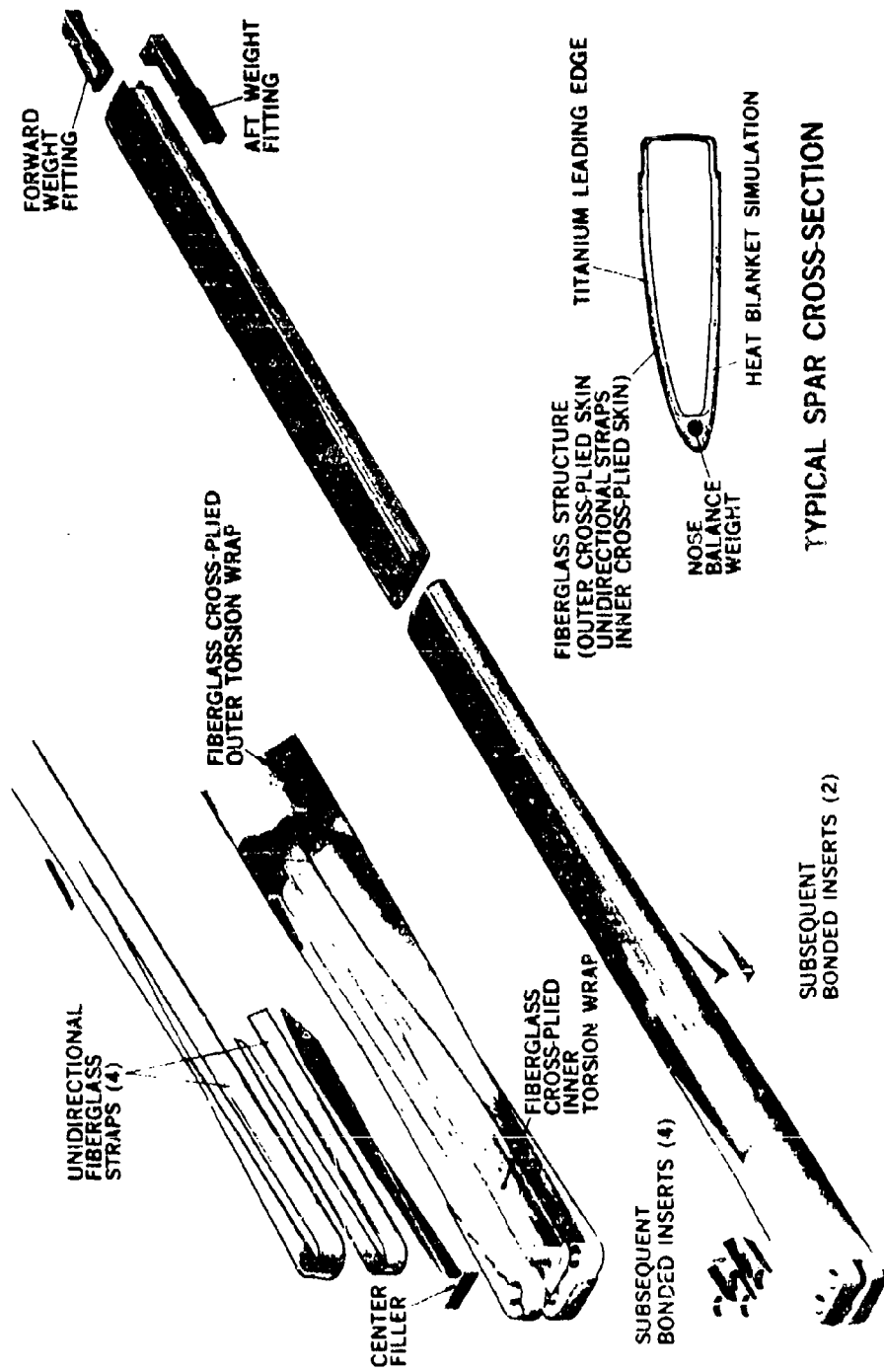


Figure 13. HLH Spar Assembly

3.4 PRELIMINARY DESIGN STUDIES AND SUPPORT TESTS

The initial blade design concept utilized the fatigue strength of fiberglass and the high stiffness, and strength-to-weight ratios of graphite to form a dual load path composite "C" spar. The skins were of crossply graphite because of its high modulus of rigidity. Design analysis showed that this concept satisfied the design fail-safe objectives. The root end attachment utilized the "coke-bottle" method, which along with the "C" spar was successfully demonstrated with all-fiberglass and all-boron advanced geometry rotor blades on the CH-47 Chinook helicopter. Dual and single spar designs with and without condition indicating systems were considered as illustrated in Figure 14.) The initial design trade studies are described in Reference 1.

Design support testing was conducted to evaluate the strength behavior of mixed modulus fiberglass/graphite composites, damage tolerance, impact tolerance, failure detection systems, and erosion. The results of these tests and further design studies had a considerable impact on the blade design, and finally led to the blade structural concept changing from a glass/graphite spar with graphite skins, crack wire detection system and polyurethane/nickel erosion strip to an all fiberglass spar, pneumatic detection system and a titanium nickel nose cap erosion system described in Paragraph 3.1. The design support test results are documented in the HLH/ATC Program Quarterly Summary Reports -2 and -3 (Reference 2).

The major reasons for the change in the structural concept are: first, metal was the only material known that would satisfy the requirements for erosion protection; second, the rapid failure mode of graphite was undesirable for a primary spar material; and third, the metal and fiberglass construction was superior in impact resistance and damage tolerance.

The addition of a metal nose cap provided inherent lightning protection and improved reliability of the deicing system. With the elimination of graphite crossply, the metal nose cap supplied the necessary torsional stiffness.

The design support tests which led to the ATC blade structural design concept are described in the following sections.

3.4.1 Phase I - Material Coupon Testing

The Phase I Material Program included the test of mixed modulus and single modulus laminates, sandwich beams and tubes. The results from 216 test specimens were used to establish the following conclusions:

1. Static modulus, static strength and fatigue strength of the graphite generally met all design goals.
2. Graphite exhibited extremely brittle failure modes.
3. Graphite crack propagation rate was rapid, both statically and in fatigue.

Figures 15, 16, and 17 show representative specimens and clearly point out the brittle nature of graphite failures characterized by rapid transverse cracks in various locations in the specimen. Failure across the fibers was expected, but not with the rapidity and severity demonstrated in these tests. The fiberglass failed as expected with longitudinal splits developing and failure progressing slowly to a point where the glass could no longer react the load. Another conclusion from this testing is that the fiberglass can act as a redundant load path.

3.4.2 Aft Fairing Damage Tolerance Test

In order to assess the effect of foreign object damage and field handling damage in service on high modulus graphite laminates, such as would be used for the fairing skins aft of the spar area, a series of test specimens were fabricated and evaluated. This is considered to be extremely important since aft fairing damage has been the cause for many blade removals in service.

Impact test parameters were the same as those used earlier to assess potential field damage to production units and consisted of gravity impact using a 2-inch diameter, one-pound ball dropped from increasing heights up to a maximum of 10 feet.

Significant differences in skin and core materials behavior were found at the 10-foot impact level. The results are summarized below:

1. No glass skin fracture occurred in any of the tests.
2. Aluminum core specimens sustained more damage than did the Nomex core specimens with the maximum impact resulting in a "permanent set" depression.
3. The graphite laminates were fractured when impact ball drops of more than 5 feet were used, with the damage being limited to less than the ball diameter in area.

Figures 18 and 19 compare the typical damage resulting from a one-pound ball dropped from heights varying from 6 inches to 10 feet on to aft fairing sections with Nomex honeycomb core and crossply fiberglass and graphite skins.

3.4.3 Whirling Arm Impact Testing

A whirling arm impact test was conducted on IR&D funding. The test was conducted by whirling typical blade sections at full-scale tip speeds and then introducing into the tip path plane hard-wood dowels of varying diameters. The test was based on a linear scaling principle with blades being scaled on an equal weight basis. It was meant to be purely qualitative and for comparative purposes only. The results of the test for both 3½-inch and 18-inch chord blade sections indicated the excellent damage tolerance of a metal fiberglass construction. In these tests, also, the brittle failure mode of graphite was evidenced by the loss of large areas of the trailing-edge fairing of all impacted specimens.

3.4.4 Crack Wire Failure Detection System Test

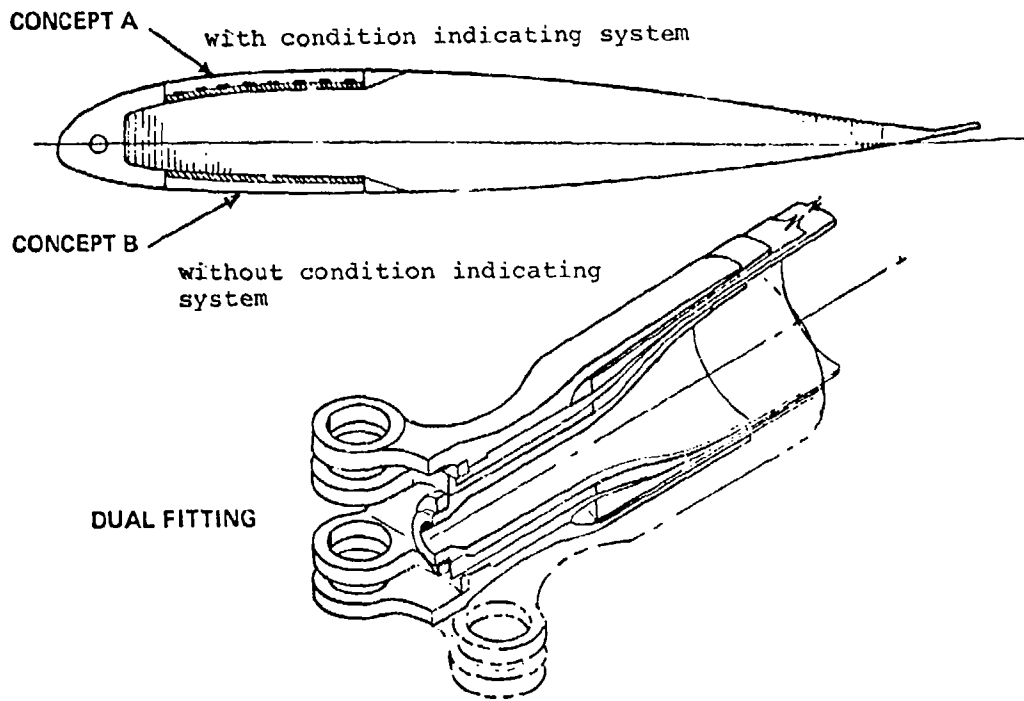
Failure detection (crack wire) tests were performed on nine 20-inch beam specimens. There was a total of 112 imbedded wires in these specimens, of which 49 were lost due to handling damage or premature failure. Of the nine beams tested, four failures were detected. The results of these tests indicate that: (1) the failure mode of graphite makes detection by crack wire adequate; (2) the failure modes of fiberglass make detection by crack wire undependable; (3) crack wires are highly susceptible to handling damage during the manufacturing processes of laminate fabrication, and (4) repair of failed imbedded wires is not possible.

3.4.5 Erosion and Lightning Protection Study

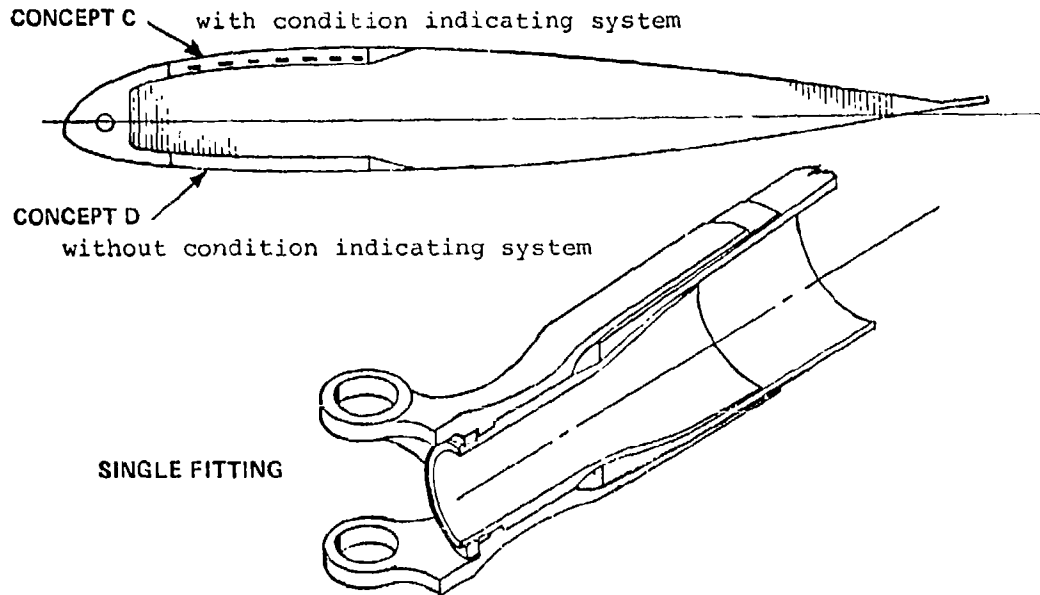
Concurrent with these material evaluations, studies were conducted to investigate erosion protection and lightning protection systems and how their requirements would be affected by blade construction and materials.

Investigation of polyurethane, which was the primary erosion protection system for the inboard 85% radius of the proposed blade indicated that it would be satisfactory for a pure sand abrasion environment. However, the rain erosion capability of urethane, especially after sand exposure, is very low and did not show promise of being improved in the near future. Polyurethane was selected originally and carried outboard to 85% radius to avoid subjecting the metal erosion strip to the critical strain zones on the blade (60%-80% radius). While it was known that urethane was inadequate for rain erosion at full-tip speeds, available data indicated that it was satisfactory to 85% radius. However, after sand exposure, the rain resistance of urethane was degraded to make it inadequate for the HLH blade. Metal at the leading edge of the blade would be required from 40% radius outboard.

The requirement for lightning protection is that the rotor blade must sustain a 200,000 amp strike without a catastrophic loss of blade, either aerodynamically or structurally. It is assumed that lightning can strike any part of the blade with a 90% probability at the tip. To satisfy these requirements, the leading edge has to have conductance equivalent to 21,000 circular mils of copper from tip to root. This lightning protection can be achieved inherently with a metal leading edge of sufficient cross-sectional area or a copper rod from tip to root and a metal tip cap connected to all other metal in the blade. The cross-sectional area for equivalent conductance is $.0164 \text{ inch}^2$ for copper, 1.64 inch^2 for Ti-6Al-4V and $.562 \text{ inch}^2$ for 301 stainless. Graphite or fiberglass aft aerodynamic fairing skins have a probable loss of 2-3 feet² without protection. However, undetected damage can occur in graphite without wire mesh protection (5-10 amps can damage graphite fiber). Therefore, a glass/graphite blade must have, in addition to a copper conductive wire, a fine grid aluminum weave over the entire blade.



(a) Dual Fiberglass Graphite Spar



(b) Single Fiberglass Spar

Figure 14. Trade Study - Rotor Blade Concepts

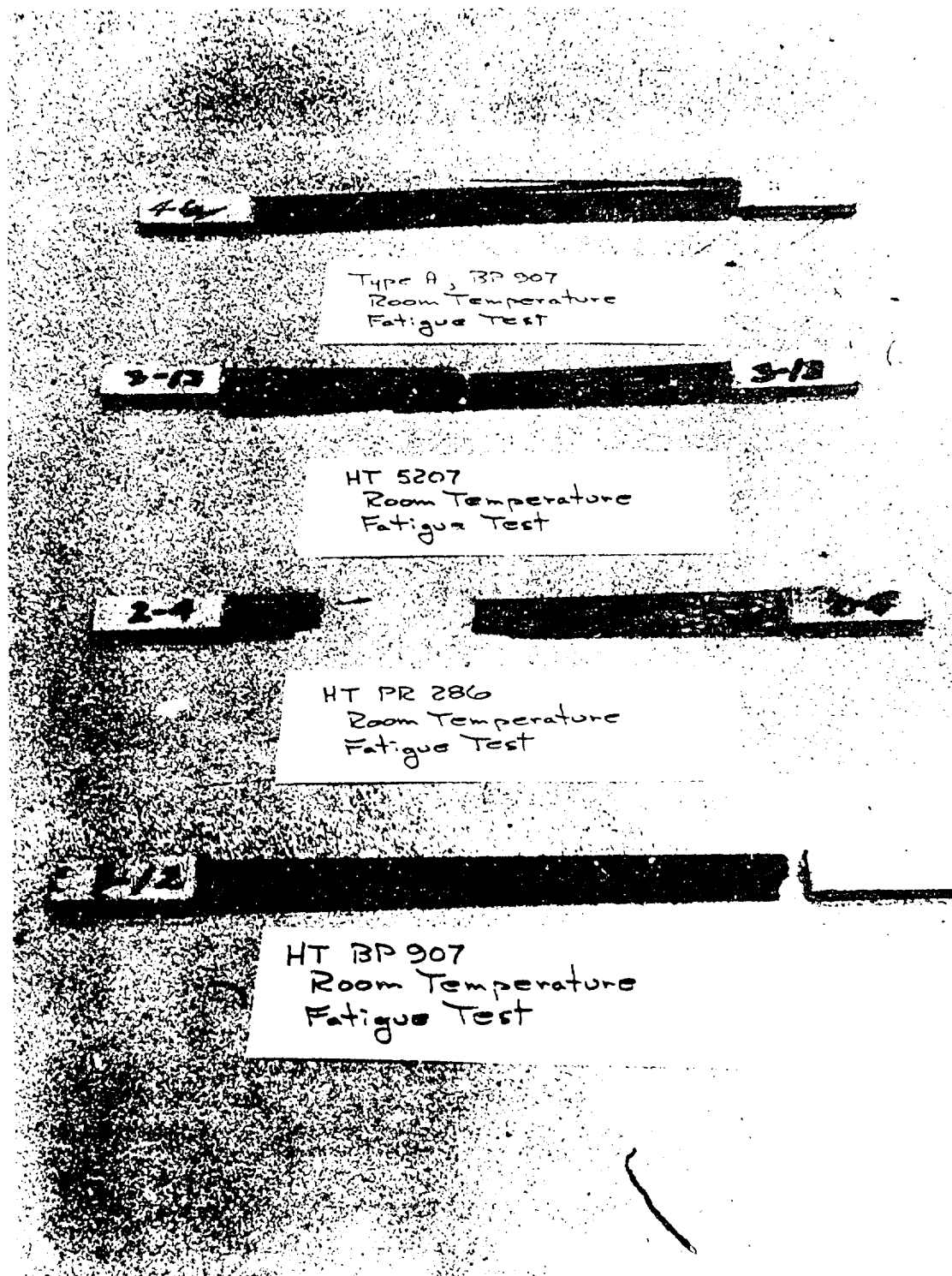


Figure 15. Tension Fatigue Failure of Graphite Composite (Room Temperature)

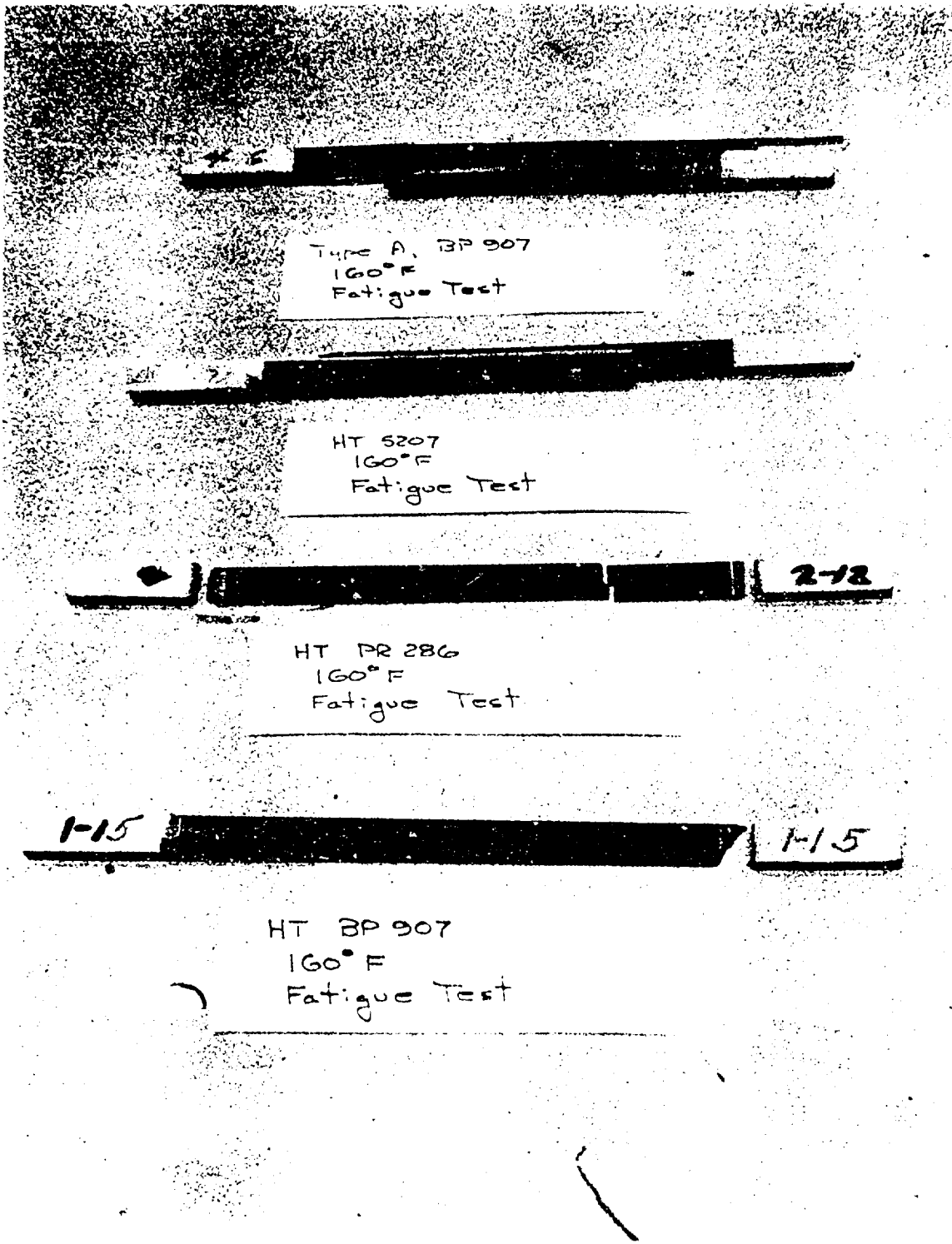


Figure 16. Tension Fatigue Failure of Graphite Composite (160°F)

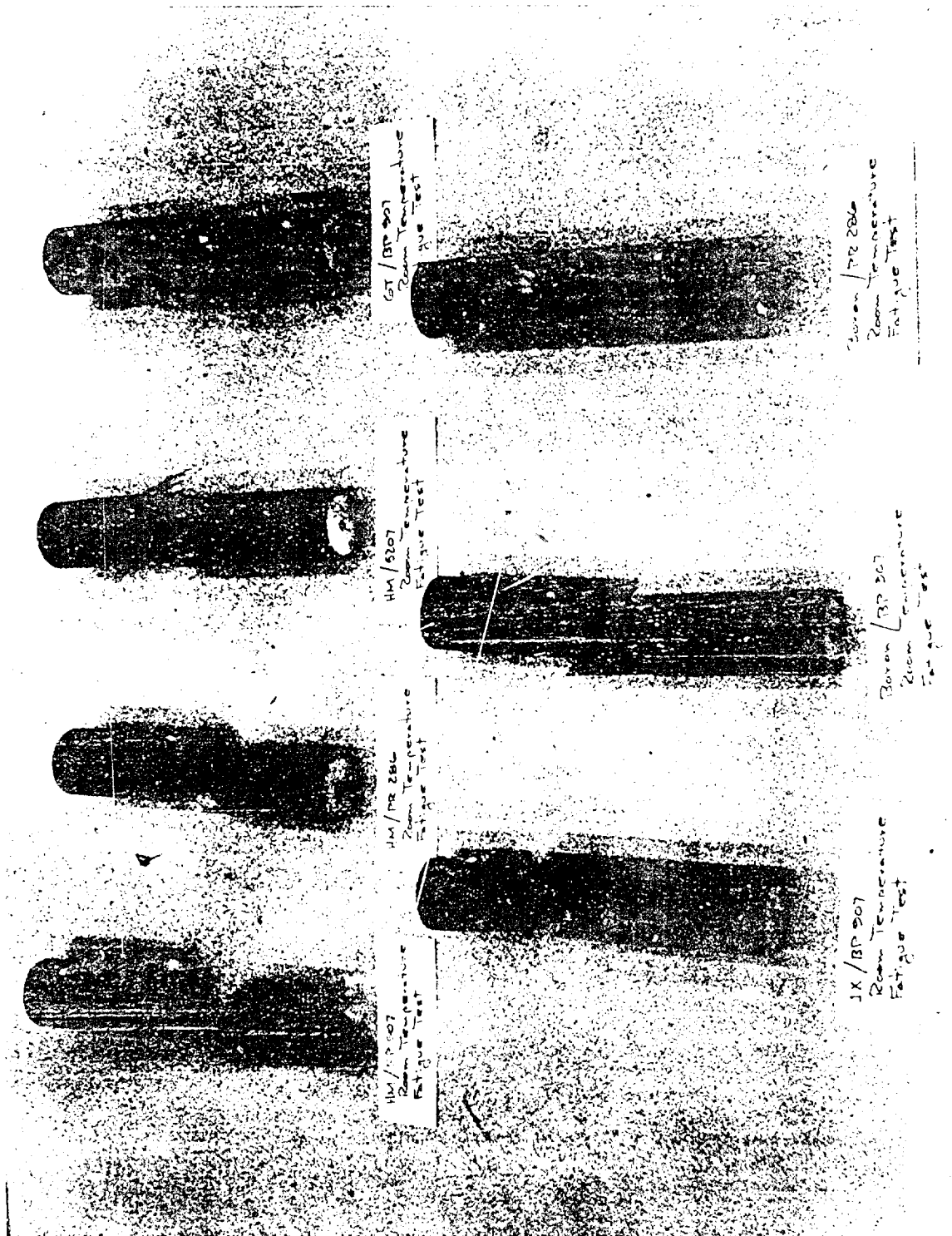


Figure 17. Shear Fatigue Failure of Graphite Composite

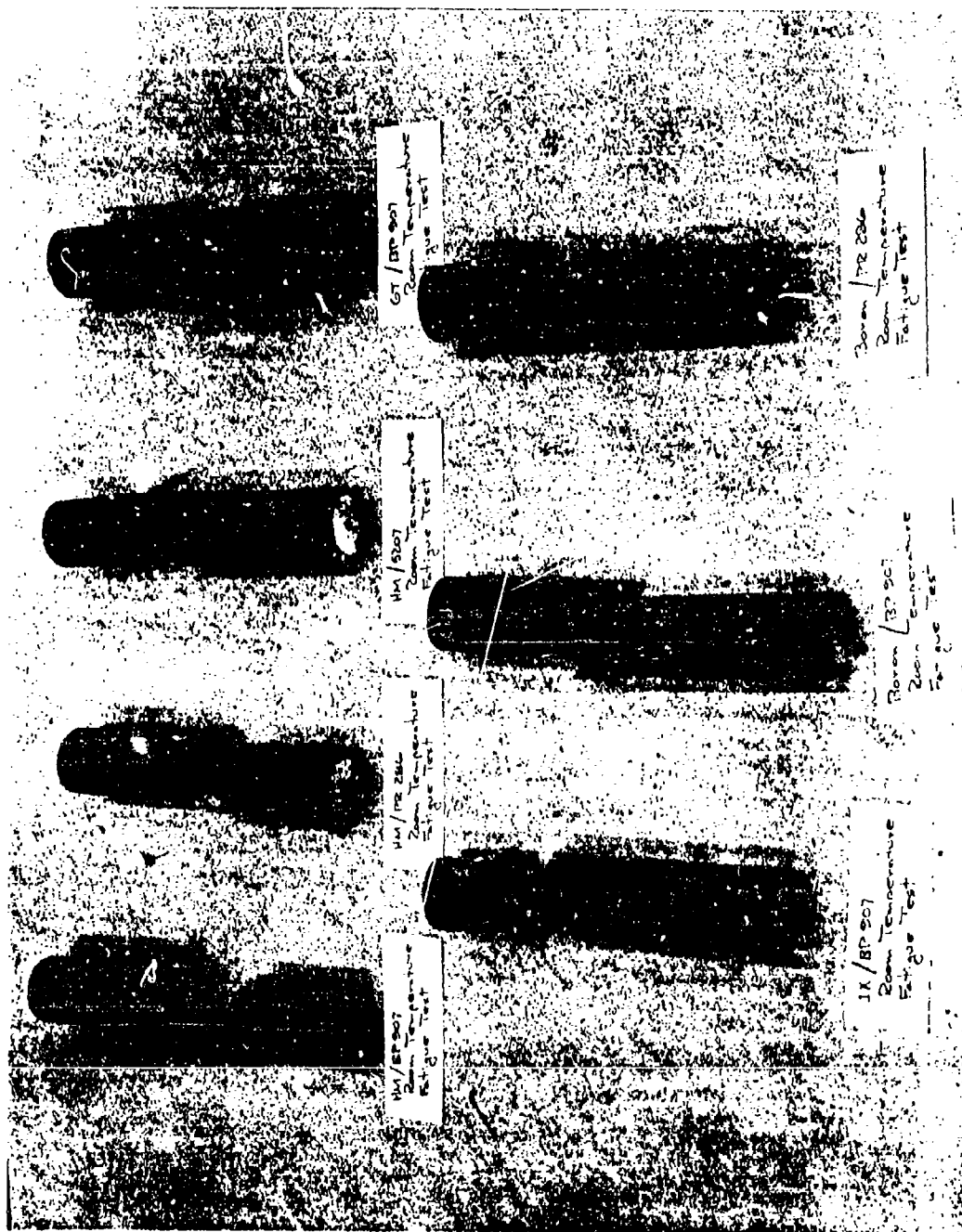


Figure 17. Shear Fatigue Failure of Graphite Composite



Figure 18. Impact Test - 1 Lb Ball on $\pm 45^\circ$
Graphite and Nomex Core

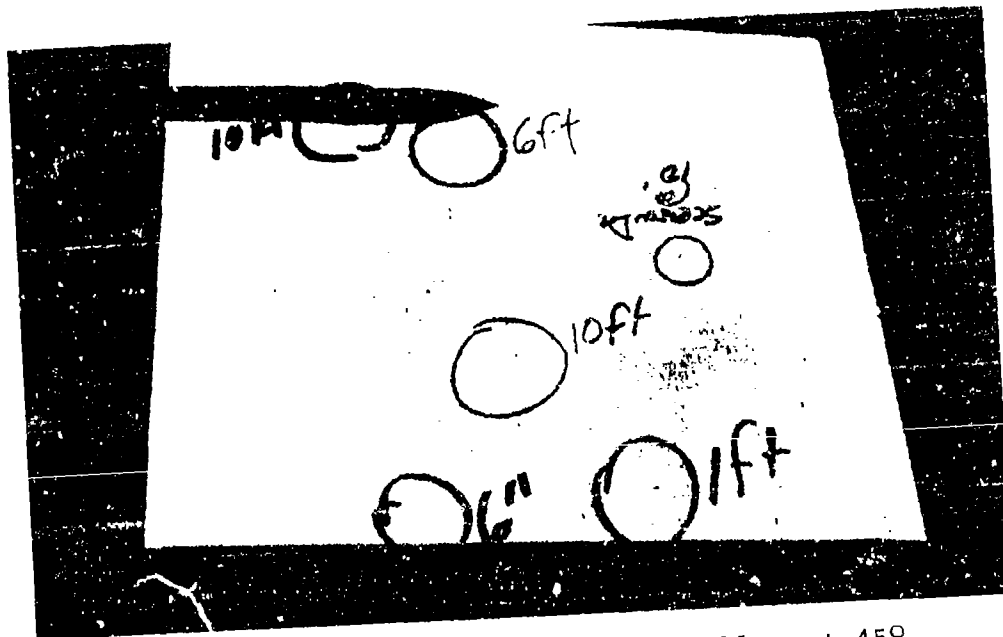


Figure 19. Impact Test - 1 Lb Ball on $\pm 45^\circ$
Glass and Nomex Core

3.5 DETAIL DESIGN OF THE ATC BLADE CONFIGURATION

The initial design studies and supporting tests led to the selection of the composite metal/fiberglass blade concept. Prior to proceeding with the detail ATC blade design, the blade parameters that were most affected by the deletion of the graphite material were reexamined. These included the blade fail safety, torsional rigidity, static droop clearance, and the failure detection system. The torsional rigidity and static droop clearance requirements were met by extending the nose cap coverage over the complete external spar upper and lower surfaces. This is due to the fact that the metal inherently provided increased torsional and flapwise stiffness and minimized the amount of crossply fiberglass. A greater proportion of the spar weight was then available for unidirectional fiberglass which yields better fatigue strength and droop properties.

The slow failure mode of fiberglass, the primary blade material, makes failure detection by crack wires undependable, and a differential pressure system was considered to be a feasible alternative.

With the basic concept defined, the detail blade design was entered into with a high level of confidence that successful development could be accomplished during the ATC program.

The detail design phase was also supported by a considerable number of tests, as summarized in Figure 20. Each major item of the blade was evaluated before finalizing the design and proceeding with the blade manufacture.

3.5.1 Spar

The spar subassembly is a closed "D" cross section of unidirectional and crossply fiberglass composite.

The change from "C" spar to "D" spar was precipitated predominantly for fabrication considerations. The tooling concept utilized for fabrication of the "C" spar for the CH-47 AGB fiberglass and boron blades required three major tools and five separate blade "cooks." This process was expensive and not production oriented. A "producible" AGB tool concept still had three major tools but required only three separate cooks. Major "C" spar fabrication problems were: core tolerances, core insertion, skin-to-spar and spar-to-core

bonding. Since the "C" spar is cured as a separate entity, and the core must be stabilized prior to insertion into the spar, the spar inside mold line and the core outside mold line must be held to a very close tolerance if they are to fit and provide a good quality bond. Hence, a tolerance and pressure problem exists in the nose of a "C" spar which is difficult to overcome. A similar problem occurred in the CH-47 AGB when the precured skins were bonded to the precured spar-core assembly. Due to the lack of flexibility in the mating surfaces, there were large unbonded or void areas over the span.

The "D" spar concept reduces the required number of major tools to one (with supplementary inserts) and completely eliminates the major core/skin-to-spar bonding problems. The fabrication sequence involves fabrication of a complete spar (titanium and fiberglass) in one cure. This spar will be virtually void-free and will ensure a superior bond to the titanium and a repeatable close tolerance airfoil contour. The aft fairing can be bonded to the fully inspected spar as a precured subassembly (which is similar to the fabrication of present day metal rotor blades) or bonded to the spar while the fairing is being cured. This latter approach was used to eliminate close control tolerances between two precured composite laminates. The "D" spar is the best construction for cost because of these fabrication and tooling advantages. Cost will be further reduced because of better inspectability, better repeatability (tracking considerations), and the capability of replacing the entire aft fairing assembly.

Other important advantages of the "D" spar over the "C" spar is that it gives the highest torsional stiffness per pound of blade weight and is adaptable to an ISIS-type pneumatic detection system.

Titanium was selected for the metal nose cap because it has the best fatigue strain capability as shown in Table 3. In addition, its creep-forming capabilities are ideally suited to the complex leading edge of the blade and its erosion properties are better per pound than 301 stainless steel and surpassed only by nickel.

Titanium possesses a 50-percent better specific torsional stiffness than does fiberglass crossply, and is equivalent to unidirectional fiberglass in specific bending stiffness; therefore, torsional stiffness can be achieved with titanium

without sacrificing droop characteristics. By extending the chordwise coverage of the titanium to .35C, the necessary torsional stiffness of the blade was achieved with a slight weight reduction compared to all fiberglass construction.

The thickness of the titanium was determined by torsional stiffness and erosion considerations. The maximum amount of unidirectional fiberglass was used in the section commensurate with bending stiffness and blade weight requirements. Fiberglass is the basic spar material with its high fatigue strength, damage tolerance, and "soft" failure modes. The specific stiffness of fiberglass is equivalent to that of metals; consequently, for the same weight, the blade has the same stiffness and frequencies as a metal blade. However, fiberglass has a fatigue strain capability 2.5 times that of steel, 3.3 times that of aluminum, and 1.6 times that of titanium.

The blade alternating strains in steady-flight conditions are much further below the endurance limit compared to the other materials. The large fatigue margin is beneficial for damage tolerance and in-service reliability.

The length of the blade eliminated the use of MIL-T-9046 hot rolled 6AL-4V titanium alloy sheet, as this is available in maximum lengths of 20 feet. Therefore, cold rolled 6AL-4V sheet to Boeing Specification BMS-7-197 (Reference 3) was selected. This material was coupon tested to provide fatigue strength properties for strength analysis and to evaluate edge treatments and the effects of heat treatment and processing required for the nose cap forming. The results of these tests are shown in Figure 21.

The endurance limit established from the coupon tests showed titanium to be acceptable from a fatigue strength point of view.

The use of the hollow "D" spar caused the wall buckling to be a critical design condition. As a result of the buckling analyses, the spar wall thickness was increased with additional unidirectional fiberglass from .25R to .75R. A buckling test of a representative spar section was conducted, which confirmed the analyses. Consideration was also given to the deflection of the spar wall, in the chordwise direction, due to differential pressure from airloading and the pneumatic failure detection system. The deflections were

limited so as to be equivalent to those for the CH-47B/C helicopter for the same conditions. This was done by adding unidirectional graphite running chordwise with its high specific stiffness at 90° to the unidirectional fiberglass. The graphite was embedded in the spar inner crossply fiberglass and the unidirectional fiberglass so as to protect it from impact damage.

Although there was no requirement for fabrication of a de-icer blanket in the ATC program, design support tests were conducted to evaluate the effect of the local blanket temperature on the surrounding fiberglass and adhesive structure. Actual energized blanket tests in a realistic ambient environment and duty cycle indicated that the critical bondline temperature never exceeded 110°F, and that the blanket located between the titanium and fiberglass would pose no structural problem. Nesting the blanket between the metal cap and the fiberglass assists the deicing process. The heat generated in the blanket flows outward to the iced surface and is not absorbed in the blade due to the insulating characteristic of the fiberglass.

3.5.2 Root End

The change from the "coke" bottle root end to the wraparound root end (Figure 22) culminated a design and analytical trade study effort spanning more than one year. Although obviously redundant, the dual coke-bottle configuration originally proposed was very expensive to fabricate and would have been extremely difficult to protect with any type of detection system. Protection of this metal root end concept would have been mandatory. Further, the disadvantage of having metal components built into the laminate which can become potential fatigue problems, and which are not replaceable, reduces the blade's serviceability and increases its potential cost.

The wraparound root end is redundant since it has four separate load paths into the hub. It has no metal components built into the laminate. The metal bushings for the attachment hardware are all replaceable. Since all lugs are separated and exposed, visual inspection is all that would be required for fail-safety. Furthermore, the wraparound root end concept is the lightest of all the concepts studied in detail. The cost of metal machining for the root end is completely eliminated.

A root end design support test (Reference 4) was conducted which demonstrated the concept's feasibility. Fatigue loading at amplitudes three times greater than V_H high-speed level flight was sustained for 3×10^6 cycles without failure of the primary load-carrying members of the root end. The specimens endured an additional $.92 \times 10^6$ cycles of fatigue loading at three times V_H flapwise bending load and maximum lag damper load applied through a lag damper arm at the blade attachment location, Station 66. Bushing fatigue failures created a requirement for a design revision. Sleeves and separate washers replaced the bushings at the blade retention pins. ISIS leaks around the lag damper arm indicated a need for a sealing bulkhead inside the spar.

The root end was capable of reacting overspeed rpm, flight maneuver, starting, and ground flapping limit load conditions without any apparent damage. The fail-safe testing showed that the root end is capable of sustaining V_H high-speed level flight loads with simulated failures at various spanwise locations, in three of the four load paths. Axial load equal to the design limit centrifugal force of 250,000 pounds was carried by the root end in the simulated failed condition.

3.5.3 Aft Fairing

The aft fairing is a single box construction, with fiberglass skins, and Nomex honeycomb core. The fairing subassembly is shown in Figure 23. Fiberglass was selected as the skin material because of the damage tolerance and durability demonstrated in years of service on the CH-47B and C helicopters. Fatigue testing of fiberglass blade skins returned from service demonstrated that fiberglass properly protected by paint shows little effect from the service exposure. Fatigue tests of the used skins fell within the scatterband of new, unexposed skins as shown in Figure 24.

The Nomex honeycomb core was selected because as a nonmetal it eliminates the corrosion problems experienced with metal honeycomb. Nomex also provides a substantial benefit in the blade's fabrication concept. When enclosed between two molds to a fixed dimension, Nomex deflects and provides a back pressure proportional to the deflection. As the temperature increases during the cure cycle, the back pressure decreases to zero and the Nomex sets in this deflected position with little or no spring back.

Fatigue, static, moisture penetration and migration tests of fiberglass/Nomex specimens were conducted and are reported in Reference 5.

The trailing-edge wedge and cusp are of fiberglass/graphite construction. The section is constant from Station 138 to the blade tip except that there is a 2-inch cusp extension between Stations 138 and 220.8. Ninety-degree uni-fiberglass is provided for chordwise trailing-edge stiffness in order to minimize in-flight cusp deflections. The zero-degree uni-fiberglass and HT-S graphite is sized by trailing-edge buckling considerations for rotor starting conditions and by the blade chordwise bending stiffness and natural frequency requirements.

The cusp stiffness limits the deflection of the cusp, as it travels around the azimuth, to ± 0.2 inch under external loading conditions.

The first chordwise natural frequency reduces by approximately .15 when coupled with the drive system. The size and stiffness of the trailing-edge wedge was determined so that the coupled frequency was greater than 4.5 per rotor revolution to ensure that, with a 4-bladed rotor, unfavorable 4 per revolution vibrations would not be transmitted to the airframe.

3.5.4 Tip Installation

The tip assembly for the rotor blade provides for a large adjustable weight capacity. The tip provides the capability for moving the dynamic balance axis forward approximately .75 percent. Advantage has been taken of the more aft location of the VR-7 and VR-8 centers of pressure by allowing the local chordwise balance axis (and, therefore, the resulting dynamic balance axis) to fall aft of the conventional quarter chord location. Wind tunnel testing has shown that no flutter exists for this configuration, but the .75 percent over-balance capability has been provided as a precaution.

The tip fittings were chopped fiber molding to be precured and secondarily bonded into the bonded blade subassembly (spar and aft fairing subassembly).

3.5.5 Fiberglass Material Specification

The fiberglass resin system for the HLH blade is SP250-1014S. The CH-47 AGB fiberglass blade was built using an SP1002S resin system curing at 350°F. The SP250 system which cures at 250°F reduces tooling and fabrication costs. It permits faster cure cycles with less heat-up and cool-down times, lesser heat requirements, and reduced warp in the co-cured spar. Coupon fatigue test results (Figure 25) showed that the SP250 resin system was at least as strong as the 1002S system.

3.5.6 Location of the Chordwise Balance Axis

Blade design practice places the center of the blade mass (Balance Axis) aft of the airfoil aerodynamic center, which for conventional airfoils is at .25C. Figure 26 presents the aerodynamic center for each of the HLH airfoil sections. The advanced airfoil permitted the balance axis to be as far aft as .26C, which resulted in a considerable weight saving. The 14-foot-diameter model rotor was tested in the Boeing Vertol Wind Tunnel with the balance axis at .257C without evidence of blade flutter.

3.5.7 Failure Detection System

The failure detection concept for the titanium/fiberglass "D" spar is a pneumatic differential pressure system utilizing an evacuated spar. Because of the very long life after titanium failure, the pneumatic system will protect only the fiberglass portion of the spar, and a failure of the titanium nose cap will be detected visually.

For normal operation of the titanium and fiberglass acting together in the spar, it is not conceivable that the fiberglass could ever fail before the titanium. In the event of fiberglass damage during manufacture or service, it is still highly improbable that continued deterioration or propagation of the damage in the fiberglass would result, without causing locally higher straining of the titanium to the point where it would fail locally permitting a leak and subsequent failure indication. Tests have confirmed these conclusions. The tests of glass composites, in combination with steel and titanium have included undamaged specimens, specimens with prior damage to the metal, specimens with prior damage to the glass, and specimens with simulated bullet damage to both the

metal and glass. In all cases, the metal failed first and the damage did not propagate to the glass.

Results of design support tests with a simulated spar section (Reference 6) and with evacuated elliptical fiberglass tubes (Reference 7) established the feasibility of the application of a pneumatic system to composites.

In order to ensure failure of the fiberglass at the blade operational stress levels, defects were built in the fiberglass, producing a spanwise discontinuity of the unidirectional fibers. The specimen section properties at the defect location were reduced by approximately 20 percent. Specimen failures occurred as titanium cracks, debonding between the titanium and fiberglass, and propagation of the built-in defect. In all cases, the failure was identified by a vacuum leak. Most failures occurred under the beam load clamp and were primarily due to the method of loading which produced high shear and local secondary stresses. The specimens were considered to be failed when the beam deflections became so large that loads could no longer be applied. At the termination of each test, all specimens were capable of carrying the test axial load equivalent to the rotor blade centrifugal force.

The conclusions obtained from the tests were:

1. Failure of the fiberglass spar under the titanium nose cap would induce a titanium failure or debonding between the titanium and the fiberglass, thus providing a vacuum leak path.
2. Following the vacuum loss indication, the blade structure will be capable of supporting normal flight loads for fatigue cycles equivalent to at least 200 hours.
3. Fiberglass laminates do not inherently leak while under high vibratory strains, a necessary requirement for the pneumatic system.
4. Fatigue failures of fiberglass laminates progress locally through the thickness of uni and are accompanied by sufficient crossply delamination to permit leakage, a necessary requirement for the pneumatic failure detection system.

5. Small defects will not propagate in fiberglass at strains of 1000μ inches or less.
6. The testing showed that even a large fiberglass defect would at first cause a titanium failure and delamination, and that fiberglass failure propagation is extremely slow.

Slow propagation was not a requirement for the detection system and no propagation time was assumed in the development of the 200-hour at (M -2σ) endurance limit criterion. It was assumed that the remaining structure, after the failure, be of sufficient section to sustain 200 hours without strains exceeding the (M -2σ) level. The inherent crack propagation capability of fiberglass makes this criterion much more conservative than originally anticipated, since initial evaluations indicate that the available detection time will exceed 200 hours.

3.5.8 Erosion Protection

Whirling arm erosion testing of nickel titanium, and stainless steel were conducted at full-scale tip speed (750 fps) and accelerated sand densities. The results of these tests are given in Reference 22. They show that the nickel/titanium leading-edge system is a substantial improvement over the stainless steel leading edge of the CH-47.

3.5.9 Blade Drawings

A complete list of the blade drawings is given in Figure 27. The blade assembly drawings are included as Figures 28 through 31.

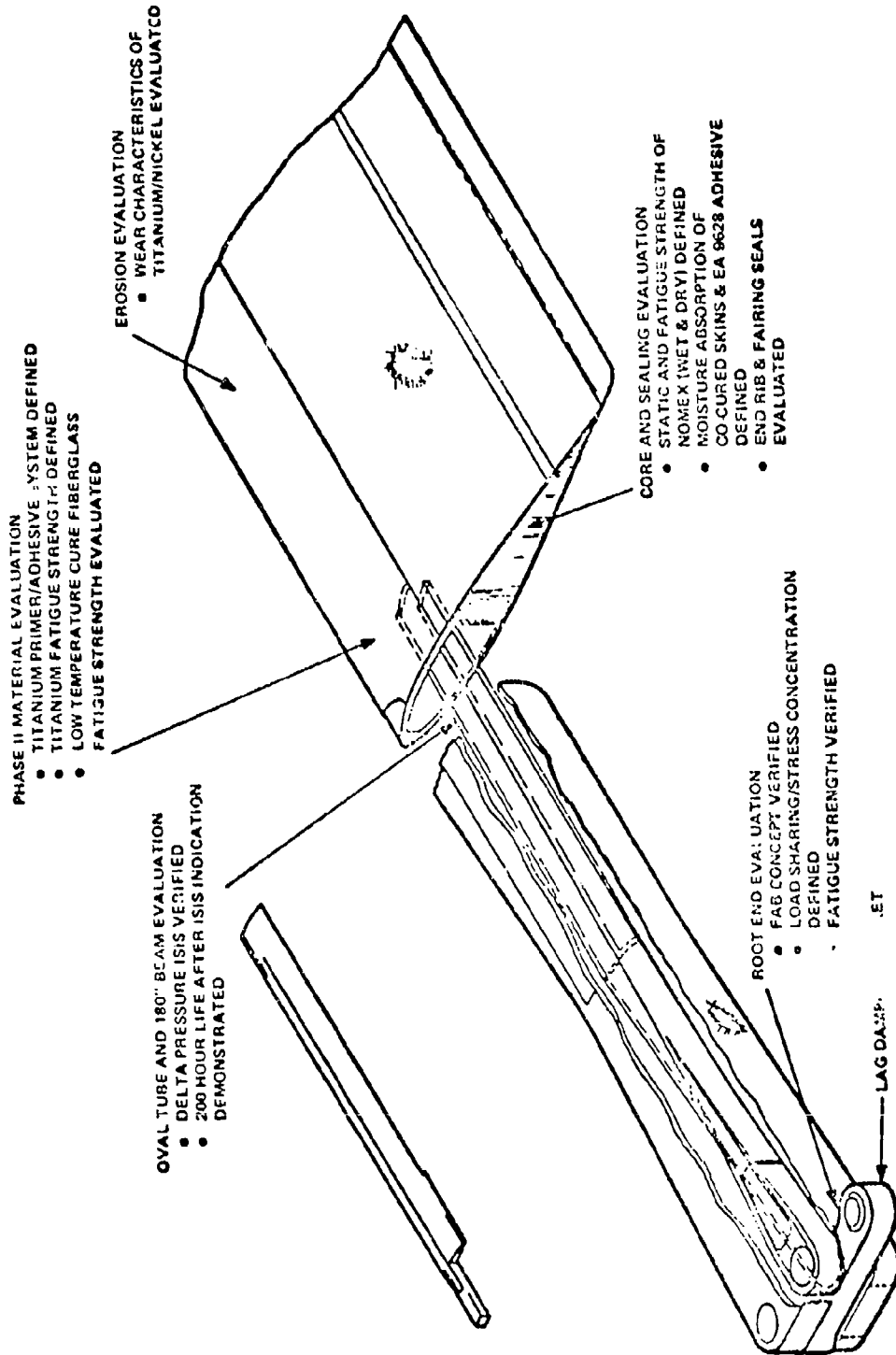


Figure 20. Design Support Tests

TABLE 3. COMPARATIVE PROPERTIES OF BLADE MATERIALS

MATERIAL	E PSI $\times 10^{-6}$	G PSI $\times 10^{-6}$	ρ LB/IN ³	ULTIMATE TENSILE STRENGTH (KSI)	FATIGUE STRENGTH (KSI) R = 0.1	FATIGUE STRAIN CAPA- BILITY μ IN/IN ϵ	SPECIFIC PROPERTIES			
							E/ ρ $\times 10^{-6}$	G/ ρ $\times 10^{-6}$	σ/ρ $\times 10^{-3}$	ϵ/ρ $\times 10^{-3}$
S CLASS UNI	6.3	0.6	0.068	175	12.5ϵ 10^8	1985	92.6	8.8	184	29.2
S GLASS X-PLY	1.8	1.8	0.068	26.2	2.56ϵ 10^8	1440	26.5	26.5	37.6	21.2
HT GRAPHITE	18.5	4.0	.055	140	40.0ϵ 10^8	2170	336	72.7	72.7	39.4
TITANIUM	16.0	6.3	.16	130	19.8ϵ 5×10^7	1235	100	39.3	124	7.7
STEEL	29.0	11.0	.284	150	23.0ϵ 10^7	795	102	38.7	81	2.4
ALUMINUM	10.0	4.0	.10	80	6.0ϵ 5×10^7	600	100	40.0	60	6.0

Cold Rolled BMS 7-197
 $t = .05$
 $K_t = 1.0$
 $R = .1$

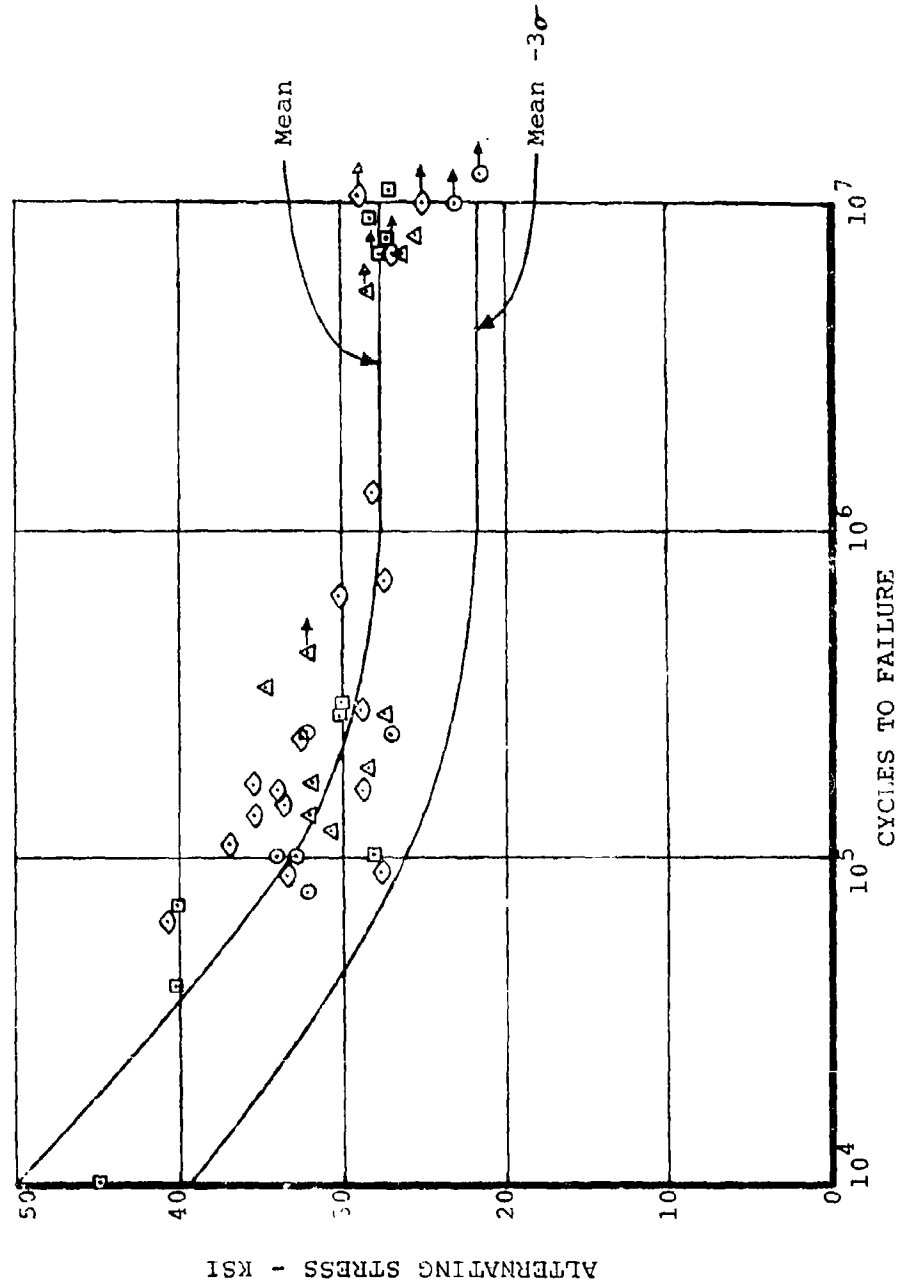


Figure 21. Coupon Fatigue Tests of 6AL4V Titanium Alloy Sheet

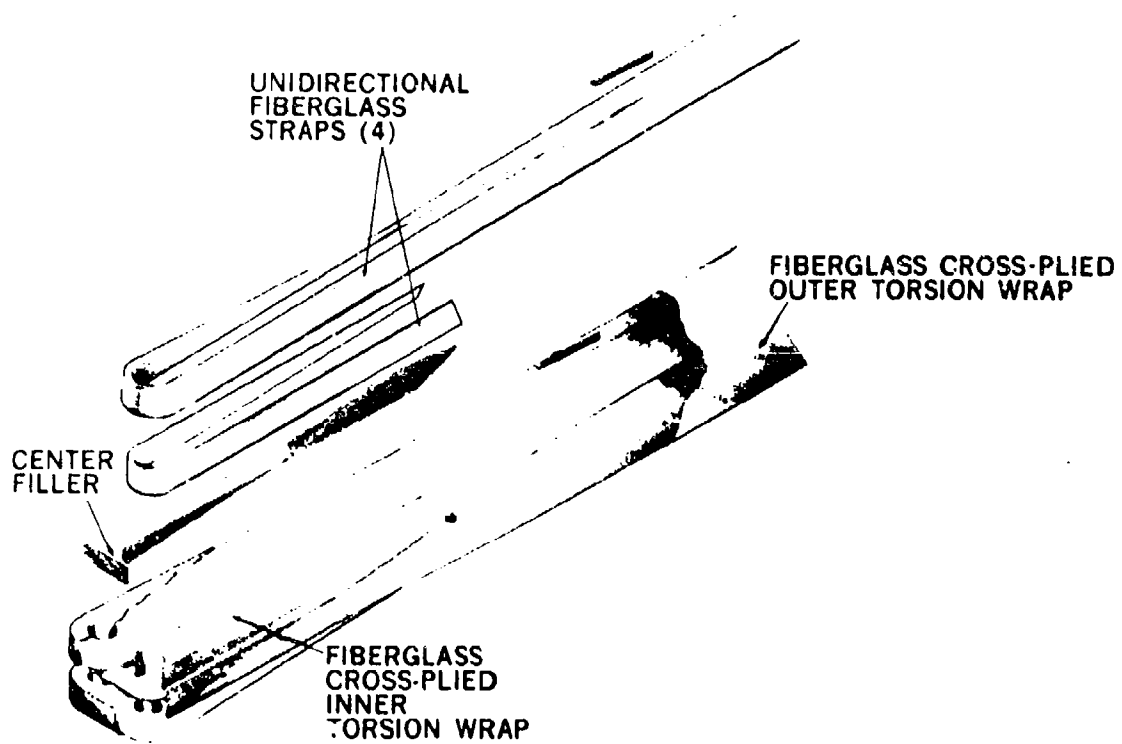
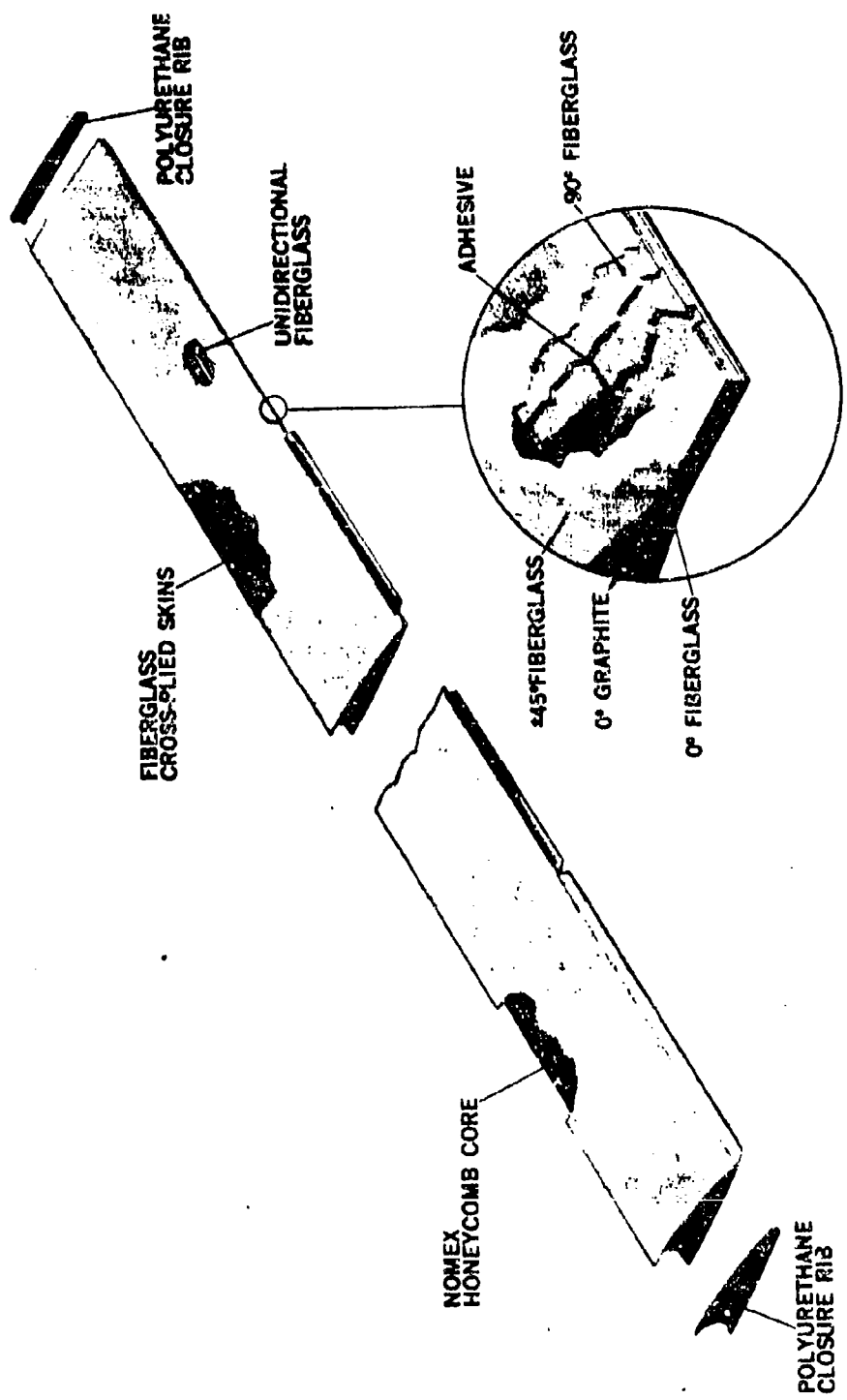


Figure 22. Wraparound Root End



TRAILING-EDGE CONSTRUCTION

Figure 23. HLH Rotor Blade Aft Fairing

Service Time

CH-47A Box Skins Painted On Outer Surface	○ —	948 Flt Hours in RVN	34 Months
		309 Flt Hours in RVN	62
	△ —	237 Flt Hours in Korea	36

■ — 1359 Flt Hours in RVN

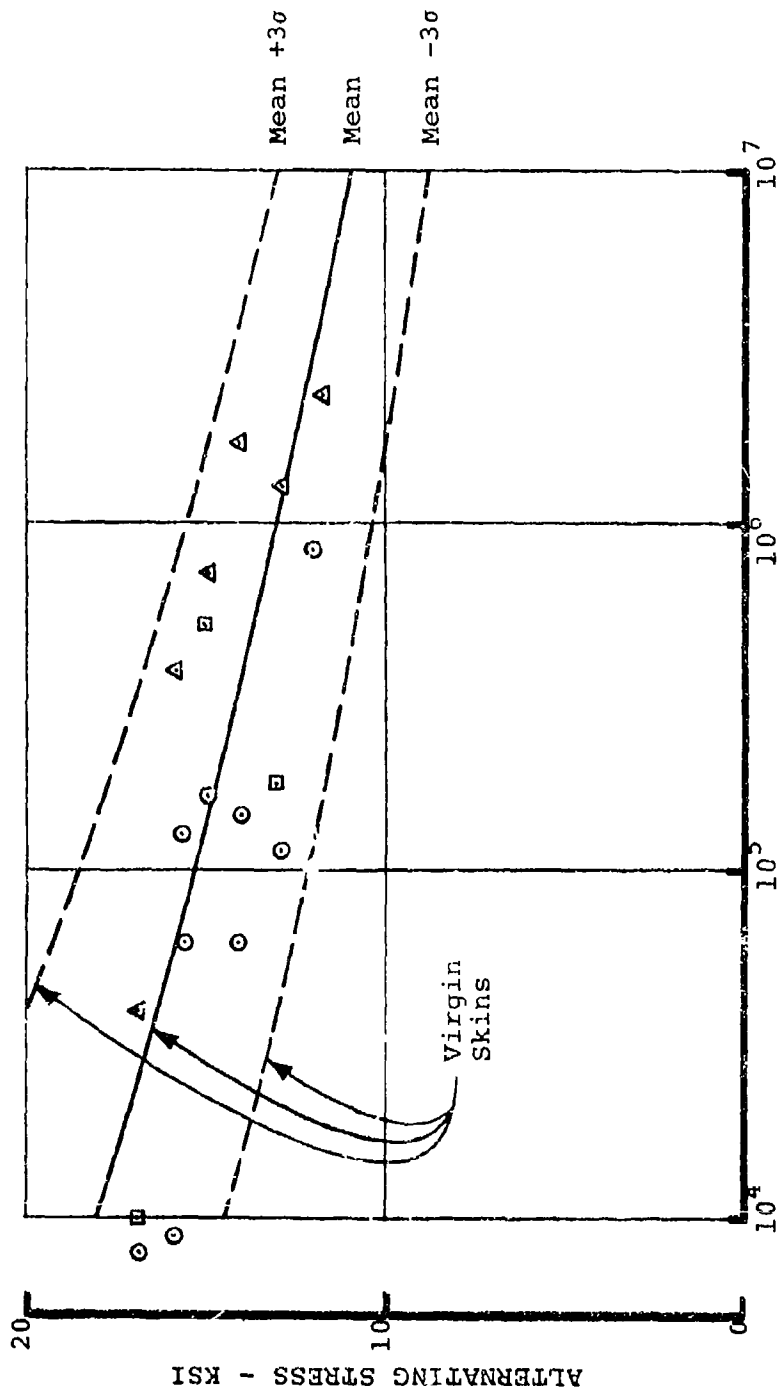


Figure 24. Fiberglass Composite Does Not Lose Strength After Operating in Service Environment

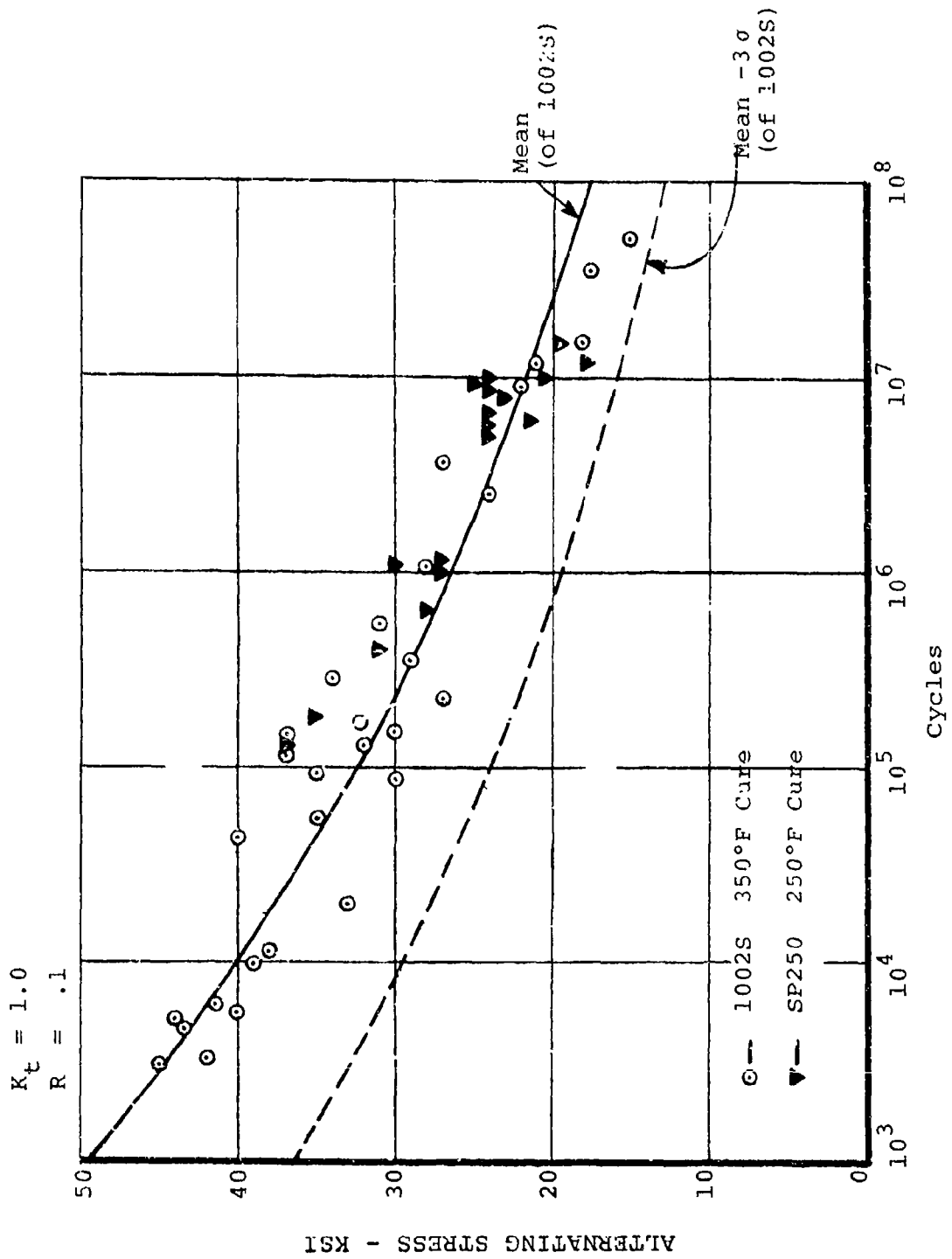
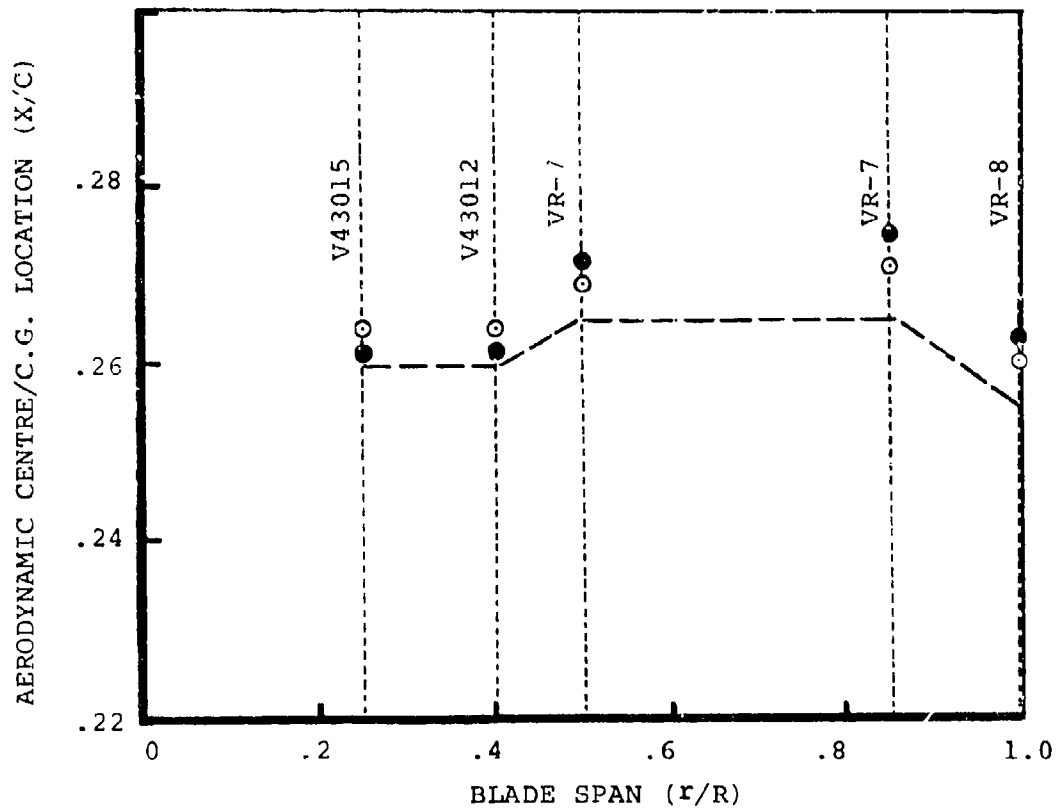


Figure 25. Comparison of Fatigue Strength of 1002S and SP250 Unidirectional Fiberglass Epoxy Composites



- ⊙ Aerodynamic Center for Hover, 750 FPS Tip Speed
- Aerodynamic Center for 170 Knots, 750 FPS Tip Speed

Figure 26. Location of Chordwise Center of Gravity

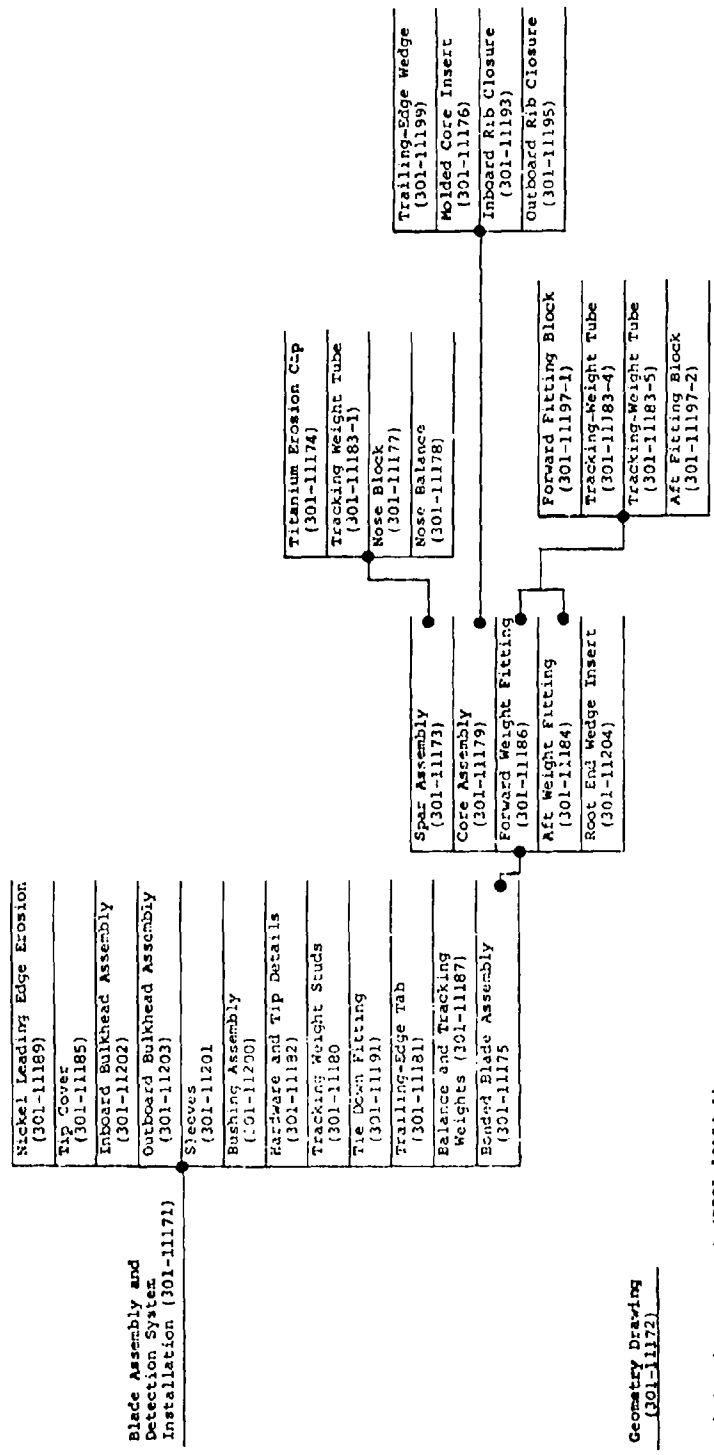


Figure 27. HLH/ATC Rotor Blade Assembly Drawing Tree

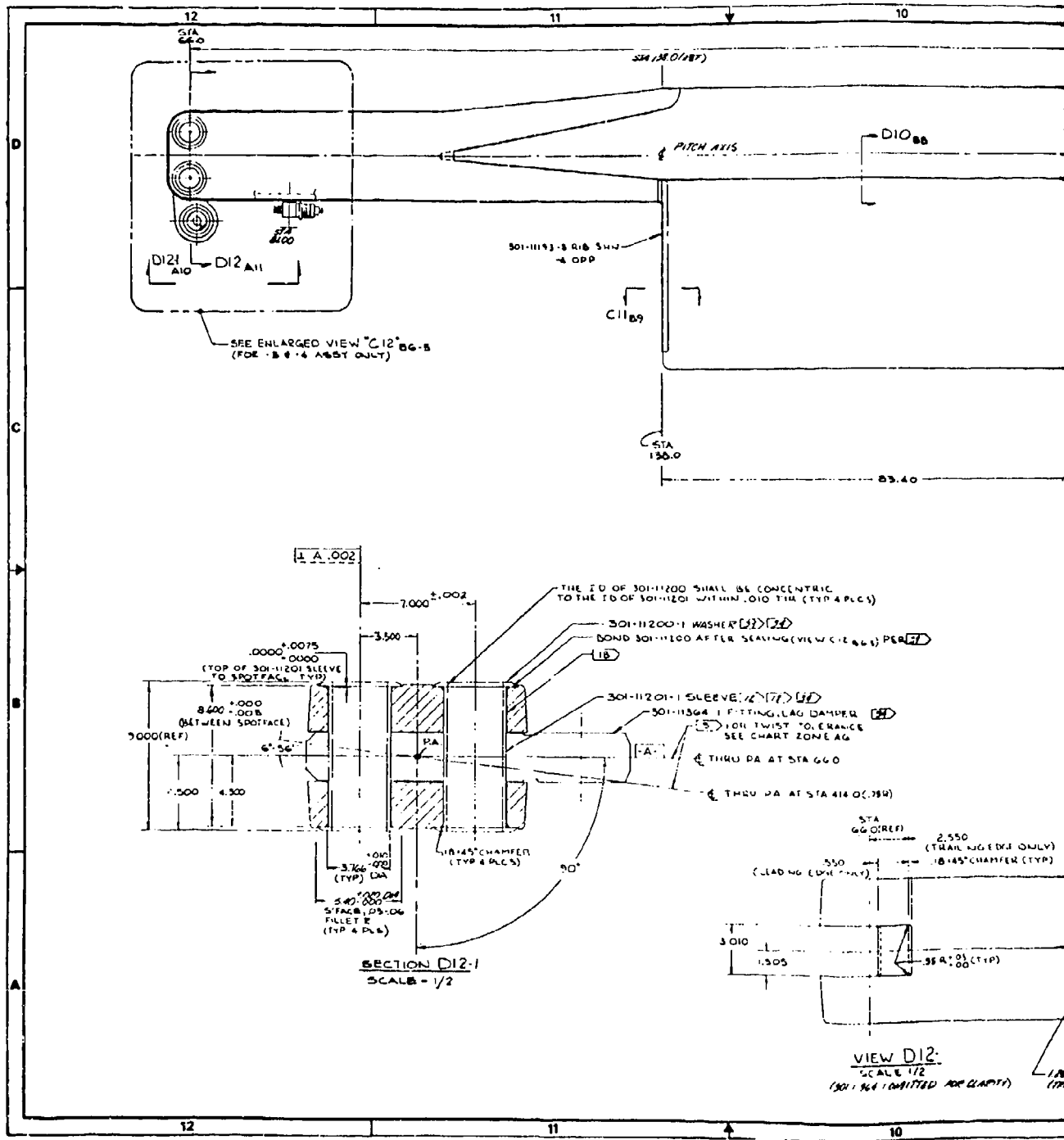


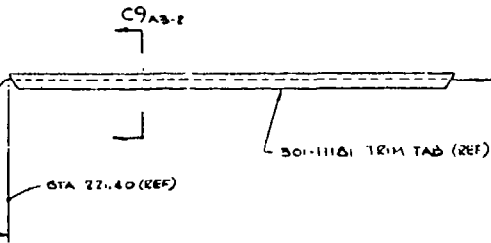
Figure 28. HLH Rotor Blade Assembly

9

8

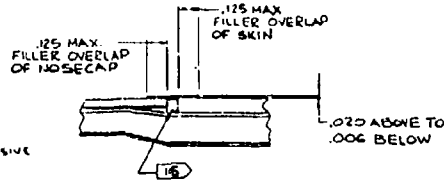
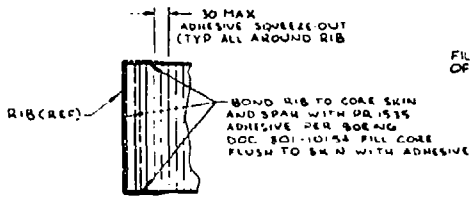
7

548.03 CB



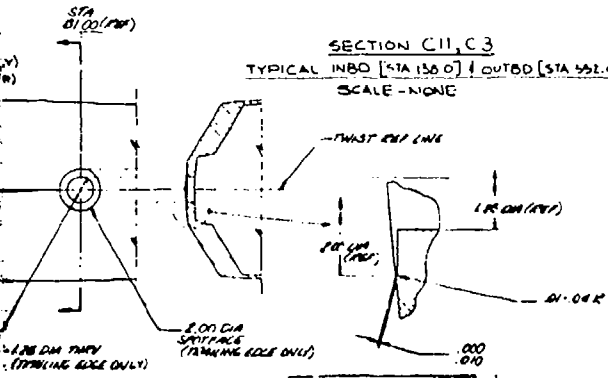
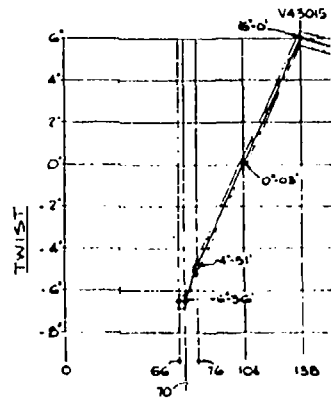
NOTE:
TWIST OMITTED FOR CLARITY

- 1 BLADE ASSEMBLY, AFT (SHOWN)
- 2 BLADE ASSEMBLY, FWD (OPP-1)
- 3 BLADE ASSEMBLY (SAME AS -1 EXCEPT
- 4 BLADE ASSEMBLY (SAME AS -2 EXCEPT



SECTION C11, C3
TYPICAL INBD [STA 150.0] / OUTBD [STA 352.0]
SCALE - NONE

SECTION D10 (ROTATED 90°)
TYPICAL UPPER & LOWER SURFACE
ALONG COMPLETE LENGTH OF BLADE
SCALE - 4/1



301-11171 81

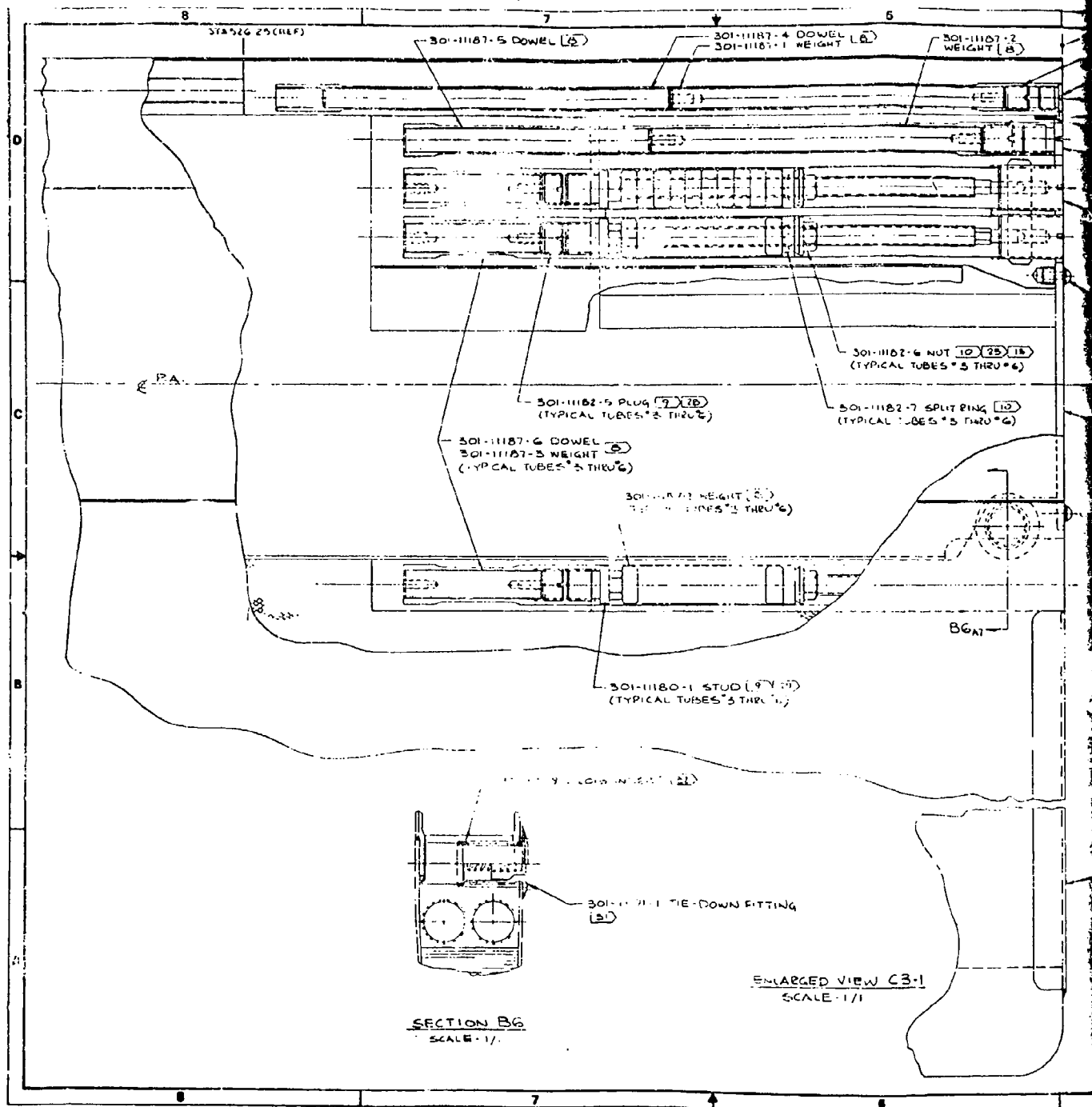
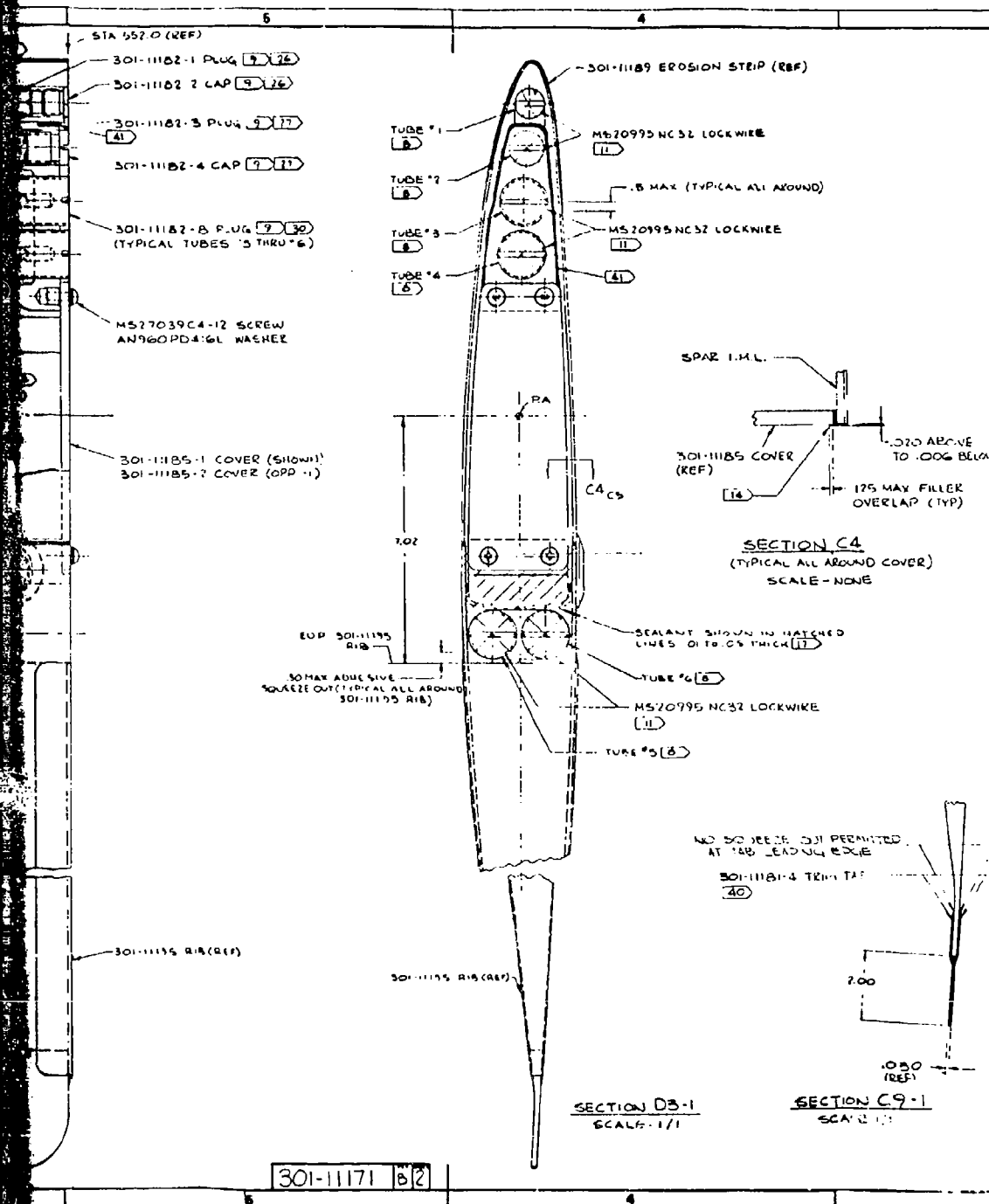


Figure 28. Continued



- NOTE
- (33) INSTALLATION OF OUTBOARD BULKHEAD P/N 301-11203:
- CLEAN SPAR I.D. (STA 546 THRU STA 552) AND ALL AREA'S WHICH WILL HAVE 1" MIN. 5-44 SEALANT APPLIED PER D301-10154-1.
 - PRIME THESE AREAS WITH 80-100S POLYURETHANE SEALANT (P/N 301-11181). APPLY A MINIMUM COAT OF PRIMER - NO LAPS OR THIN AREAS PERMITTED.
 - APPLY 80-100S SEALANT ALONG SPAR AND FITTINGS (END 8 AFT) JOINTS AS SHOWN. NO VOIDS PERMITTED AT FAYING SURFACES. APPLY AND CURE PER D301-10154-1.
 - PREFABR BULKHEAD PER D301-10154-1.
 - LOCATE BULKHEAD IN SPAR AS SHOWN.
 - APPLY 80-100S SEALANT, FILLING CAVITY AS SHOWN. NO VOIDS PERMITTED AT FAYING SURFACES OF SPAR AND SEALANT. APPLY AND CURE PER D301-10154-1.
- (34) INSTALLATION OF 301-11204 COVER FITTING (SLEEVES A PREPARE SPAR SURFACES PER D301-10154-1 REQUIREMENTS OF D301-10154-1):
- REMOVE COVER FITTING FROM SPAR. FITTING MUST BE KEPT IN SPAR AT ALL TIMES.
 - COAT FAYING SURFACES OF SPAR AND FITTING WITH 80-100S POLYURETHANE SEALANT AS SHOWN. USE SEALANT PER D301-10154-1.
 - PREFABR 301-11204-1 SLEEVES FOR 80-100S SEALANT PER D301-10154-1. PREPARE SPAR SURFACES TO BE SEALANT APPLIED PER D301-10154-1.
 - INSTALL SLEEVES PER D301-10154-1. FULL LENGTH INTERFERE IS TO BE USED AS A LOCATING BAND SLEEVES PER (27)
 - SEAL SLEEVES PER (33)
 - INSTALL WASHERS 301-11190-1 INTO WELT DMS 5-44 SEAL AROUND OUTER DIA OF WASHERS PER DETAIL C18.
- (35) INSTALLATION OF INDICATOR ASSY P/N 11482100 AND EVACUATION VALVE ASSY P/N 301-11190:
- CLEAN AREA'S OF MOUNT, INDICATOR, AND VALVE WHERE D-RINGS WILL SEAL PER D301-10154-1. COAT FAYING SURFACES OF MOUNT, INDICATOR AND VALVE WITH DMS 5-44 (DO NOT CURE).
 - INSTALL INDICATOR AND VALVE WITH D-RINGS IN PLACE, TO THE MOUNT FITTING.
 - TORQUE EVACUATION VALVE TO 100-140 IN. LB.
 - TORQUE INDICATOR TO 100-140 IN. LB.
 - CHECK TORQUES 15 MINUTES AFTER INITIAL INST. 2.
 - VERIFY INDICATOR VALUE PER D301-10154-1.
 - APPLY DMS 5-44 SEALANT TO FORM A FILLET AROUND INDICATOR AND VALVE AT MOUNT FITTING JUNCTURE AS SHOWN.
 - CURE DMS 5-44 PER D301-10154-1.
- (36) WHEN INSTALLING THE INDICATOR ASSY P/N 11482100 USE THE FOLLOWING PRECAUTIONS:
- DO NOT PERMIT SOLVENTS TO CONTACT LEAKAN SURFACE.
 - WHEN TORQUING INDICATOR DO NOT AFFIX WRENCH TO RING AT BASE OF LEAKAN COVER. GET ATTACHING POINTS AT BASE OF INDICATOR.
- (37) LEAK TEST OF DETECTION SYSTEM:
- PERFORM A FINAL SYSTEM LEAK TEST PER D301-10154-1.
 - SYSTEM LEAK RATE CRITERIA IS 7.5 X 10⁻⁵ ATMG'S CC/SEC OF HELIUM.
 - EVACUATE GEAR TO 50 TO 5.5 PSIA.
 - TORQUE VALVE JAM NUT TO 20 IN. LB AFTER EVACUATION AND WHILE PUMP IS ON.
 - INSTALL VALVE CAP AND TORQUE TO 5-10 IN. LB.
 - INSTALL LOCKWIRE PER D301-10154-1 DOUBLE TWIST METHOD.
- (38) PARKER SEAL CO. IS V. OF PARKER HANNIFIN CORP LEXINGTON KY
- (39) PRIOR TO INSTALLATION OF WASHERS SEAL FAYING SURFACES OF SLEEVE & SPAR AROUND COMPLETE CIRCUMFERENCE USING DMS 5-44 PER D301-10154-1.
- (40) BOND TRIM TAB P/N 301-11181 TO BLADE PER D8-0274 TYPE II ADHESIVE BONDING SYSTEM USING SCENT CURE.
- (41) FILL GAPS BETWEEN FITTING AND SPAR WITH SEALANT PER D301-10154-1.

301-11171 82

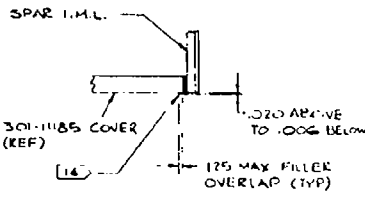
(NOTES CONTINUED ON SHEET)

109 EROSION STRIP (REF)

995 NC32 LOCKWIRE

B MAX (TYPICAL ALL AROUND)

1095 NC32 LOCKWIRE



SECTION C4
(TYPICAL ALL AROUND COVER)
SCALE - NONE

SEALANT SHOWN IN HATCHED LINES 0.1 TO .05 THICK (17)

TUBE #6 (8)

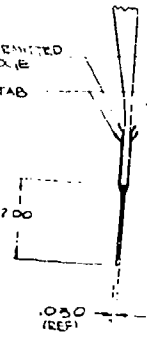
MS20995 NC32 LOCKWIRE

(11)

#6 (A)

NO SCREWS BUT PERMITTED AT TAB LEADING EDGE

301-1184 TRIM TAB (20)



SECTION C9-1
SCALE 1/1

D3-1
-1/1

(33) INSTALLATION OF OUTBOARD BULKHEAD P/N 301-11203

- A. CLEAN SPAR ID (STA 546 THRU STA 552) AND ALL AREAS WHICH WILL HAVE P/N 301-11203 SEALANT APPLIED PER D301-10154-1.
- B. FILL THE CAVITY WITH AN ANTI-SEIZE COMPOUND PER D301-10154-1. NO VOID PERMITTED.
- C. APPLY P/N 544 SEALANT ALONG SPAR AND FITTINGS. END FAYING JOINTS AS SHOWN. NO VOIDS PERMITTED AT FAYING SURFACES. APPLY AND CURE PER D301-10154-1.
- D. PREPARE BULKHEAD PER D301-10154-1.
- E. LOCATE BULKHEAD IN SPAR AS SHOWN.
- F. APPLY ANTI-SEIZANT FILLING CAVITY AS SHOWN. NO VOIDS PERMITTED AT FAYING SURFACES OF SPAR AND SEALANT. APPLY AND CURE PER D301-10154-1.

(34) INSTALLATION OF 301-1184 COVER FITTING (SEERS)

- A. PREPARE COVER FITTING PER D301-10154-1.
- B. APPLY ANTI-SEIZANT FILLING CAVITY AS SHOWN. NO VOIDS PERMITTED AT FAYING SURFACES OF SPAR AND SEALANT. APPLY AND CURE PER D301-10154-1.
- C. COAT FAYING SURFACES OF SPAR AND FITTING WITH ANTI-SEIZANT PER D301-10154-1.
- D. INSTALL COVER FITTING IN PLACE. TORQUE TO 100-150 IN LBS.
- E. APPLY ANTI-SEIZANT FILLING CAVITY AS SHOWN. NO VOIDS PERMITTED AT FAYING SURFACES OF SPAR AND SEALANT. APPLY AND CURE PER D301-10154-1.
- F. INSTALL SLEEVE PER D301-1189. USE LEAD WIRE TO LOCATE SLEEVE IN PLACE.
- G. SEAL SLEEVE PER (17).
- H. INSTALL WIRE PER D301-1189. USE LEAD WIRE TO LOCATE WIRE IN PLACE.

(35) INSTALLATION OF INDICATOR BODY P/N 1185 DO AND EVACUATION VALVE ASSEMBLY P/N 301-1189

- A. CLEAN AREAS OF MOUNT, INDICATOR, AND VALVE. WIPER OFF SURFACES. SEAL PER D301-10154-1. COAT FAYING SURFACES OF MOUNT, INDICATOR, AND VALVE WITH P/N 544 (DO NOT USE).
- B. INSTALL INDICATOR AND VALVE IN PLACE. TORQUE TO THE MOUNT FITTING.
- C. TORQUE EVACUATION VALVE TO 100-150 IN LBS.
- D. TORQUE INDICATOR TO 100-150 IN LBS.
- E. CHECK TORQUES. RECHECK AFTER INITIAL TEST.
- F. APPLY ANTI-SEIZANT FILLING CAVITY AS SHOWN. NO VOIDS PERMITTED AT FAYING SURFACES OF SPAR AND SEALANT. APPLY AND CURE PER D301-10154-1.
- G. APPLY P/N 544 SEALANT TO FORM A FILLET AROUND NO. 2 AND VALVE AT MOUNT FITTING. FAYING AS SHOWN.
- H. CURE P/N 544 PER D301-10154-1.

(36) WHEN INSTALLING THE INDICATOR BODY VALVE USE THE FOLLOWING PRECAUTIONS

- A. DO NOT PERMIT SOLVENTS TO CONTACT LEXAN SURFACE.
- B. WHEN TORQUING INDICATOR DO NOT APPLY FORCE TO DOG AT BASE OF LEXAN TUBES. USE ATTACHING POINTS AT BASE OF INDICATOR.

(37) LEAK TEST OF DETECTION SYSTEM

- A. FILL UP A FINAL SYSTEM LEAK TEST PER D301-10154-1.
- B. SYSTEM LEAK RATE CRITERIA IS 1.0 INCH AT 100 PSI FOR 15 MINUTES.
- C. EVACUATE FUEL TO 100 INCHES Hg.
- D. TORQUE VALVE AND MOUNT TO 100 INCHES Hg.
- E. INSTALL LEAK CAP AND TORQUE TO 50 INCHES Hg.
- F. INSTALL LEAK PER PER FAC 501 DOUBLE TWIST METHOD.

(38) PARKER SEAL CO. O-RING PARKER HANNIFIN CORP. LEXINGTON KY

(39) PRIOR TO INSTALLATION OF WARNERS SEAL FAYING SURFACES TO BE FILLED & SEAL AROUND COMPLETE CIRCUMFERENCE USING P/N 544 PER D301-10154-1.

(40) HOLD TRIM TAB IN POSITION IN PLACE PER D301-10154-1 TYPE II ADHESIVE BONDING SYSTEM USING FIBER CLOTH (14).

(41) FILL AND FAIR CAVITY BETWEEN FITTING AND SPAR AS SHOWN USING DOW 92-018 SEALANT PER D301-10154-1.

NOTES - CONTINUED FROM SHEET 1

(10) APPLY MIL-L-7859B 2000 FIRM LUB. TO TAPERED SURFACE PER BAC 5811 METHOD 2.

(11) INSTALL PER BAC 5018.

(12) INSTALL PER BAC 5455.

(13) ANTI-SEIZE COMPOUND TT-A-58010 BE USED ON THREADS WHEN INSTALLING NUTS P/N 301-1182. AFTER INSTALLATION OF NUTS REMOVE ALL EXCESS COMPOUND.

(14) SEAL JOINT BETWEEN COVER P/N 301-1185 AND SPAR I.M.L. AS SHOWN USING DOW 92-018 SEALANT PER BONDING DOCUMENT D301-10154-1 (SEE SECT. C4-2).

(15) BOND EROSION STRIP P/N 301-1189 TO BLADE USING FC-2719 ADHESIVE PER D301-10154-1 USING 50/50 CLOTH (14). FAIR EDGES ALL AROUND AS SHOWN IN ZONE C4-2.

(16) FILL AND FAIR CAVITY BETWEEN TRAILING EDGE OF EROSION CAP AND LEADING EDGE OF FAIRING SURFACES AS SHOWN USING FC-2719 ADHESIVE PER D301-10154-1. REMOVAL OF EXISTING RESIN OR ADHESIVE IN CAVITY NOT REQUIRED. CLEAN UP TO BE FACED AS SHOWN USING DOW 92-018 SEALANT PER D301-10154-1. THERE SHALL BE NO DISCONTINUITY GREATER THAN .06.

(17) BOND SLEEVE P/N 301-1189 IN PLACE USING FC-2719 ADHESIVE PER D301-10154-1. LEAD WIRE PER D301-1189. USE LEAD WIRE TO LOCATE SLEEVE IN PLACE.

(18) SEAL SLEEVE PER (17).

(19) APPLY POLYURETHANE (POLYETHER BASE) HAVING 2500 PSI AT 60°F TO THE CONTACT SURFACES AT BREAK 2700 PSI MIN. ELONGATION AT BREAK 60% MIN. MAY BE PURCHASED FROM QUANTUM CORP. BARNES INDUSTRIAL PARK WALLINGFORD, CONN. 06472

(20) TORQUE TO 100-150 IN LBS.

(21) TORQUE TO 100-150 IN LBS.

(22) TORQUE TO 100-150 IN LBS.

(23) TORQUE TO 100-150 IN LBS.

(24) TORQUE TO 100-150 IN LBS.

(25) TORQUE TO 100-150 IN LBS.

(26) TORQUE TO 100-150 IN LBS.

(27) TORQUE TO 100-150 IN LBS.

(28) TORQUE TO 100-150 IN LBS.

(29) TORQUE TO 100-150 IN LBS.

(30) TORQUE TO 100-150 IN LBS.

(31) TORQUE TO 100-150 IN LBS.

(32) TORQUE TO 100-150 IN LBS.

(33) TORQUE TO 100-150 IN LBS.

(NOTES CONTINUED ON SHEET 3)

REV	DESCRIPTION	DATE	BY	CHKD
A	DCN A			
B	SEC DCN B			

REV	DESCRIPTION	DATE	BY	CHKD
1	BLADE ASSEMBLY			
2	HLH			
3	ROTOR BLADE			
4	J17272			
5	301-11171			

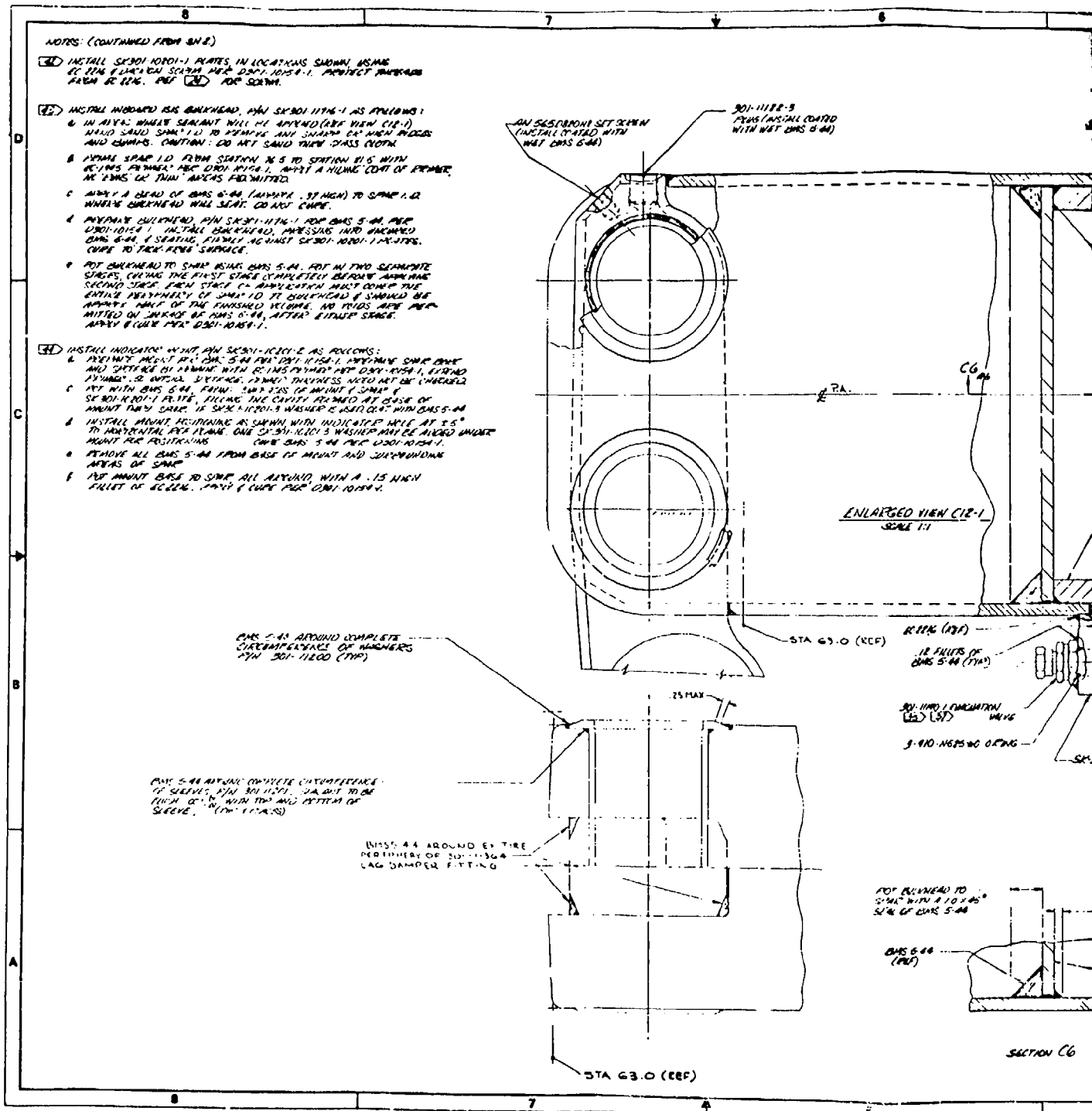
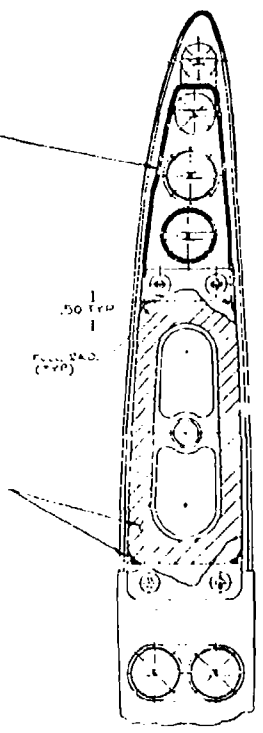
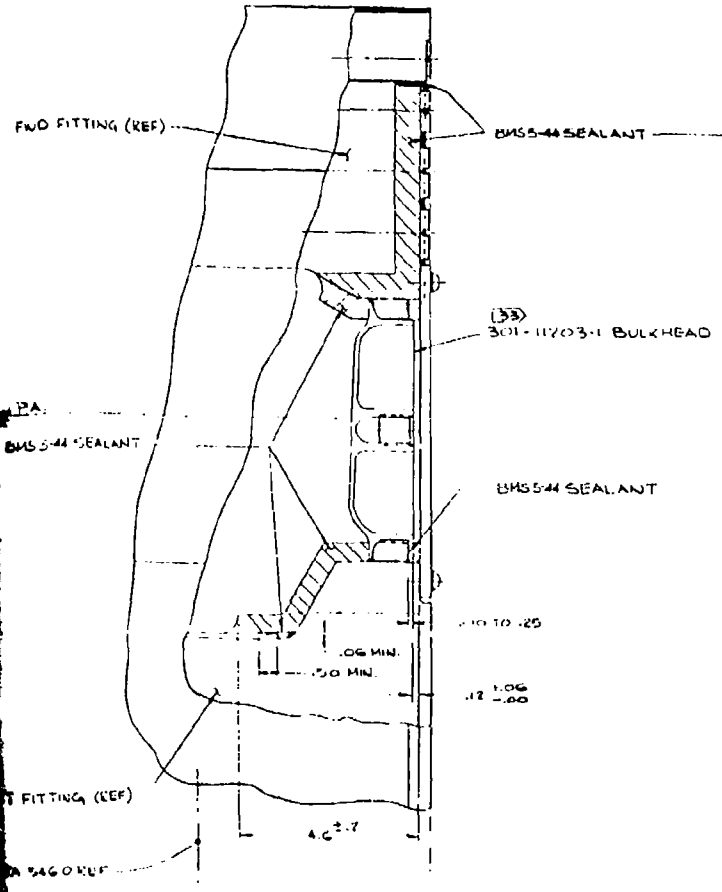


Figure 28. Continued

REV	BY	DATE
A	THIS SHEET ADDED	04/17/77
B	SEE DRAWING	10-18-77



NO	DESCRIPTION	QTY	UNIT
1	WASHER		
2	SCREW		
3	WASHER		
4	SCREW		
5	WASHER		
6	SCREW		
7	WASHER		
8	SCREW		
9	WASHER		
10	SCREW		
11	WASHER		
12	SCREW		
13	WASHER		
14	SCREW		
15	WASHER		
16	SCREW		
17	WASHER		
18	SCREW		
19	WASHER		
20	SCREW		
21	WASHER		
22	SCREW		
23	WASHER		
24	SCREW		
25	WASHER		
26	SCREW		
27	WASHER		
28	SCREW		
29	WASHER		
30	SCREW		
31	WASHER		
32	SCREW		
33	WASHER		
34	SCREW		
35	WASHER		
36	SCREW		
37	WASHER		
38	SCREW		
39	WASHER		
40	SCREW		
41	WASHER		
42	SCREW		
43	WASHER		
44	SCREW		
45	WASHER		
46	SCREW		
47	WASHER		
48	SCREW		
49	WASHER		
50	SCREW		
51	WASHER		
52	SCREW		
53	WASHER		
54	SCREW		
55	WASHER		
56	SCREW		
57	WASHER		
58	SCREW		
59	WASHER		
60	SCREW		
61	WASHER		
62	SCREW		
63	WASHER		
64	SCREW		
65	WASHER		
66	SCREW		
67	WASHER		
68	SCREW		
69	WASHER		
70	SCREW		
71	WASHER		
72	SCREW		
73	WASHER		
74	SCREW		
75	WASHER		
76	SCREW		
77	WASHER		
78	SCREW		
79	WASHER		
80	SCREW		
81	WASHER		
82	SCREW		
83	WASHER		
84	SCREW		
85	WASHER		
86	SCREW		
87	WASHER		
88	SCREW		
89	WASHER		
90	SCREW		
91	WASHER		
92	SCREW		
93	WASHER		
94	SCREW		
95	WASHER		
96	SCREW		
97	WASHER		
98	SCREW		
99	WASHER		
100	SCREW		

REV	BY	DATE
A	THIS SHEET ADDED	04/17/77
B	SEE DRAWING	10-18-77

BLADE ASSEMBLY
 HLH
 ROTOR BLADE
 301-11171

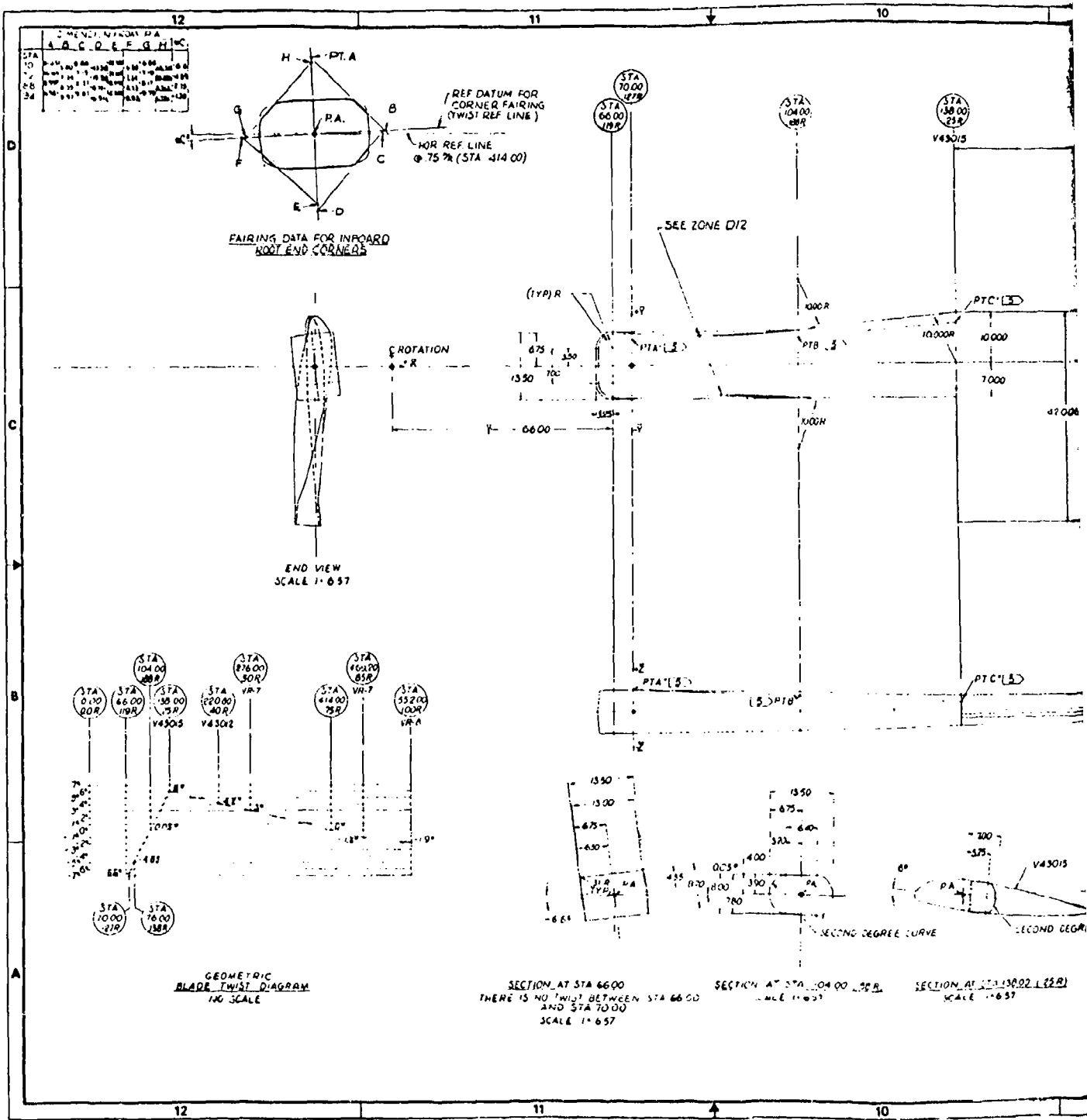
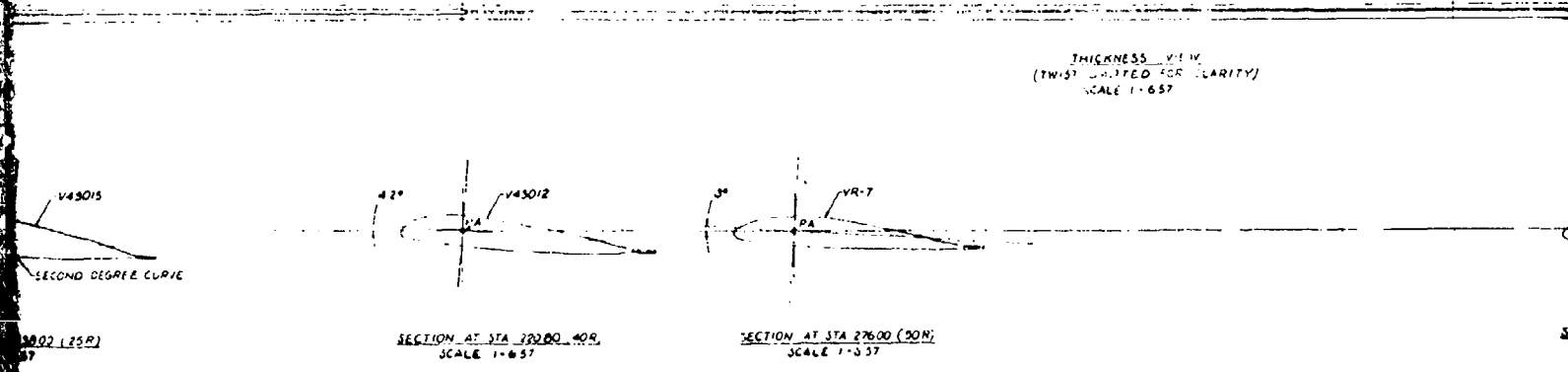
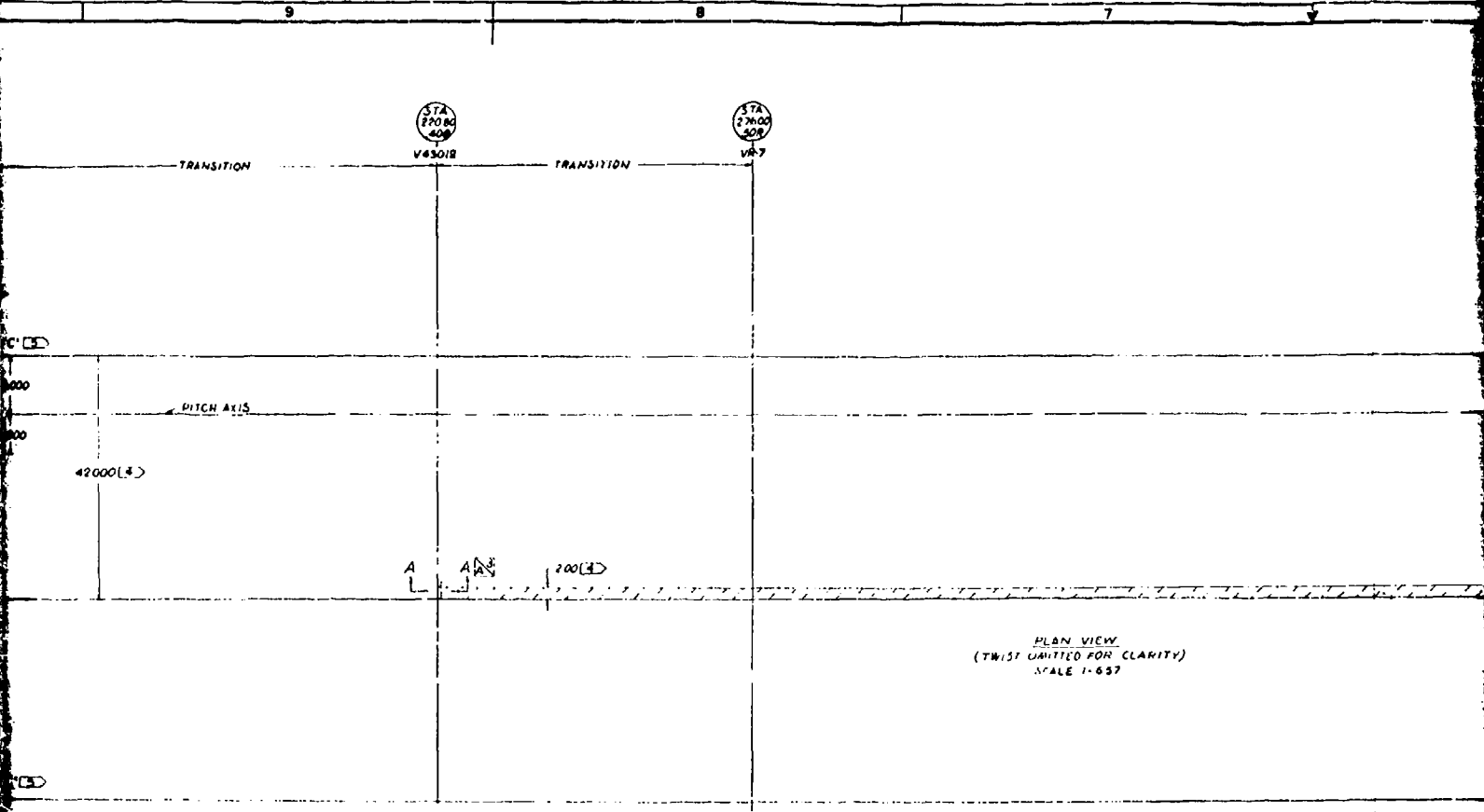


Figure 29. Geometry Two-Pin, Fittingless HLH Rotor Blade



301-11172 41

P-69

2

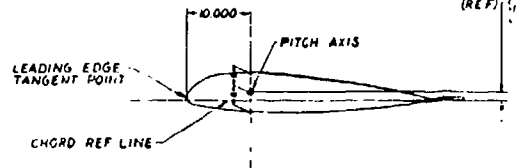
STA
41400
73R

STA
44920
85R
VR-7

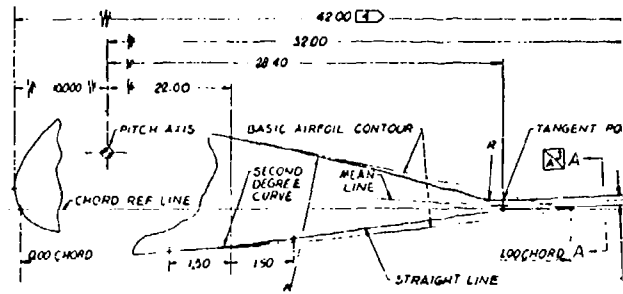
STA
55200
100R
VR-8

TRANSITION

3376 FOR VERN
(REF) 1.3250 - V43
1.2192 - VR-
.4875 - VR-



PITCH AXIS LOCATION IN AIRFOILS [1]
SCALE 1:6.57



CUSP GEOMETRY [2]
SCALE 1:1

STA
2208
40R



SECTION AT STA 4140 [73R]
SCALE 1:6.57

SECTION AT STA 4492 [85R]
SCALE 1:6.57

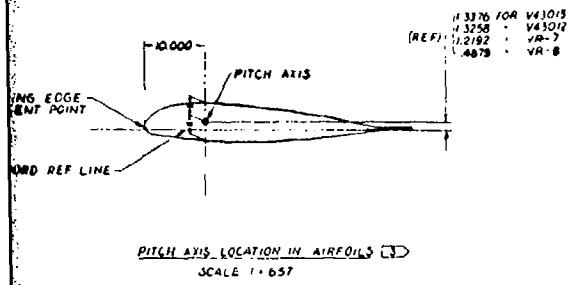
SECTION AT STA 5520 [100R]
SCALE 1:6.57

SECTION A-A
SCALE 1:1

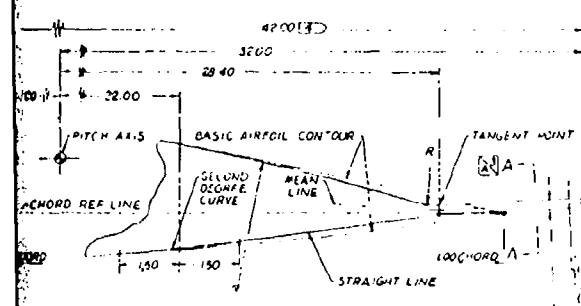
NOTES:

1. THE INFORMATION ON THIS DRAWING IS IN ACCORDANCE WITH DATA SHOWN ON DESIGN DECISION NO BDD 301-1 & DOCUMENT D301-10136-1.
2. AIRFOIL CONTOURS PER ORDINATES SHOWN ON ENCLOSURE II OF BDD 301-1 BASED ON A 4000" CHORD LENGTH.
3. ALL AIRFOILS ARE ALIGNED SO THAT THEIR LEADING EDGE TANGENT POINT TOUCHES A PERPENDICULAR LINE ON THE CHORD REFERENCE LINE ON A PARALLEL LINE 1000" TO THE LEADING EDGE LINE MIDWAY BETWEEN THE AIRFOIL O.M.'S ESTABLISH THE PITCH AXIS POINT, THESE POINTS MUST BE ALIGNED KEEPING ALL CHORD REFERENCE LINES PARALLEL. THEN AIRFOILS ARE TO BE TWISTED PER TWIST DIAGRAM SHOWN IN ZONE A-2. THE TRAILING EDGES OF THE AIRFOILS ARE MODIFIED AS SHOWN IN THE CUSP GEOMETRY IN ZONE B-3.
4. THE 4200" DIMENSION INCLUDES A 200" CUSP EXTENSION FROM STA 22000+40R TO STA 55200(100R) SOME OR ALL OF THE 200" EXTENSION WILL BE TRIMMED BACK.
5. DEVELOPMENT OF BLADE ROOT END TRANSITION CONTOURS.
 - A. ESTABLISH SECTION POINTS PTA, PTB AND PTC SUCH THAT PROJECTED POINTS PTA', PTB' AND PTC' IN PLANE Y-Y ARE LOCATED AT A CONSTANT PERCENT OF CHORD.
 - B. PROJECT POINTS PTA, PTB AND PTC TO Z-Z PLANE LOCATING POINTS PTA'', PTB'' AND PTC''.
 - C. GENERATE A CUBIC EXPRESSION DEFINING A LINE INTERSECTING POINTS PTA'', PTB'' AND PTC''. THE SLOPE OF THE CUBIC AT POINTS PTA'' AND PTB'' IS SET TO ZERO FOR A STATION BETWEEN STA 7000 AND 10400, AND AT POINTS PTA'' AND PTC'' FOR A STATION BETWEEN STA 10400 AND 13800.
 - D. A POINT ON ANY INTERMEDIATE STATION SECTION IS LOCATED BY THE COORDINATE DIMENSIONS OF Z-Z COMPUTED VALUE FROM THE CUBIC EQUATION OF STEP C, AND Y-Y CONSTANT PERCENT OF CHORD FOR THE SELECTED STATION.
6. THE TECHNIQUE USED TO TRANSITION FROM AIRFOIL TO AIRFOIL OUTBOARD OF STA 55200 IS AS FOLLOWS. AT ANY GIVEN PERCENT OF CHORD AT A GIVEN STATION, AN ORDINATE VALUE CAN BE EXTRACTED FROM THE CONTAINING AIRFOILS AT THE SAME PERCENT OF CHORD USING THESE COORDINATE VALUES AND THE STATION VALUES AT WHICH THE CONTAINING CONTINUOUS AIRFOILS EXIST. A THICKNESS (NEAR VIEW) COORDINATE SYSTEM IS SET UP (STATION VS ORDINATE) IN THIS VIEW, TANGENT CIRCLES OF EQUAL RADII ARE USED TO CONNECT THE TWO POINTS. THE ORDINATE VALUE AT THE GIVEN STATION AND THE GIVEN PERCENT OF CHORD WOULD BE EXTRACTED FROM THE APPLICABLE CIRCULAR ARC SEE ZONE A-2 FOR ILLUSTRATION.

REVISION	NO.	DATE	BY	CHKD
1	A	SEE DCN A		



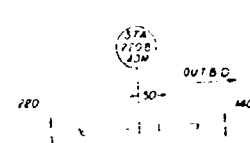
PITCH AXIS LOCATION IN AIRFOILS
SCALE 1:657



CUSP GEOMETRY
SCALE 1:1

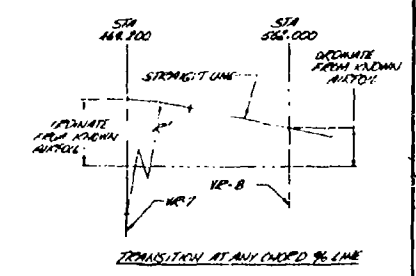
- 1070 FROM 40 TO 100R (STA 2213 TO 5520)
- 110 FROM 25 TO 40R (STA 1380 TO 2208)
- 140 FROM 40 TO 100R (STA 2213 TO 5520)
- 220 FROM 25 TO 40R (STA 1380 TO 2208)

4.5° FROM 25%R TO 50%R
G.C. FROM 52%R TO 100%R
LINEAR TRANSITION FROM 4.5° TO 60° BETWEEN 50%R & 52%R



SECTION A-A
SCALE 1:1

TRANSITION BETWEEN KNOWN AIRFOILS AT ANY CHORD PERCENT LINE IS
SCALE NONE



REVISION	NO.	DATE	BY	CHKD
1	A	SEE DCN A		
GEOMETRY				
TWO PIN, FITTINGLESS				
HLW ROTOR BLADE				
PART NO.		77272 301-11172		
REV.		1		

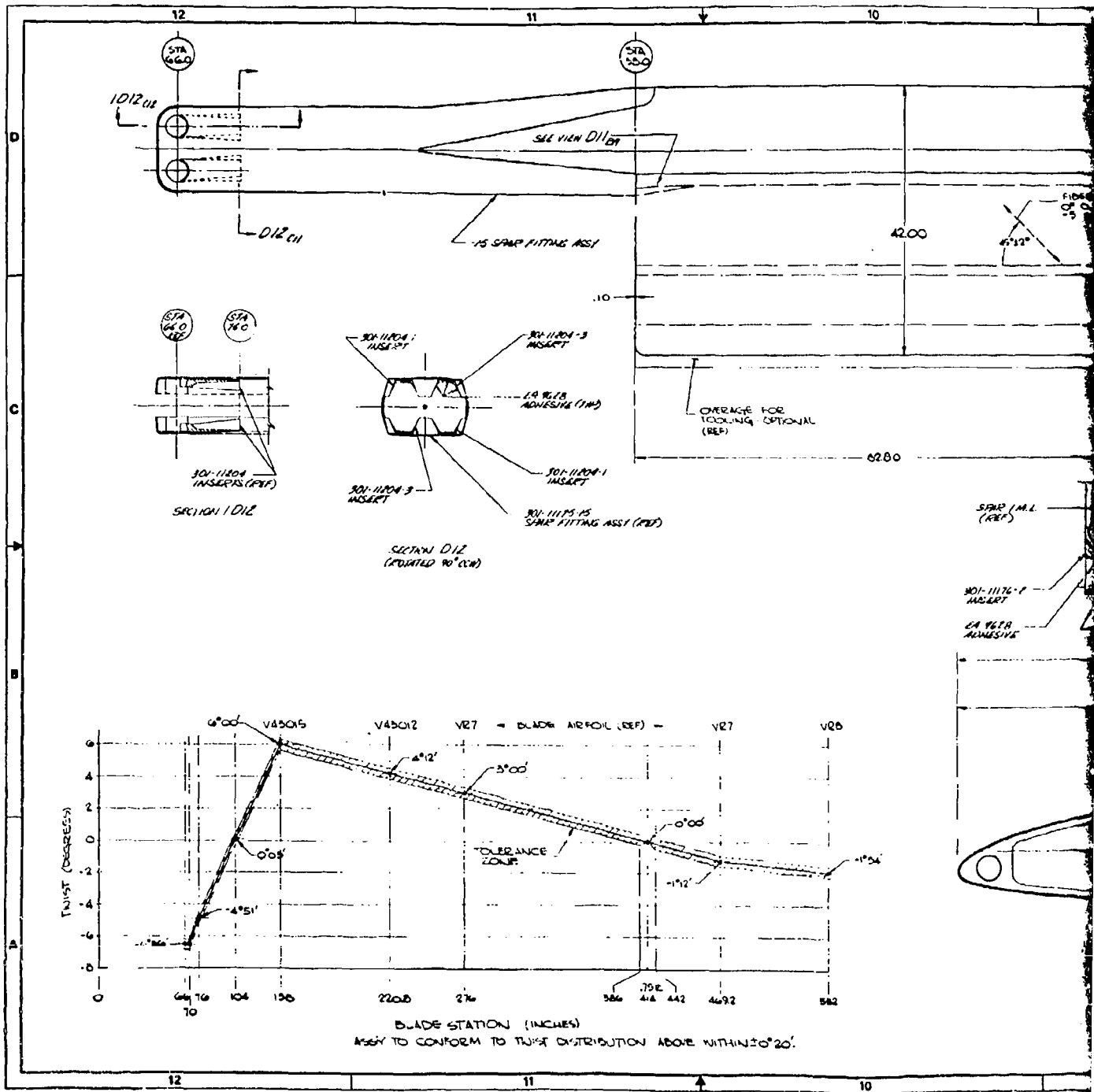
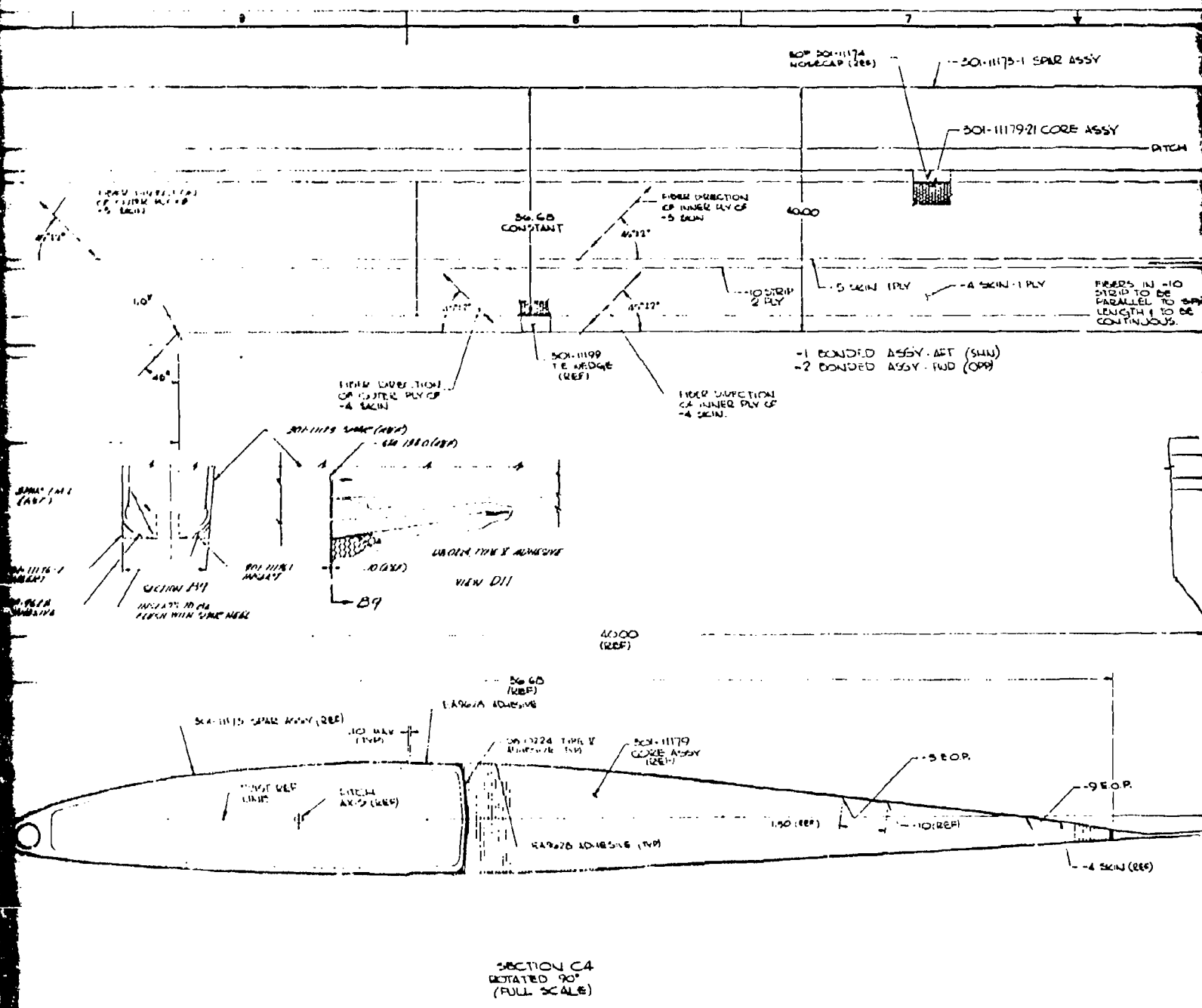
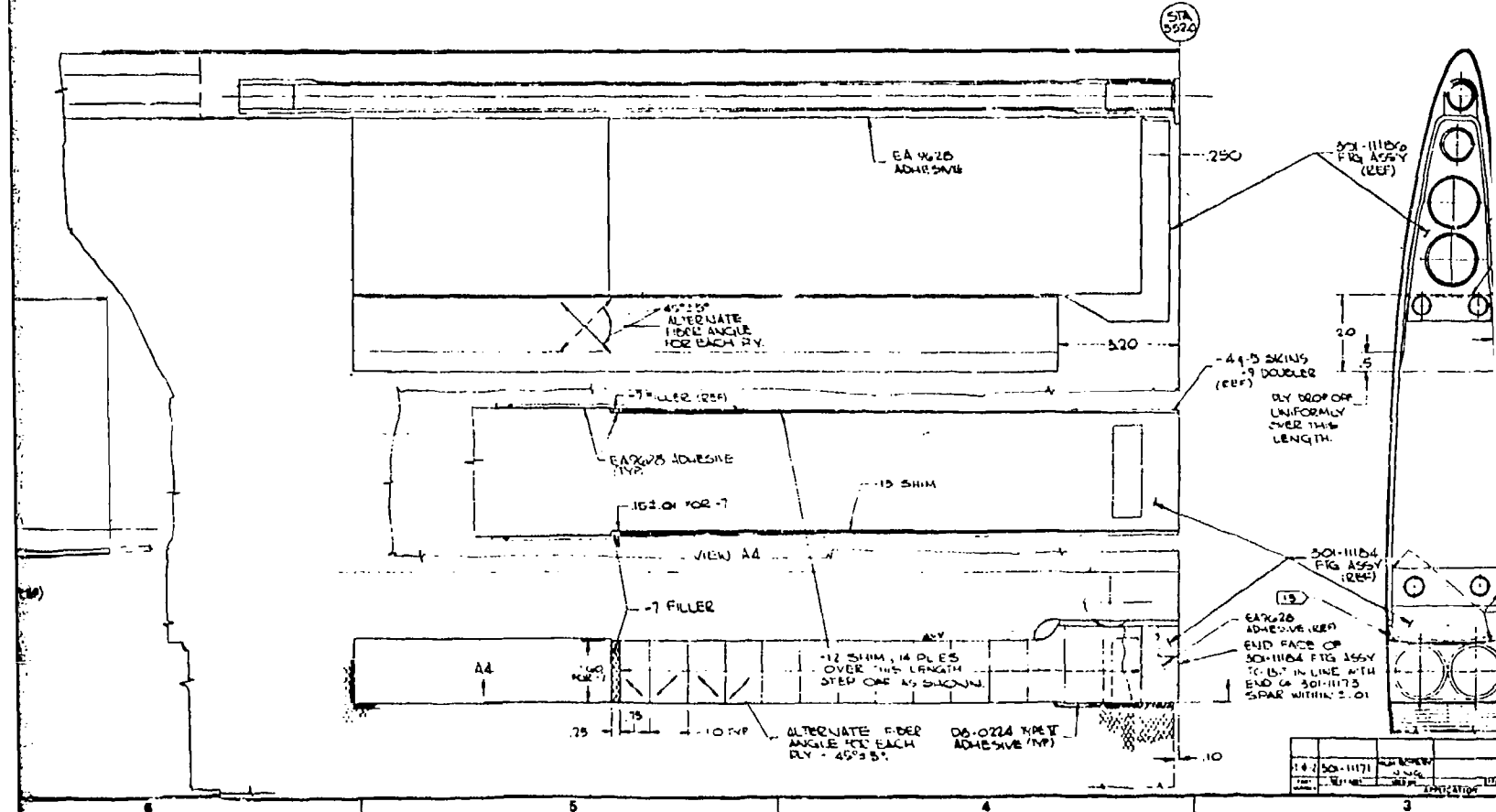
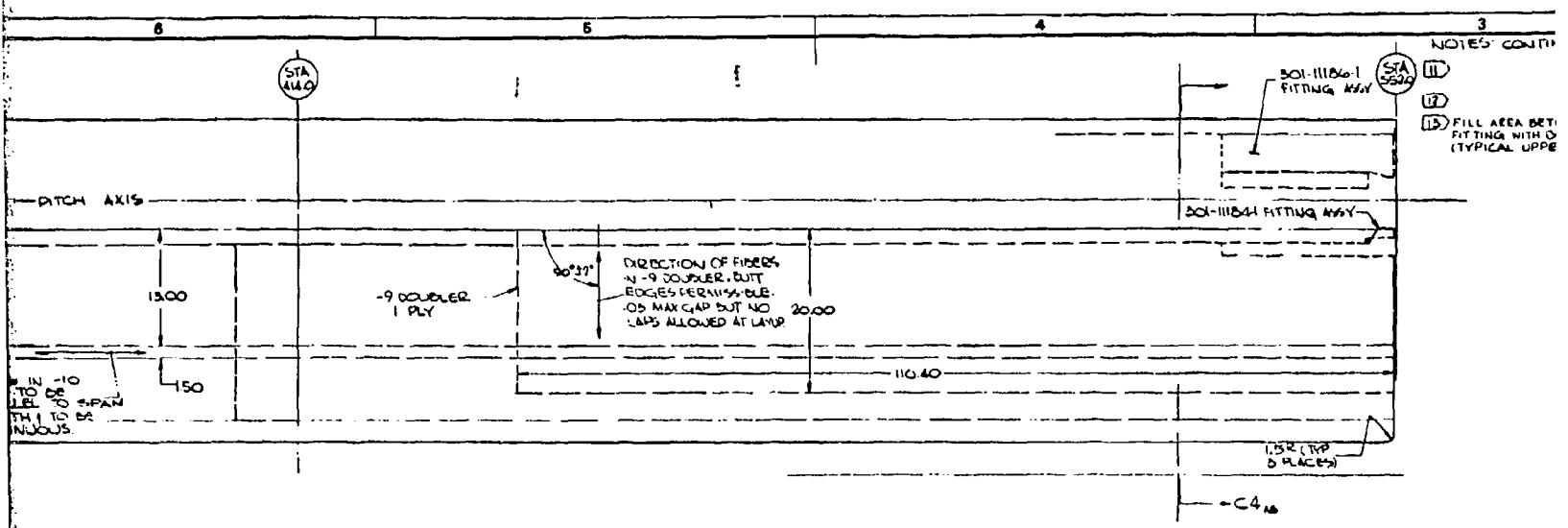


Figure 30. Bonded Assembly - Rotary Wing - HLH



30-11175 INT



3

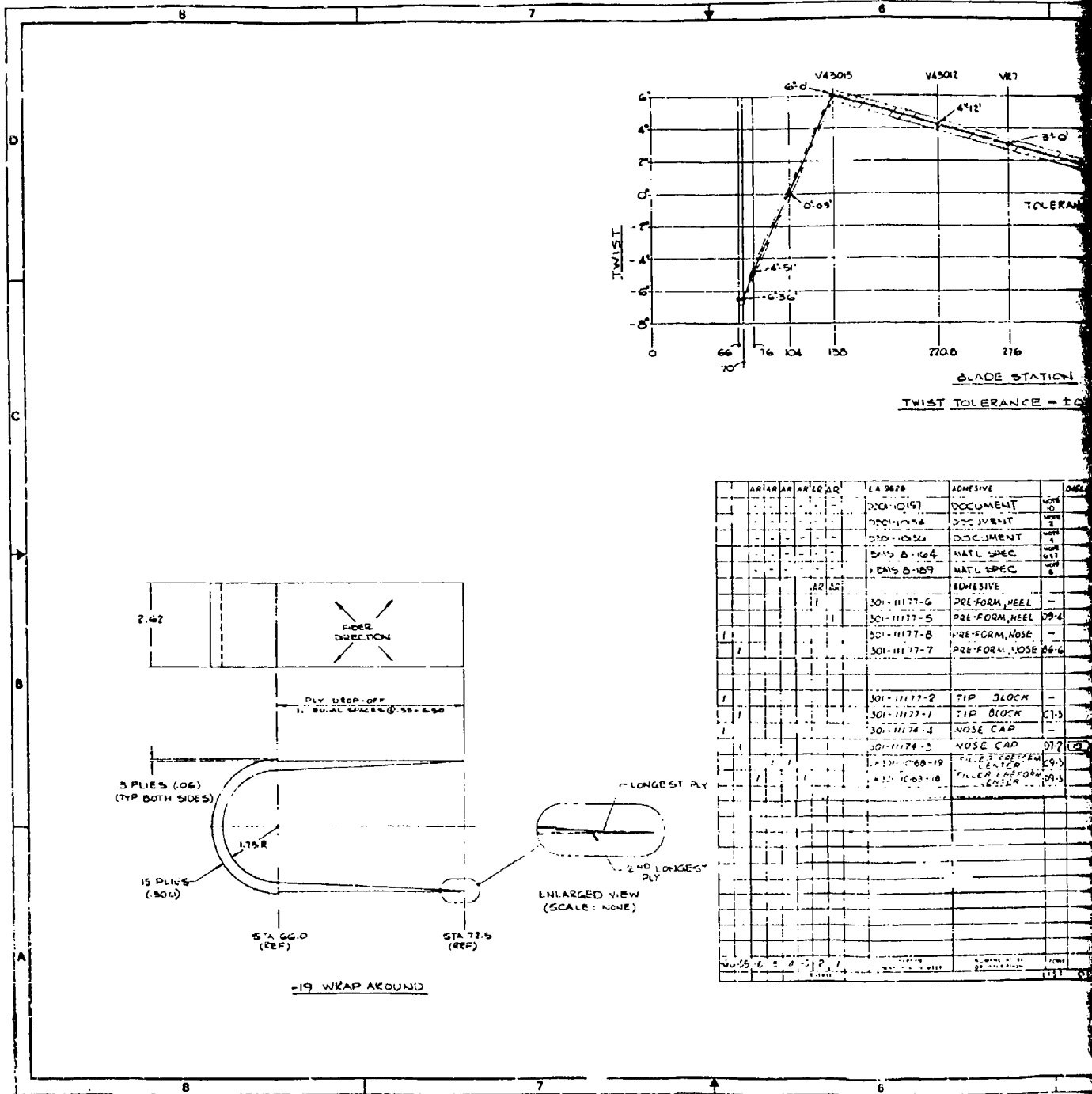
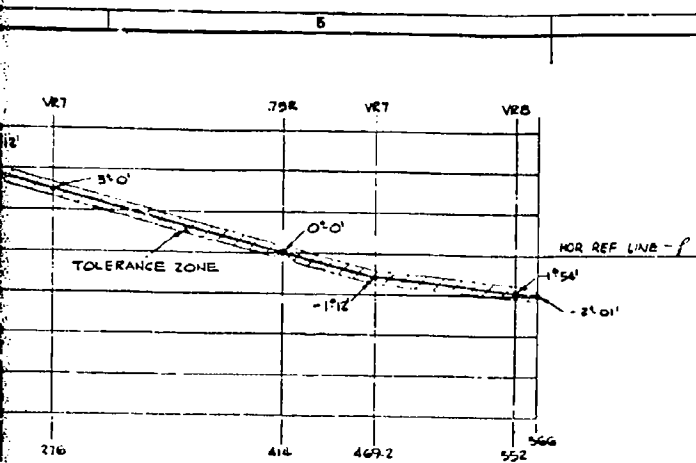


Figure 31. Spar Assembly for Two Pin, Fittingless HLH Rotor Blade



- 16) APPLY ADHESIVE PER D 301-10154-1
- 17) CAUTION TO EXERCISED IN HANDLING & THRU-OUT FAB CYCLE OF THESE SUB-ASSEMBLYS TO AVOID MARKING, SCRATCHING, TWISTING, OR ABUSE WHICH COULD BE DETRIMENTAL TO THE HIGH QUALITY OF THIS STRUCTURE.
- 18) TOOLING TO FORM CAVITY, MUST MATCH TOOLING FOR 301-11204 INSERT, STATIONS 66.0 THRU 76.50
- 19) 301-11174-1 NOSE CAP IS AN ACCEPTABLE SUBSTITUTE FOR 301-11174-3 NOSE CAP ON TOOL PROVER BLADE ONLY
- 20) BALANCE RODS OF NOS 301-11178-5 & -6 TO BE SELECTED PER WEIGHT & BALANCE DOC D 301-10155-1.
- 21) PRIOR TO INSTALLING 301-11178 BALANCE RODS, WRAP WITH ONE LAYER OF ADHESIVE PER DOC D 301-10154-1.
- 22) MAT'L PER BMS R-164 CLASS A, TYPE I (2.62" WIDE) WITH LEAD TRACER PER D 301-10154-1.
- 23) ORIENTATION OF 25 & 12 PER SH 5.
- 24) THIS IS A CLASS B CRITICAL PART AND PROVIDES ALL TESTS & REVISIONS SPECIFIED IN MS N. 00

GRADE STATION
TOLERANCE = ±0.20'

QTY	DESCRIPTION	UNIT	REMARKS
	ADHESIVE PER D 301-10154-1		
	FORM, NOSE		
	FORM, HEEL		
	FORM, NOSE		
	FORM, NOSE		
	BLOCK		
	BLOCK		
	CAP		
	CAP		
	ENTER		
	ENTER		
	ENTER		

QTY	DESCRIPTION	UNIT	REMARKS
66	GLAND	AS 6	
65	FILLER	AS 6	
64	MID INNER SKIN	AS 6	
63	MID LOWER SKIN	AS 6	
62	MID UPPER SKIN	AS 6	
61	MID LOWER SKIN	AS 6	
60	MID UPPER SKIN	AS 6	
59	NOSE CAP ASST	AS 6	OPP TO -59
58	NOSE CAP ASST	AS 6	OPP TO -57
57	NOSE CAP ASST	AS 6	OPP TO -55
56	WEDGE LOCKER	AS 6	OPP TO -53
55	WEDGE LOCKER	AS 6	OPP TO -51
54	WEDGE LOCKER	AS 6	OPP TO -49
53	WEDGE LOCKER	AS 6	
52	WEDGE LOCKER	AS 6	
51	WEDGE LOCKER	AS 6	
50	WEDGE LOCKER	AS 6	
49	WEDGE LOCKER	AS 6	
48	WEDGE LOCKER	AS 6	
47	WEDGE LOCKER	AS 6	
46	WEDGE LOCKER	AS 6	
45	WEDGE LOCKER	AS 6	
44	WEDGE LOCKER	AS 6	
43	WEDGE LOCKER	AS 6	
42	WEDGE LOCKER	AS 6	
41	WEDGE LOCKER	AS 6	
40	WEDGE LOCKER	AS 6	
39	WEDGE LOCKER	AS 6	
38	WEDGE LOCKER	AS 6	
37	WEDGE LOCKER	AS 6	
36	WEDGE LOCKER	AS 6	
35	WEDGE LOCKER	AS 6	
34	WEDGE LOCKER	AS 6	
33	WEDGE LOCKER	AS 6	
32	WEDGE LOCKER	AS 6	
31	WEDGE LOCKER	AS 6	
30	WEDGE LOCKER	AS 6	
29	WEDGE LOCKER	AS 6	
28	WEDGE LOCKER	AS 6	
27	WEDGE LOCKER	AS 6	
26	WEDGE LOCKER	AS 6	
25	WEDGE LOCKER	AS 6	
24	WEDGE LOCKER	AS 6	
23	WEDGE LOCKER	AS 6	
22	WEDGE LOCKER	AS 6	
21	WEDGE LOCKER	AS 6	
20	WEDGE LOCKER	AS 6	
19	WEDGE LOCKER	AS 6	
18	WEDGE LOCKER	AS 6	
17	WEDGE LOCKER	AS 6	
16	WEDGE LOCKER	AS 6	
15	WEDGE LOCKER	AS 6	
14	WEDGE LOCKER	AS 6	
13	WEDGE LOCKER	AS 6	
12	WEDGE LOCKER	AS 6	
11	WEDGE LOCKER	AS 6	
10	WEDGE LOCKER	AS 6	
9	WEDGE LOCKER	AS 6	
8	WEDGE LOCKER	AS 6	
7	WEDGE LOCKER	AS 6	
6	WEDGE LOCKER	AS 6	
5	WEDGE LOCKER	AS 6	
4	WEDGE LOCKER	AS 6	
3	WEDGE LOCKER	AS 6	
2	WEDGE LOCKER	AS 6	
1	WEDGE LOCKER	AS 6	

301-11173 2/1

301-11173	HLN ATC		
301-11173	HLN ATC		
301-11173	HLN ATC		

2

- NOTE
1. FABRICATE PER DOCUMENT D301-10154-1
 2. FABRICATE PER DOCUMENT D301-10154-1
 3. BLADE GEOMETRY PER DRAWING 101-11172
 4. SPAR CONTOURS PER DOCUMENT D301-10154-1
 5. MAT'L PER BMS 8-164 CL A TYPE I (262 WIDE)
 6. MAT'L PER BMS 8-164 CL A TYPE III
 7. MAT'L PER BMS 8-164 CL A TYPE I
 8. MAT'L PER BMS 8-189 TYPE II, CLASS A, EXCEPT THE TRACER FIBER DOES NOT APPLY.
 9. LAY UP 11, 10, 15, 17 SKINS WITH FIBERS AS SHOWN TO PITCH AXIS
 10. INSPECT ASSY PER DOING DOC D301-10157
 11. FINISH OF CONTIGUOUS ASSY TO MATCH BLADE CHIL PER DOC D301-10156 WITHIN 1.005.
 12. FLAP SIDE STITCH MAY BE IN ONE OR BOTH DIRECTIONS AND WIND RATE OF BOND DOES NOT EXCEED 100 INCHES PER FOOT OF SPAR LENGTH.
 13. IF DISCREPANCY DOC 10, 16, 17 MAY END OR JET MEASURED BETWEEN STATION 108 & 152.
 14. MATERIAL REQUIRED ON L.M.L. IN THIS AREA.
 15. MATERIAL REQUIRED ON ENTIRE O.H.L. EXCEPT NOSECAP W/ 301-11174.

REV	DATE	BY	CHKD
1	1/1		
2	1/2		
3	1/3		
4	1/4		
5	1/5		
6	1/6		

REV	DATE	BY	CHKD
A	1/1		
B	1/2		
C	1/3		
D	1/4		

QTY	DESCRIPTION	UNIT	REF
66	GLUE	1/2	(6)
65	FILLER	1/2	(6)
64	FIB D INNER SKIN	AS G	(6)
63	FIB D LOWER SKIN	AS G	(6)
62	FIB D UPPER SKIN	AS G	(6)
61	FIB D INNER SKIN	AS G	(6)
60	FIB D LOWER SKIN	AS G	(6)
59	FIB D UPPER SKIN	AS G	(6)
58	NOSE CAP ASSY	1	(6)
57	WEDGE (UPPER)	1	(6)
56	WEDGE (LOWER)	1	(6)
55	TRACER (HEAT BLANKET)	1	(6)
54	FILLED STRAP (L&E LOWER)	1	(6)
53	FILLED STRAP (L&E UPPER)	1	(6)
52	SPRINKLED	1	(6)
51	SPRINKLED	1	(6)
50	SPRINKLED	1	(6)
49	SPRINKLED	1	(6)
48	SPRINKLED	1	(6)
47	SPRINKLED	1	(6)
46	SPRINKLED	1	(6)
45	SPRINKLED	1	(6)
44	SPRINKLED	1	(6)
43	SPRINKLED	1	(6)
42	SPRINKLED	1	(6)
41	SPRINKLED	1	(6)
40	SPRINKLED	1	(6)
39	SPRINKLED	1	(6)
38	SPRINKLED	1	(6)
37	SPRINKLED	1	(6)
36	SPRINKLED	1	(6)
35	SPRINKLED	1	(6)
34	SPRINKLED	1	(6)
33	SPRINKLED	1	(6)
32	SPRINKLED	1	(6)
31	SPRINKLED	1	(6)
30	SPRINKLED	1	(6)
29	SPRINKLED	1	(6)
28	SPRINKLED	1	(6)
27	SPRINKLED	1	(6)
26	SPRINKLED	1	(6)
25	SPRINKLED	1	(6)
24	SPRINKLED	1	(6)
23	SPRINKLED	1	(6)
22	SPRINKLED	1	(6)
21	SPRINKLED	1	(6)
20	SPRINKLED	1	(6)
19	SPRINKLED	1	(6)
18	SPRINKLED	1	(6)
17	SPRINKLED	1	(6)
16	SPRINKLED	1	(6)
15	SPRINKLED	1	(6)
14	SPRINKLED	1	(6)
13	SPRINKLED	1	(6)
12	SPRINKLED	1	(6)
11	SPRINKLED	1	(6)
10	SPRINKLED	1	(6)
9	SPRINKLED	1	(6)
8	SPRINKLED	1	(6)
7	SPRINKLED	1	(6)
6	SPRINKLED	1	(6)
5	SPRINKLED	1	(6)
4	SPRINKLED	1	(6)
3	SPRINKLED	1	(6)
2	SPRINKLED	1	(6)
1	SPRINKLED	1	(6)

QTY	DESCRIPTION	UNIT	REF
30	SPRINKLED	1	(6)
29	SPRINKLED	1	(6)
28	SPRINKLED	1	(6)
27	SPRINKLED	1	(6)
26	SPRINKLED	1	(6)
25	SPRINKLED	1	(6)
24	SPRINKLED	1	(6)
23	SPRINKLED	1	(6)
22	SPRINKLED	1	(6)
21	SPRINKLED	1	(6)
20	SPRINKLED	1	(6)
19	SPRINKLED	1	(6)
18	SPRINKLED	1	(6)
17	SPRINKLED	1	(6)
16	SPRINKLED	1	(6)
15	SPRINKLED	1	(6)
14	SPRINKLED	1	(6)
13	SPRINKLED	1	(6)
12	SPRINKLED	1	(6)
11	SPRINKLED	1	(6)
10	SPRINKLED	1	(6)
9	SPRINKLED	1	(6)
8	SPRINKLED	1	(6)
7	SPRINKLED	1	(6)
6	SPRINKLED	1	(6)
5	SPRINKLED	1	(6)
4	SPRINKLED	1	(6)
3	SPRINKLED	1	(6)
2	SPRINKLED	1	(6)
1	SPRINKLED	1	(6)

1-2	301-1175	NEW ATC	
-----	----------	---------	--

3	301-1175	NEW ATC	
---	----------	---------	--

301-1175	NEW ATC		
SPAR ASSEMBLY TWO PIN-FITTINGLESS 11LH ROTOR BLADE J-772, 301-11173			

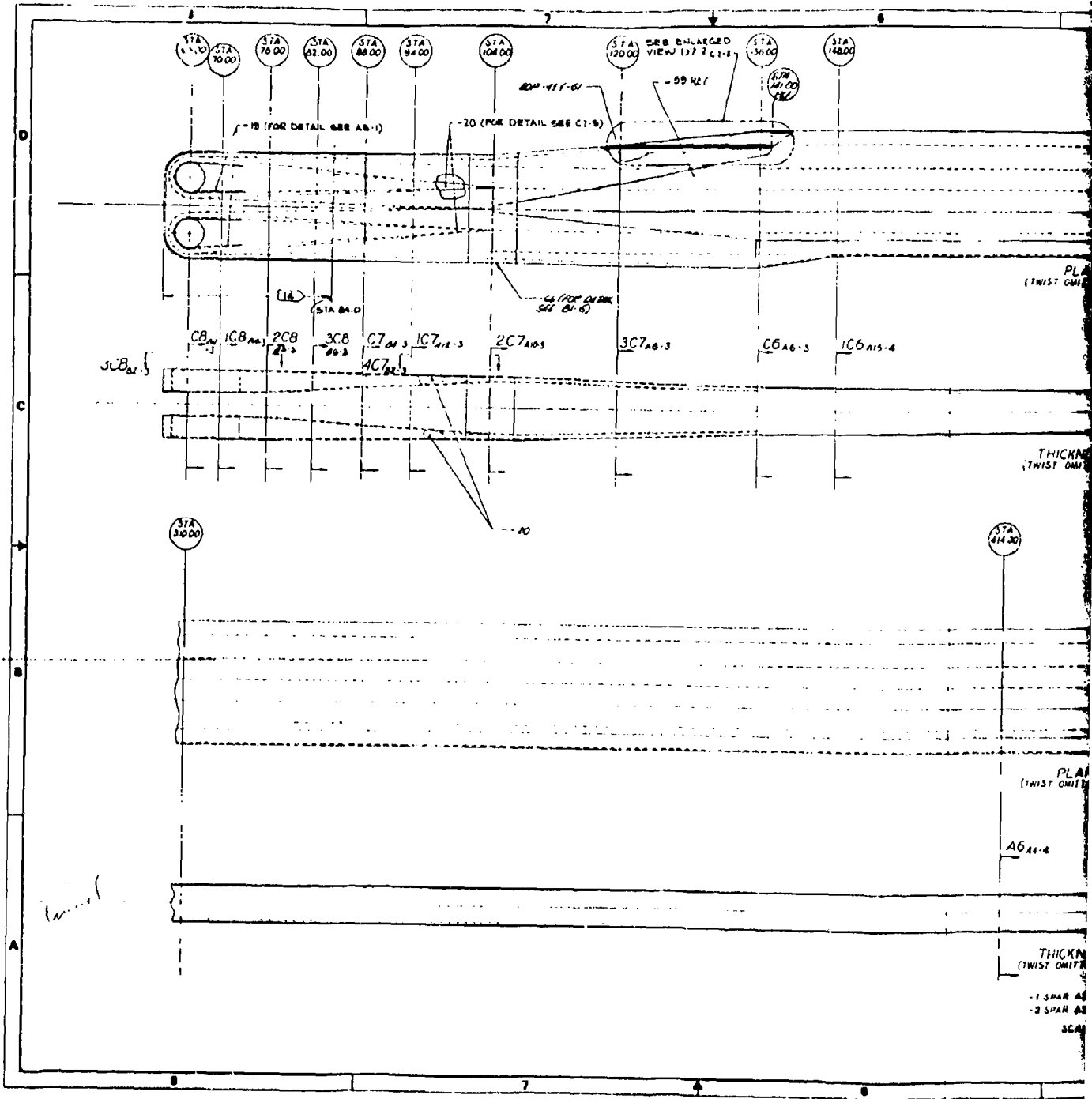
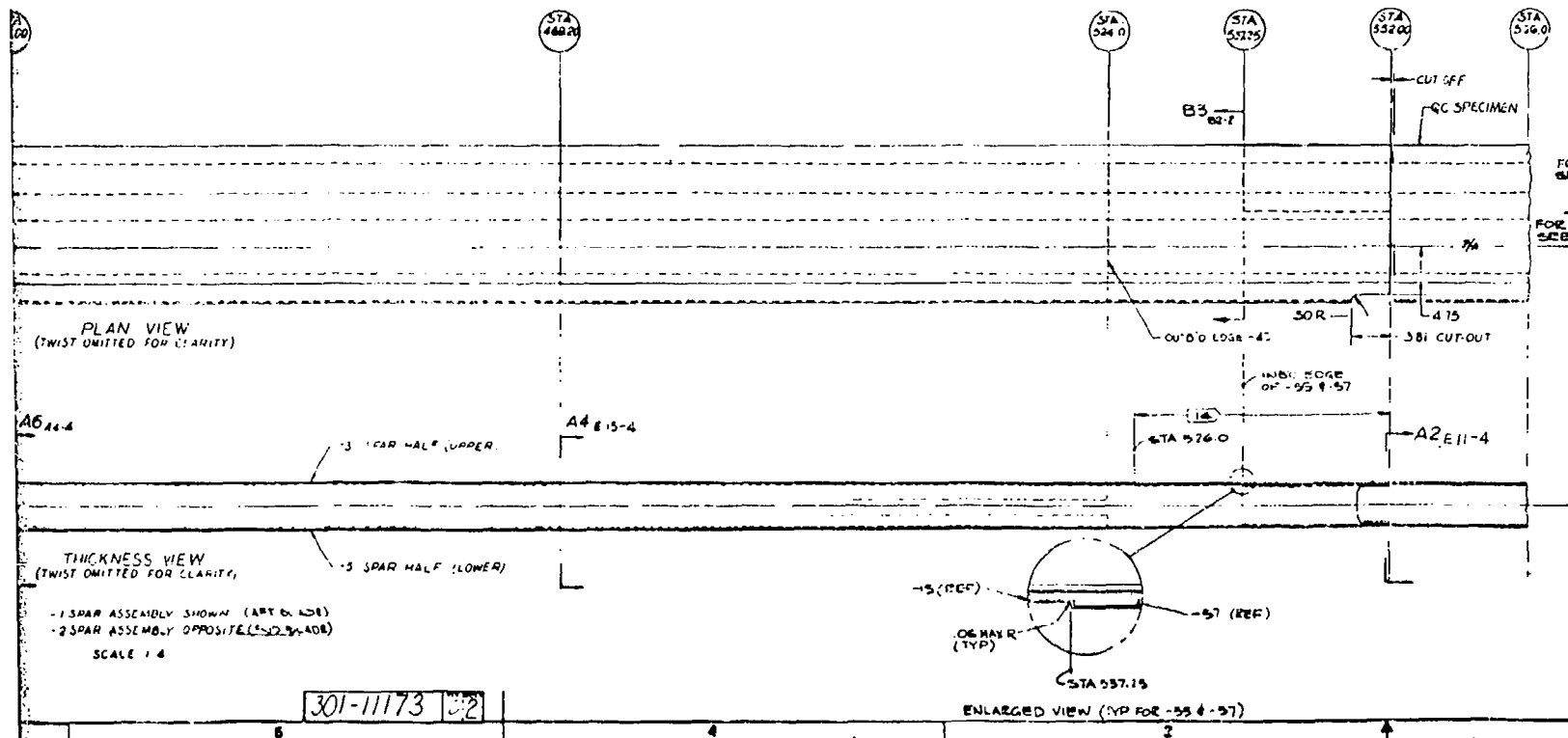
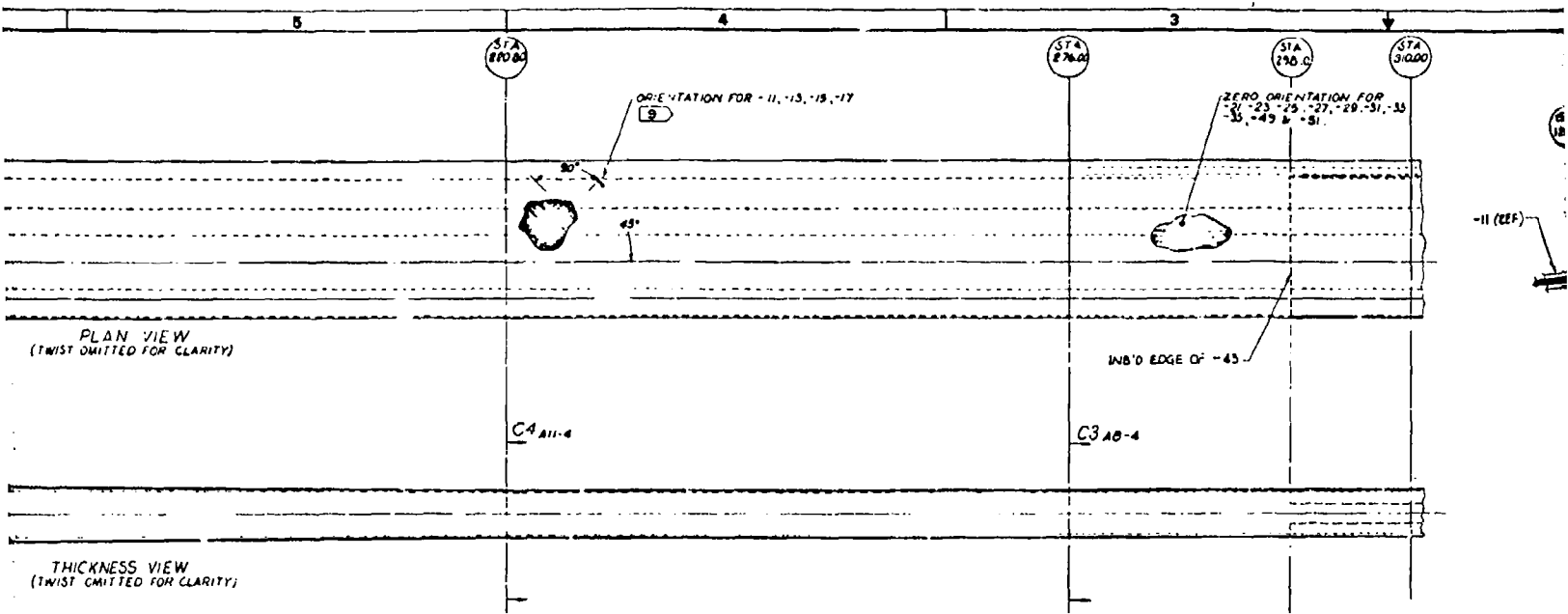
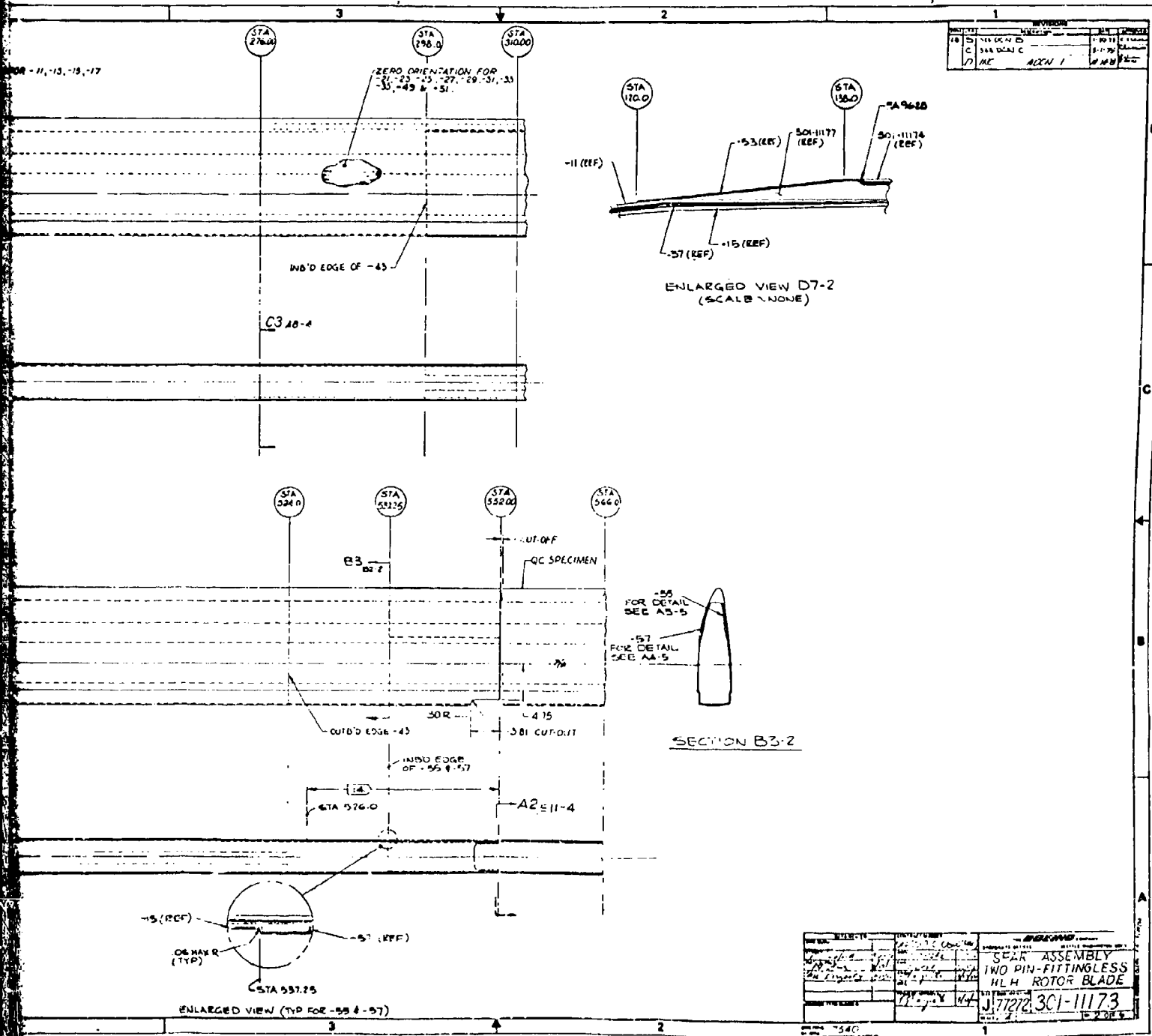


Figure 31. Continued



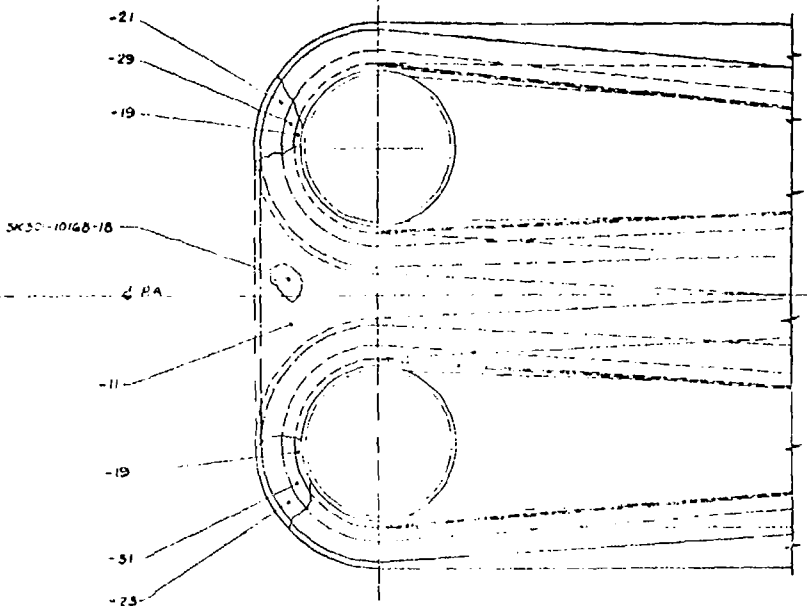
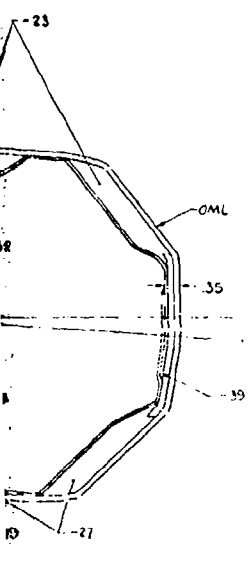
2



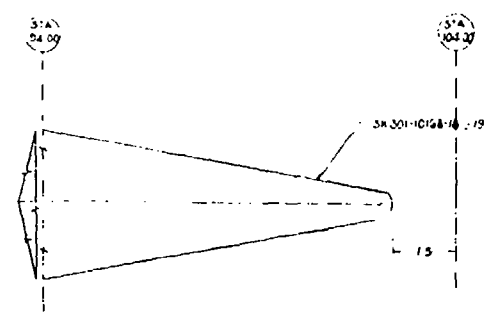
NO.	DESCRIPTION	DATE	BY
1	SEALED	11-17-72	J. J. [unclear]
2	SEALED	11-17-72	J. J. [unclear]
3	SEALED	11-17-72	J. J. [unclear]
4	SEALED	11-17-72	J. J. [unclear]
5	SEALED	11-17-72	J. J. [unclear]
6	SEALED	11-17-72	J. J. [unclear]
7	SEALED	11-17-72	J. J. [unclear]
8	SEALED	11-17-72	J. J. [unclear]
9	SEALED	11-17-72	J. J. [unclear]
10	SEALED	11-17-72	J. J. [unclear]

SEALED ASSEMBLY
 TWO PIN-FITTINGLESS
 HLH ROTOR BLADE
 J. J. [unclear] 301-11173
 11-17-72

REVISIONS		BY	DATE
A	210,433 REV - WITH CAG		5-1-54
B	SIC DEC 5		1-30-54
C	ORR DEC 5		1-30-54
D	SEE DRWG		5-1-54
D		MC HORN LES	
E		MAILED UNDER PATENT	
F		WITH 3 SETS OF DRAWINGS	
G		ANY SIZE 10-11-1954	
H		REPLACE WITH THIS DRG	
I		SHEET 6	



VIEW 308-2



100% OF SP AND
100% OF STA 1160

PART NO. 301-11173	QUANTITY 1	DATE 1-30-54	BY J. J. [unclear]	CHECKED [unclear]	APPROVED [unclear]
3-PAIR ASSEMBLY NO PIN FITTINGLESS HLH ROTOR BLADE J17727 301-11173					

C
B
A

4

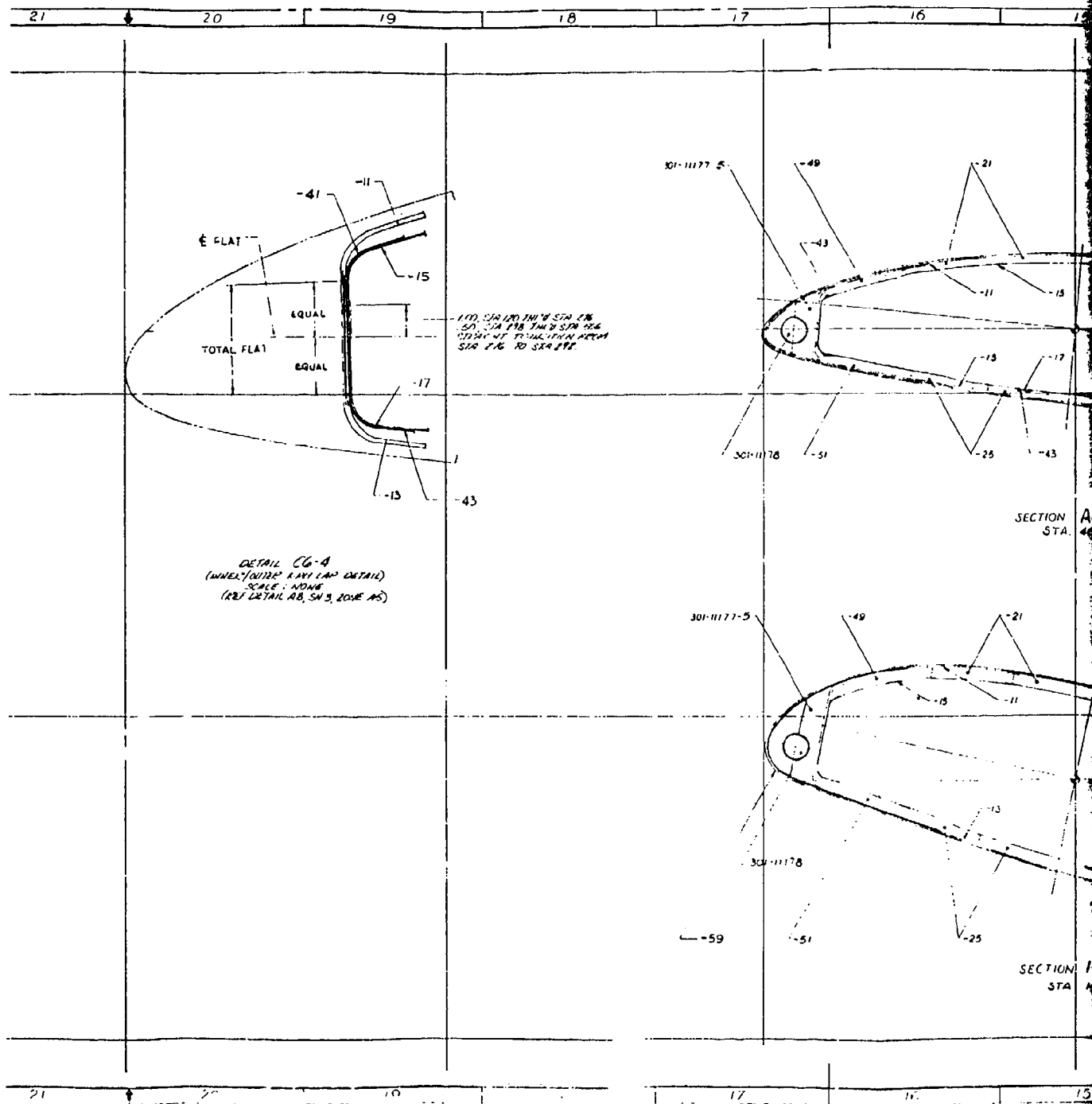
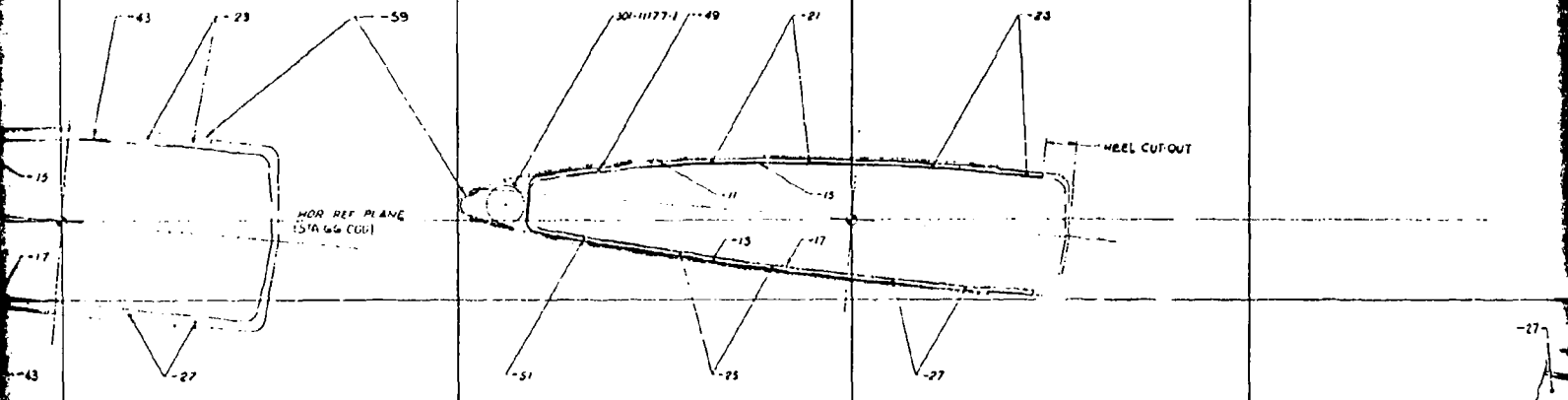


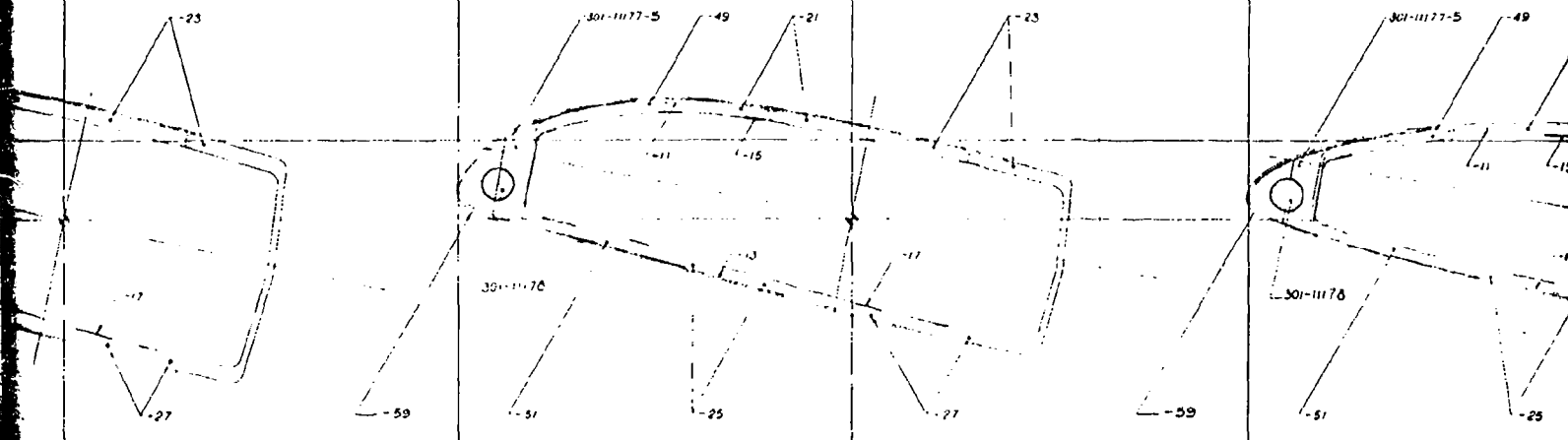
Figure 31. Continued

15 14 13 12 11 10 9



SECTION A4-2
STA 469.20

SECTION A2-2
STA 552.00

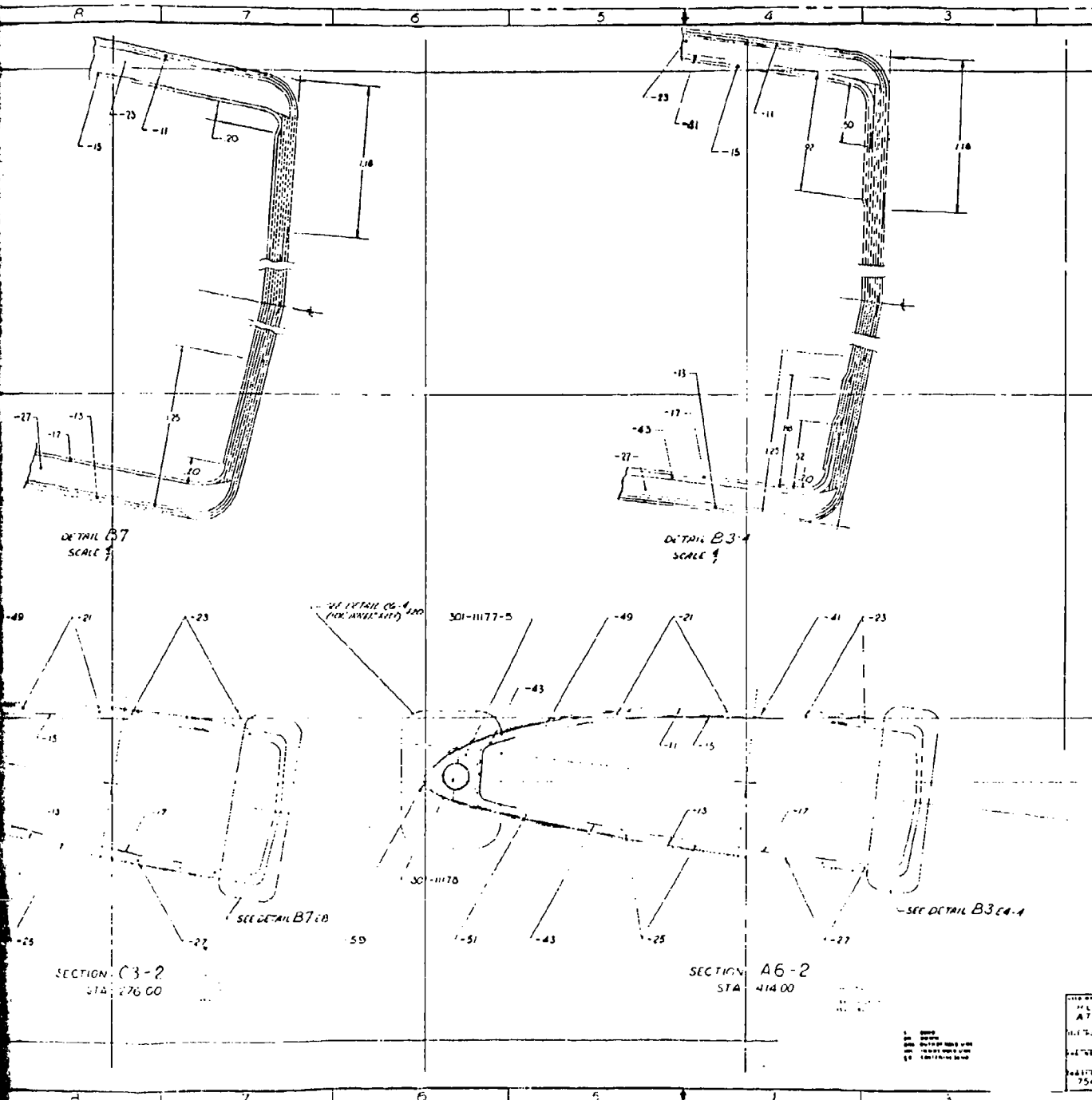


SECTION C6-2
STA 140.00

SECTION C4-2
STA 220.0

15 14 13 12 11

2



REV	DATE	BY	CHK
1	568	DCN B	
2		SEE DCN C	
3		PC	ALC 106

NO. OF SHEETS	DATE	PROJECT	NO. OF SHEETS
ATC		STAR	100
		TWO PIN	
		HLH RC	
DATE			
7540		J. M. J.	5

3

PCM

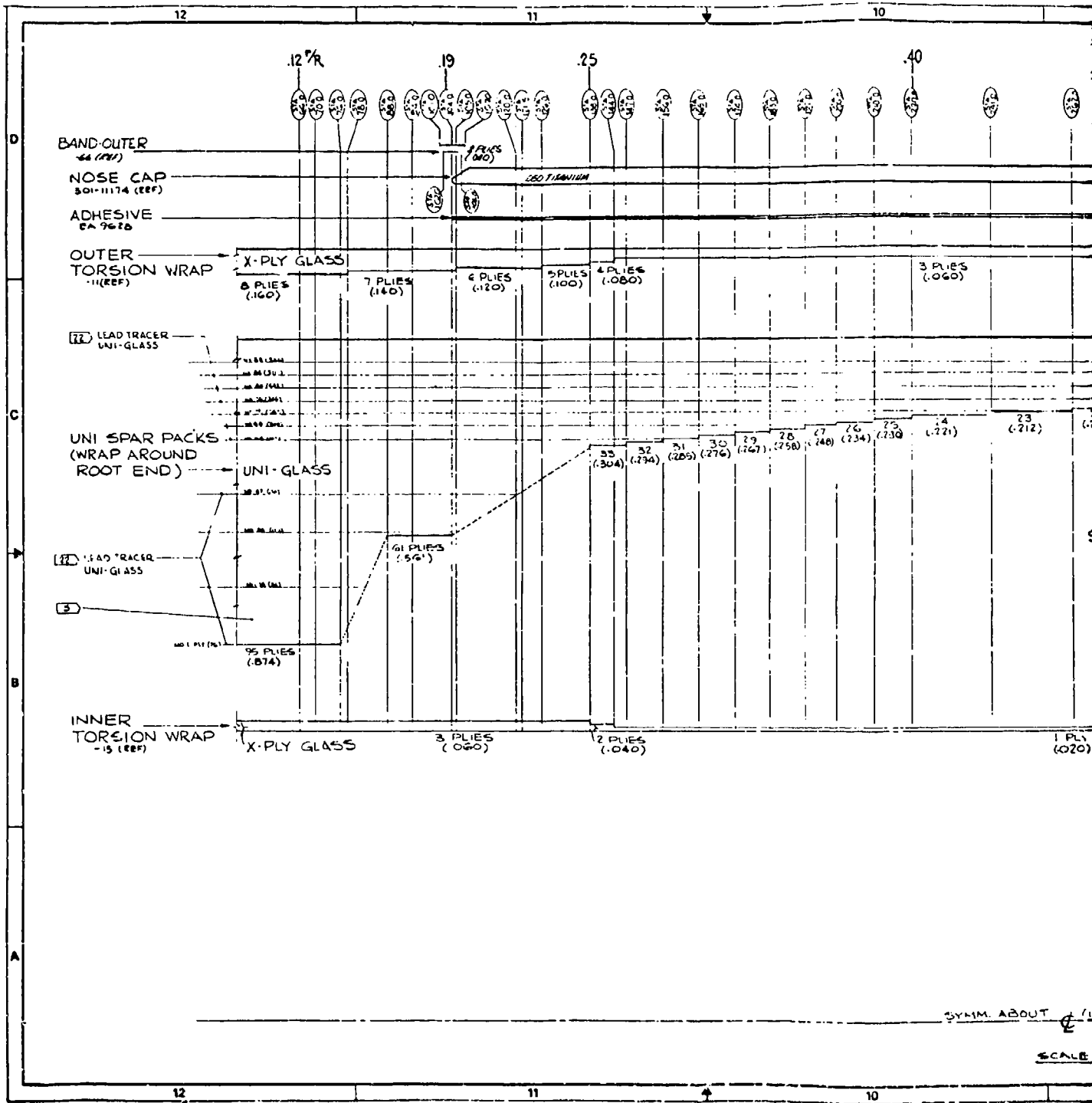
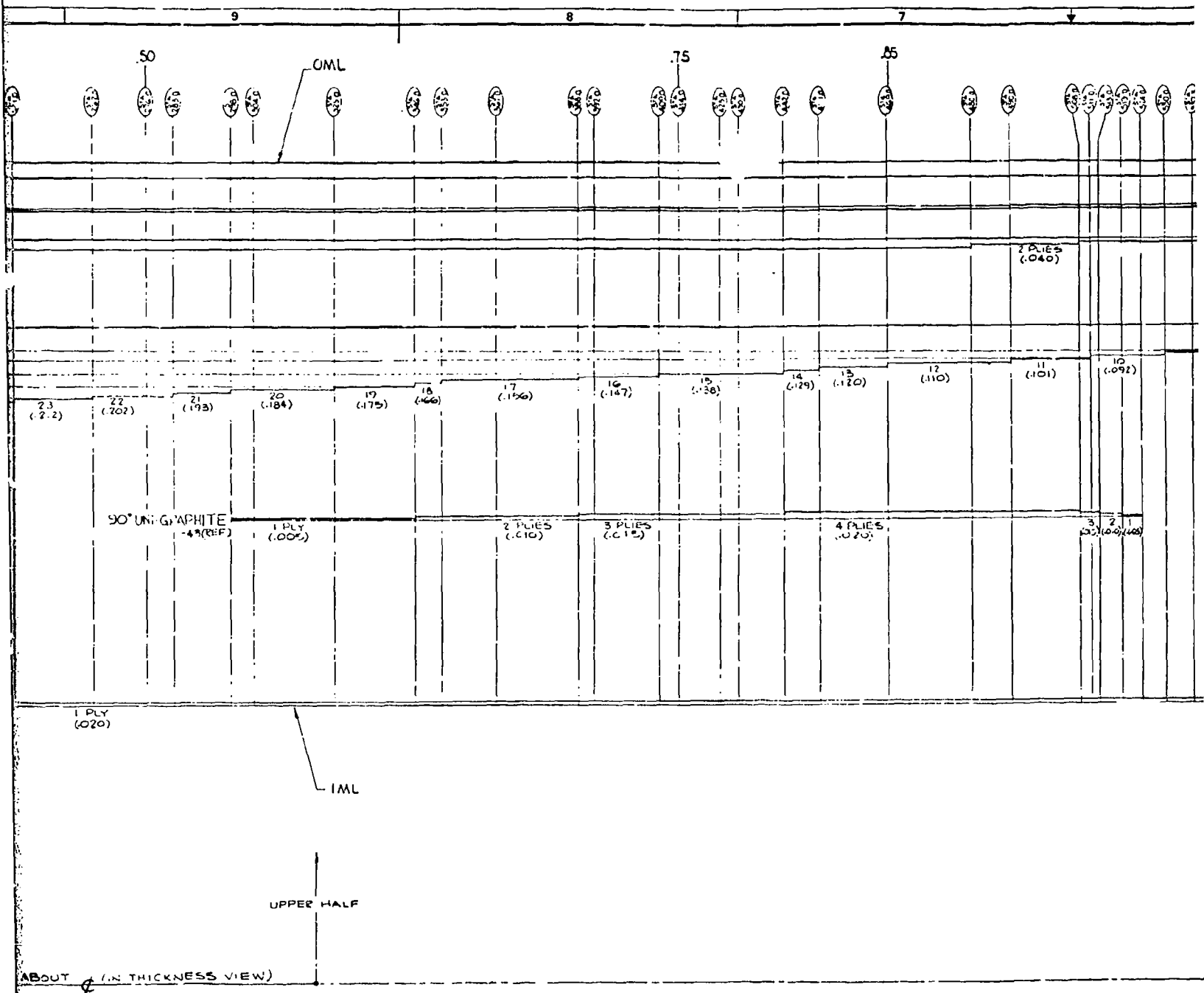


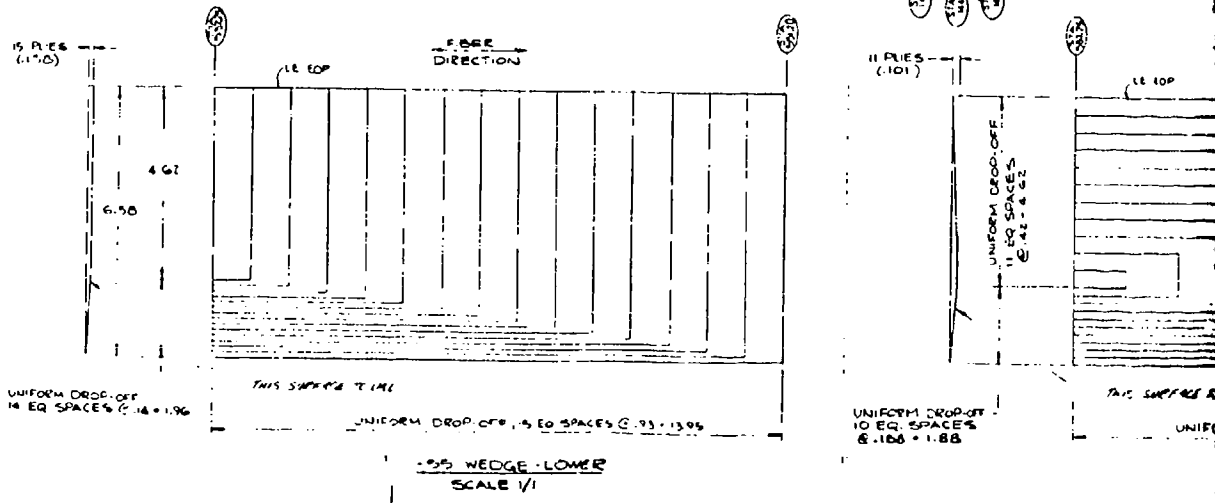
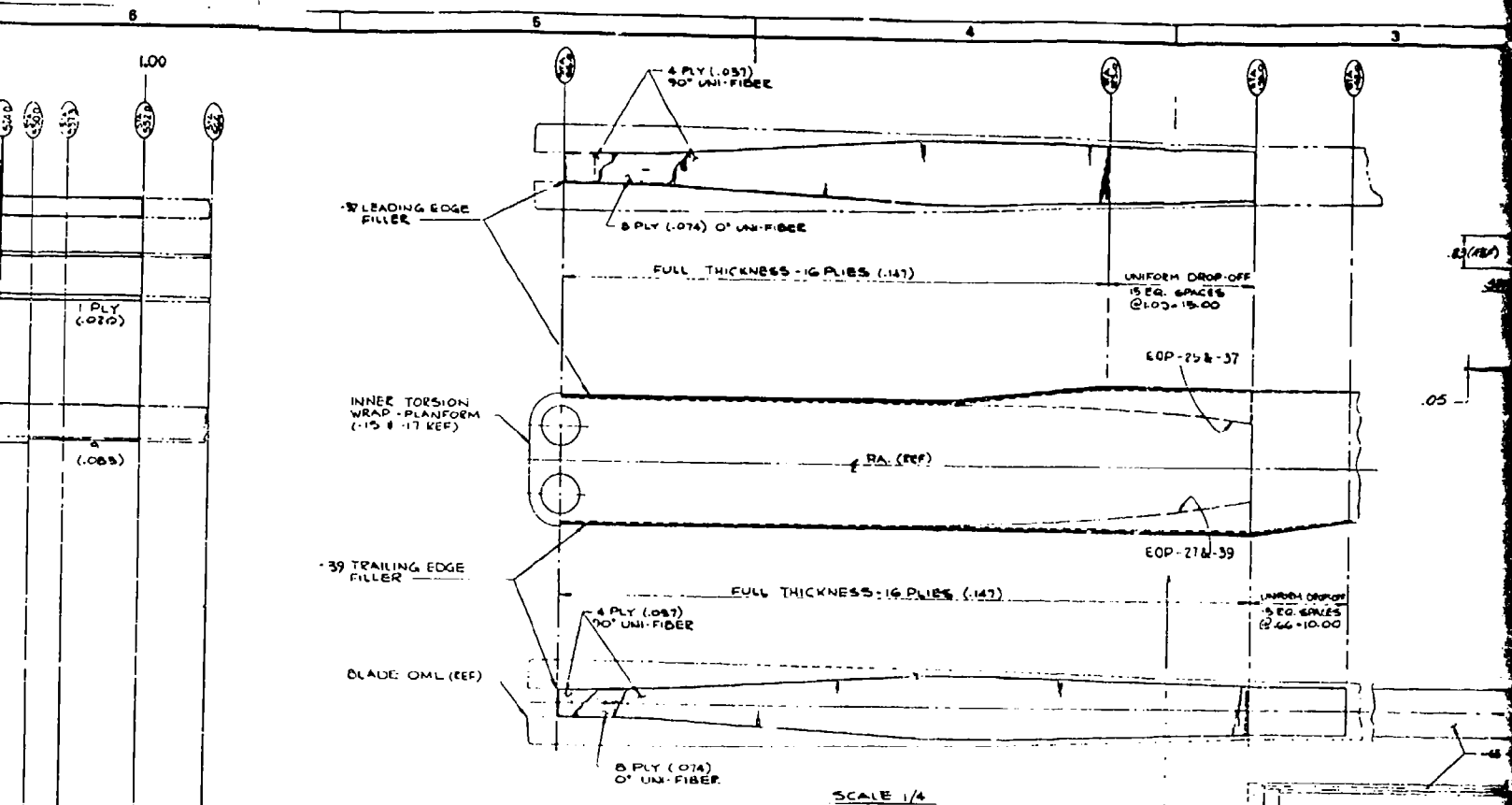
Figure 31. Continued



SCALE NONE

301-11173 25

2



3

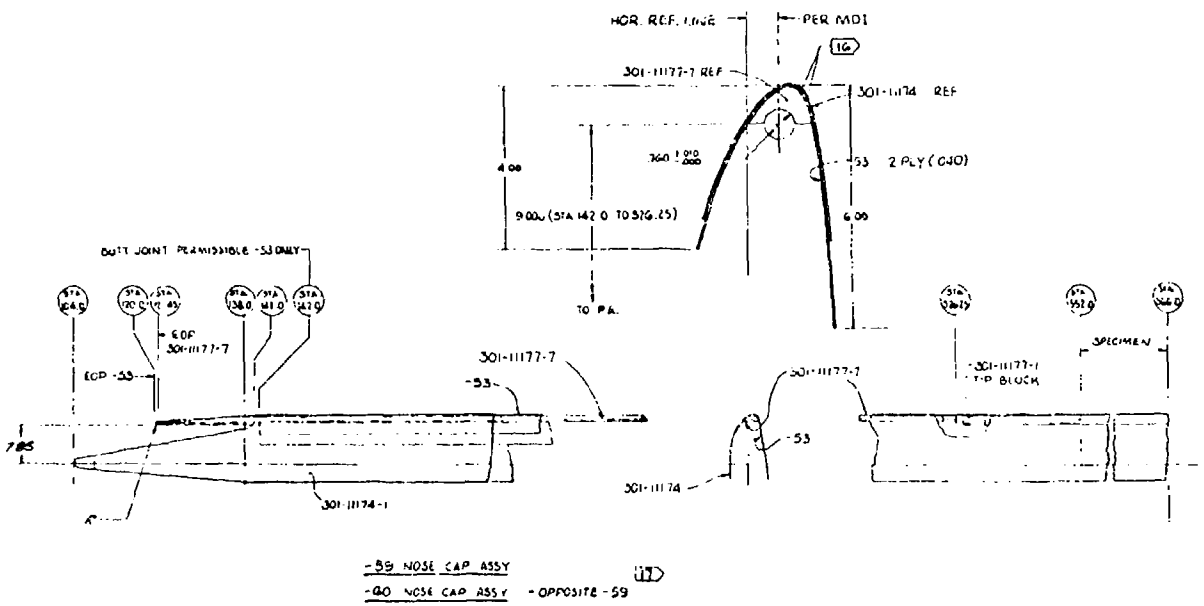
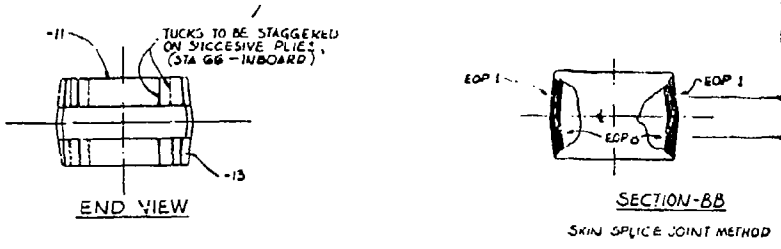
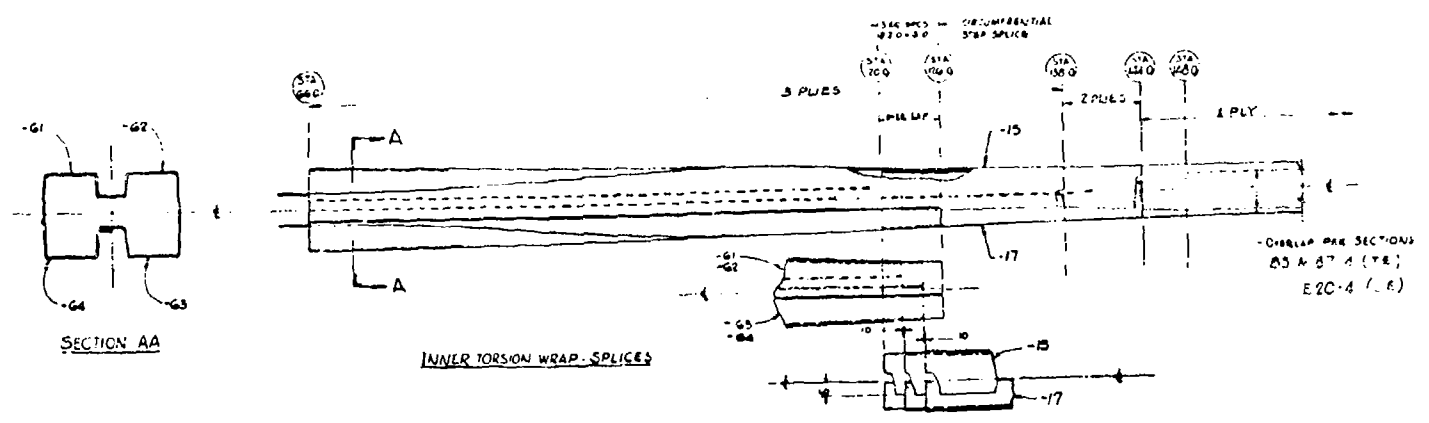
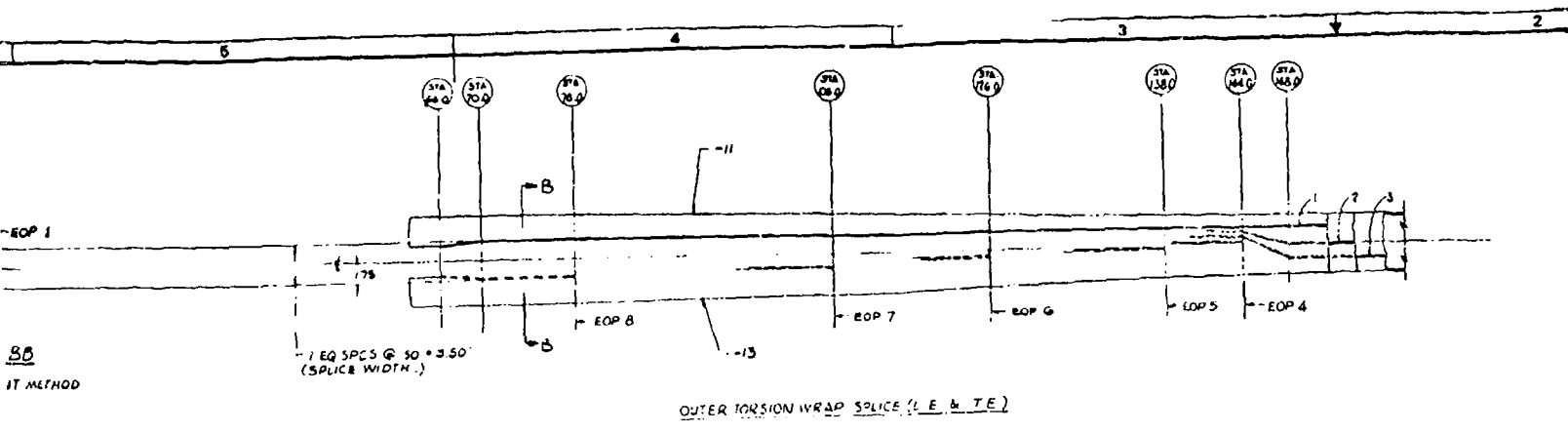
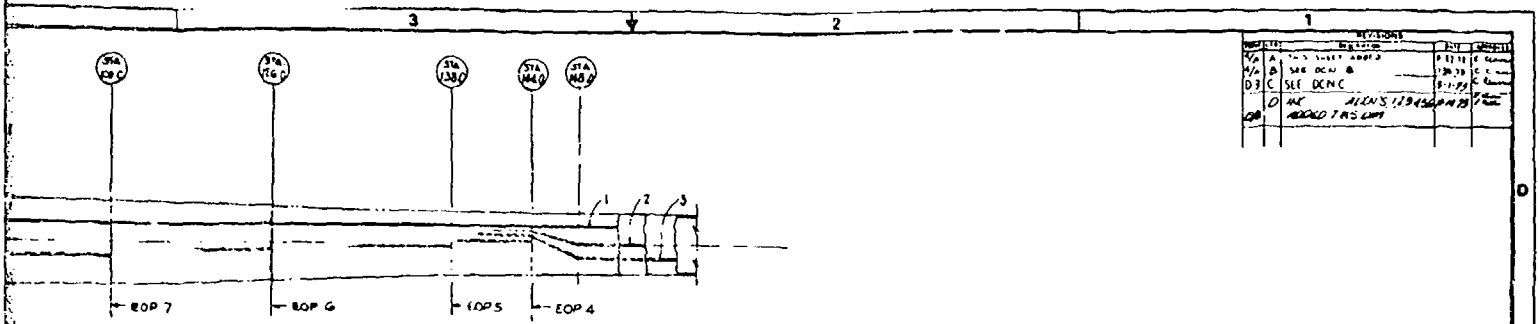


Figure 31. Continued



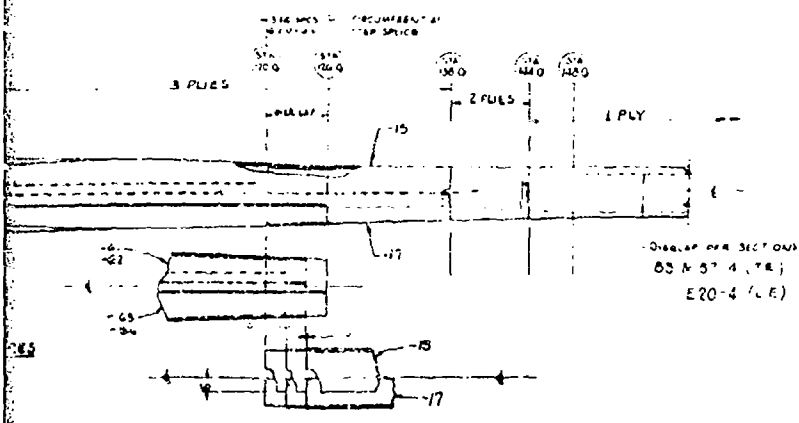
301-11173 26

2



NO.	REVISIONS	DATE	BY	CHKD
1	ISSUED	8-11-78	J. J. [unclear]	[unclear]
2	SEE DCN 8	7-20-78	[unclear]	[unclear]
3	SEE DCN C	8-11-78	[unclear]	[unclear]
4	ALLEN'S 1294564M78			
5	ADDED T.R.S. COPY			

TORSION WRAP SPLICE (L.E. & T.E.)



NO.	REVISIONS	DATE	BY	CHKD
1	ISSUED	8-11-78	J. J. [unclear]	[unclear]
2	SEE DCN 8	7-20-78	[unclear]	[unclear]
3	SEE DCN C	8-11-78	[unclear]	[unclear]
4	ALLEN'S 1294564M78			
5	ADDED T.R.S. COPY			

SPAR ASSEMBLY
TWO PIN FITTINGLESS
HLM ROTOR BLADE
J 77272 301-11173

3.6 DETAIL DESIGN OF THE PROTOTYPE BLADE CONFIGURATION

The basic structural concept for the blade for the prototype helicopter is identical to that of the ATC configuration. Rotor blade design improvements that developed out of manufacturing experience and demonstration testing of the ATC configuration were incorporated into the HLH prototype design. These modifications, summarized in Figure 32, include the following items:

1. Lightning protection
2. Titanium nose cap material substitution
3. Tip fitting installation and hardware
4. Precured spar heel
5. Lag damper arm and sleeve
6. ISIS integral spar inspection system
7. Internal droop stop wedges
8. Outboard spar wall stiffener
9. Aft fairing core and skin

The purpose of these changes was to reduce the manufacturing cost and to improve the structural capability of the rotor blade.

3.6.1 Lightning Protection

Lightning tests on an ATC rotor blade segment indicated that the titanium cap is almost an order of magnitude better than predicted in its ability to transmit lightning. Consequently, the coverage provided by the ATC titanium nose cap is much more than is needed to transmit a 200,000 amp strike.

It was anticipated that the titanium nose cap would be more attractive to lightning than the graphite trailing-edge wedge, but this was not the case. Since the graphite acts as a conductor, two issues must be addressed as a result of this situation. The graphite suffers some microscopic damage when current flows through it (the fiber-to-resin bond breaks down) which would result in a loss of some strength and stiffness in the composite. Since the graphite trailing edge was not grounded in the blade design, the lightning must arc from the trailing edge to the spar and would choose the path through the aft fairing, which would produce internal damage to the blade.

The first issue, loss of stiffness in the trailing-edge, is not safety of flight since the trailing edge wedge has three independent unidirectional load paths. Any damage to the wedge, even undetected damage, would result in a change in in-plane stiffness, and a vibration level change would occur.

The second issue, trailing edge to spar arcing, could present a situation where safety of flight would be affected. Therefore, it was concluded that graphite in the trailing edge must be grounded and protected.

The pigtail arrangement used to ground the inboard end to the titanium is expensive and requires excessive processing to make the brass-to-titanium-to-wire termination.

During lightning testing, an aluminum sheath or covering was placed over the trailing edge area. This new conductor successfully shielded the trailing-edge wedge from the remaining lightning strikes. A complete Faraday cage is provided by a weave of aluminum. Figure 33 shows the modified design compared to that for the ATC blade.

3.6.2 Titanium Nose Cap

The original Specification (BMS7-197) for the nose cap material required minimum differences between properties in the longitudinal and transverse directions. Preliminary tests indicated that when the directionality (texture) of the material is pronounced, improved high-cycle fatigue strength properties are obtained in the longitudinal direction. Further tests, reported in Reference 8, confirmed this phenomenon and showed that the heat treatment for forming the nose cap has no degrading effects. The highly directional material was selected for the prototype nose caps to take advantage of the higher strength. The highly directional product is also easier to fabricate and should prove to be a substantial cost saving.

3.6.3 Tip Fitting Installation and Hardware

Obtaining an acceptable fit of the precured tip weight fitting to the inside mold lines (IML) of the spar proved to be a very difficult and expensive procedure. The difficulty in obtaining an exact fit resulted in questionable bond integrity.

The internal hardware of the ATC tip-weight configuration required many parts that were difficult to install. ISIS pressure leaked through the upper and lower precured halves of the tip fitting into the tracking tubes, causing an invalid failure indication.

The prototype configuration reduced the number of tip hardware parts and thus simplified the installation. A unidirectional fiberglass fitting was co-cured with the spar to eliminate the close fitting requirements and to eliminate the ISIS leaks. This co-cured configuration also reduced the cost of the tip fitting assembly.

3.6.4 Spar Heel

Sporadic wrinkling of the crossply fiberglass in the "D" spar heel area occurred on the ATC blades manufactured (Figure 34). The wrinkling is unacceptable structurally as it caused an early failure of a spar section during a limit torsion test as reported in Reference 9.

The wrinkling originated during the installation or transfer of uncured composite material into the curing mold. The solution to this problem incorporated in the prototype design is to precure the heel (Figure 35) as a structural member in a separate operation prior to the spar assembly.

3.6.5 Lag Damper Arm and Sleeve

The root end demonstration test showed that the stresses in the lag damper arm were higher than calculated. The high stresses caused a failure at the trailing pin hole. This failure was due in part to improperly applied test load. The failure origin occurred at fretting between the steel sleeve and the titanium damper arm. The sermetal coating on the inner diameter surface of the sleeve was unsatisfactory for eliminating fretting, showing wear that progressed all the way through the coating.

For the prototype design, stress levels were reduced by increasing the thickness of the lag damper arm in the critical area around the trailing pin hole. Improved fretting protection was provided with a fiberglide coating applied to the inner and outer diameter surfaces of the steel sleeves. The fiberglide was proven in the CH-47 socket where it was subjected to operating bearing pressures similar to those of the HLE.

The number two HLH root end specimen with the new arm and the fiberglide fretting inhibitor was tested at high-speed level flight (V_H) loading for 258 equivalent flight hours. Fretting between the steel sleeve and the titanium damper arm was eliminated and the fiberglide on the sleeve was in excellent condition.

3.6.6 ISIS Integral Spar Inspection System

The root end ISIS bulkhead for the ATC design was located at Station 80, outboard of the chopped fiberglass internal droop stop wedges.

The installation was difficult to inspect and/or repair once the sleeves and damper arm were installed. Reconfiguration of the droop stop wedges permitted the relocation of the inboard ISIS bulkhead to Station 70. The mounting block was eliminated, thereby reducing the number of parts and the overall cost. Repositioning the valve away from the indicator makes the evacuation system failsafe. The weight of this installation is less than the ATC. The installation is more repairable without root end disassembly.

The initially specified internal pressure of 3.5 psia for the evacuated spar was selected on the basis of metal blade experience where, because of the rapid crack propagation and the requirement to detect crack lengths of approximately 0.10 inch, a completely active system is required. A completely active system has a pressure set to always provide a differential pressure between internal spar and external air for all flight conditions from sea level at -65°F to 8000 feet at 100°F .

For the prototype blade, an intermediate internal pressure of 7.5 psia was specified based on the following characteristics of composite rotor blades:

1. Very slow damage propagation.
2. Residual strength of section with extensive damage which would obviously leak on the ground or in the air still provides 200 hours of safe life.

The 7.5 psia pressure provides a differential pressure for all ground conditions between sea level -65°F and 8000 feet at 100°F . The fail-safe test data obtained for the composite

blade failure mode and rate indicate that the continuous ISIS system could be replaced with a periodic "pump down" ground check and still retain the required fail safety.

3.5.7 Internal Droop Stops

The ATC design used four fittings to react the compressive loads at the root end due to ground conditions with zero or low blade centrifugal force. Each fitting was hot bonded to the internal surface of the spar. The variation in surface contour required considerable hand fitting of the blocks prior to bonding. The root end structural tests showed the hot bond to be unsatisfactory. An interim fix using cold bonded EC-2216 fittings capable of receiving the design loads was used on the whirl tower and DSTR blades. For the prototype design, the droop fittings were cured in place with the spar, eliminating the fit and bonding problems experienced.

3.6.8 Aft Fairing

Simulated airloads testing of the ATC airfoil sections resulted in premature shear failures of the Nomex honeycomb core at the bond of the core to the spar heel. The results of these tests are reported in Reference 9. The premature failure was attributed to the core height and to deflection of the spar heel. Full-size coupon tests verified the height and stiffness effects. In addition, the tests showed that curing temperature and crushing of the core during assembly did not degrade the core strength.

The prototype design substantially increased the stiffness of the spar heel by adding graphite into the heel web at 90° to the spar direction. Figure 36 compares the ATC and prototype designs of the heel.

Repeat of the simulated airload tests (Reference 9) verified that the modification met the design load conditions for the prototype helicopter. In addition to the spar heel stiffening, a horizontal stabilizer was introduced into the outboard section of the prototype fairing to improve its strength. The core density of the intermediate section of the prototype fairing was increased to 3 pounds. The 2-pound core behind the vertical splice was introduced as a weight saving scheme, since the increased strength is not required in this area.

These changes are illustrated in Figure 37. The total weight penalty for the prototype core modification is 7.5 pounds.

Local fairing skin changes were introduced to eliminate skin cracks that occurred during final cure due to thermal conditions and the pressure necessary to deform the core. These cracks only occurred in the three-pound core region where the 90° material terminated.

The following modifications (Figure 38) were made to the prototype fairing skin:

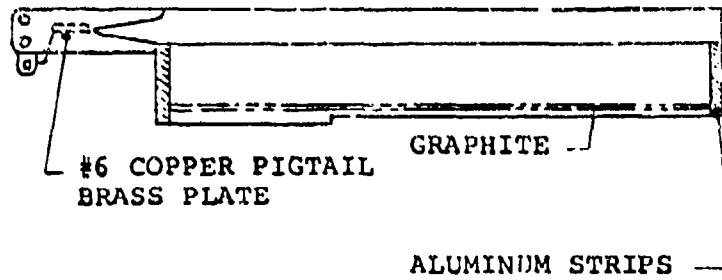
1. Extended 90° uni to trailing edge wedge.
2. Shortened inner skin by .5 inch to have core splice coincide with 0° rib strip.
3. Trailing-edge wedge will have all 90° material added to fairing in subsequent assemblies for additional tolerance (forward only).

3.6.9 Pendulum Vibration Absorbers

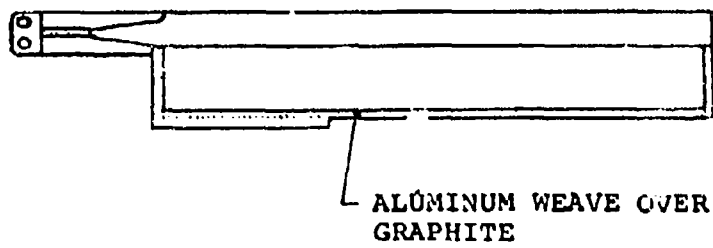
Provisions were made on the HLH rotor blade for the installation of pendulum vibration absorbers (Ref. Drawing No. 301-59800). These pendulum absorbers are masses mounted on a fiberglass collar (Ref. Drawing No. 301-55117) that is bonded to and clamped around the blade spar between the attachment pins and the airfoil cutout. These masses are designed to minimize vertical root shear forces by flapping about a horizontal axis. Two types of absorbers were designed, one tuned to react 3/rev root shears, and the other tuned to 4/rev. The mounts are positioned such that either the 3/rev, the 4/rev, or a combination of both can be installed at one time. The structural qualification test described in test plan report number D301-10115-23 (Reference 10) was not conducted before the program was terminated.

3.6.10 Blade Drawings

A complete list of the prototype blade drawings is given in Figure 39. The blade assembly drawings are included in Figures 40, 41, and 42.

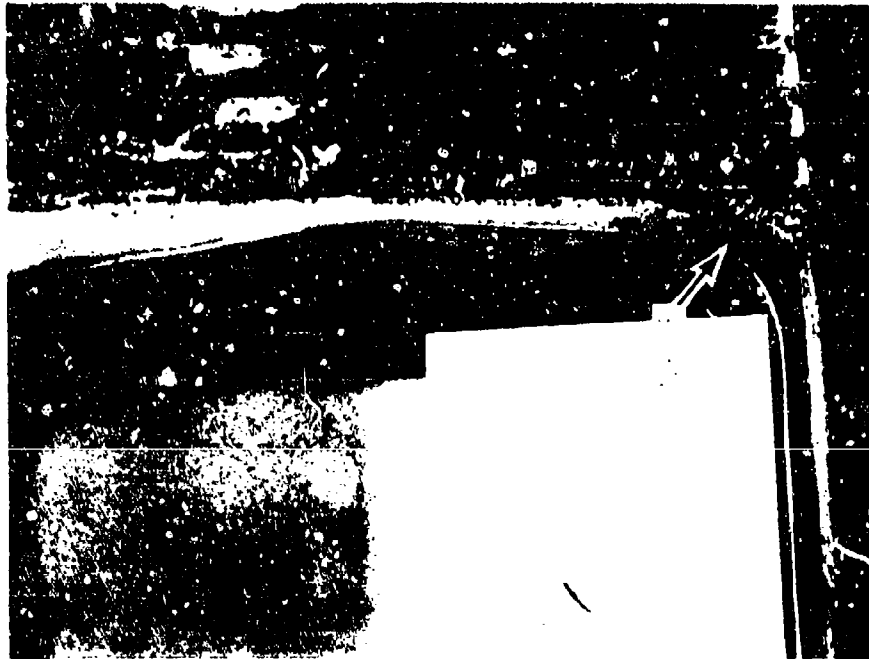


ATC CONFIGURATION

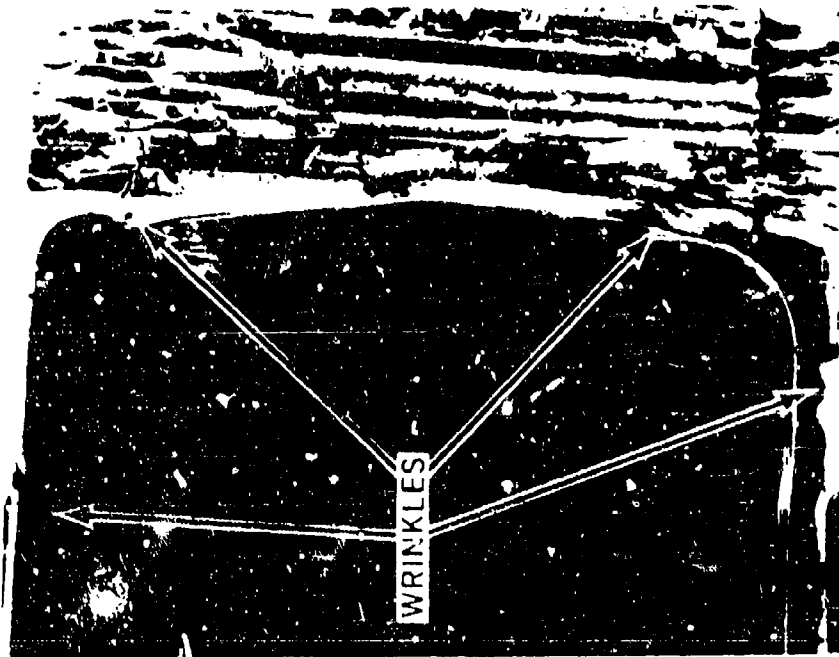


PROTOTYPE CONFIGURATION

Figure 33. Lightning Protection



HLH SPAR SECTION FROM NO 2 BLADE
MINOR IN NATURE



HLH SPAR SECTION FROM NO 1 BLADE
VERY SEVERE IN NATURE

Figure 34. Typical Crossply Wrinkles in Spar Heel Area

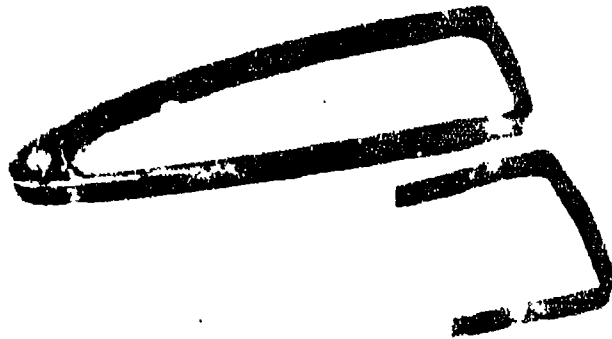


Figure 35. 1-Inch Section of HLH Prototype Spar
Precured Heel, Fiberglass and Graphite

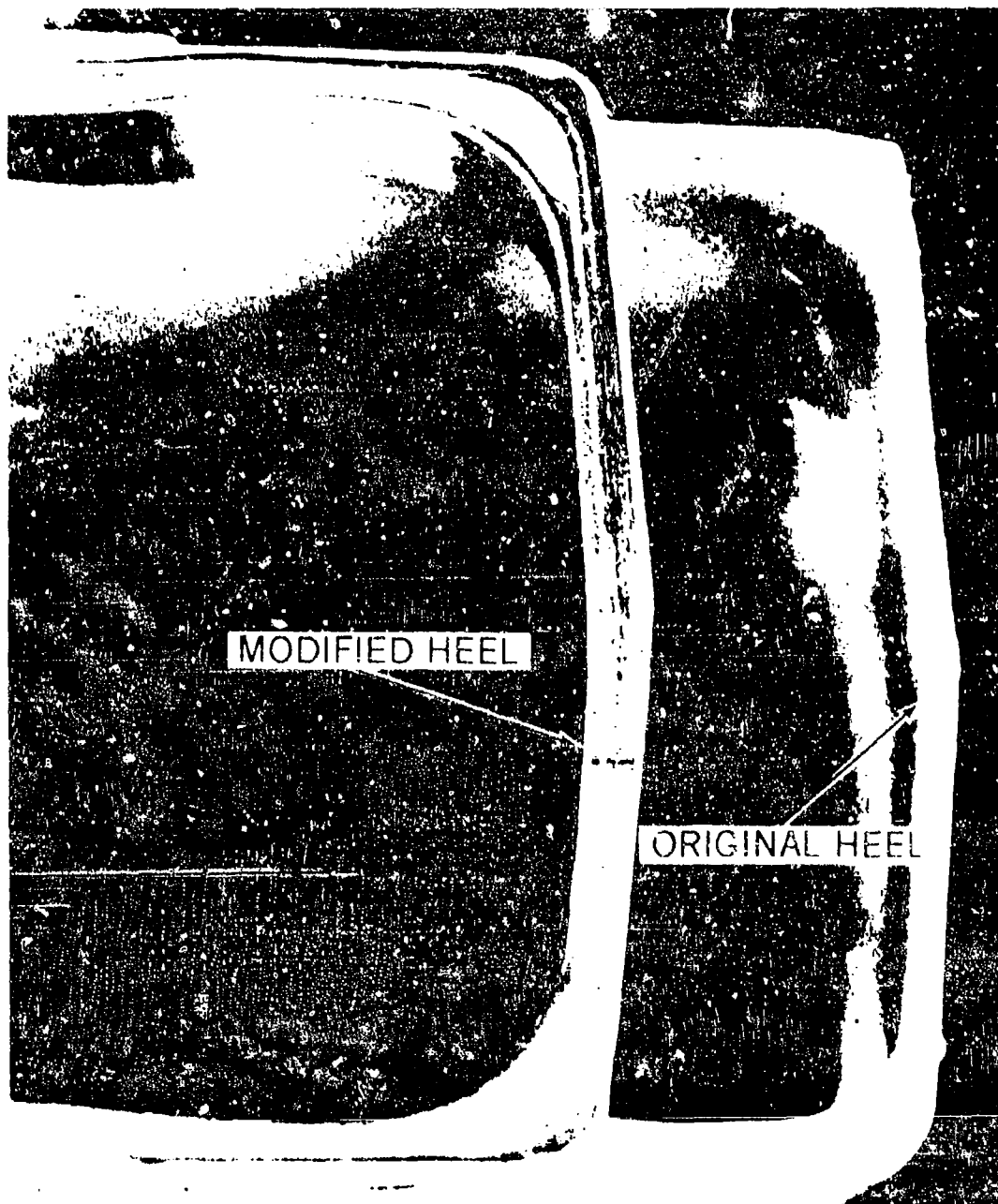
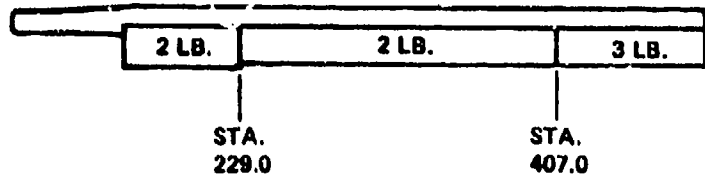
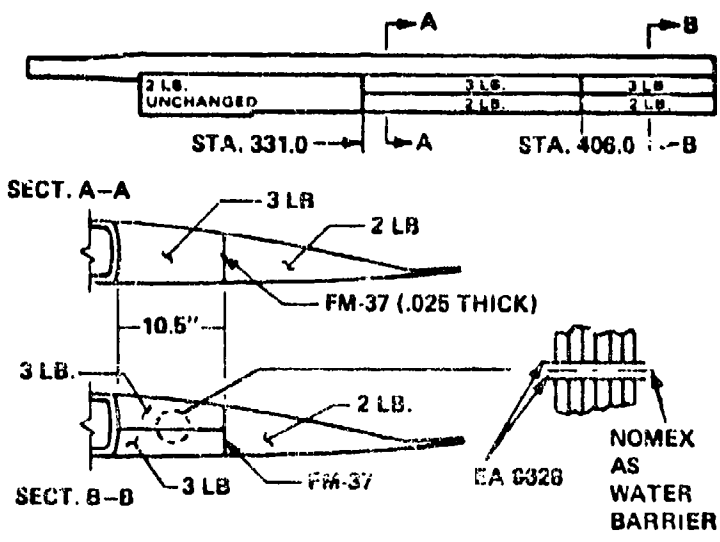


Figure 36. Comparison of HLH Spar Heels Before and After Modifications



ATC CONFIGURATION



PROTOTYPE CONFIGURATION

Figure 37. Aft Fairing Core

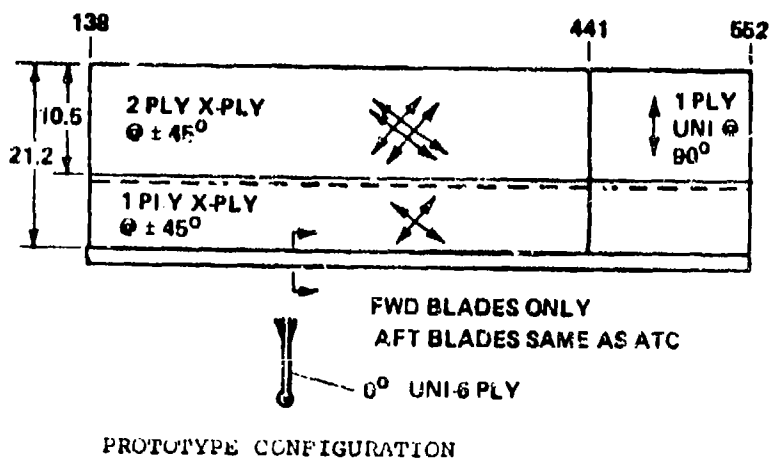
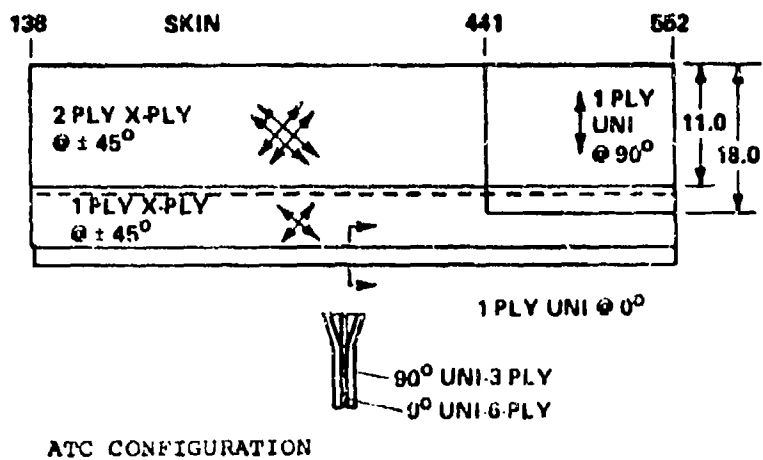


Figure 38. Aft Fairing Skin

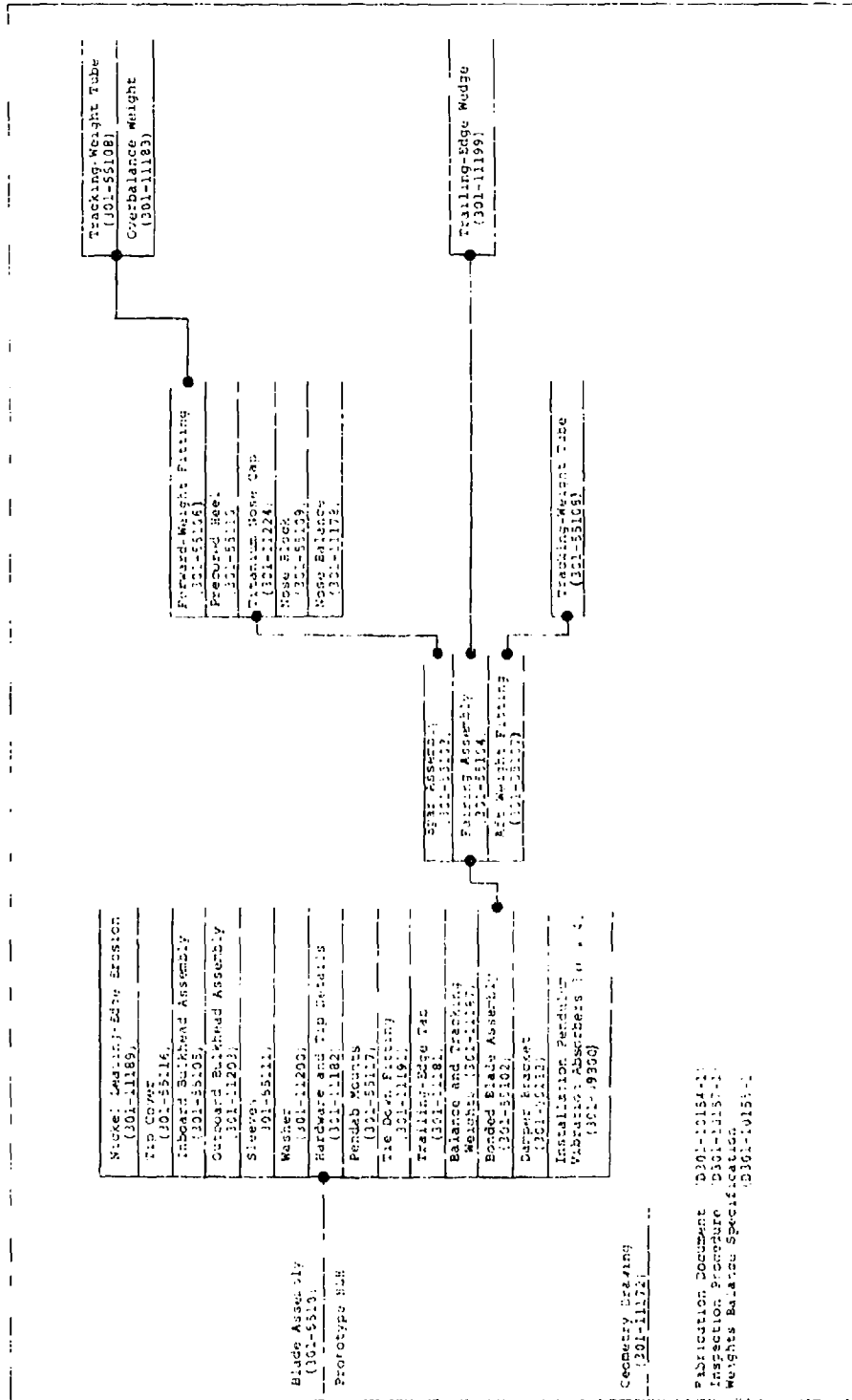


Figure 39. HLE/Prototype Rotor Blade Assembly Drawing Tree

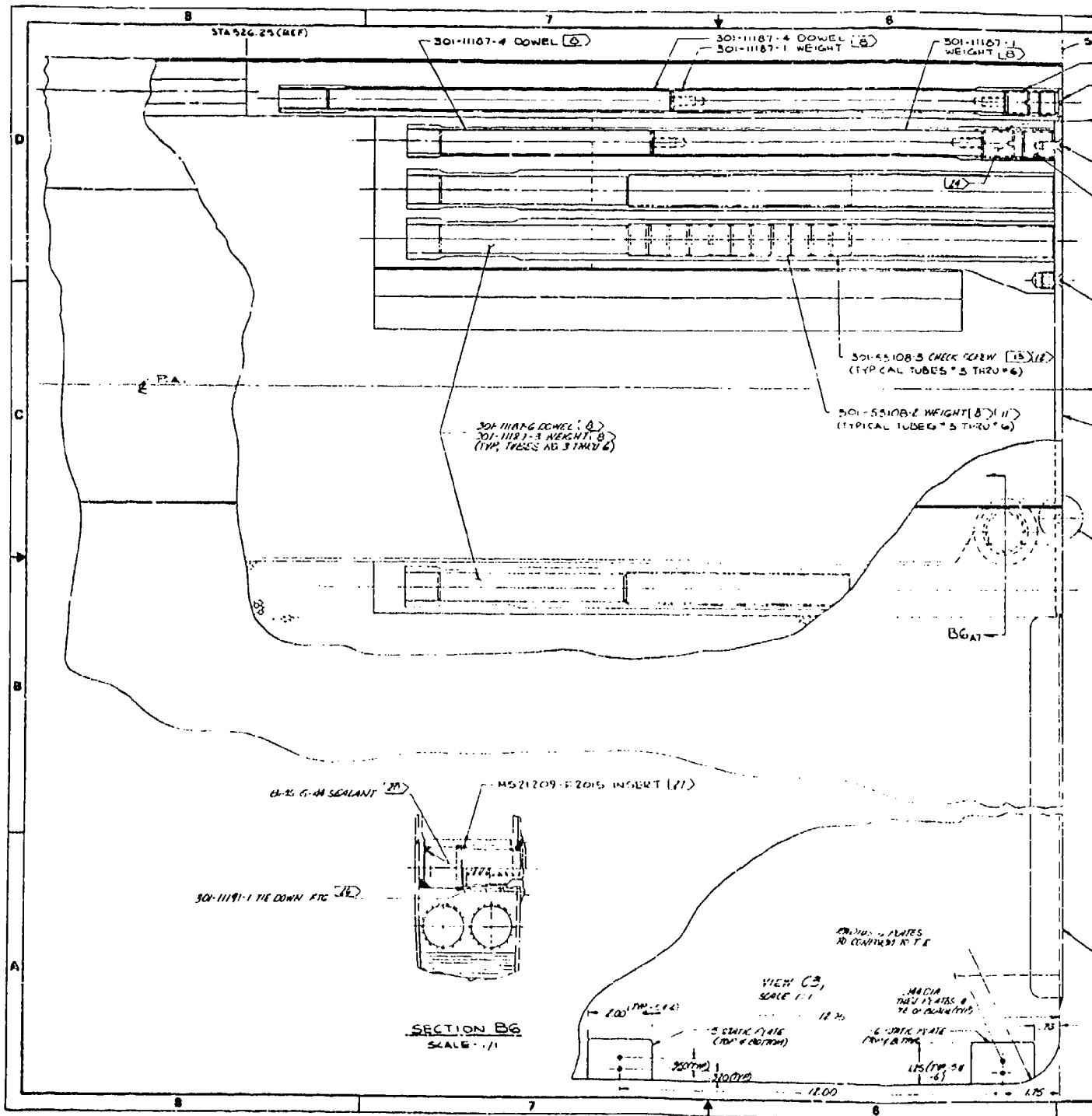


Figure 40. Continued

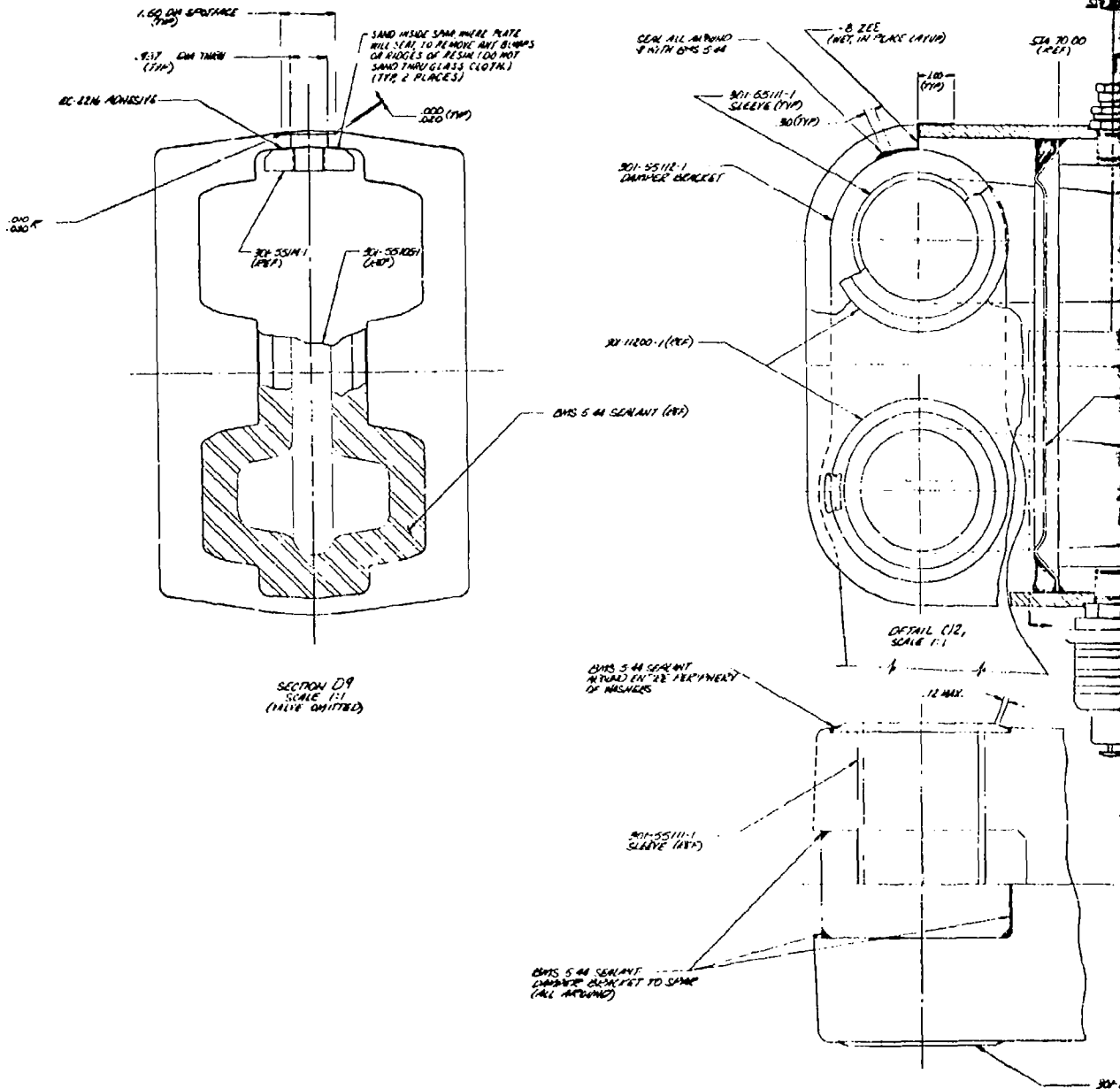


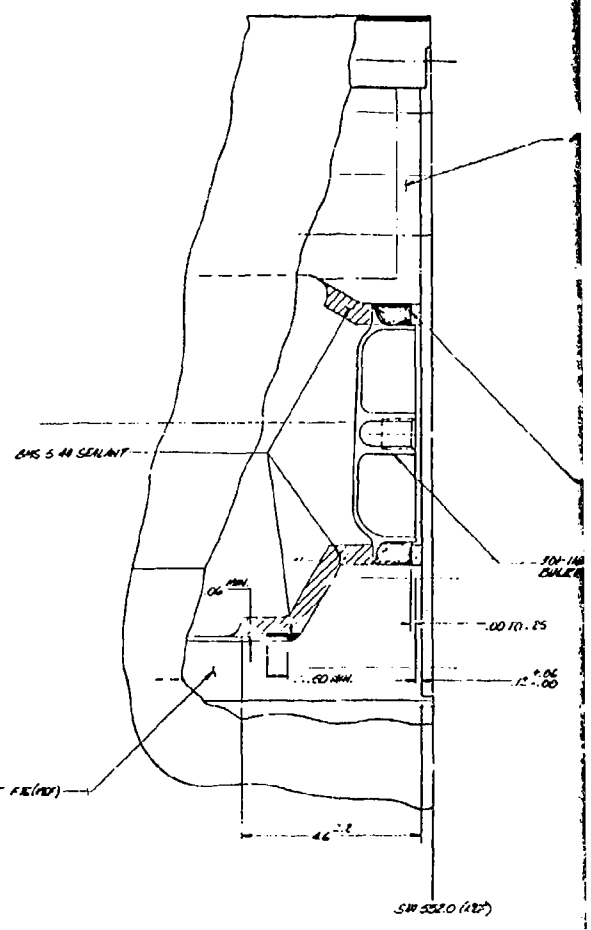
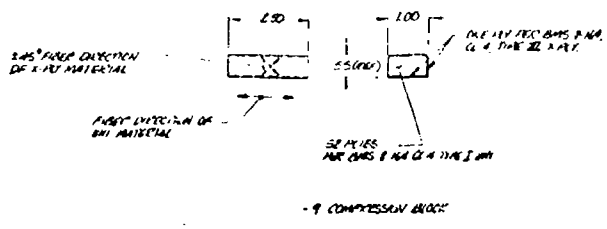
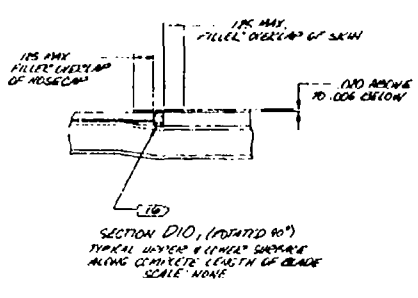
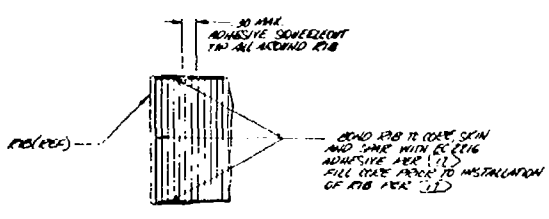
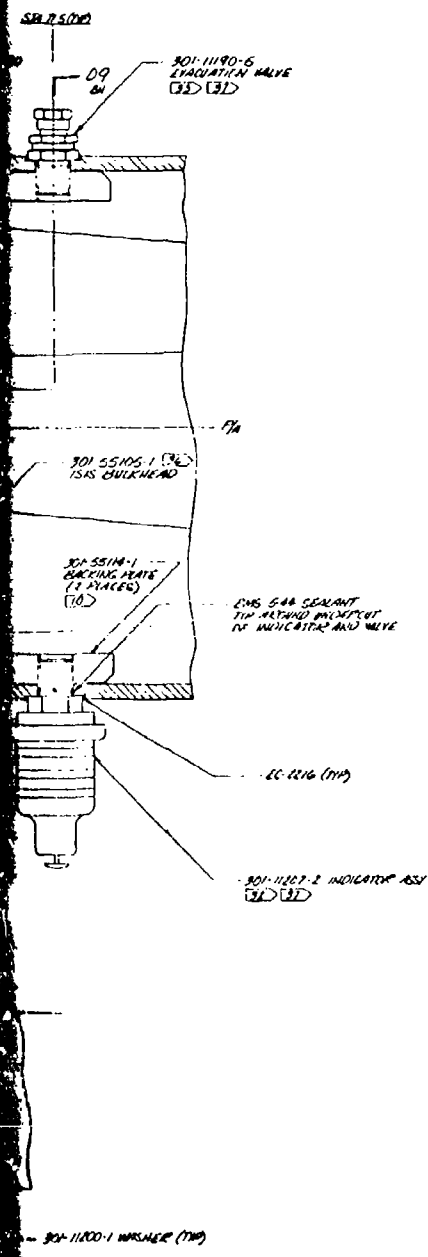
Figure 40. Continued

9

8

7

6



301-55.01 A3

9 8 7

WOP 301-11214 NOBECAP (REF) 301-65102 SPAR ASSY

301-55104 FAIRING ASSY

PIT

FIBER DIRECTION OF OUTER PLY OF -5 SKIN

45°12'

36 GB CONSTANT

FIBER DIRECTION OF INNER PLY OF -5 SKIN

45°12'

4000

10°

45°

45°12'

45°12'

-10 STRIP 2 PLY

-5 SKIN - 1 PLY

-4 SKIN - 1 PLY

FIBERS IN STRIP TO BE PARALLEL TO LENGTH & TO CONTINUE

-1 BONDED ASSY. AIT (SHN)
-2 BONDED ASSY. PAD (OPF)

FIBER DIRECTION OF OUTER PLY OF -4 SKIN

FIBER DIRECTION OF INNER PLY OF -4 SKIN

301-1 TE WEDGE (REF)

EOP - 7 SKIN
-18 DOUBLER
-19 SKIN
-9 DOUBLER

EOP - 4 SKIN, STA 1410-5550.0

-18 DOUBLER & 1 PLY STA 139-226.8 (10° WHT)

-19 (0° WHT) 1 PLY STA 140-5550.0

-17 SKIN (10° WHT) 1 PLY, STA 1410-411.00

DETAIL AT (EOP-2 ASSY)

301-1116-2 (REF)

(1)

301-1116-2 INSERT
24-9678 ADHESIVE (2 PLYS)

SECTION B9

INSERTS TO BE FLUSH WITH SPAR HULL

301-55103 SPAR (REF)

SM 1580 (REF)

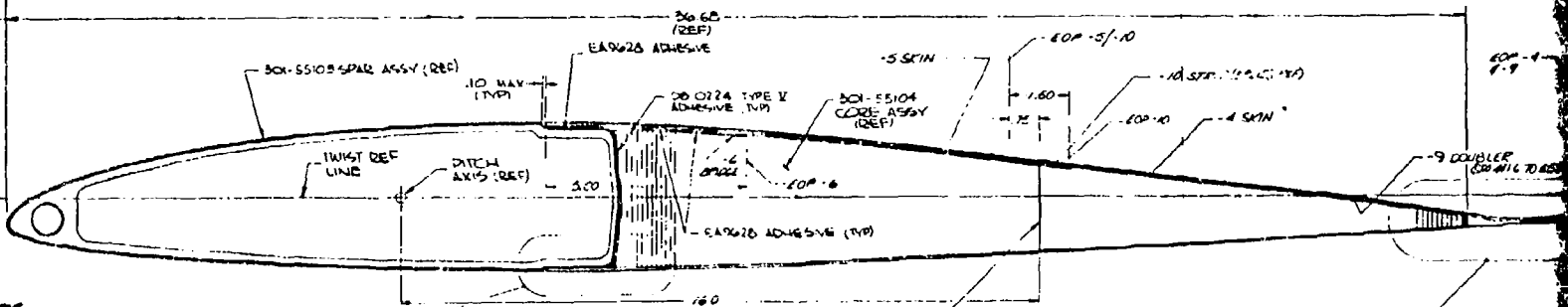
DB 0224 TYPE X ADHESIVE

10 (REF)

VIEW D11

B9

4000 (REF)



301-55102 SPAR ASSY (REF)

EA9628 ADHESIVE

-5 SKIN

EOP - 5/10

-10 STRIP (2 PLYS) (REF)

EOP - 10

-4 SKIN

EOP - 4/9

WING REF LINE

DITCH AXIS (REF)

500

36 GB (REF)

EA9628 ADHESIVE

DB 0224 TYPE X ADHESIVE (TYP)

301-55104 CORE ASSY (REF)

10 (REF)

EOP - 6

EA9628 ADHESIVE (TYP)

1.60

75

0.1" SPACE, SM 5510 TO STA 5550.0 (REF)

SECTION AT EOP - 2, AND B9 ASSY ONLY



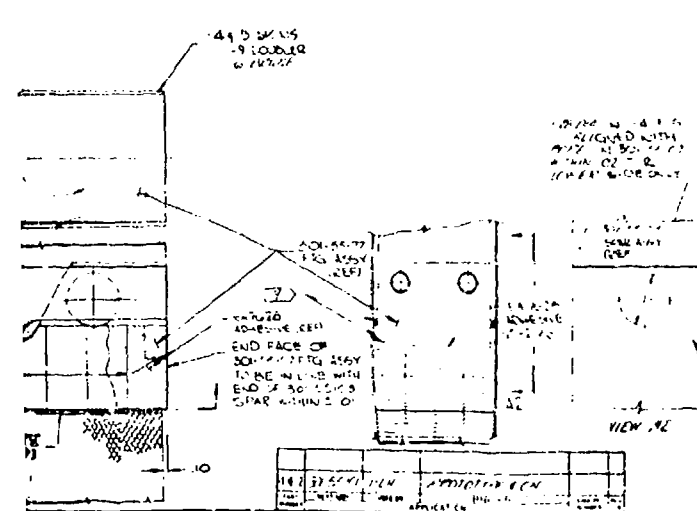
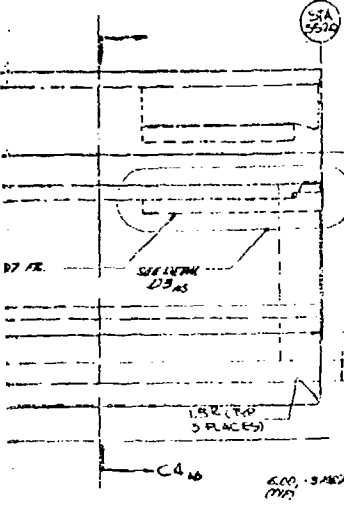
SECTION C4 ROTATED 90° (FULL SCALE)

301-55102B11

9 8 7

NOTES CONTINUED

- (K) IN PLACES OF BUSHING ASSETS AND ON 65471 FITTING CHANGES... (SEE DRAWING 301-55100 FOR DETAILS)
- (L) SEE DRAWING 301-55100 FOR DETAILS... (SEE DRAWING 301-55100 FOR DETAILS)
- (M) SEE DRAWING 301-55100 FOR DETAILS... (SEE DRAWING 301-55100 FOR DETAILS)



REV	DATE	BY	CHKD	APP'D	REVISION
1					
2					

2. FABRICATE PER DRAWING DOC 0301-10134-1.
3. CHORDWISE BOND OF ASSY TO BE MAX. OF .50 IN OR ART MEASURED BETWEEN STATION 158 & 552.
4. OUTSIDE CONTOUR OF ASSY TO MATCH BLADE BASIC OML DEFINED BY DRAWING DOC 0301-10136 WITHIN ±.05.
5. FLAPWISE BOND OF ASSY MEASURED WITH ASSY STANDING ON ITS LEADING EDGE TO BE .50 MAX IN EITHER DIRECTION BETWEEN STATION 158 & 552.
6. BONDED ASSY TO BE INSPECTED PER WORKING INSPECTION PROCEDURE DOC 0301-10157.
7. TAKE ALL CRITICAL PARTS ASSEMBLY AND ACQUIRE ALL TESTS AND REPORTS... (SEE DRAWING 301-55100 FOR DETAILS)

NO.	DESCRIPTION	QTY	UNIT	REMARKS
1	301-1126-2	1	WASHER	OH
2	301-1126-1	1	WASHER	OH
3	301-1126-1	1	WASHER	OH
4	0301-10157	1	INSPECTION DOCUMENT	OH
5	0301-10156	1	INSPECTION DOCUMENT	OH
6	0301-10155	1	INSPECTION DOCUMENT	OH
7	DB-0274	1	ADHESIVE SPEC	(FM-57)
8	BA 967A	1	ADHESIVE	PER 0301-10134-1
9	BA 967A	1	ADHESIVE	PER 0301-10134-1
10	BA 967A	1	ADHESIVE	PER 0301-10134-1
11	BA 967A	1	ADHESIVE	PER 0301-10134-1
12	BA 967A	1	ADHESIVE	PER 0301-10134-1
13	BA 967A	1	ADHESIVE	PER 0301-10134-1
14	BA 967A	1	ADHESIVE	PER 0301-10134-1
15	BA 967A	1	ADHESIVE	PER 0301-10134-1
16	BA 967A	1	ADHESIVE	PER 0301-10134-1
17	BA 967A	1	ADHESIVE	PER 0301-10134-1
18	BA 967A	1	ADHESIVE	PER 0301-10134-1
19	BA 967A	1	ADHESIVE	PER 0301-10134-1
20	BA 967A	1	ADHESIVE	PER 0301-10134-1
21	BA 967A	1	ADHESIVE	PER 0301-10134-1
22	BA 967A	1	ADHESIVE	PER 0301-10134-1
23	BA 967A	1	ADHESIVE	PER 0301-10134-1
24	BA 967A	1	ADHESIVE	PER 0301-10134-1
25	BA 967A	1	ADHESIVE	PER 0301-10134-1
26	BA 967A	1	ADHESIVE	PER 0301-10134-1
27	BA 967A	1	ADHESIVE	PER 0301-10134-1
28	BA 967A	1	ADHESIVE	PER 0301-10134-1
29	BA 967A	1	ADHESIVE	PER 0301-10134-1
30	BA 967A	1	ADHESIVE	PER 0301-10134-1
31	BA 967A	1	ADHESIVE	PER 0301-10134-1
32	BA 967A	1	ADHESIVE	PER 0301-10134-1
33	BA 967A	1	ADHESIVE	PER 0301-10134-1
34	BA 967A	1	ADHESIVE	PER 0301-10134-1
35	BA 967A	1	ADHESIVE	PER 0301-10134-1
36	BA 967A	1	ADHESIVE	PER 0301-10134-1
37	BA 967A	1	ADHESIVE	PER 0301-10134-1
38	BA 967A	1	ADHESIVE	PER 0301-10134-1
39	BA 967A	1	ADHESIVE	PER 0301-10134-1
40	BA 967A	1	ADHESIVE	PER 0301-10134-1
41	BA 967A	1	ADHESIVE	PER 0301-10134-1
42	BA 967A	1	ADHESIVE	PER 0301-10134-1
43	BA 967A	1	ADHESIVE	PER 0301-10134-1
44	BA 967A	1	ADHESIVE	PER 0301-10134-1
45	BA 967A	1	ADHESIVE	PER 0301-10134-1
46	BA 967A	1	ADHESIVE	PER 0301-10134-1
47	BA 967A	1	ADHESIVE	PER 0301-10134-1
48	BA 967A	1	ADHESIVE	PER 0301-10134-1
49	BA 967A	1	ADHESIVE	PER 0301-10134-1
50	BA 967A	1	ADHESIVE	PER 0301-10134-1

NO.	DESCRIPTION	QTY	UNIT	REMARKS
1	BA 967A	1	ADHESIVE	PER 0301-10134-1
2	BA 967A	1	ADHESIVE	PER 0301-10134-1
3	BA 967A	1	ADHESIVE	PER 0301-10134-1
4	BA 967A	1	ADHESIVE	PER 0301-10134-1
5	BA 967A	1	ADHESIVE	PER 0301-10134-1
6	BA 967A	1	ADHESIVE	PER 0301-10134-1
7	BA 967A	1	ADHESIVE	PER 0301-10134-1
8	BA 967A	1	ADHESIVE	PER 0301-10134-1
9	BA 967A	1	ADHESIVE	PER 0301-10134-1
10	BA 967A	1	ADHESIVE	PER 0301-10134-1
11	BA 967A	1	ADHESIVE	PER 0301-10134-1
12	BA 967A	1	ADHESIVE	PER 0301-10134-1
13	BA 967A	1	ADHESIVE	PER 0301-10134-1
14	BA 967A	1	ADHESIVE	PER 0301-10134-1
15	BA 967A	1	ADHESIVE	PER 0301-10134-1
16	BA 967A	1	ADHESIVE	PER 0301-10134-1
17	BA 967A	1	ADHESIVE	PER 0301-10134-1
18	BA 967A	1	ADHESIVE	PER 0301-10134-1
19	BA 967A	1	ADHESIVE	PER 0301-10134-1
20	BA 967A	1	ADHESIVE	PER 0301-10134-1
21	BA 967A	1	ADHESIVE	PER 0301-10134-1
22	BA 967A	1	ADHESIVE	PER 0301-10134-1
23	BA 967A	1	ADHESIVE	PER 0301-10134-1
24	BA 967A	1	ADHESIVE	PER 0301-10134-1
25	BA 967A	1	ADHESIVE	PER 0301-10134-1
26	BA 967A	1	ADHESIVE	PER 0301-10134-1
27	BA 967A	1	ADHESIVE	PER 0301-10134-1
28	BA 967A	1	ADHESIVE	PER 0301-10134-1
29	BA 967A	1	ADHESIVE	PER 0301-10134-1
30	BA 967A	1	ADHESIVE	PER 0301-10134-1

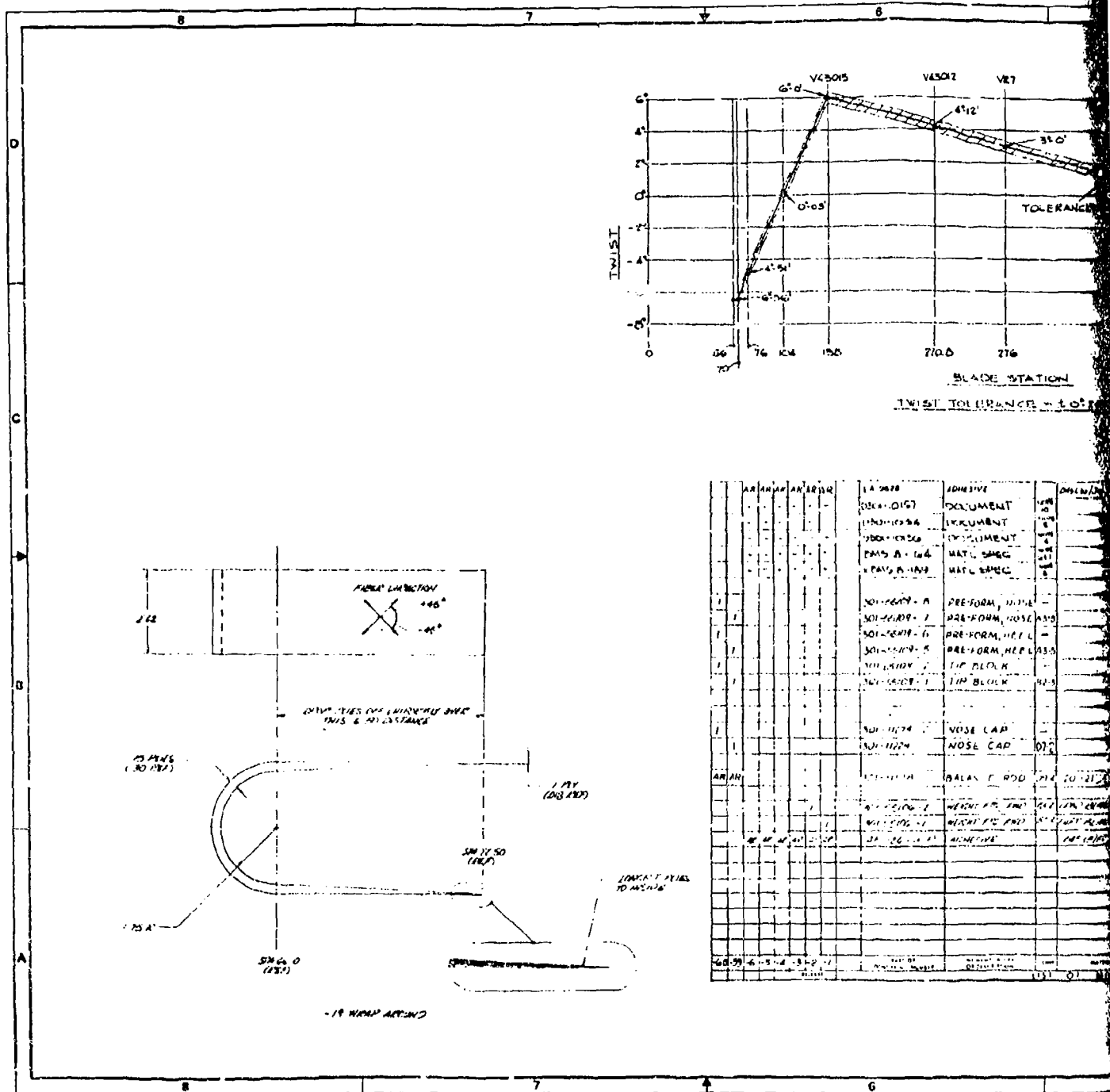
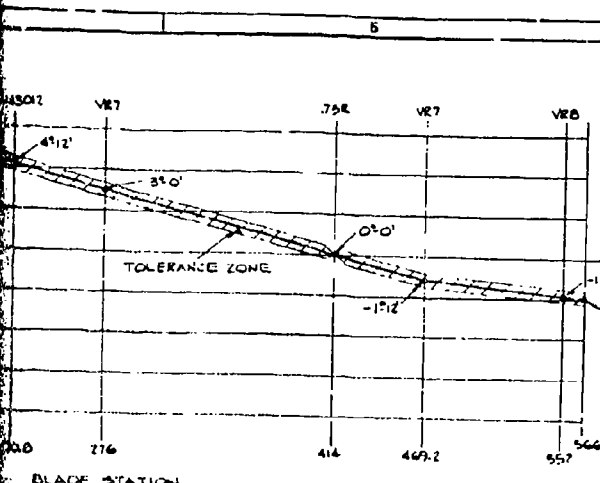


Figure 42. Spar Assembly Two-Pin, Fittingless HLH Rotor Blade



- 26 ADD 0.1" OF INTERLAYER RESIN AS IT GOES TO IMPROVE A SMOOTH TRANSITION OF .55 & .37 TO UNIT SPARK FRACES
- 27 ADD ONE PLY OF EA-9301 ADHESIVE IN THIS AREA PER D301-10154-1
- 28 PREPARE 7.75" BOND BY WIPING DECREASE METHOD PER D301-10154-1
- 29 ADD ONE PLY OF EA-9301 ADHESIVE BETWEEN .41 & .45, PER D301-10154-1
- 30 CURE THE SPACER STRIP THE .41 & .45 WILL COVER 2010 IN THIS AREA. IF FACILITY PERMITS ONE SET OF EA-9301 ADHESIVE MAY BE APPLIED OVER .41 & .45, 1.00 WIDE, PER .41 & .45 SPAN
- 31 PLACE 10 WIDE STRIPS OF EA-9301 ADHESIVE OVER .41 AND .45 IN A 4" x 4" SQUARE FROM STA 505.0 START AT 21.0 (TOP), ELEVATION 1.200 @ BOTTOM
- 32 THE 10 WIDE EA-9301 ADHESIVE STRIPS ARE TO BE POSITIONED FROM THE BOTTOM EDGE TO THE TOP. ONLY THE BOTTOMS OF CONTACT AREA STRIPS TO BE POSITIONED. THE STRIPS TO BE POSITIONED AT 500 INCHES FROM THE 10 WIDE STRIPS WITH 10 WIDE SPACES AND ALL LAYERS AND UNITS OF STRIP BOND
- 33 VERIFY THE INSTALLATION OF EACH STRIP WITH THIS AREA MAY BE FACILITY FROM A FLIGHT STRIP. THE 10 WIDE UNITS MUST BE A MINIMUM OF ONE PLY OF ADHESIVE. THE UNITS MUST BE AT EACH LOCATION - CHECK FOR EACH STRIP

- 16 APPLY ADHESIVE PER D301-10154-1
- 17 CAUTION TO EXERCISE IN HANDLING & THRU-OUT FAB CYCLE OF THESE SUB-ASSYS TO AVOID MARKING, SCRATCHING, TWISTING OR ABUSE WHICH COULD BE DETRIMENTAL TO THE HIGH QUALITY OF THIS STRUCTURE.
- 18 MATERIAL PER: BMS 3-20, TYPE 2, FILLER COMPOUND.
- 19 .45 IS THE SAME AS SK-301-10168-1B, TRIMMED TO 1.5 DIMENSION SAME IN ZONE A2-3.
- 20 BALANCE RODS OF NOS 301-11178-5 & 6 TO BE SELECTED PER WEIGHT & BALANCE DOC U-301-10155-1.
- 21 PRIOR TO INSTALLING 301-11178 BALANCE RODS, WRAP WITH ONE LAYER OF ADHESIVE PER DOC. D-301-10154-1
- 22 MAT'L PER BMS B-164 CLASS A, TYPE 1 (2.62" WIDE) WITH LEAD TRACER PER D-301-10154-1.
- 23 LOCATION OF 22 AND 23 SHOWN ON SHEET 5.
- 24 THIS IS A CORE OF OPTICAL PAINT AND PROVIDES ALL POSITIVE MARKERS SPECIFIED IN AFS 14.00
- 25 THE END ITEM KNITTED MESH WIRE 12.21 OY 1.50 SINGLE PLY. COARSE PLY. PAPER CORE. PER NEW DRAWING PD EDITION 1.1
- 26 .41 & .45 ARE MADE UP OF SIX PLYS OF ALTERNATING 2.45" FIBER MESH
- 27 THIS SUB-ASSY IS PREFORMATED AND ASSEMBLED AT NETS ASY INCH 62

BLADE STATION
TOLERANCE = ±0.20

ADHESIVE	QTY	UNIT	DESCRIPTION
ADHESIVE			D301-10154-1
DOCUMENT			
DOCUMENT			
DOCUMENT			
MAT'L W/REG			
MAT'L W/REG			
PRE-FORM, NOSE			
PRE-FORM, NOSE			
PRE-FORM, NOSE			
PRE-FORM, NOSE			
PRE-FORM, NOSE			
TIP BLOCK			
TIP BLOCK			
NOSE CAP			
NOSE CAP			
BALANCE ROD			
MESH WIRE			
MESH WIRE			
ADHESIVE			

QTY	UNIT	DESCRIPTION
66	BOND	
67	INTER STRIP	
68	PREP INNER SKIN	
69	PREP LOWER	
70	PREP INNER SKIN	
71	PREP LOWER	
72	PREP INNER SKIN	
73	PREP LOWER	
74	PREP INNER SKIN	
75	PREP LOWER	
76	NOSE CAP ASST	
77	NOSE ST	
78	WEDGE UPPER	
79	WEDGE LOWER	
80	WEDGE LOWER	
81	WEDGE LOWER	
82	WEDGE LOWER	
83	WEDGE LOWER	
84	WEDGE LOWER	
85	WEDGE LOWER	
86	WEDGE LOWER	
87	WEDGE LOWER	
88	WEDGE LOWER	
89	WEDGE LOWER	
90	WEDGE LOWER	
91	WEDGE LOWER	
92	WEDGE LOWER	
93	WEDGE LOWER	
94	WEDGE LOWER	
95	WEDGE LOWER	
96	WEDGE LOWER	
97	WEDGE LOWER	
98	WEDGE LOWER	
99	WEDGE LOWER	
100	WEDGE LOWER	

301-55103/41

1-2-301-220-62 PROTOTYPE

2

AS ADD TO REVISE
"301-51 TO INV. 50A"
ADHESIVE IN THE AREA
INCREASE METHOD
THINNESS BETWEEN -41-43,
44-45 WILL BE CUT TO 0.025 IN THIS
AREA THE 1/16 IN. ADHESIVE
WILL BE 1.00 INCH, THE 1/16 IN. SPACER
WILL BE 1/16 IN. ADHESIVE OVER -41
AND 1/16 IN. SPACER 305.0 SPACER
WILL BE 1/16 IN. ADHESIVE.

THIS AREA TO BE PROTECTED FROM
CONTACT WITH THE SURFACE OF THE
PART. IT MAY BE REMOVED TO REPAIR
OR REWORK. THE SURFACE OF THE
PART SHOULD BE KEPT CLEAN.
NOTE: THE NEW THIS AREA WILL
BE PROTECTED WITH A 1/16 IN. ADHESIVE
WILL BE 1.00 INCH, THE 1/16 IN. SPACER
WILL BE 1/16 IN. ADHESIVE.

- (16) APPLY ADHESIVE PER D301-10154-1
- (17) CAUTION TO EXERCISED IN HANDLING & THRU-OUT
FAB CYCLE OF THESE SUB-ASSYS TO AVOID MARKING
SCRATCHING, TWISTING, OR ABUSE WHICH COULD BE
DETRIMENTAL TO THE HIGH QUALITY OF THIS STRUCTURE.
- (18) MATERIAL PER:
BMS 5-28, TYPE 2, FILLER COMPOUND.
- (19) -45 IS THE SAME AS 301-10160-10, TRIMMED TO
1.5 DIMENSION SA-MIN IN ZONE A2-3.
- (20) BALANCE RODS, PT NOS 301-11174-5 & -6 TO BE SELECTED
PER WEIGHT & BALANCE DOC D301-10155-1
- (21) PRIOR TO INSTALLING 301-11178 BALANCE RODS, WRAP
WITH ONE LAYER OF ADHESIVE PER DOC D301-10154-1
- (22) MAT'L PER BMS 8-16 CLASS A, TYPE I (2.62" WIDE)
WITH LEAD TRACER PER D301-10154-1.
- (23) LOCATION OF (23) AND (22) SHOWN ON SHEET 5.
- (24) THIS IS A CLASS C FIBER AND PROVIDES ALL
FIBER PROPERTIES SPECIFIED IN AS M. 02.
- (25) THE DR ALUM FINISHED MESH WIRE, 1/2 IN. DIA. SINGLE WIRE,
OBTAIN FROM: METEL CORP. 700 NEW BRUNSWICK RD EDISON, N.J.
- (26) -43-48 THE WIRE OF SIX PAGES OF ALTERNATIVE 246"
FIBER MESH.
- (27) THIS SUB ASSY IS INVESTIGATED QND, AND INSTALLED AT
LAST ASSY DRAWING.

- NOTES
1. THIS IS A CLASS C FIBER AND PROVIDES ALL FIBER PROPERTIES SPECIFIED IN AS M. 02.
 2. FABRICATE PER DOCUMENT D301-10154-1
 3. BLADE GEOMETRY PER DRAWING 301-11172
 4. SPAR CONTOURS PER DOCUMENT D301-10156-1
 - (28) MAT'L PER BMS 8-164 CL. A, TYPE I (2.62" WIDE)
 - (29) MAT'L PER BMS 8-164 CL. A, TYPE III
 - (30) MAT'L PER BMS 8-164 CL. A, TYPE I
 - (31) MAT'L PER BMS 8-180 TYPE II, CLASS A,
EXCEPT THE TRACER FIBER DOES NOT APPLY.
 - (32) LAY UP -11, -13, -15, -17 TWINS WITH FIBERS
45° ± 5° TO PITCH AXIS
 - (33) INSPECT ASSY PER BORING DOC
D301-10157
 - (34) OUTSIDE CONTOUR OF ASSY TO MATCH
BLADE CML PER DOC D301-10158 WITHIN ±.015.
 - (35) FURNISH FROM MAY BE 1/4 IN. OR BOTH
DIRECTIONS PROVIDED RATE OF BOW DOES
NOT EXCEED .005 INCHES PER FOOT OF
SPAR LENGTH.
 - (36) OVERLAP BOW TO BE 1.0 MAX
FWD OR AFT MEASURED BETWEEN STATION
150 & 552.
 - (37)
 - (38)

REV	DATE	DESCRIPTION	BY	CHKD
1	11/11/62			
2	11/11/62			
3	11/11/62			
4	11/11/62			
5	11/11/62			
6	11/11/62			

REV	DESCRIPTION	QTY	UNIT	REMARKS
62	BAND	1	EA	
63	INTERIOR STRIP	1	EA	
64	UPPER INNER SKIN	1	EA	
65	UPPER LOWER SKIN	1	EA	
66	UPPER LOWER SKIN	1	EA	
67	UPPER LOWER SKIN	1	EA	
68	UPPER LOWER SKIN	1	EA	
69	UPPER LOWER SKIN	1	EA	
70	UPPER LOWER SKIN	1	EA	
71	UPPER LOWER SKIN	1	EA	
72	UPPER LOWER SKIN	1	EA	
73	UPPER LOWER SKIN	1	EA	
74	UPPER LOWER SKIN	1	EA	
75	UPPER LOWER SKIN	1	EA	
76	UPPER LOWER SKIN	1	EA	
77	UPPER LOWER SKIN	1	EA	
78	UPPER LOWER SKIN	1	EA	
79	UPPER LOWER SKIN	1	EA	
80	UPPER LOWER SKIN	1	EA	
81	UPPER LOWER SKIN	1	EA	
82	UPPER LOWER SKIN	1	EA	
83	UPPER LOWER SKIN	1	EA	
84	UPPER LOWER SKIN	1	EA	
85	UPPER LOWER SKIN	1	EA	
86	UPPER LOWER SKIN	1	EA	
87	UPPER LOWER SKIN	1	EA	
88	UPPER LOWER SKIN	1	EA	
89	UPPER LOWER SKIN	1	EA	
90	UPPER LOWER SKIN	1	EA	
91	UPPER LOWER SKIN	1	EA	
92	UPPER LOWER SKIN	1	EA	
93	UPPER LOWER SKIN	1	EA	
94	UPPER LOWER SKIN	1	EA	
95	UPPER LOWER SKIN	1	EA	
96	UPPER LOWER SKIN	1	EA	
97	UPPER LOWER SKIN	1	EA	
98	UPPER LOWER SKIN	1	EA	
99	UPPER LOWER SKIN	1	EA	
100	UPPER LOWER SKIN	1	EA	

REV	DESCRIPTION	QTY	UNIT	REMARKS
30	UPPER LOWER SKIN	1	EA	
31	UPPER LOWER SKIN	1	EA	
32	UPPER LOWER SKIN	1	EA	
33	UPPER LOWER SKIN	1	EA	
34	UPPER LOWER SKIN	1	EA	
35	UPPER LOWER SKIN	1	EA	
36	UPPER LOWER SKIN	1	EA	
37	UPPER LOWER SKIN	1	EA	
38	UPPER LOWER SKIN	1	EA	
39	UPPER LOWER SKIN	1	EA	
40	UPPER LOWER SKIN	1	EA	
41	UPPER LOWER SKIN	1	EA	
42	UPPER LOWER SKIN	1	EA	
43	UPPER LOWER SKIN	1	EA	
44	UPPER LOWER SKIN	1	EA	
45	UPPER LOWER SKIN	1	EA	
46	UPPER LOWER SKIN	1	EA	
47	UPPER LOWER SKIN	1	EA	
48	UPPER LOWER SKIN	1	EA	
49	UPPER LOWER SKIN	1	EA	
50	UPPER LOWER SKIN	1	EA	
51	UPPER LOWER SKIN	1	EA	
52	UPPER LOWER SKIN	1	EA	
53	UPPER LOWER SKIN	1	EA	
54	UPPER LOWER SKIN	1	EA	
55	UPPER LOWER SKIN	1	EA	
56	UPPER LOWER SKIN	1	EA	
57	UPPER LOWER SKIN	1	EA	
58	UPPER LOWER SKIN	1	EA	
59	UPPER LOWER SKIN	1	EA	
60	UPPER LOWER SKIN	1	EA	
61	UPPER LOWER SKIN	1	EA	
62	UPPER LOWER SKIN	1	EA	
63	UPPER LOWER SKIN	1	EA	
64	UPPER LOWER SKIN	1	EA	
65	UPPER LOWER SKIN	1	EA	
66	UPPER LOWER SKIN	1	EA	
67	UPPER LOWER SKIN	1	EA	
68	UPPER LOWER SKIN	1	EA	
69	UPPER LOWER SKIN	1	EA	
70	UPPER LOWER SKIN	1	EA	
71	UPPER LOWER SKIN	1	EA	
72	UPPER LOWER SKIN	1	EA	
73	UPPER LOWER SKIN	1	EA	
74	UPPER LOWER SKIN	1	EA	
75	UPPER LOWER SKIN	1	EA	
76	UPPER LOWER SKIN	1	EA	
77	UPPER LOWER SKIN	1	EA	
78	UPPER LOWER SKIN	1	EA	
79	UPPER LOWER SKIN	1	EA	
80	UPPER LOWER SKIN	1	EA	
81	UPPER LOWER SKIN	1	EA	
82	UPPER LOWER SKIN	1	EA	
83	UPPER LOWER SKIN	1	EA	
84	UPPER LOWER SKIN	1	EA	
85	UPPER LOWER SKIN	1	EA	
86	UPPER LOWER SKIN	1	EA	
87	UPPER LOWER SKIN	1	EA	
88	UPPER LOWER SKIN	1	EA	
89	UPPER LOWER SKIN	1	EA	
90	UPPER LOWER SKIN	1	EA	
91	UPPER LOWER SKIN	1	EA	
92	UPPER LOWER SKIN	1	EA	
93	UPPER LOWER SKIN	1	EA	
94	UPPER LOWER SKIN	1	EA	
95	UPPER LOWER SKIN	1	EA	
96	UPPER LOWER SKIN	1	EA	
97	UPPER LOWER SKIN	1	EA	
98	UPPER LOWER SKIN	1	EA	
99	UPPER LOWER SKIN	1	EA	
100	UPPER LOWER SKIN	1	EA	

1-2	301-51/52/53/54/55/56/57/58/59/60/61/62	PROTOTYPE
-----	---	-----------

1	301-51/52/53/54/55/56/57/58/59/60/61/62	PROTOTYPE
---	---	-----------

1	301-51/52/53/54/55/56/57/58/59/60/61/62	PROTOTYPE
---	---	-----------

SPAR ASSEMBLY
TWO PIN - FITTINGLESS
HLH ROTOR BLADE
J7722 301-55103

3

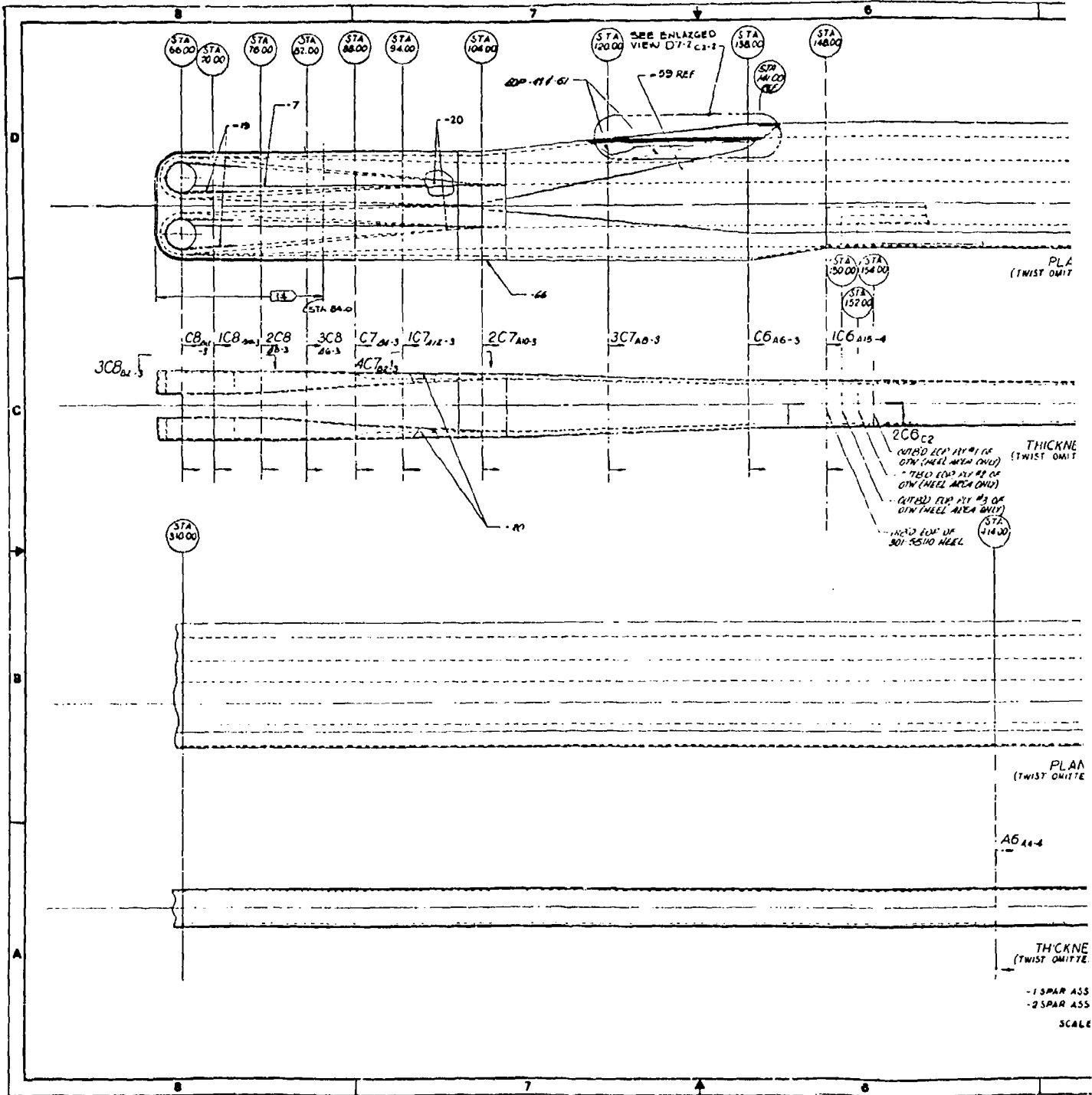
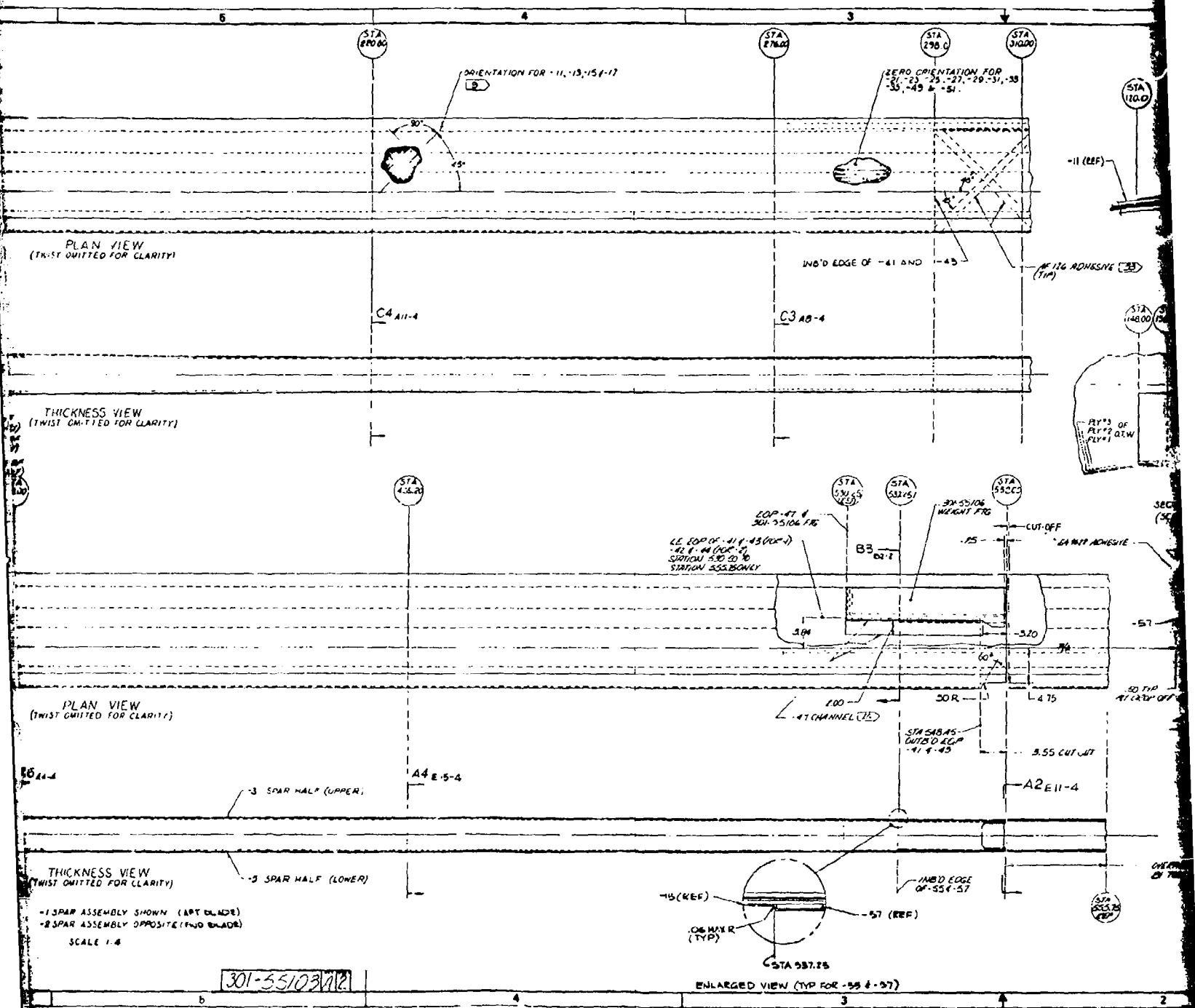
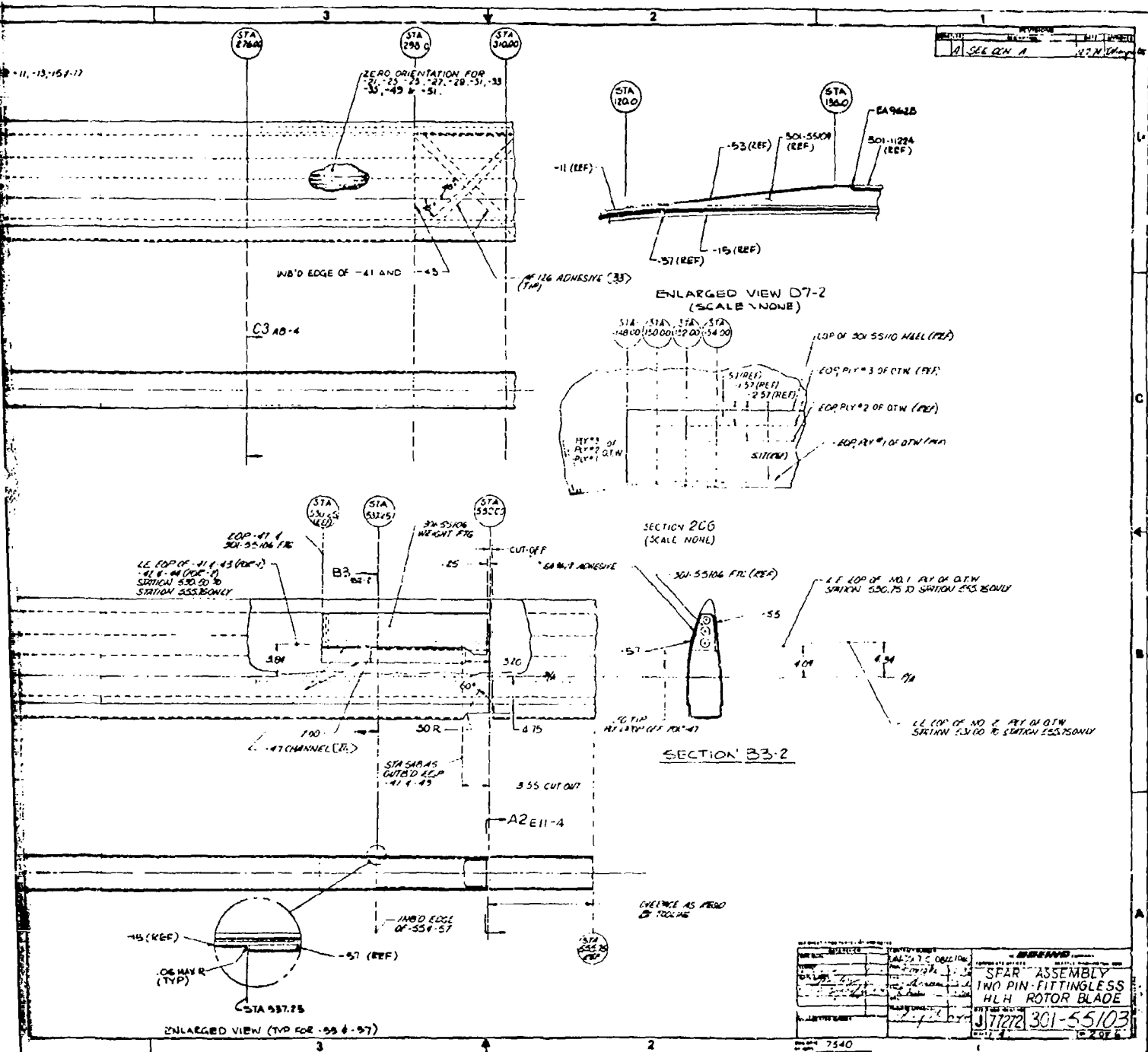


Figure 42. Continued



2



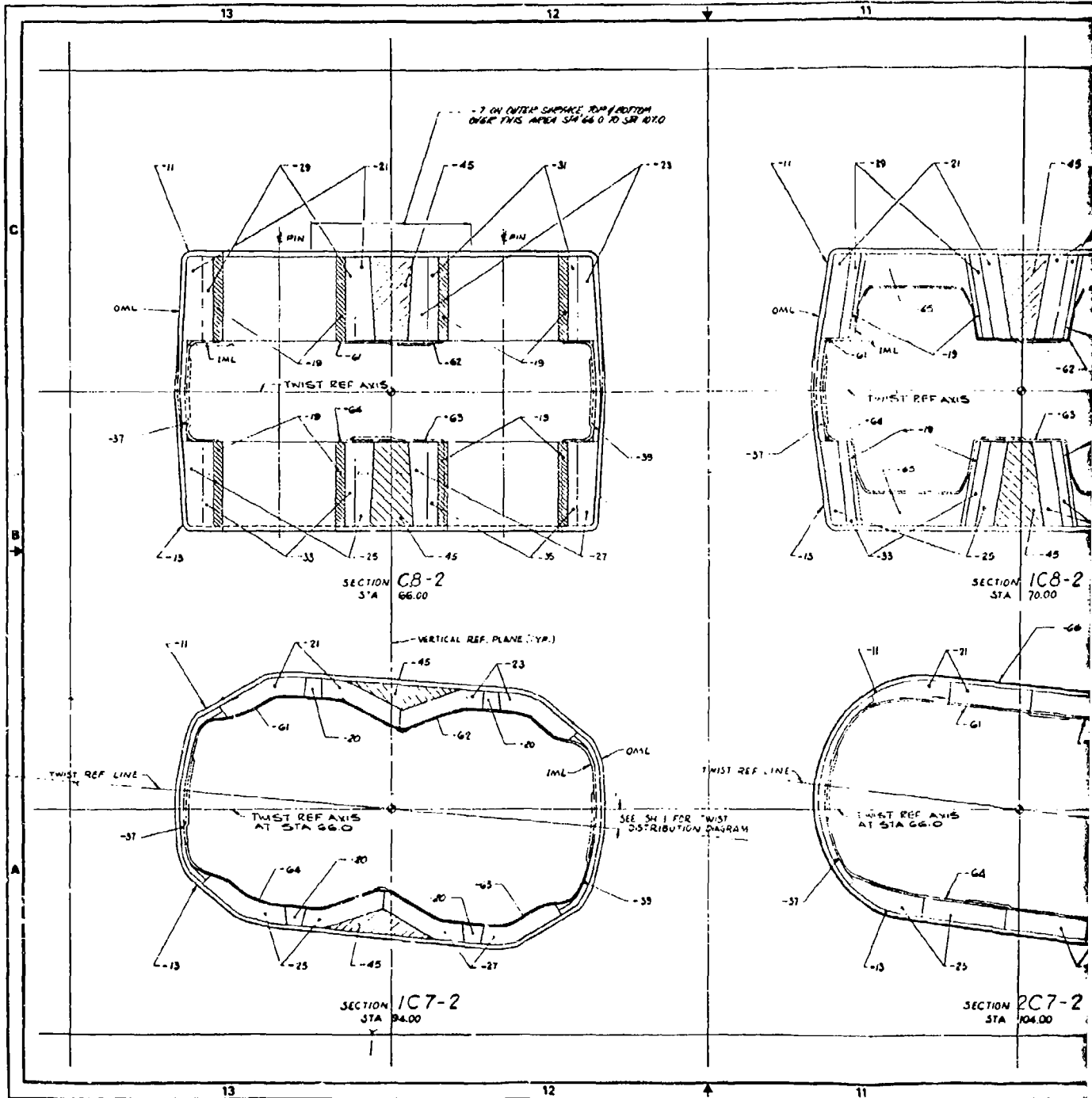
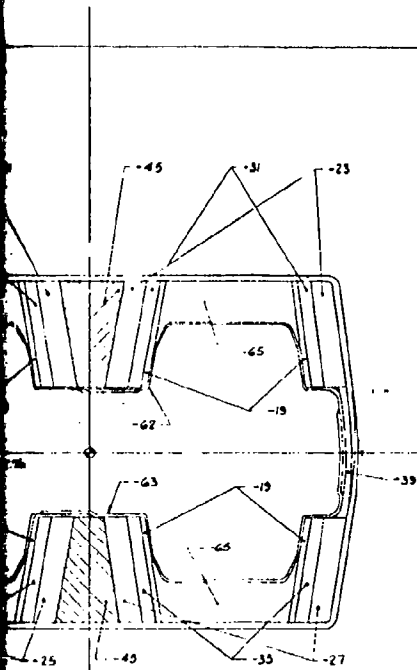
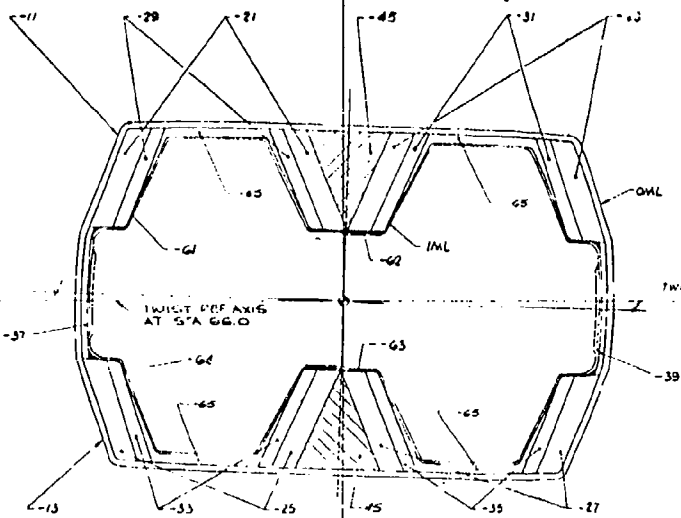


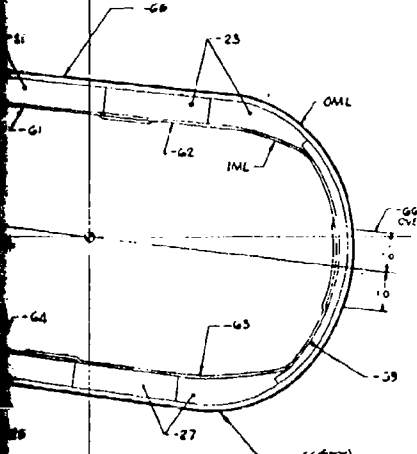
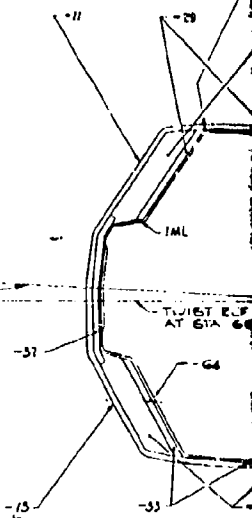
Figure 42. Continued



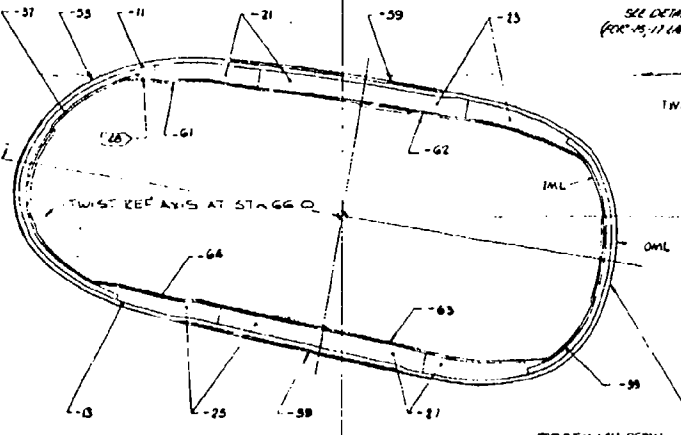
SECTION 1C8-2
STA 70.00



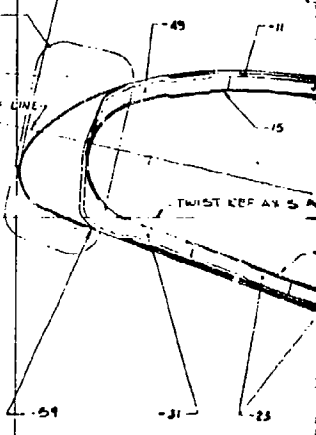
SECTION 2C8-2
STA 76.00



SECTION 2C7-2
STA 106.00

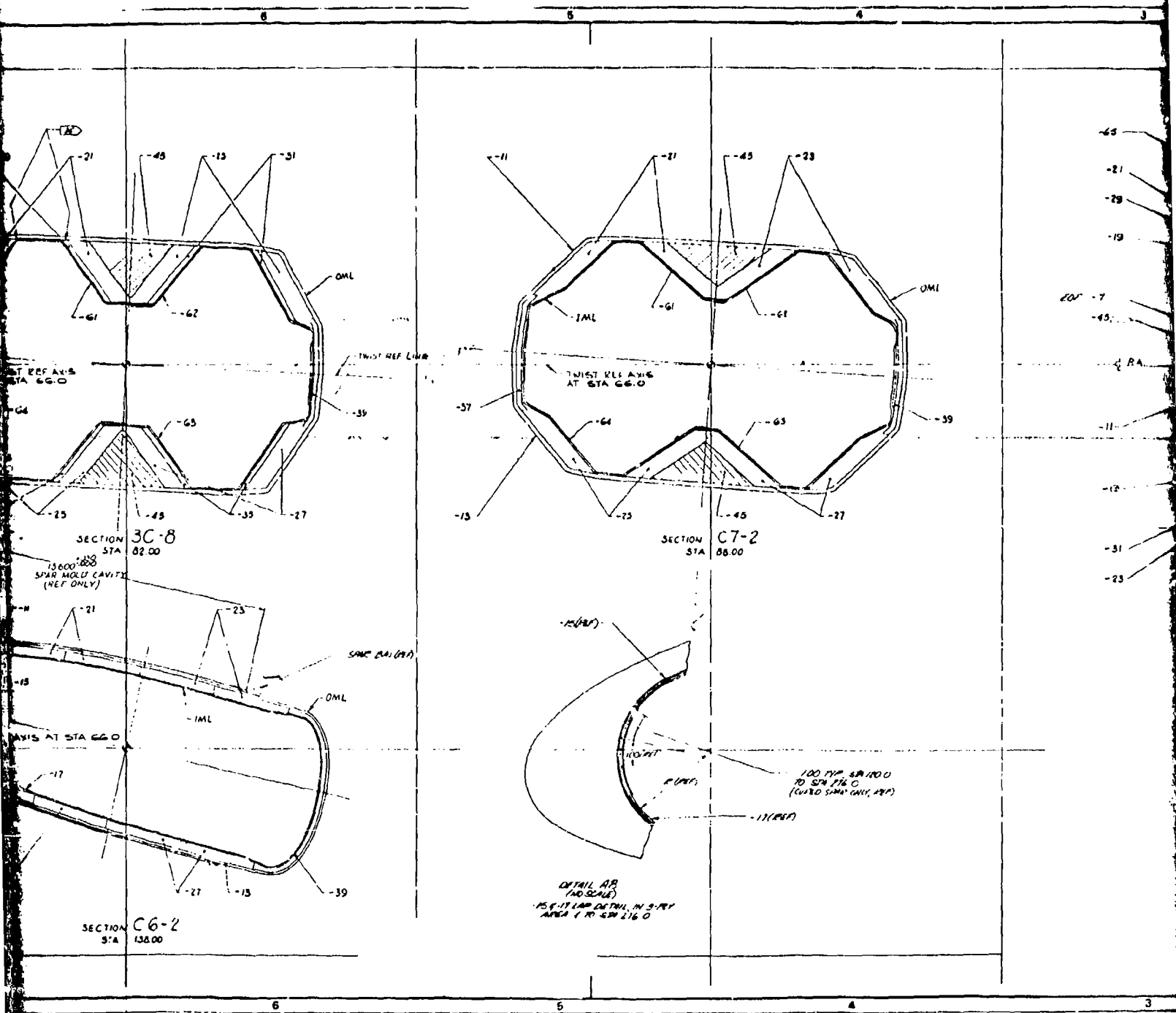


SECTION 3C7-2
STA 120.00

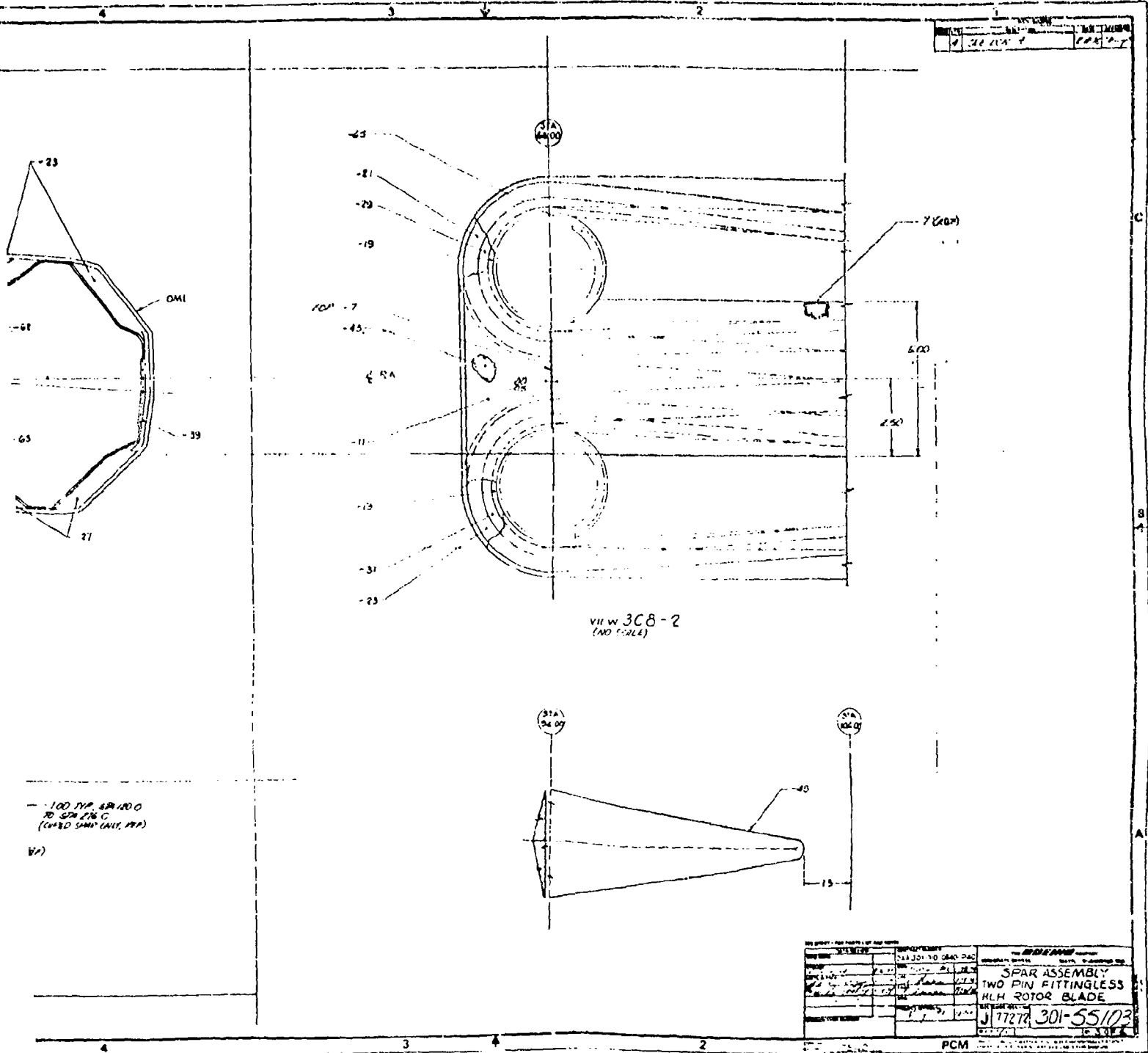


301-55103/13

2



3



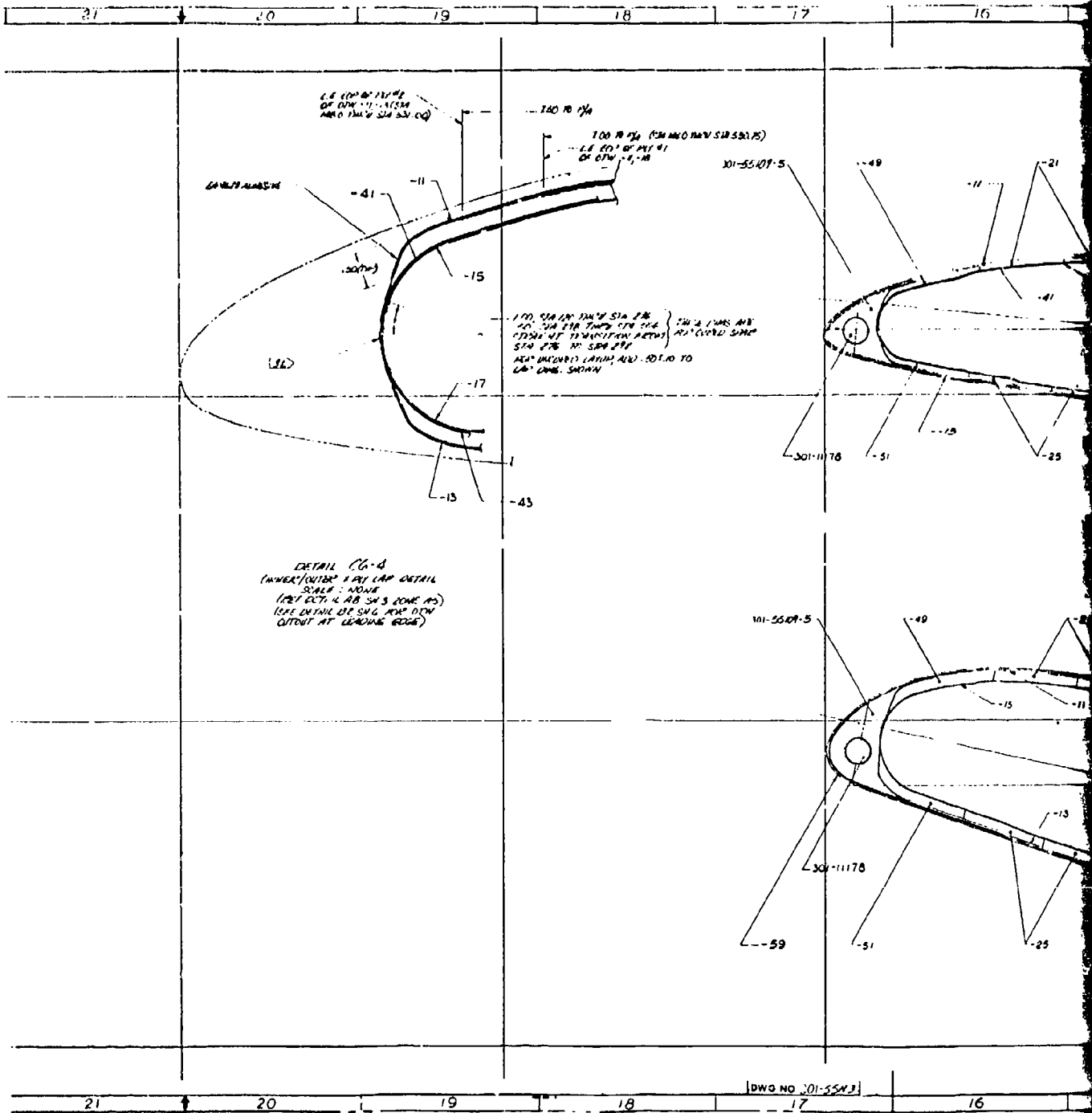
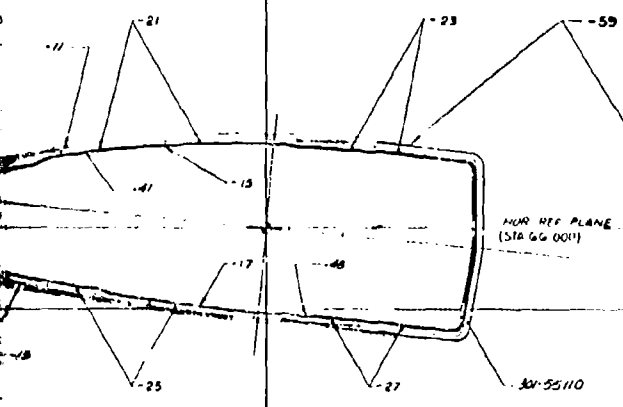
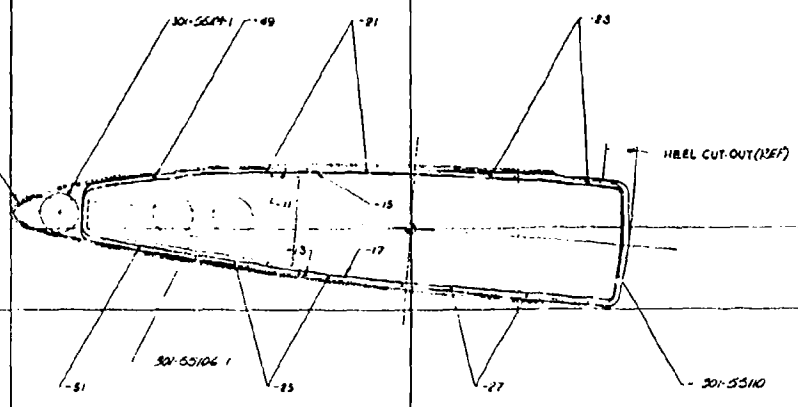


Figure 42. Continued

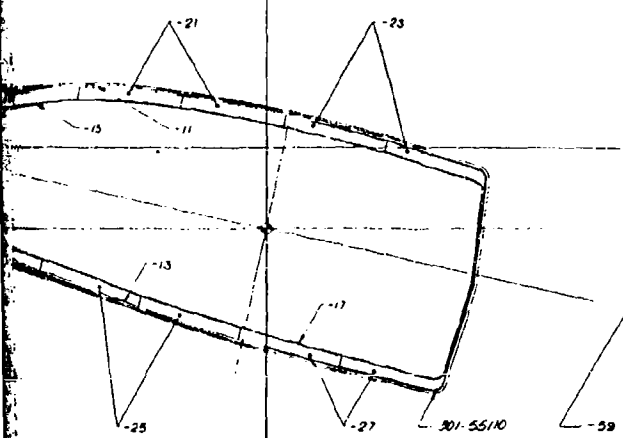
16 15 14 13 12 11 10



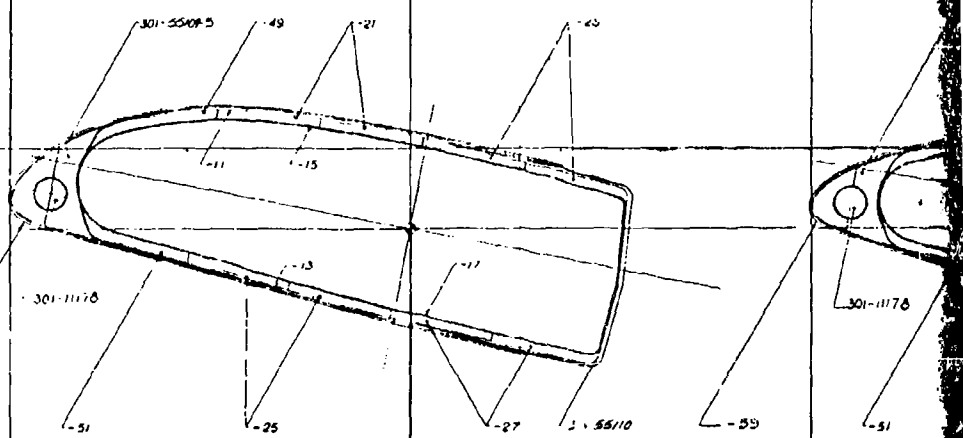
SECTION A4-2
STA 469.20



SECTION A2-2
STA 552.00



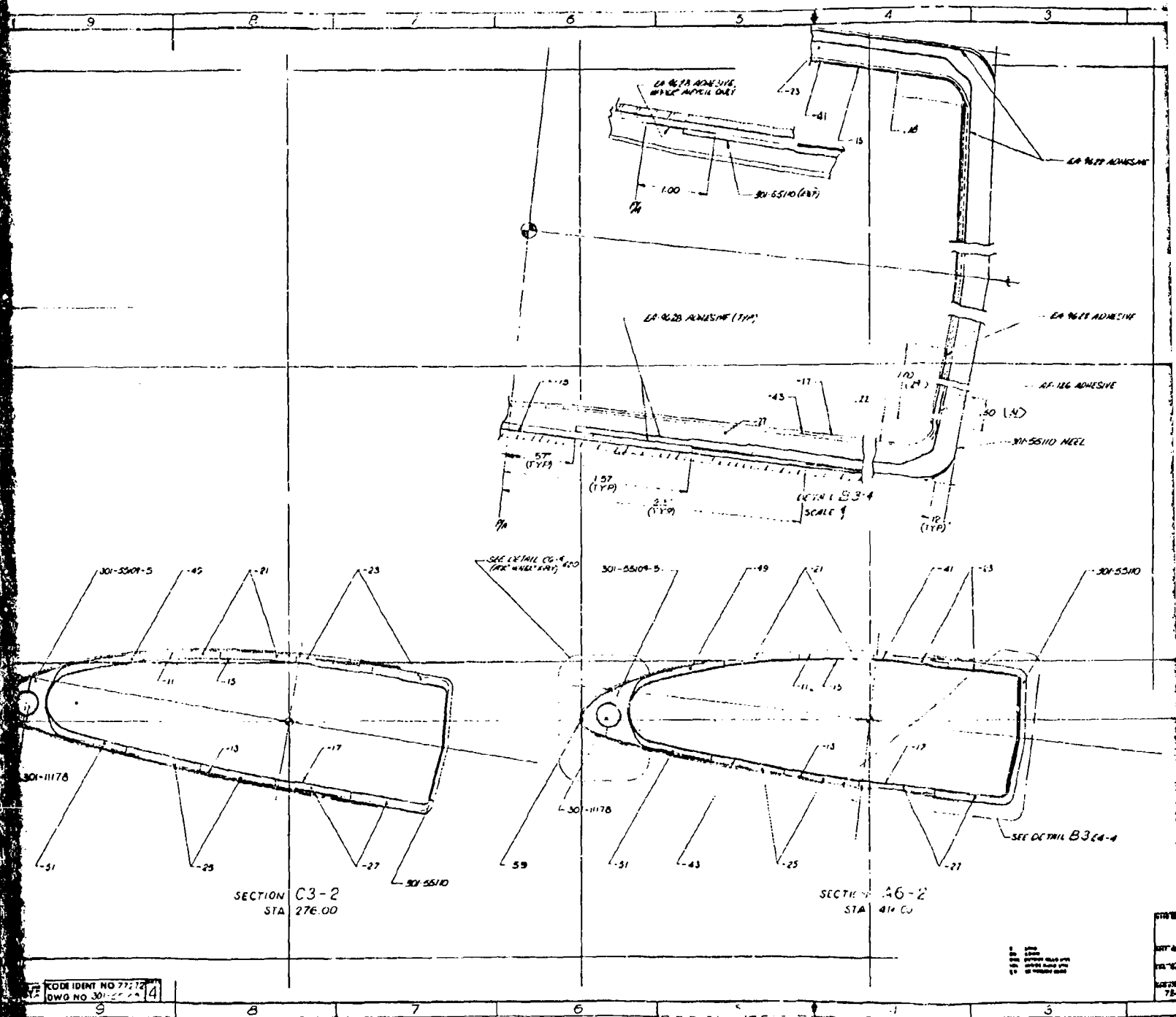
SECTION 1C6-2
STA 148.00



SECTION C4-2
STA 220.80

16 15 14 13 12 11 10

KODS IDB
DWG NO.



SECTION C3-2
STA 276.00

SECTION A6-2
STA 414.00

KODE IDENT NO 77272
DWG NO 301-5510-14

NOTES:
1. ALL DIMENSIONS ARE IN METERS
2. UNLESS OTHERWISE SPECIFIED,
ALL MATERIALS SHALL BE AS SHOWN
ON THE DRAWING

DATE: 11/14/60
SCALE: 75:1

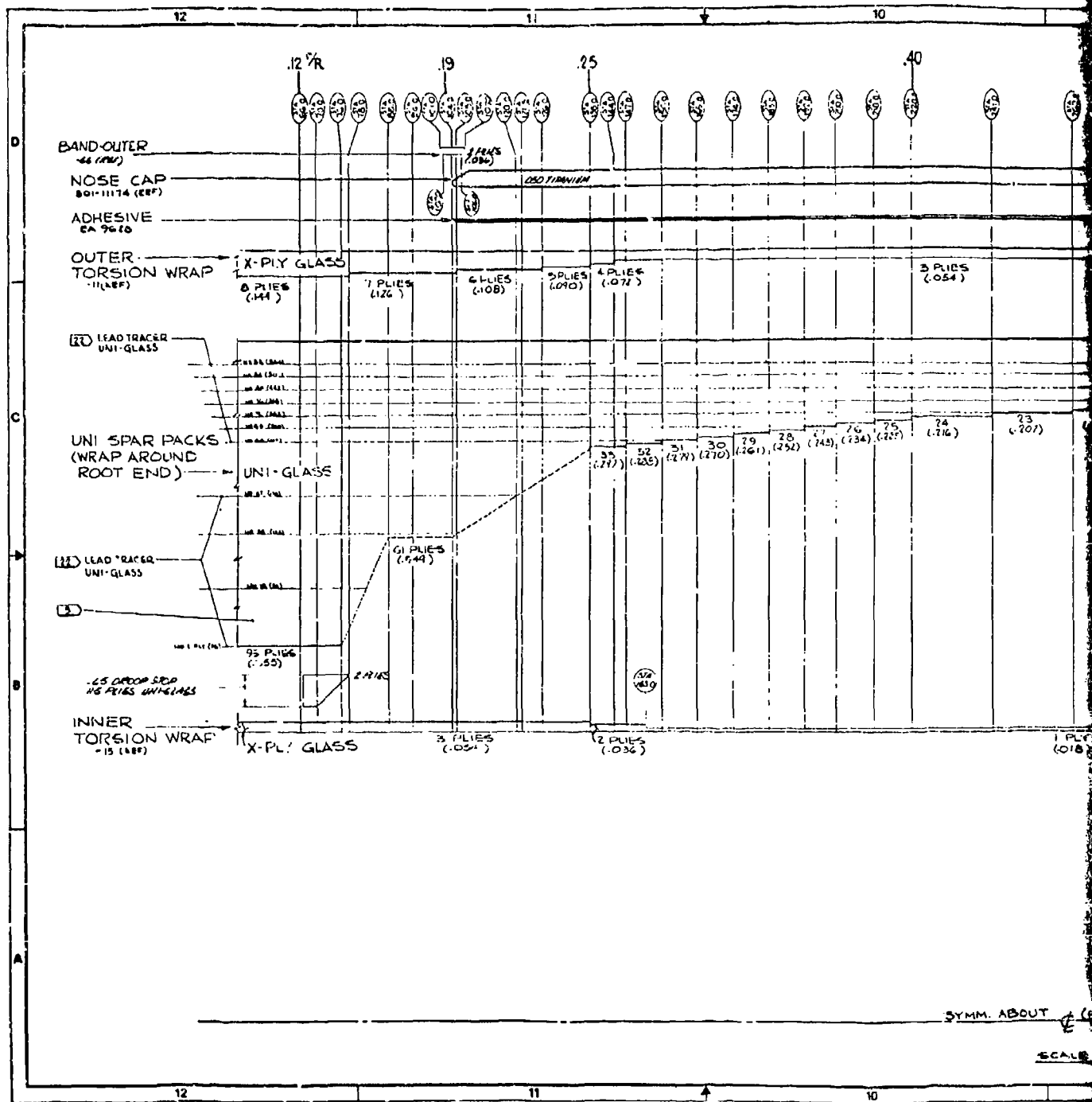
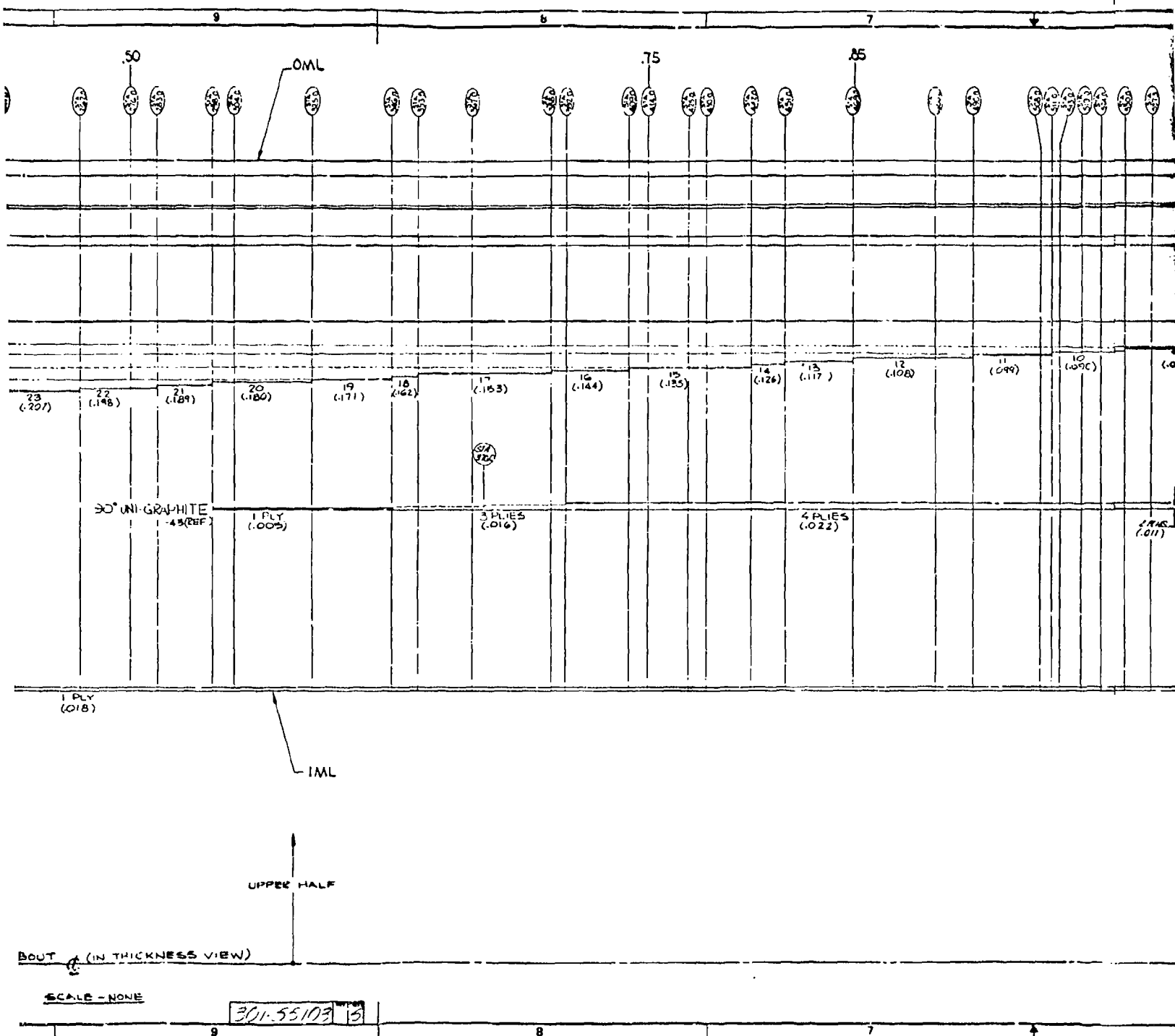
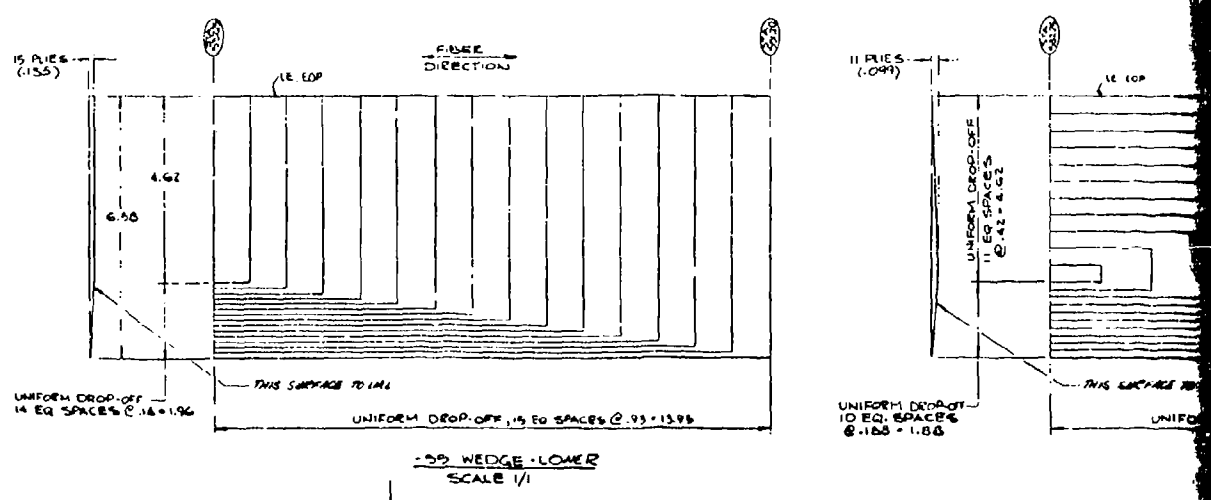
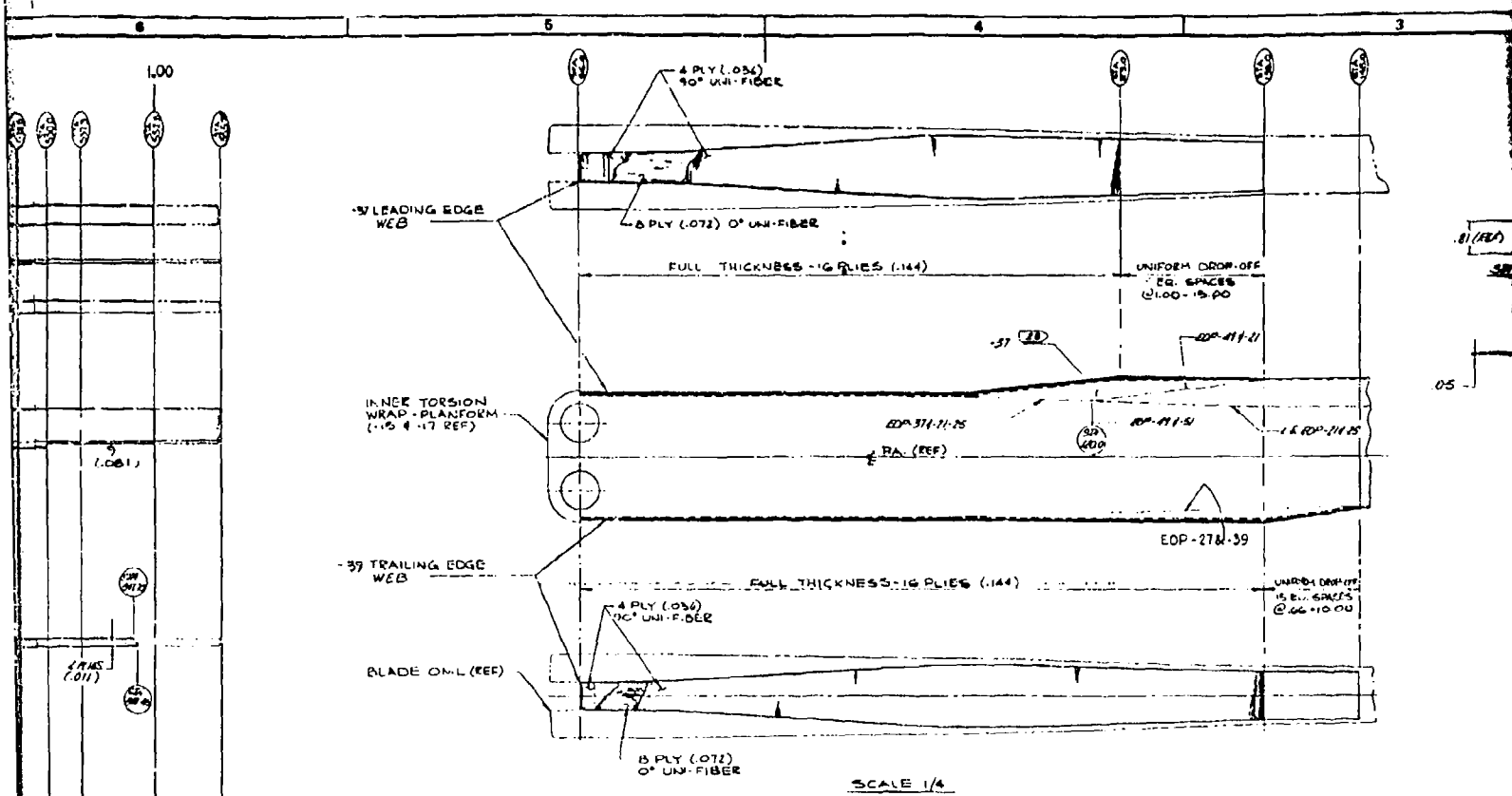


Figure 42. Continued



2



3

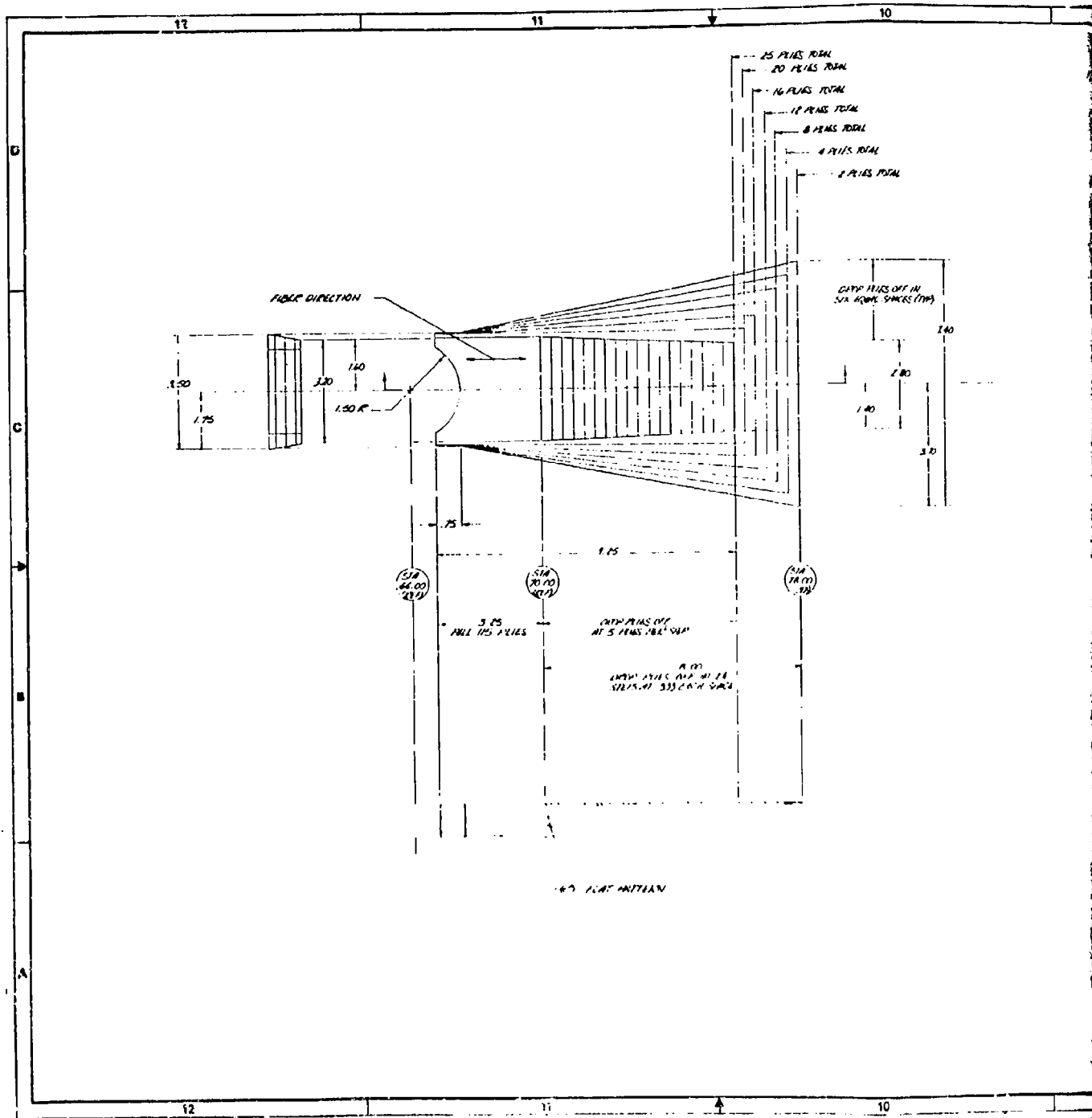
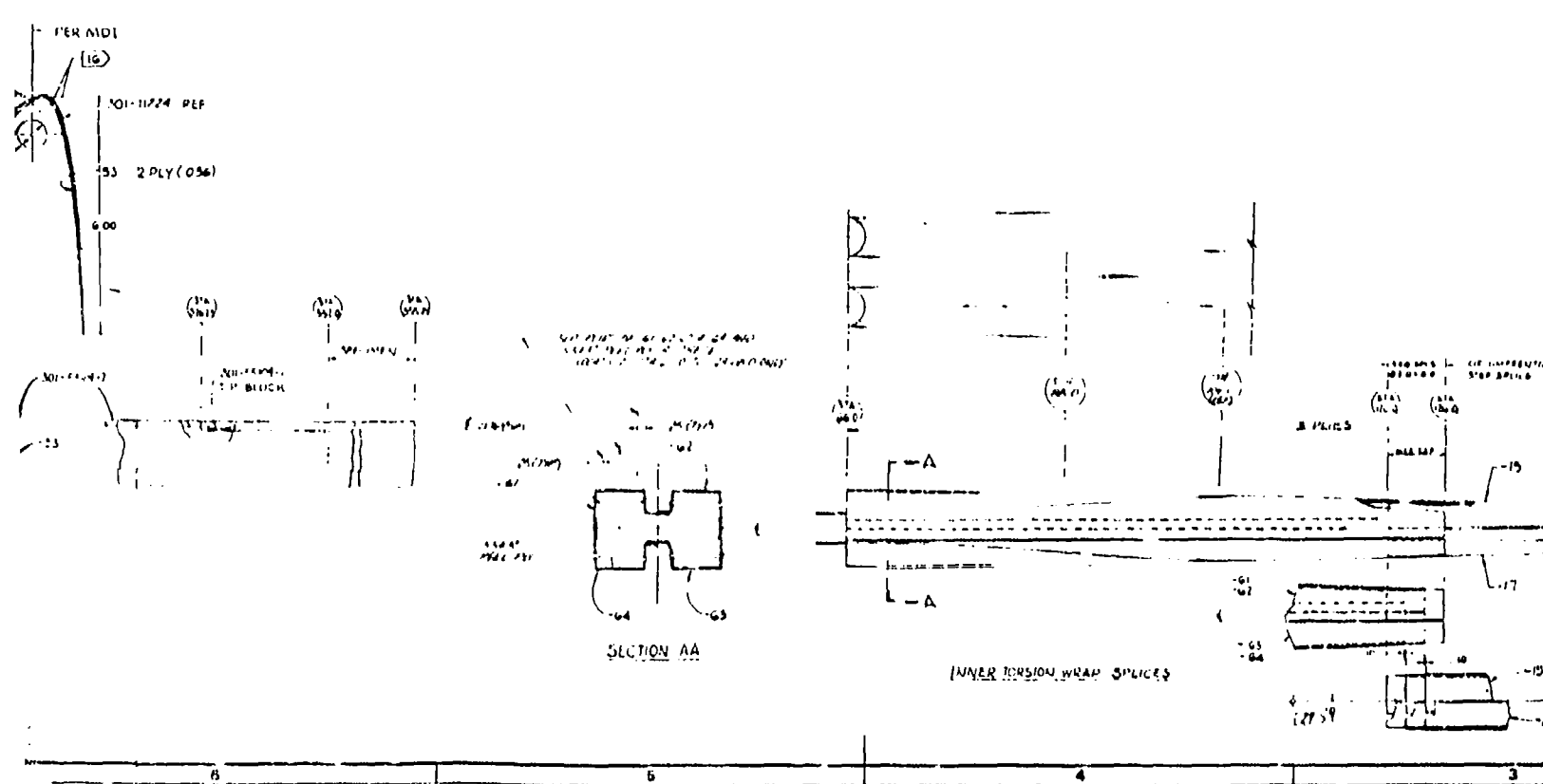
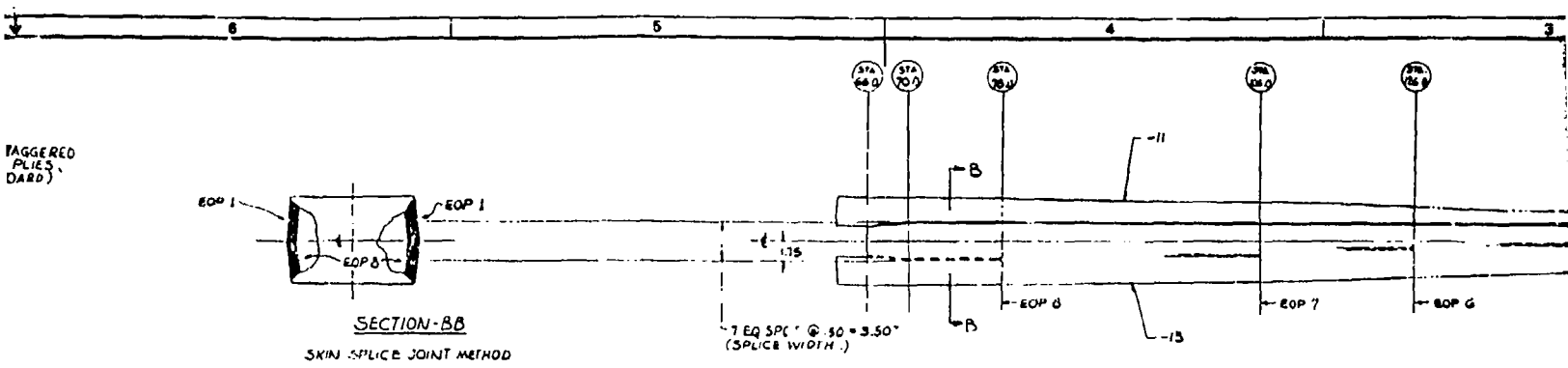
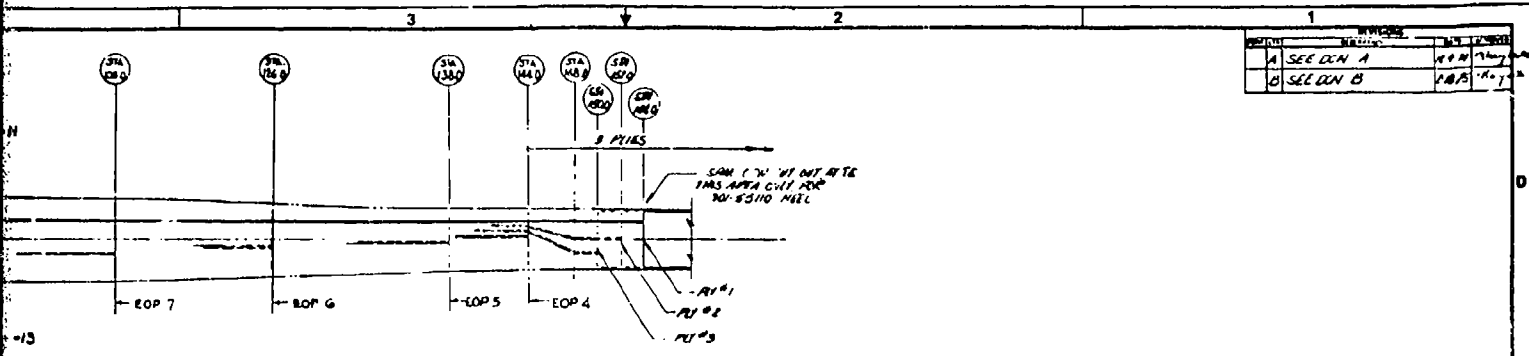


Figure 42. Continued

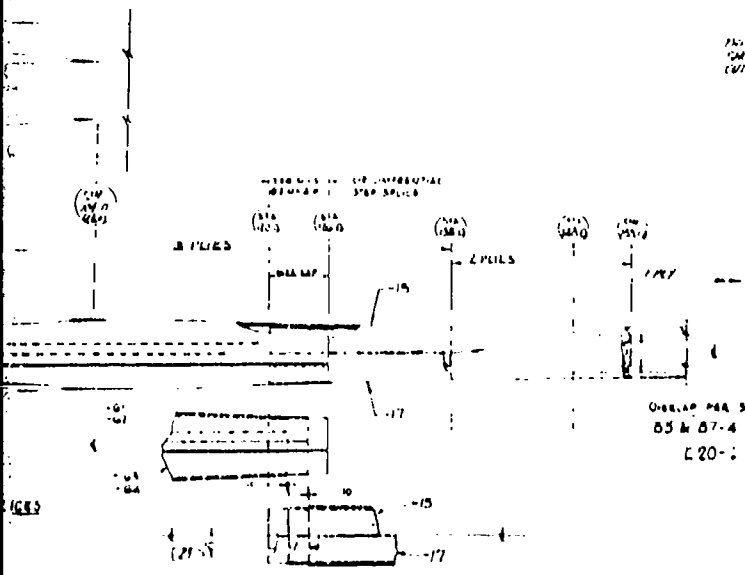
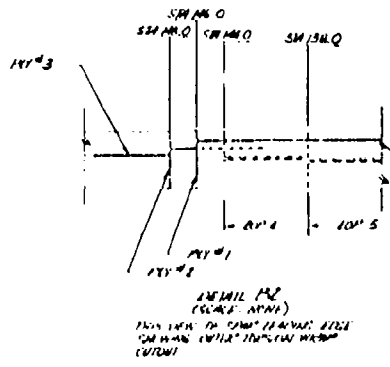


3

SECTION	REVISION	DATE	BY
A	SEE CON A		
B	SEE CON B		



TORSION WRAP SPICE
 SEE CON A FOR SPICE IN HOLE AREA
 OF STA 1510



NO.	DESCRIPTION	DATE	BY
1	ASSEMBLY		
2	TWO PIN FITTINGLESS		
3	IN H. WATER BLADE		

11272 301-55103

4.0 STRUCTURAL AND AEROELASTIC ANALYSES

The structural analyses used in the design development and preliminary structural substantiation of the HLH rotor blade are contained in Reference 11. The report contains rotor loads analyses, physical properties, natural frequencies, and detailed stress analyses.

4.1 CRITERIA AND REQUIREMENTS

The design criteria for the rotor blade limit and fatigue loading are in accordance with the requirements of AR-56, Reference 12, for a crane helicopter except as noted in the deviations contained in Reference 13, PIDD Revision E. Basic requirements for the HLH helicopter are summarized in Figure 43. The design maximum level flight airspeed, V_H , at the basic design gross weight is 150 knots.

The design requirement specifies that the fatigue safe life shall be equal to or greater than 3600 hours based on mean minus 3 sigma ($M - 3\sigma$) allowables and top of scatter measured loads. The loading schedule used to calculate the design fatigue safe life is given in Table 4. The safe life is based on the airspeed distribution for flight maneuvers given in Table 5.

The failsafety requirement is that the blade shall have a minimum operating life of 200 hours after a failure detection with a confidence level associated with mean -2 sigma ($M - 2\sigma$) allowables. In the case of a redundant structure, a minimum of 100 hours of safe life is required after complete failure of one of the load paths using mean minus one sigma ($M - 1\sigma$) allowables. The failsafe life is calculated using the same loads and airspeed distribution as in the safe life calculation.

4.2 LIMIT AND ULTIMATE LOADS

The critical limit load conditions are:

- 2.5g flight pullup maneuver
- Rotor starting
- Rotor braking
- Ground flapping at 4.67 "g" ultimate load

Figure 44 defines the spanwise distributions of rotor blade flight maneuver limit loads.

A factor of safety of 1.5 is applied to the limit load to determine the ultimate design load.

4.3 DESIGN FATIGUE FLIGHT LOADS

The rotor blade design fatigue loads are based on theoretical predictions for high-speed level flight condition and on maneuver load factors from CH-47 helicopter measured flight data. The L-02 computer program for aeroelastic rotor blade loads analysis with its nonuniform downwash option was used to predict the flapwise and chordwise bending moment at the level flight design condition of 118,000-pound gross weight and 150-knot forward speed (V_H) at sea level/95°F. The root end chordwise moment was established using the lag damper characteristics with predicted vibratory lag angles. These predictions for bending moment are shown in Figure 45. The corresponding rotor blade centrifugal force distribution is shown in Figure 46. CH-47 flight test measured pitch link load data was combined with the L-02 analysis to establish the spanwise distribution of rotor blade torsion shown in Figure 45. The maneuver load factors based on flight experience and the complete listing of mission profile loads are given in Reference 11.

4.4 MATERIAL PROPERTIES

Material properties are required to establish the weight and stiffness of the rotor blade, which in turn are required to predict natural frequencies and loads. The fatigue and ultimate strengths of the materials are also required to design a structurally adequate rotor blade. The material properties and strengths for the basic rotor blade materials are summarized in Table 6. The properties for the blade composite materials and titanium nose cap are not contained in military specifications and were determined by coupon testing as required to support the design.

The properties of the isolated materials are not necessarily the same as when they are combined to form the rotor blade structure. This is especially true in the case of composites where the combined strength of the elements is often different from the individual materials. The component tests described in Section 6 of this report investigate the combined material

strength of the total rotor blade structure that is required to demonstrate its load-carrying capability. These tests are used to substantiate the analytically predicted structural capability of the rotor blade.

The stress/load cycle (S-N) curves and the stress ratio effects on fatigue strength are defined in Paragraph 11 of rotor blade structural substantiation report, Reference 11.

The strength of the Nomex honeycomb core was defined during the demonstration testing and is discussed in Section 6.1 of this report and in the Full Scale Blade Fatigue Test Report, Reference 9.

4.5 BLADE PHYSICAL PROPERTIES

The rotor blade physical properties were developed during the design phase to meet the requirements for blade weight and centrifugal force, loads and frequencies. These properties shown in Table 7 and Figures 47 and 48 include the spanwise distribution of:

Weight	Pitch Inertia
Axial Stiffness	Chordwise Neutral Axis
Chord Stiffness	Shear Center
Flap Stiffness	Static Balance Axis
Torsion Stiffness	

The design loads were calculated using the properties for the ATC blade configuration. The basic structural concept for the prototype blade is identical to that for the ATC blade and the minor differences in properties will not significantly change the design loads.

4.6 ULTIMATE STRENGTH ANALYSIS

The ultimate loads are obtained by multiplying the limit loads by the 1.5 ultimate factor of safety. The minimum margins of safety (MS) calculated for the primary structural components are shown in Table 8. The margin of safety is defined by the following formula:

$$MS = \frac{\text{Ultimate Strength}}{\text{Ultimate Load}} - 1$$

These margins use the blade loads and material strengths described in Paragraphs 4.2 and 4.4 of this report.

ITEM	DESIGN GROSS WEIGHT	MAX. ALTERNATE DESIGN G.W.	MIN. MISSION PROFILE G.W.
Gross Weight	118,000 lb	148,000 lb	73,000 lb
Limit Maneuver Load Factor	+2.5/-0.5	+2.0/-0.5	+2.5/0.5

Center of Gravity Range	MOST FORWARD	MOST AFT
	60 in. fwd	40 in. aft

DESIGN ROTOR SPEED RPM	POWER ON	POWER OFF
Minimum	155.7	140.1
Normal	155.7	-
Maximum	155.7	176.9
Limit	171.3	194.6

Figure 43. Basic Design Requirements

TABLE 4. BASIC FATIGUE LOADING SCHEDULE

<u>CONDITION</u>	<u>% OCCUR.*</u>	<u>GROSS WEIGHT (LBS)</u>	<u>% TIME</u>
Ground Conditions	1.0		
Take Off	(400)		
Steady Hovering	30.0	78,000	45
Turns Hovering	(2000)	118,000	50
Hover Control Reversals	(2000)	148,000	5
Sideward Flight	2.0		
Rearward Flight	1.0		
Landing Approach	(765)		
Forward Flight			
20% V _H	5.0		
40% V _H	2.0		
50% V _H	2.0		
60% V _H	5.0		
70% V _H	8.0		
80% V _H	9.0		
90% V _H	16.8		
V _H	1.0		
115% V _H	1.0		
Climb, T. O. Power	3.0		
Climb, Full Power	4.0		
Partial Power Descent	(500)		
Turns	5.2		
	(1000)		
Control Reversals	(815)		
Pull Up	(270)		
Power to Autorotation	(60)		
Autorotation to Power	(60)		
Steady Autorotation	1.1		
Autorotation Turns	0.4		
	(160)		
Autorotation Control Rev.	(40)		
Autorotation Landing	(40)		
Autorotation Pull Up	(40)		
Ground-Air-Ground	(100)		
Power Dive	2.5		

*Bracketed numbers are occurrences per 100 flight hours.

TABLE 5. MANEUVER AIRSPEED DISTRIBUTION

<u>FORWARD LEVEL FLIGHT</u>		<u>MANEUVER</u>	
<u>% VH</u>	<u>% TIME</u>	<u>% TIME OR OCCURRENCES</u>	
20	5.0	}	
40	2.0		
50	2.0		
60	5.0		64
70	8.0		
80	9.0		
90	16.8	33	
100	1.0	3	
TOTAL	48.8		

The % maneuver or occurrences from the basic fatigue schedule are distributed with airspeed as given in right hand column.

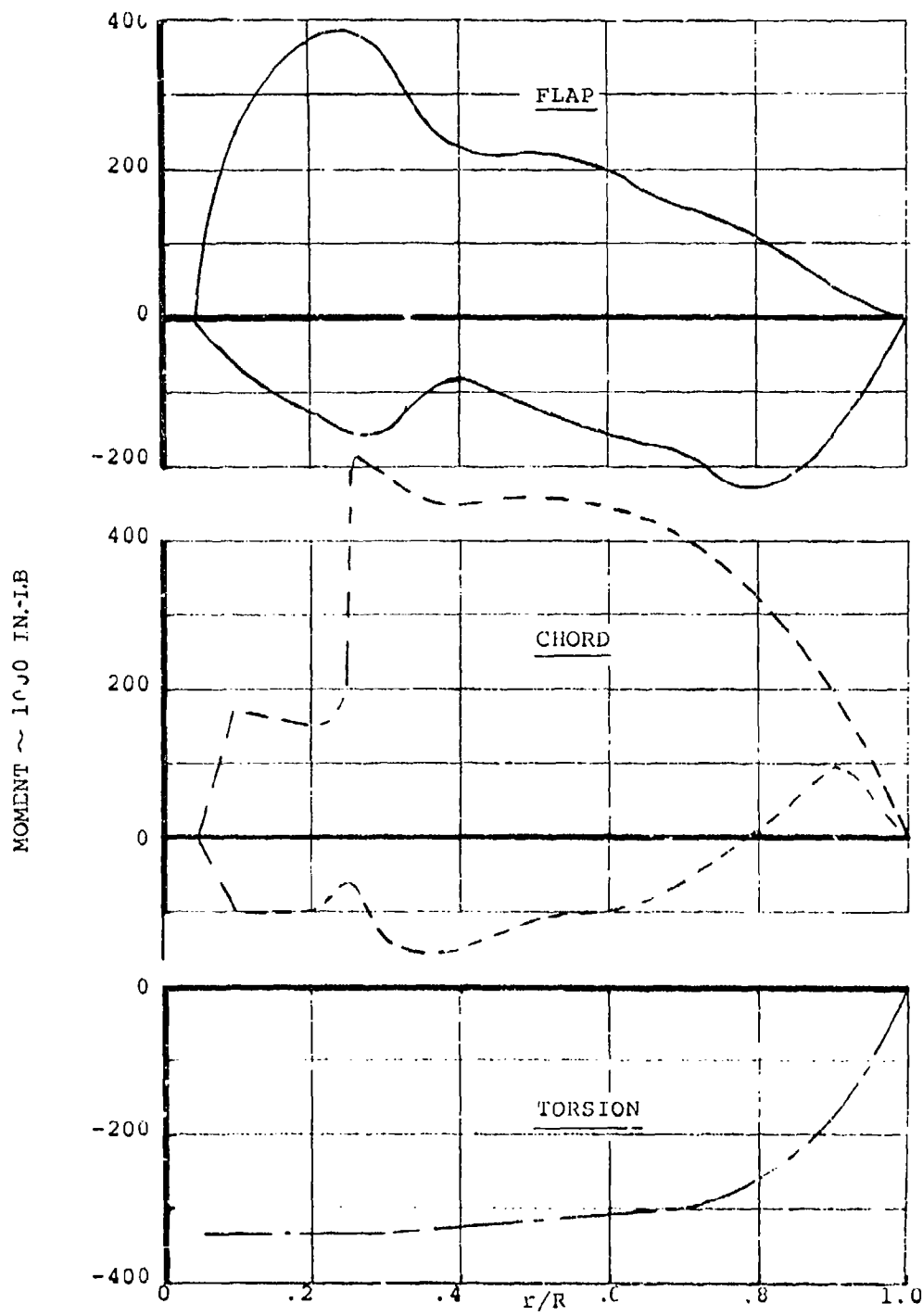


Figure 44. Rotor Blade Moments for Design Limit Maneuver Condition

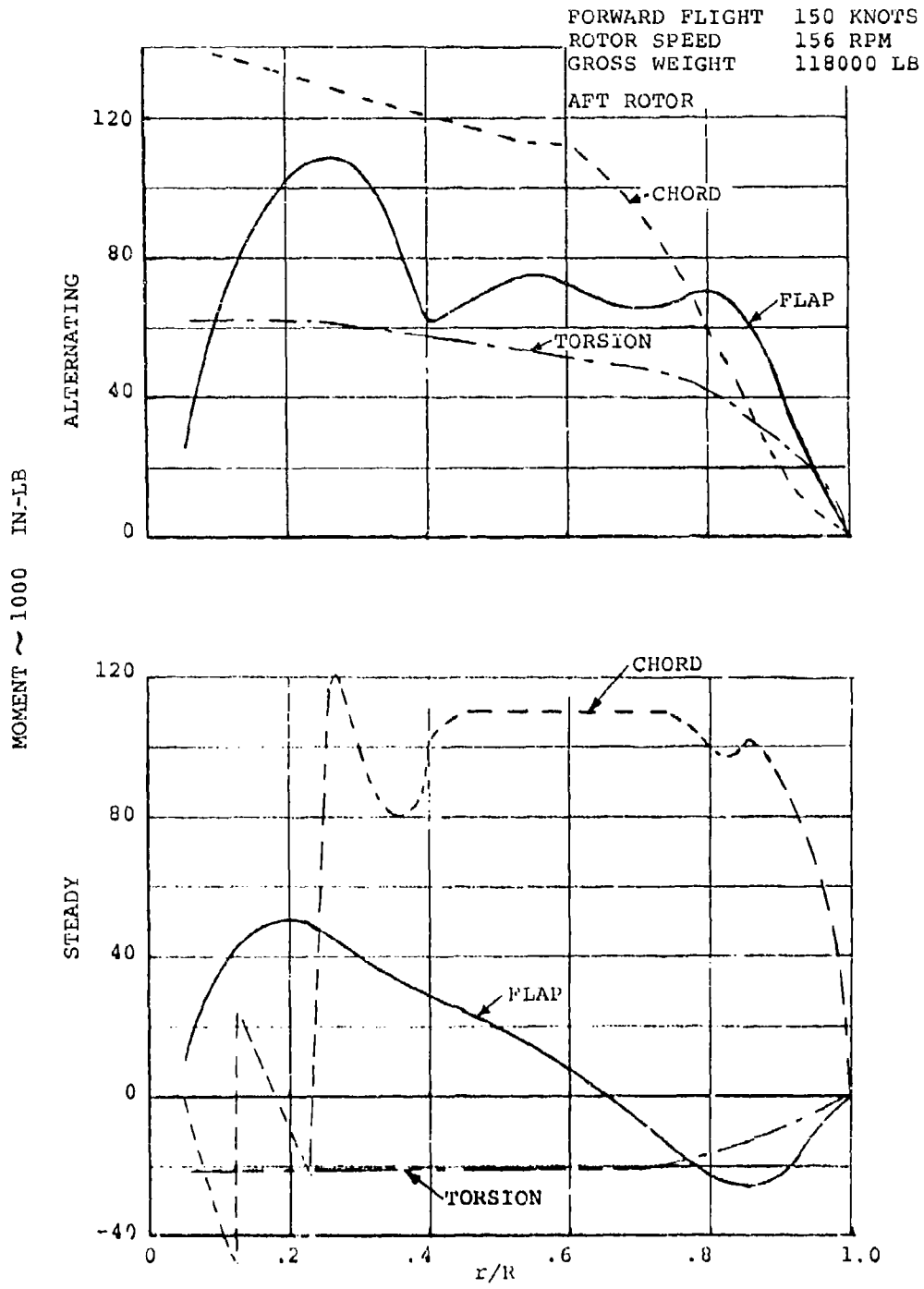


Figure 45. Rotor Blade Design Moments for High-Speed Level Flight

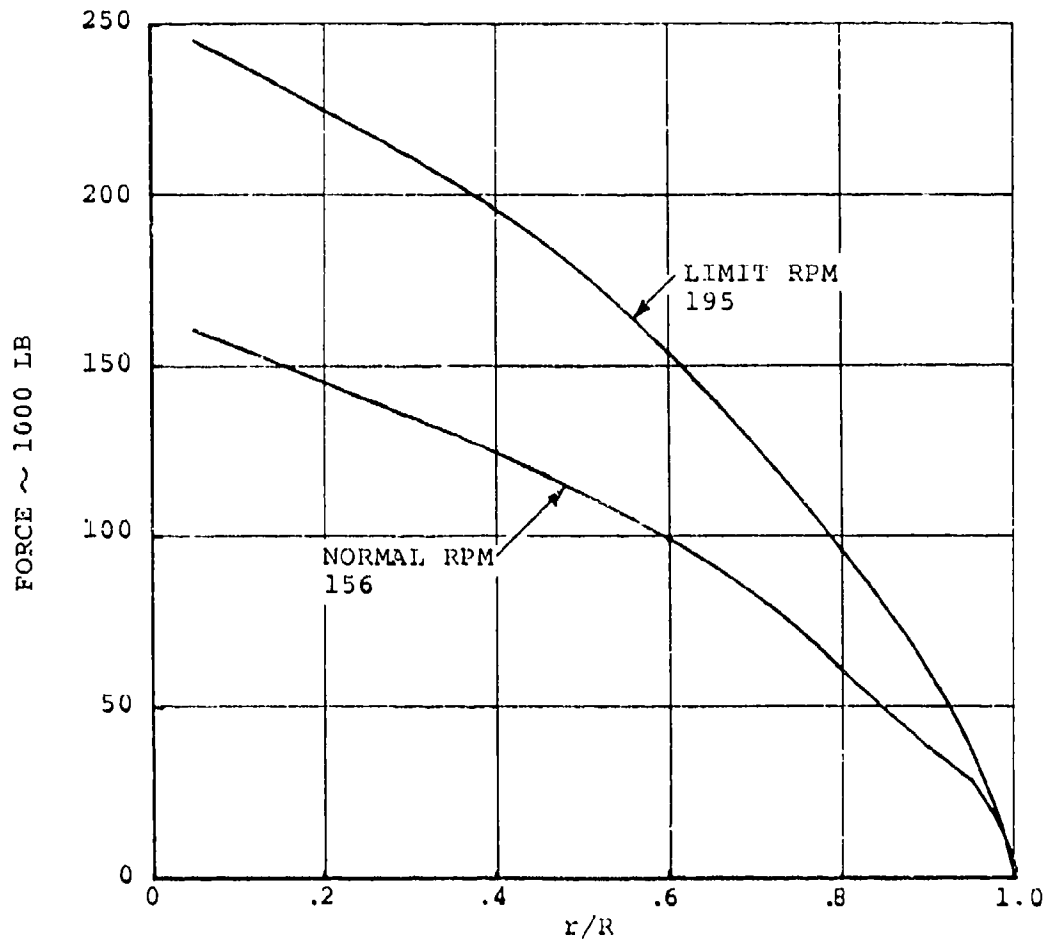


Figure 46. Rotor Blade Centrifugal Force

TABLE 6. MATERIAL PROPERTIES AND DESIGN ALLOWABLES SUMMARY

ITEM	Exlc ⁶ PSI	F _{TU} PSI	f _{te} PSI R=.10	Gx10 ⁶ PSI	F _{su} PSI	f _{se} PSI	ρ LB/IN ³	α x10 ⁻⁶ IN/IN/°F 70°F-250°F
Fiberglass SP 250S 0°	6.3	153000	13600	.52	6940	1600	.067	2.22
90°	1.74	2980	560	.52	6510	1600	.067	20.0
+45°	1.78	23100	2680	1.67	46500	5000	.067	4.09
HT-GRAPHITE								
0°	18.0	140000	39400	.70	7450		.055	-.4
90°	2.0	5450		.70			.055	18.0
TITANIUM 6AL-4V ANNEALED SHEET	16.0	134000	24500	6.2	79000	14150	.160	5.05
17- 4PH 150-170KSI	28.5	150000	20800	11.2			.282	6.0
AISI 301 SS 1/2 HARD	26.0	141000	23000	11.5	77000	13280	.286	8.4
I157 MOLDING COMPOUND	1.21	11040			14800		.065	
4340 STL 125-145KSI	29.	125000	20000	11.0	75000		.283	
AISI 304 SS	29.	95000		12.5	42000		.290	
NICKEL ELECTRO- FORMED	25	114000	28500					

TABLE 7. CALCULATED WEIGHT AND CENTRIFUGAL FORCE

<u>Component</u>	<u>Weight LB</u>	<u>CF - LB at Bearing</u>
BASIC ATC BLADE (Ref. 1, D301-10227, Vol. I, Pg. 121)	747.83	150,000
Tungsten Nose Weights*	8.67	2,920
ISIS Hardware	4.05	219
ATC Blade Total	760.55	153,139
Hub Hardware	370.70	10,160
ATC TOTAL	<u>1,131.25</u>	<u>163,299</u>
PROTOTYPE CHANGES		
Aft Fairing Core & Skin		
ATC	-121.41	-28,000
Prototype	119.16	27,900
ISIS Mounting	-3.41	-215
Tip Hardware	-3.84	-1,430
Spar Wall (ISIS Beef Up)	3.00	1,070
Precured Heel (Balanced)	21.45	5,860
Prototype Blade Total	774.50	158,324
Hub Hardware	370.70	10,160
Lag Damper Arm	35.33	1,610
Damper Preload	--	-8,000
PROTOTYPE TOTAL	<u>1180.53</u>	<u>162,094</u>
PENDULUM ABSORBERS		
4/Rev Assembly	36.72	2,675
4/Rev Mount	10.19	675
3/Rev Mount	10.40	750
3/Rev Hardware	1.54	105
PENDULUM TOTAL	<u>58.85</u>	<u>4,205</u>
PROTOTYPE WITH PENDULUM ABSORBERS		
Blade	833.35	162,529
Total	1239.38	166,299

* Added to move dynamic balance axis forward.

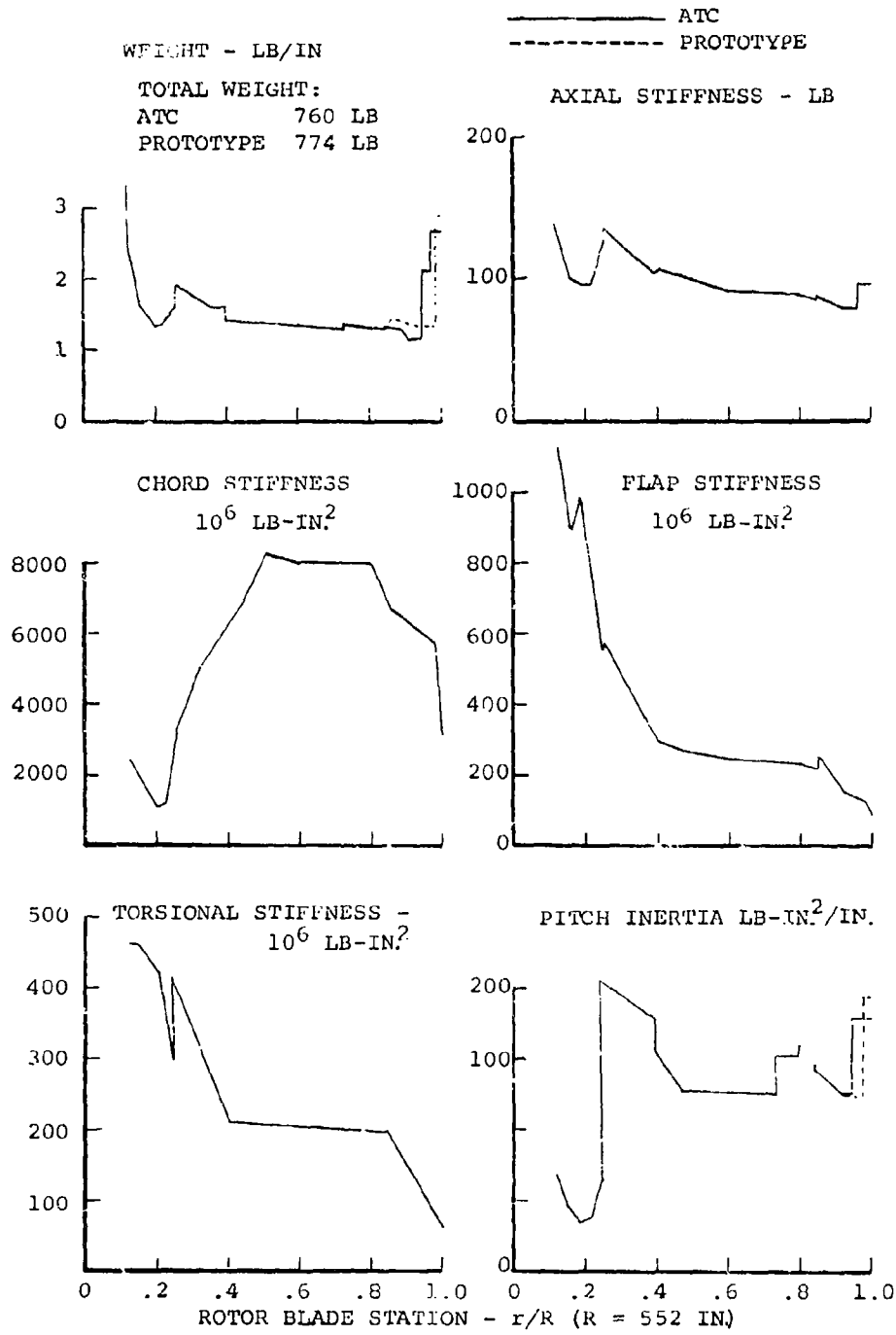
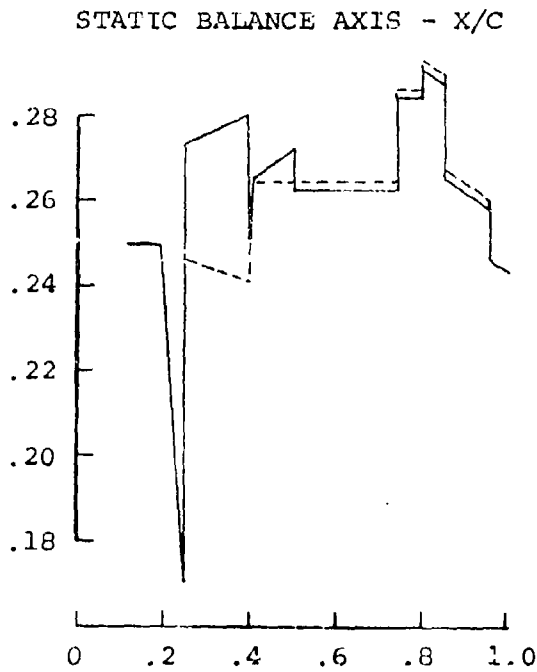
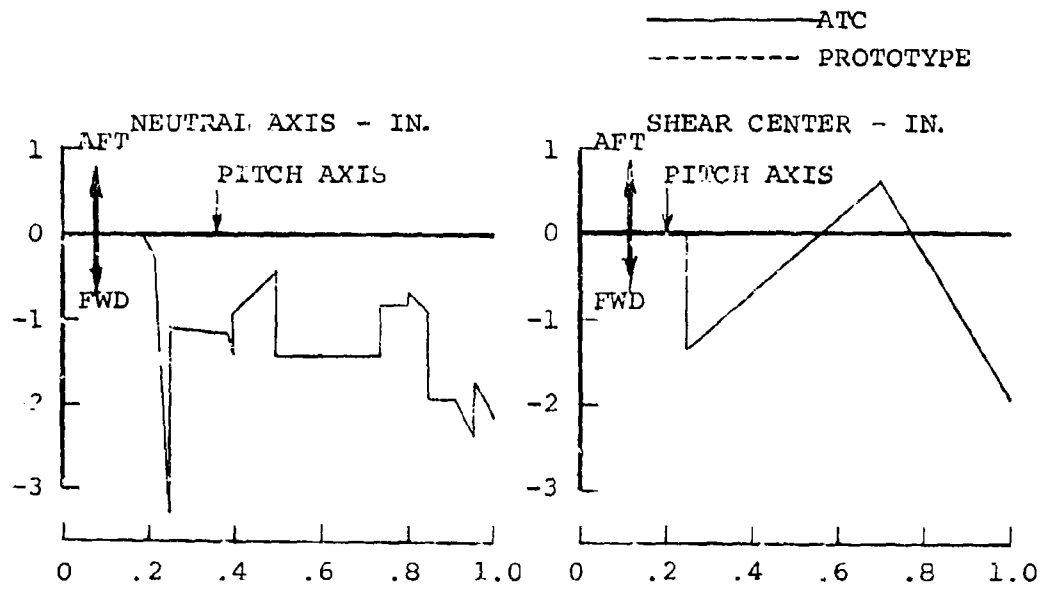


Figure 47. Spanwise Distribution of Mass and Stiffness



ROTOR BLADE STATION - r/R
 ($R = 552$ IN.)

Figure 48. Spanwise Distribution of Blade Axis

TABLE 8. MINIMUM MARGINS OF SAFETY

PART NO.	COMPONENT	CRITICAL SPAN STATION	STRESS CONDITION	LOADING CONDITION	ULTIMATE
		ULT.			MS
301-11199-1	Trailing Edge Strip X-Ply F/G	497	Tension	Flt. Loads	.18
301-11199-3	Trailing Edge Wedge 0° Uni. Graphite	216	Tension	Flt. Loads	1.68
		276	Compression Buckling	Rotor Starting	.175 (Lim.)
		221	Tension	Rotor Braking	2.17
301-11181	Trim Tab	258	Tension	Flt. Loads	.12
301-11179	Core	407	Shear	Airloads	.38
301-11175	Skin	138		Shear/Tension	.46
301-11189	Nickel Erosion Strip	469	Tension	Flt. Loads	.18
301-11174-3	Titanium Nose cap	276	Tension	Flt. Loads	.02
301-11173-1	Spar Assy.	220	Compression Buckling	Ground Flapping	0 (Lim.)
		386	Tension	Flt. Loads	.18
		276	Tension	Flt. Loads	.53
		104	Tension	Rotor Braking	1.95
301 11204	Insert	66	Bearing	Ground Flapping	.65
EA 4628	Adhesive	138	Shear	Airloads & T.E. Loads	1.47
		104	Shear	Nose cap Termination	.52
		66 (Insert)	Shear	Ground Flapping	.11

4.7 SAFE LIFE FATIGUE ANALYSIS

The fatigue criterion specifies that the safe life shall be at least 3600 hours in order to ensure maximum service reliability. Maximum flight safety is obtained by retiring the blades at the time the safe life expires in order to virtually eliminate the possibility of a catastrophic failure during the life of the fleet. The safe life is based on top of scatter loads and mean minus three sigma ($M - 3\sigma$) allowables. Allowables are based on coupon test results of the individual blade materials.

During the initial design, all blade components were sized for unlimited fatigue life at a load equal to 1.2 times the high-speed level flight (V_H) design condition load. The critical element for the ATC rotor blade was the fiberglass crossply skin that had unlimited life for 1.16 times the V_H design load. The endurance limits for unidirectional fiberglass and titanium were 1.31 and 1.43 times the V_H design load.

Safe life of the titanium nose cap was calculated using the flight spectrum loads including the combined effects of alternating tension and shear stresses. The results of this calculation led to safe life prediction of 15,500 hours. The safe life of the fiberglass crossply was calculated at 185,500 hours, indicating that this element is less critical than the titanium even though the fiberglass crossply unlimited life factor is lower.

4.8 FAIL SAFE ANALYSES

Analyses were performed to evaluate the structural adequacy of the rotor blade after the occurrence of a partial failure.

In the structurally redundant root end attachment, the fail-safe criterion requires that at least 100 hours of safe life exist after the complete failure of one load path. The critical lug that normally reacts the highest flight load was assumed to be failed. The remaining safe life prediction with one lug failed was 1754 hours based on mean minus one sigma ($M - 1\sigma$) allowables and top of scatter flight loads. The ultimate margin of safety for the failed lug condition is .75.

For the outer portion of the rotor blade, the failsafe design criterion requires that 200 hours of safe life exist after a readily detectable failure has occurred. The complete titanium nose cap and one-half of the lower zero degree unidirectional fiberglass spar was assumed to be failed, thereby representing a readily detectable failure. With the unidirectional fiberglass failed, the $\pm 45^\circ$ crossply fiberglass material was considered capable of maintaining torsional continuity of the section. This mode of failure was considered to realistically represent a potential in-service failure that has been demonstrated during the oval tube testing to initiate an ISIS system warning while still providing the beam continuity required to carry axial and torsional loading regardless of the spanwise extent to which the unidirectional material failure has progressed.

The remaining safe life of 1006 hours was calculated. The required confidence level for this mode of failure is achieved by using top of scatter loads and mean minus two sigma ($M - 2\sigma$) allowables. The ultimate margin of safety for the failsafe mode on the outer portion of the rotor blade is .35.

4.9 NATURAL FREQUENCY ANALYSIS

The rotor blade flapwise, chordwise and torsional natural frequencies are predicted using the Leone-Myklestad method (L-01 computer program). The natural frequencies at normal operating rotor speed are summarized in Table 9. The spectrums plotted in Figure 49 define the variation of the natural frequencies with rotor speed from stationary (0 rpm) to normal at 156 rpm. Comparisons with measured frequencies are made in Section 6.2.

TABLE 9. NONDIMENSIONAL NATURAL FREQUENCY

Mode		Natural Frequency ATC	Per Rev at 156 RPM Prototype
Flapwise	1st	2.67	2.69
	2nd	5.11	5.09
	3rd	8.70	8.52
	4th	13.21	12.82
Chordwise	1st	4.80	4.67
	2nd	12.12	11.52
Torsion	1st	6.46	6.43
	2nd	12.79	12.77

4.10 CLASSICAL FLUTTER

The results of the classical flutter analysis using the L-01 computer program indicate that the rotor blade is free from flutter up to 1.15 times the limit rotor speed (224 rpm) for forward speeds up to 1.15 V_D (209 kts). This favorable characteristic is attributed to the blade shear center location and the mass center both lying forward of the aerodynamic center. The separation of flap and torsion natural frequencies also contributes to the avoidance of classical flap-pitch flutter. The stability conclusion applies to both 0° and 26.5° of δ_3 kinematic flap pitch coupling.

4.11 ROTOR BLADE TORSIONAL DIVERGENCE

AR-56, Paragraph 3.6.2, "Aeroelasticity," states that, "...The rotor blades...shall be free of flutter, divergence and any other aeroelastic instability at rotor speeds up to 1.15 times the design limit rotor speed with and without power at 1.15 V_D ." HLH blade motions and loads were analyzed to assure compliance with this requirement, and the high-speed dive condition was tested during the test of the dynamically scaled 14-foot diameter HLH rotor model. The results of the analysis have been previously reported in Reference 11, and the results of the wind tunnel test are reported in Reference 14. Only the conclusions of the analysis and test will be summarized here and the reader is referred to the references for further detail.

The analysis was performed using the Boeing Vertol C-60 Blade Load Analysis Computer Program supplemented by a manual calculation to add coupled drag and lift moments about the torsional axis due to blade bending. The results showed that torsional loads are not excessive and do not cause unstable torsional tip deflections. The method of analysis was validated by its application to a CH-47C high-speed flight test point; it compared favorably with the measured data. Analyses of other HLH flight conditions were also performed without incident. Sensitivity studies of the results to blade stiffness and twist were also conducted and showed no indication of divergence, but rather a moderate increase in loads. Airfoil characteristics and their relation to these analyses were also evaluated.

The wind tunnel test results were consistent with the analytical findings. The test condition was flown at the 1.15 V_{Dive} speed and normal rotor rpm resulting in a 200-knot forward speed, an advance ratio $\mu = .45$, and an advancing blade tip Mach No. = .975. The test results are shown in Figures 50 and 51. Figure 50 shows measured model blade torsion loads vs. μ for the dive condition shown by the triangle test points compared to level flight trim condition test results shown by the circle points. It may be noted that the measured loads at the 1.15 V_{Dive} speed are just about equal to the scaled endurance limit load which in general represents a good match between fatigue design and load level. Figure 51 shows a comparison of the waveform of the pitch link load measured in the 14-foot model test compared with the waveform predicted in the Reference 11 analysis for the same condition. Remarkable agreement is shown in this correlation. Additional test results are shown in Reference 14.

4.12 PITCH LAG STABILITY

The stability boundaries are determined by the procedures of Reference 15 based on the lag damper critical damping ratio of 26 percent. The forward rotor boundary is less critical due to the incorporation of delta -3. The region designated "level flight" includes all gross weight/cg/airspeed conditions within the HLH flight envelope. The "maximum g pull-up" yields the most adverse combination of large coning and large lag angle while the "steep turns in autorotation" combine the most adverse high coning and low pitch angle conditions.

All flight conditions investigated are well within the current range of experience, and provide ample clearance to the stability boundaries.

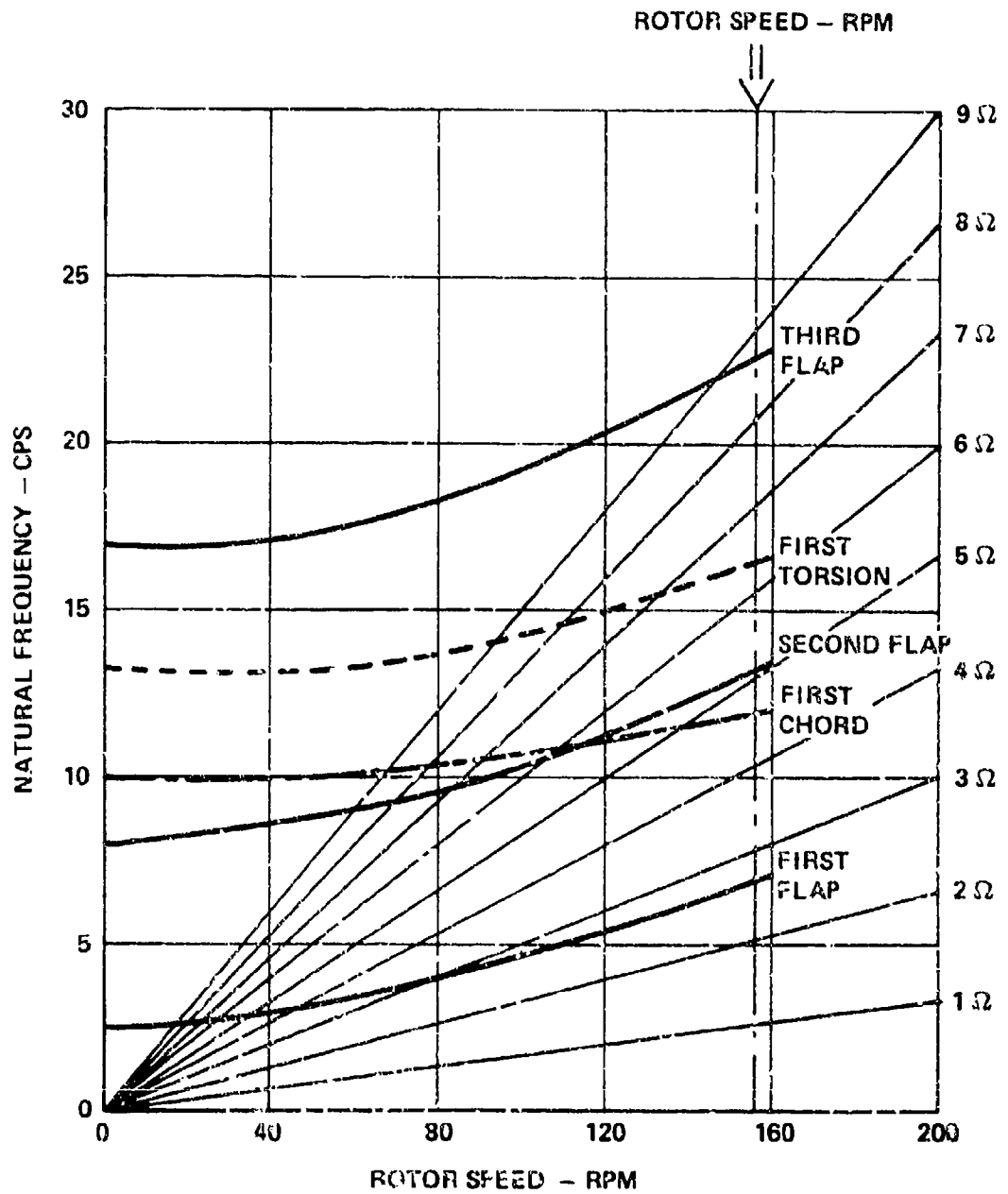


Figure 49. Rotor Blade Frequency Spectrum

SCALED WIND TUNNEL TEST DATA

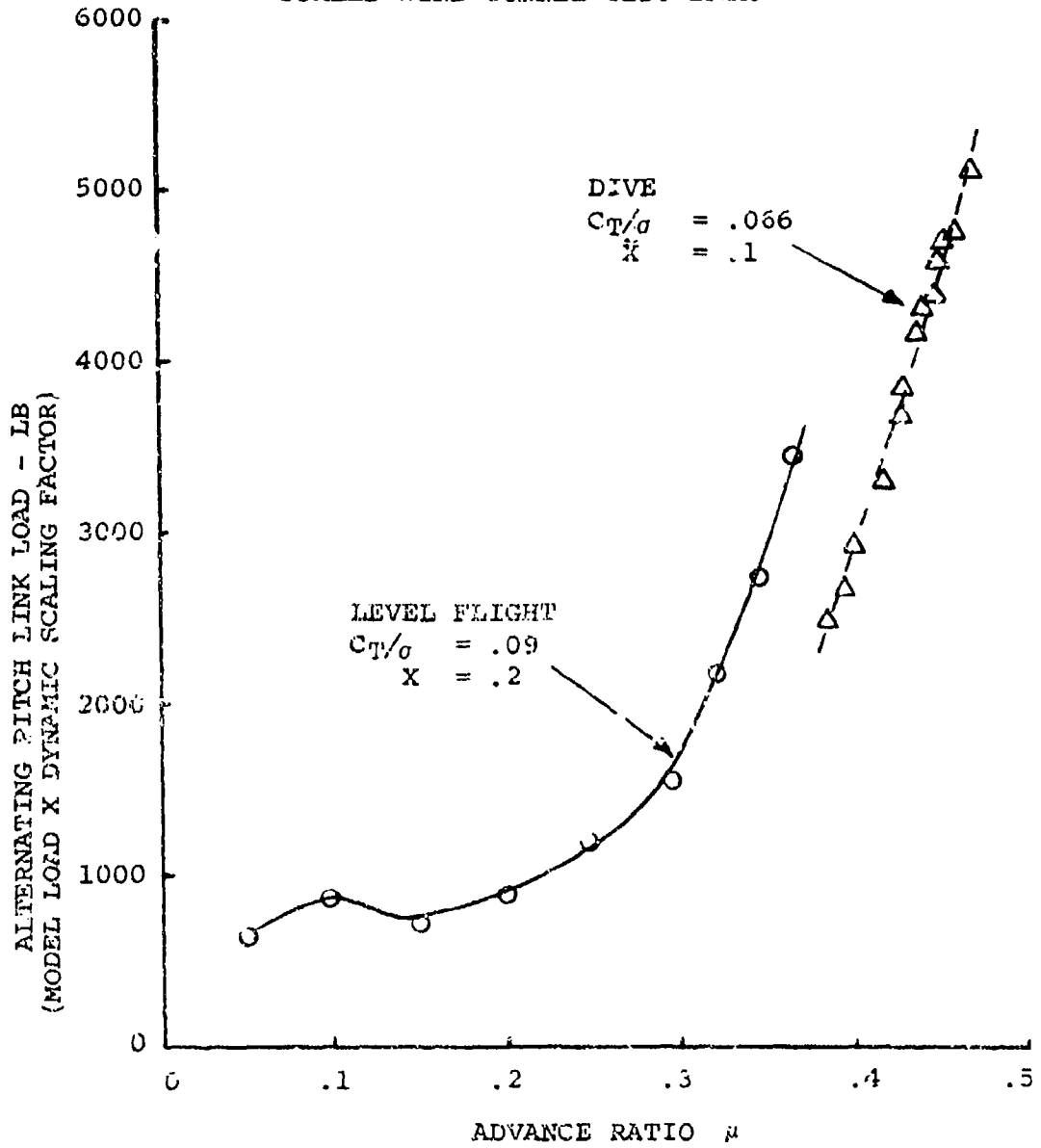


Figure 50. Demonstration of Blade Torsional Aeroelastic Stability at High Speed With 14-Ft-Diameter Model Rotor

V = 200 KNOTS
GROSS WEIGHT 118,000 LB
V_{TIP} = 750 FPS
SEA LEVEL/STD

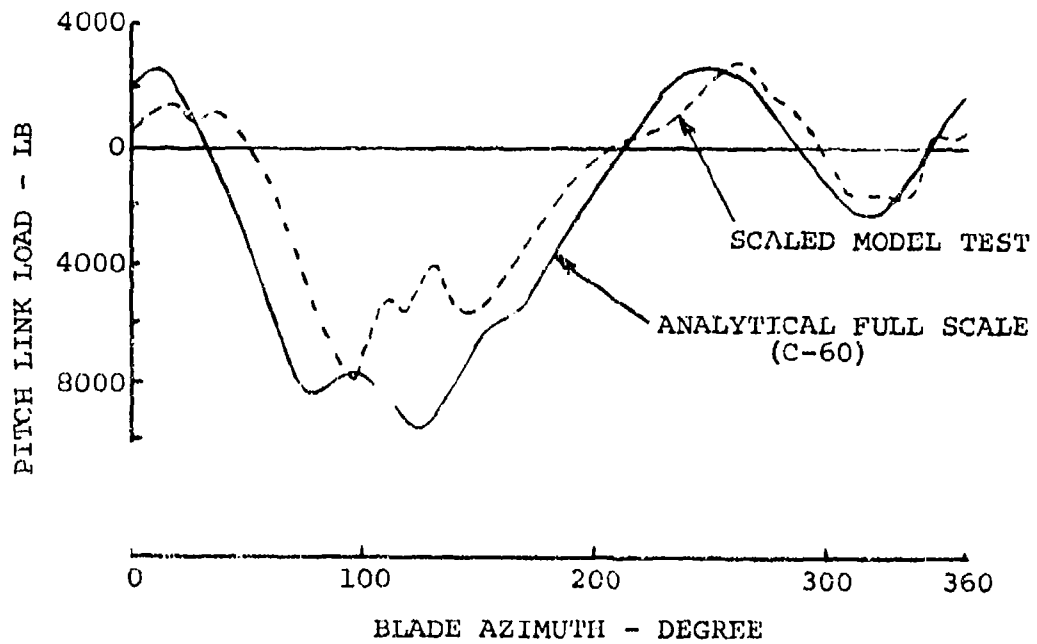


Figure 51. Comparison of Analytical Pitch Link Load With 14-Ft-Diameter Rotor Wind Tunnel Test Load for Limit Design Dive Speed

5.0 MANUFACTURING DEVELOPMENT

The HLH advanced composite rotor blade is fabricated with electrically heated, zone-temperature controlled, match metal dies using internal pressure.

The use of computer-based Master Dimensioning Information was extremely successful in coordinating the fabrication of the various tools required and ensuring that the advanced aerodynamic rotor blade contours were attained. The composite spar is co-cured with the titanium nose cap. The matched metal tools assure airfoil surfaces and blade physical properties that are consistent and repeatable from unit to unit. The HLH rotor blade design possesses many inherent features directed toward the use of automated tooling for high-rate production which will result in reductions in unit cost. Nondestructive test techniques have been developed and are now available to provide the high level of quality assurance needed for production of composite rotor blades.

The most important aspects of the tooling, titanium forming, fiberglass fabrication inspection methods, and the results of fabrication of the initial prototype blades are described in this section.

5.1 SPAR FABRICATION

The fabrication involves the assembly of details on a bag and mandrel, installation of a leading edge assembly, and the wiring operation. The detailed manufacturing development of the HLH rotor blade is given in D301-10280-1, Reference 16.

Figure 52 and the flow chart in Figure 53 show the major events in the manufacturing sequence of the HLH ATC rotor blade. The steps that go into each major event are defined in the flow charts of Figures 54 through 62.

5.1.1 Fabrication Results

The fabrication concept was not intended to be a "production process" when it was devised, but it was intended to be a stepping stone to the production process. Conceptually, the results were highly successful and satisfactory. Laminate quality and integrity in this matched die concept were uniform and excellent, and successful results were achieved in the following areas:

- Spar laminate fiber orientation, density and uniformity
- Skin laminate bond to honeycomb
- Bond integrity of co-cured titanium cap and fiberglass spar
- Contour repeatability of matched die tooling
- Consistency of lugs
- Weight control
- Outstanding accuracy of NDT techniques

The two problem areas that emerged were:

- Wrinkling of the "D" spar heel and shank fiberglass crossply caused by handling of the uncured layup
- Secondary bonding of cured fittings to the spar

The steps taken to eliminate these problem areas are discussed in the following paragraphs.

Crossply Wrinkles

The crossply wrinkles in the shank (spar inboard of airfoil fairing) area were eliminated by adding unidirectional fiberglass to fill the spaces between the spar packs and by improved control of the lay-up procedure. The solution chosen to eliminate the heel crossply wrinkles for a production blade configuration is to precure the heel as a structural member in a separate operation prior to the spar assembly. The layup and cure of this detail is an additional cost; but the heel permits the elimination of another cure and thus pays for itself.

Secondary Bonding of Cured Fittings

Difficulty was encountered in the bonding of the precured fiberglass fittings at the root end and tip. The contours of the matching parts could not be maintained without time-consuming and costly hand fitting. This was particularly true for hot bonds where the thickness of the bond line could not be controlled. An interim solution for the ATC configuration

was to cold bond (with EC-2216) the fittings in place. The prototype fittings and intended production approach was to cure the fittings with the spar.

5.2 TOOLING

The blade spar and airfoil section molds are made from Mechanite H.S. The molds are integrally heated and self-contained. A photograph of the complete tool is shown in Figure 63. Steel was selected for the tool material for its durability and compatibility of thermal coefficient of expansion with those for the spar materials as shown in Table 10. A photograph of the spar curing tool is shown in Figure 64. An electrically heated tool system was selected over liquid (oil) and steam-heated systems. The objection to the latter was primarily potential contamination of the composition with oil or moisture which would result in poor bonding.

The temperature was regulated by a 60-zone computer-controlled on/off switching system. During the cure of the first tool proving spar, computer control system operation proved that it was capable of automatically controlling zone temperature to within required limits as shown in the heat chart in Figure 65.

The tool base has an integral air system used for cooling the fixtures after the cure cycle.

5.3 FORMING OF THE TITANIUM CAP

The titanium cap is formed to the outer contour of the blade and later becomes an integral part of the spar when it is bonded to the fiberglass during the fiberglass cure. The forming of the cap presented a difficult task due to the sharpness of the leading nose radius, blade twist, and airfoil thickness variation. In addition, titanium forming was not common industry practice. The changing airfoils require stretching in some areas and shrinking in others throughout the 40-foot length.

The initial forming concept consisted of preforming the leading edge radius on a brake using conventional punch and die. The cap was then formed using male and female ceramic dies and heated to 1450°F for 2 hours to produce the desired shape. The formed parts using this method were good; however, the ceramic dies developed cracks, preventing their use for further production.

The second approach changed the tool material to Inconel 802 and eliminated the female die. The cap was drape-formed over the mandrel by attaching weights to the edges and heating to 1500°F for a little less than 2 hours. This time and temperature kept scaling to a minimum, and the phosphate flouride etching required was kept in the region of .008 inch. Figure 66 shows a creep formed titanium cap with the weights attached.

These experiences on the ATC blade program provided background for the improvement of certain areas in the fabrication of subsequent titanium nose caps for the HLH Prototype Program. Areas for improvement included:

- (1) Radius of leading edge, and
- (2) chordwise bow of the outboard blade section.

Changes to the method and tools are shown in Figure 67. For example, 3000 pounds of additional weights have been added to improve forming of the leading edge radius. A cap made of refrasil, a refractory silicone blanket material, is being used on the cap's leading edge during the forming operation to help control cool-down of the part. A ceramic female upper cap has been added to approximately 10 feet of the outboard blade section to improve nose radius forming.

5.4 QUALITY ASSURANCE

The quality level of the HLH/ATC rotor blades was achieved through the control of processes used in blade development and by thorough inspections of details, subassemblies, and the finished product. Specimens were fabricated from the materials used in the blade construction to check the validity of the inspection techniques. These techniques, which were later used to inspect the rotor blade itself, gave a high degree of confidence in the quality of materials and processes.

The critical characteristics of each blade subassembly were inspected during fabrication, after assembly into the blade, and after blade component specimen tests. Final inspection of the assembled blades was performed to assure compliance with design requirements.

A Quality Assurance Capability Analysis was made to ensure that component characteristics were measured and processes adequately controlled during development of the blade.

The basic element of the Capability Analysis was the Quality Assurance Flow Chart, Figure 68, which shows schematically the processes involved from the receipt of materials to final assembly of the blade.

Nondestructive Testing (NDT). Both ultrasonic and penetrating radiation (X-ray) techniques were used to determine the presence of voids, delaminations, unbonded areas and fiber orientation. The ultrasonic inspection was performed on the "D" spar using a Dondicator Bond Tester at the root end and heel areas, and then using the Custom Machine semiautomatic scanning system to inspect the upper and lower airfoil sections. The size and location of all detected indications equal to or greater than 1/4-inch diameter were recorded and kept on file.

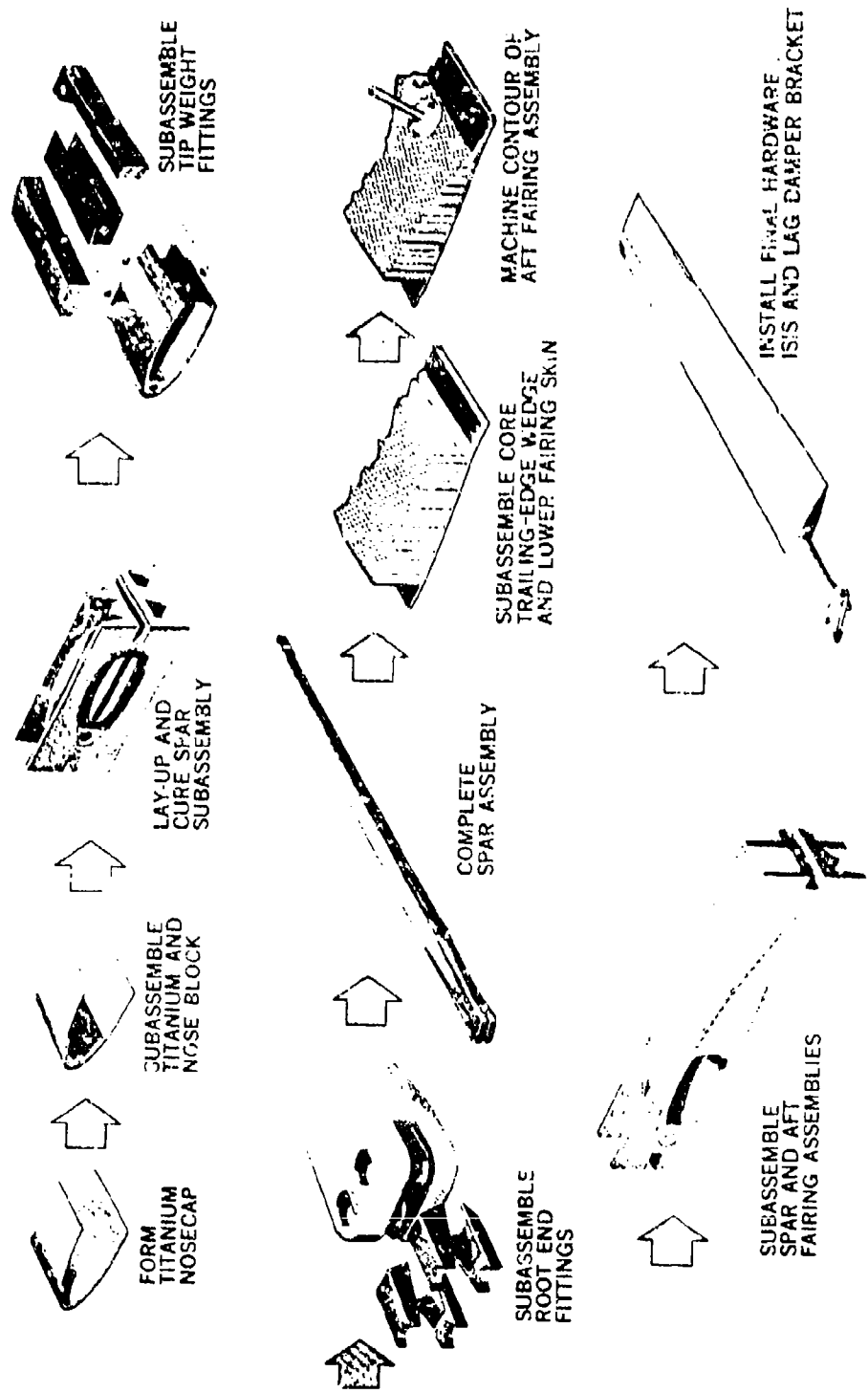


Figure 52. HLH Rotor Blade Fabrication Sequence

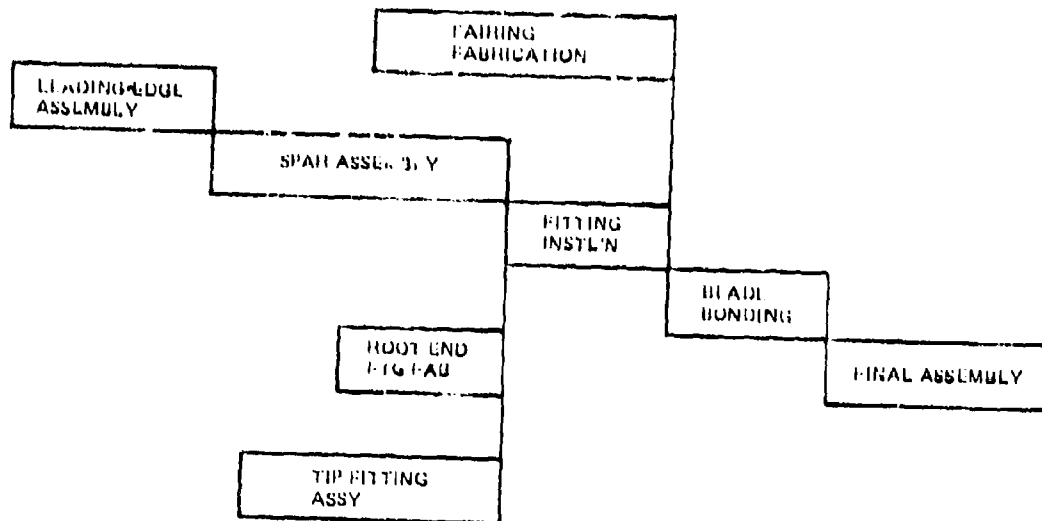


Figure 53. HLH Blade Fabrication Flow Diagram

FABRICATION SEQUENCE

- LEADING-EDGE ASSEMBLY
- SPAR ASSEMBLY
- ROOT END FITTING FABRICATION
- TIP FITTING ASSEMBLY
- FITTING INSTALLATION
- FAIRING FABRICATION
- BLADE BONDING
- DAMPER ARM ASSEMBLY
- FINAL ASSEMBLY

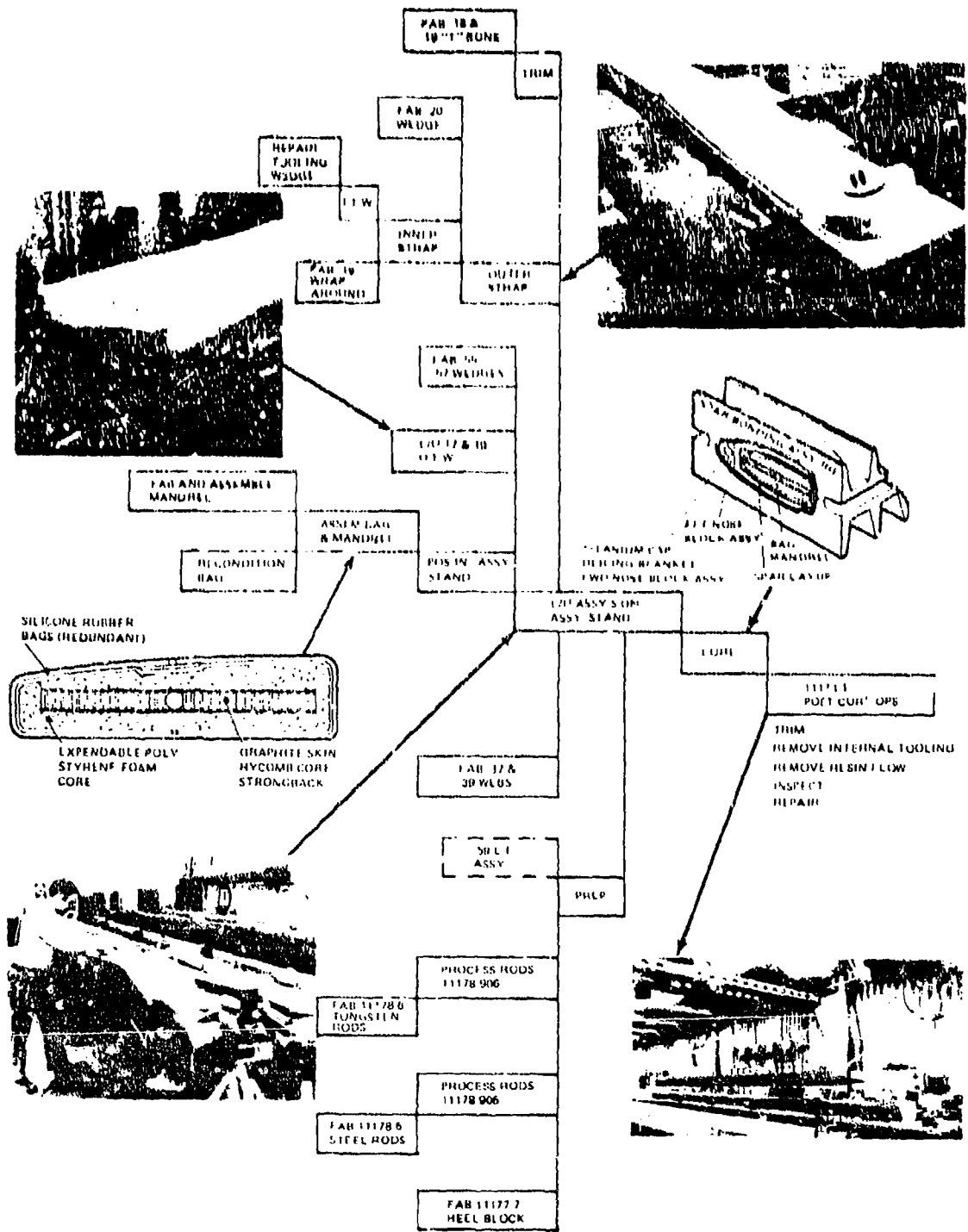
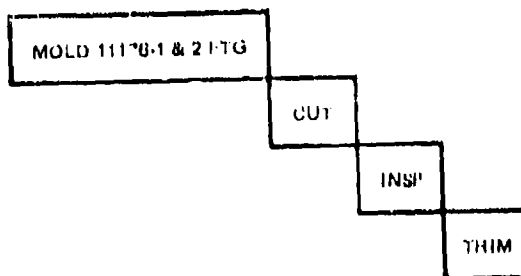


Figure 55. Spar Assembly Flow Chart

INSERT FITTING
301-11178-1 & 2



CLOSURE FITTING
301-11204-1 & 3

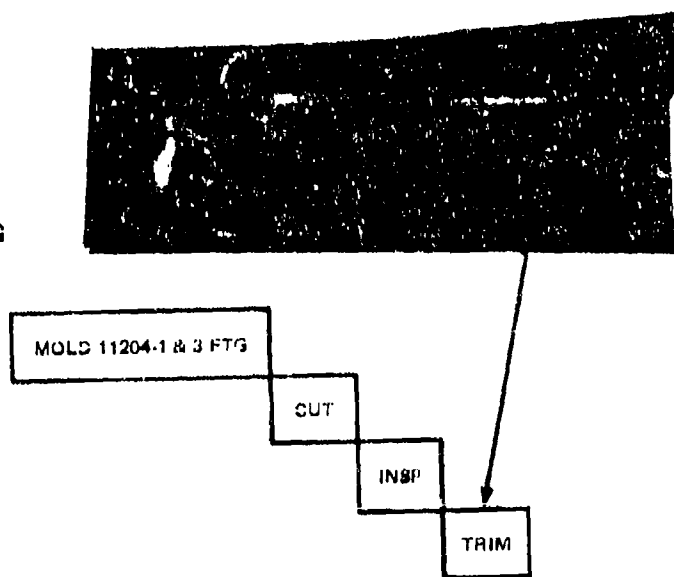


Figure 56. Root End Fitting Fabrication Flow Chart

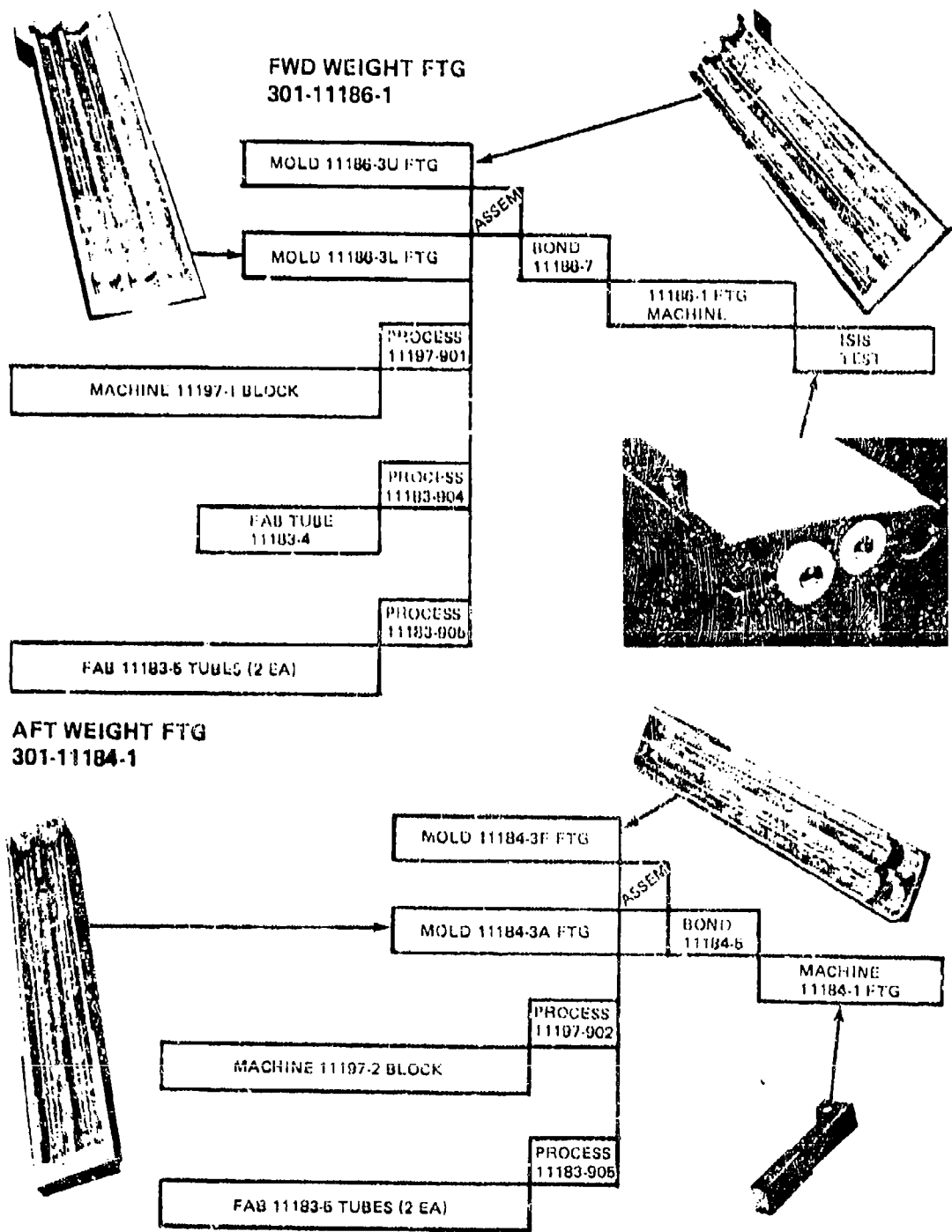


Figure 57. Tip Fitting Assembly Flow Chart

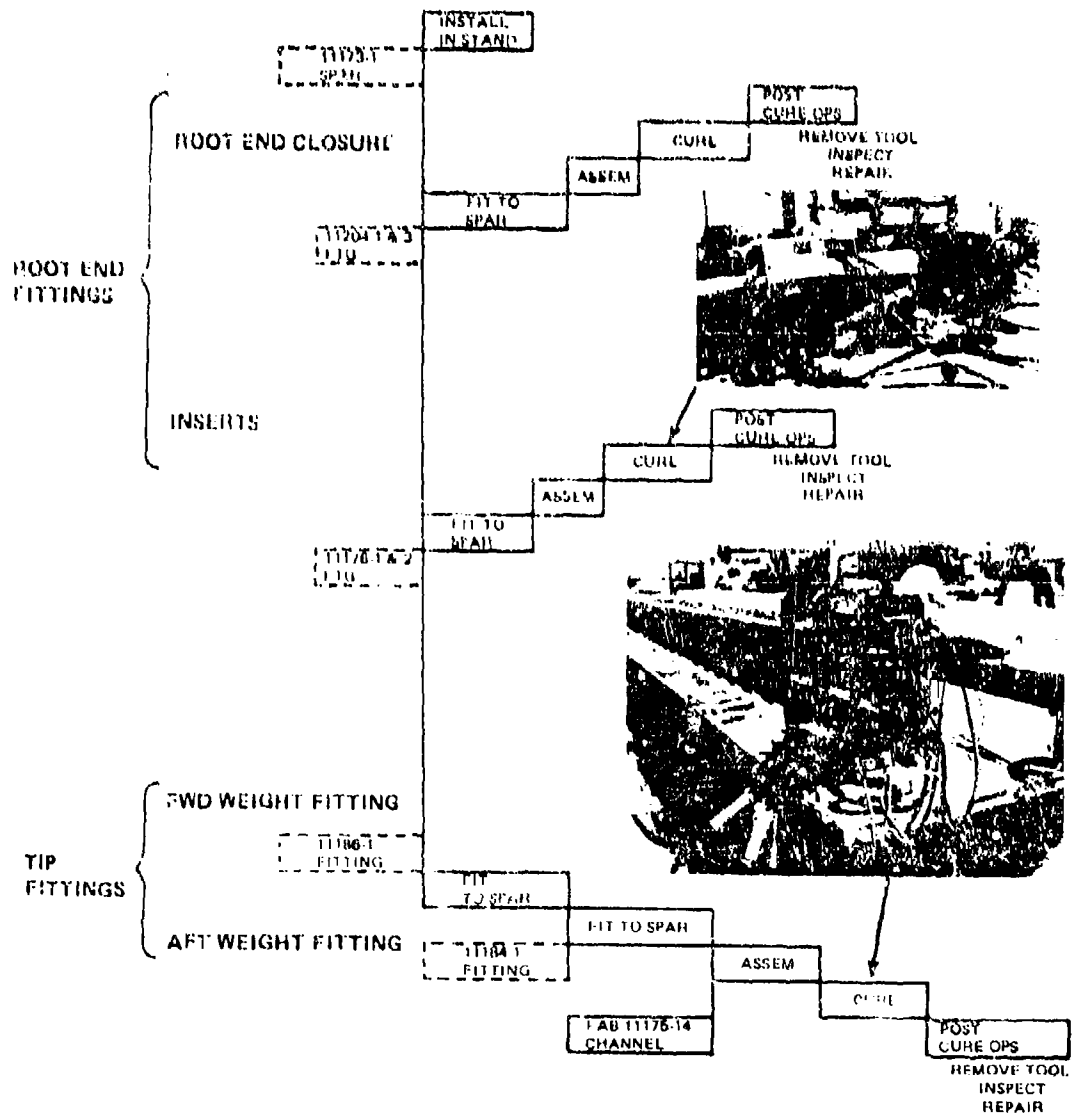


Figure 58. Fitting Installation Flow Chart

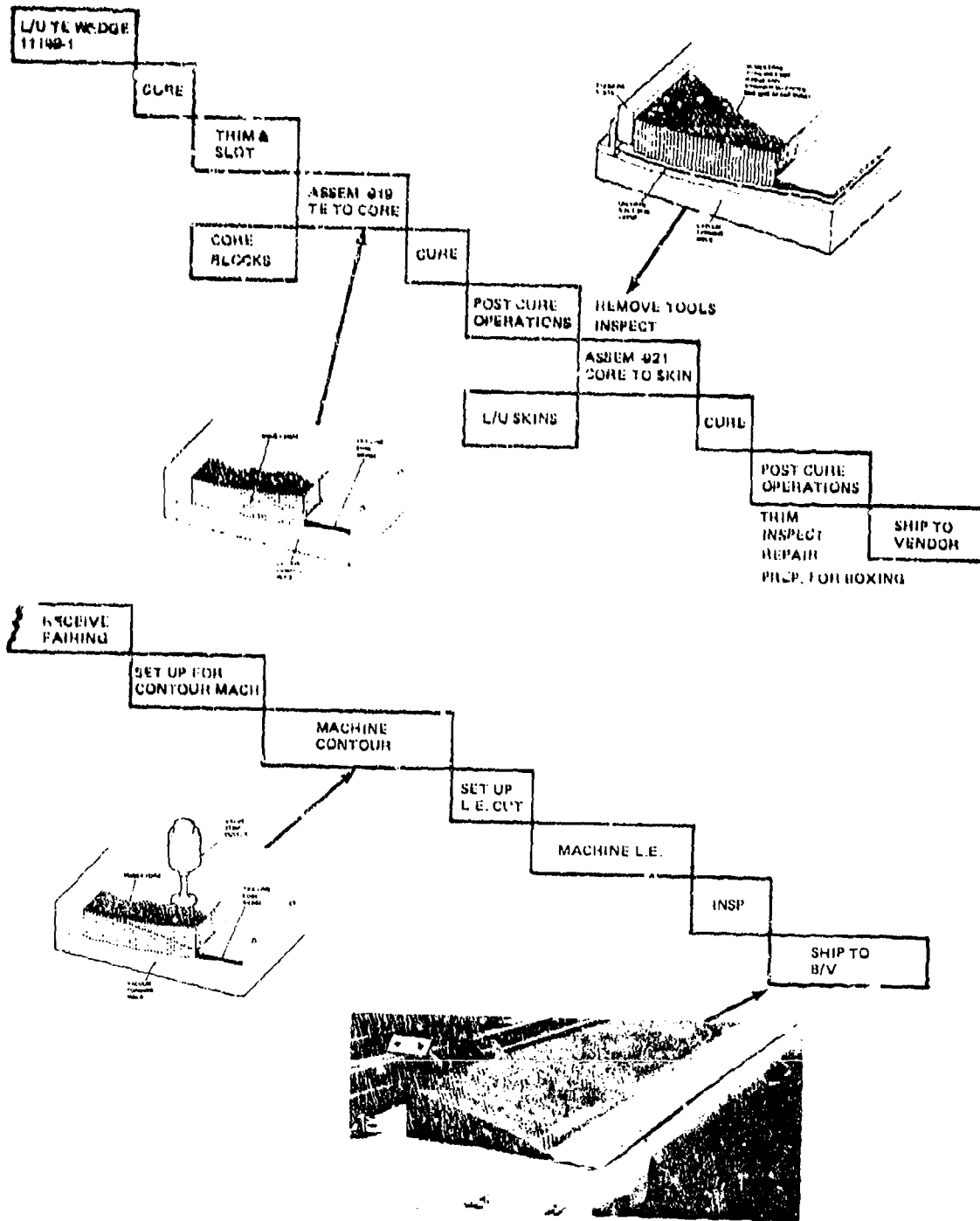


Figure 59. Pairing Fabrication Flow Chart

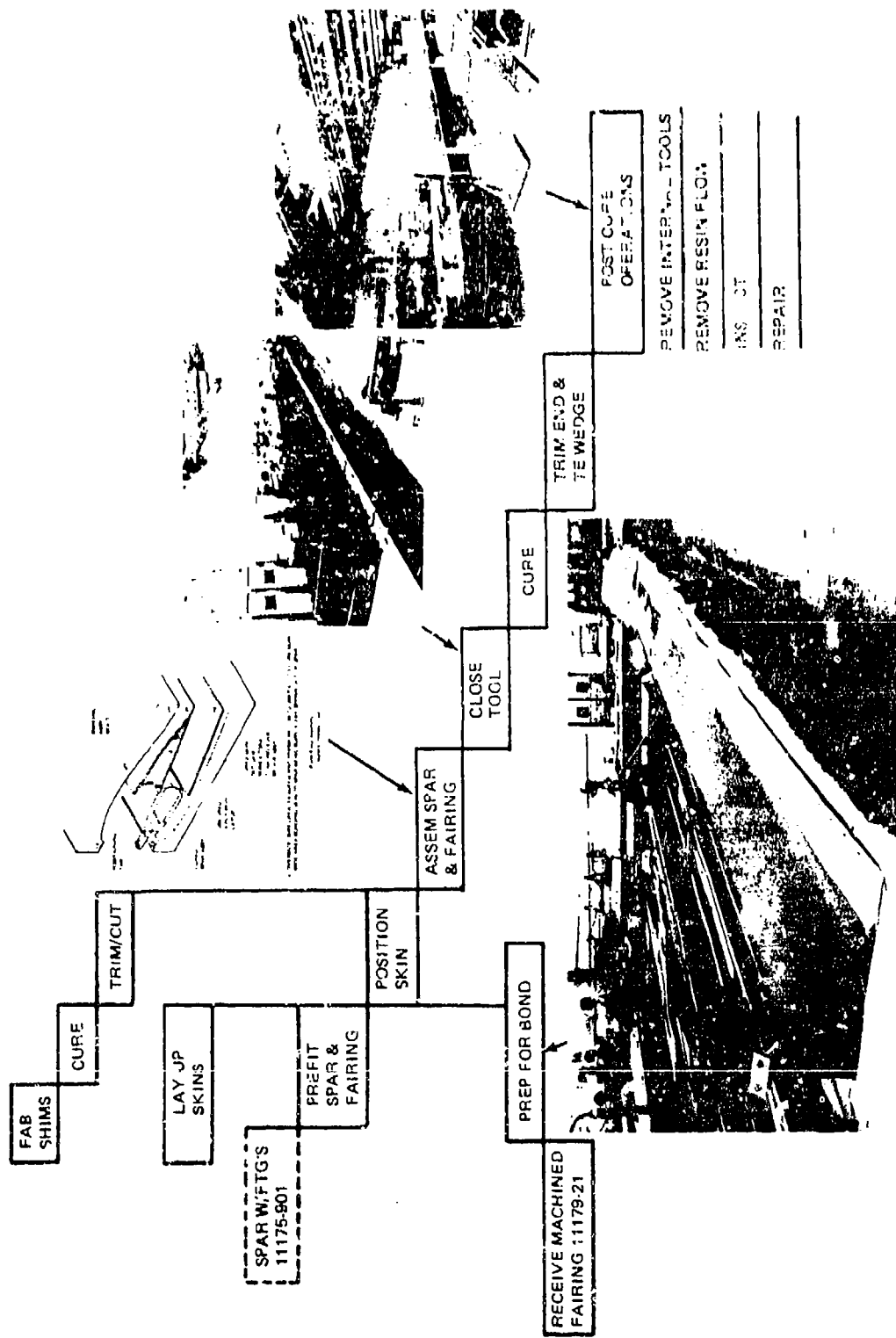


Figure 60. Blade Bonding Flow Chart

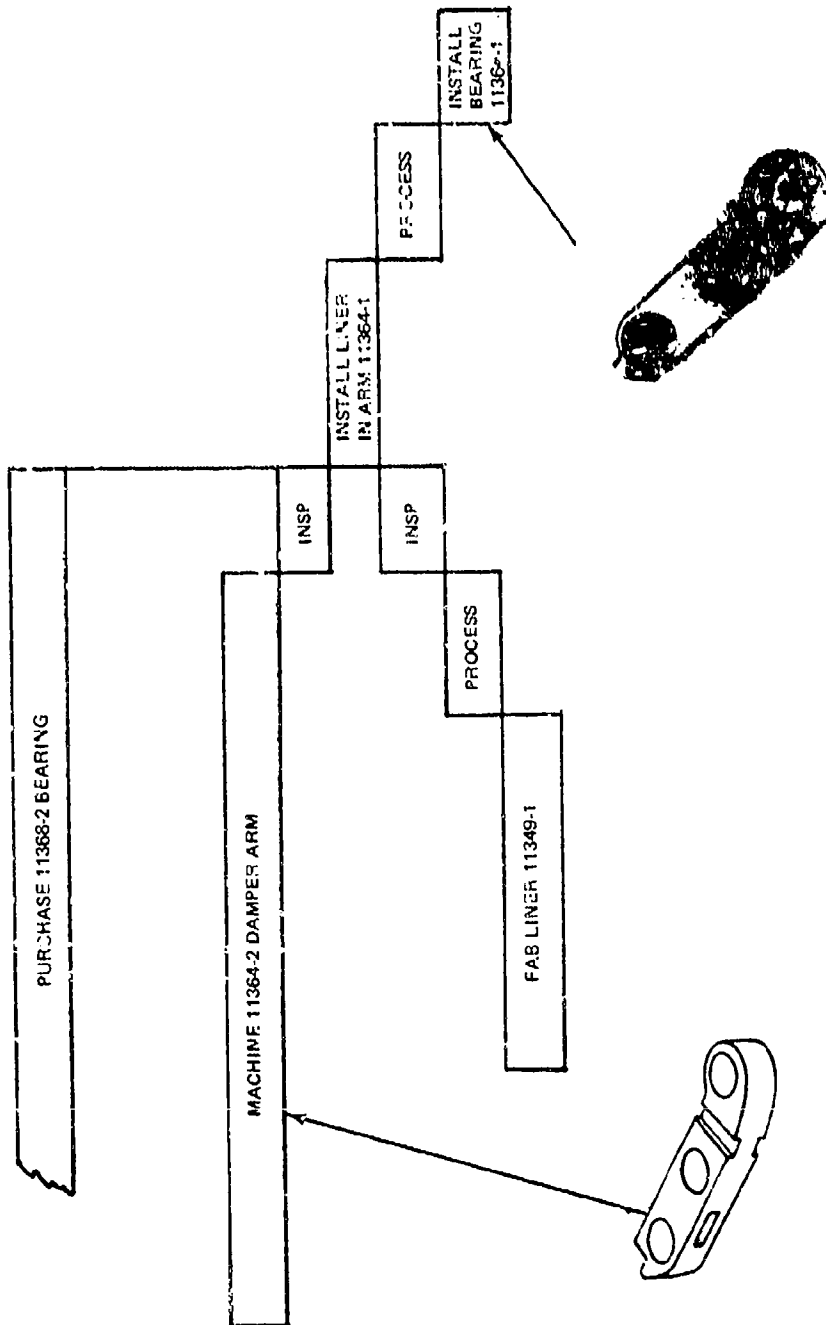


Figure 61. Damper Arm Assembly Flow Chart

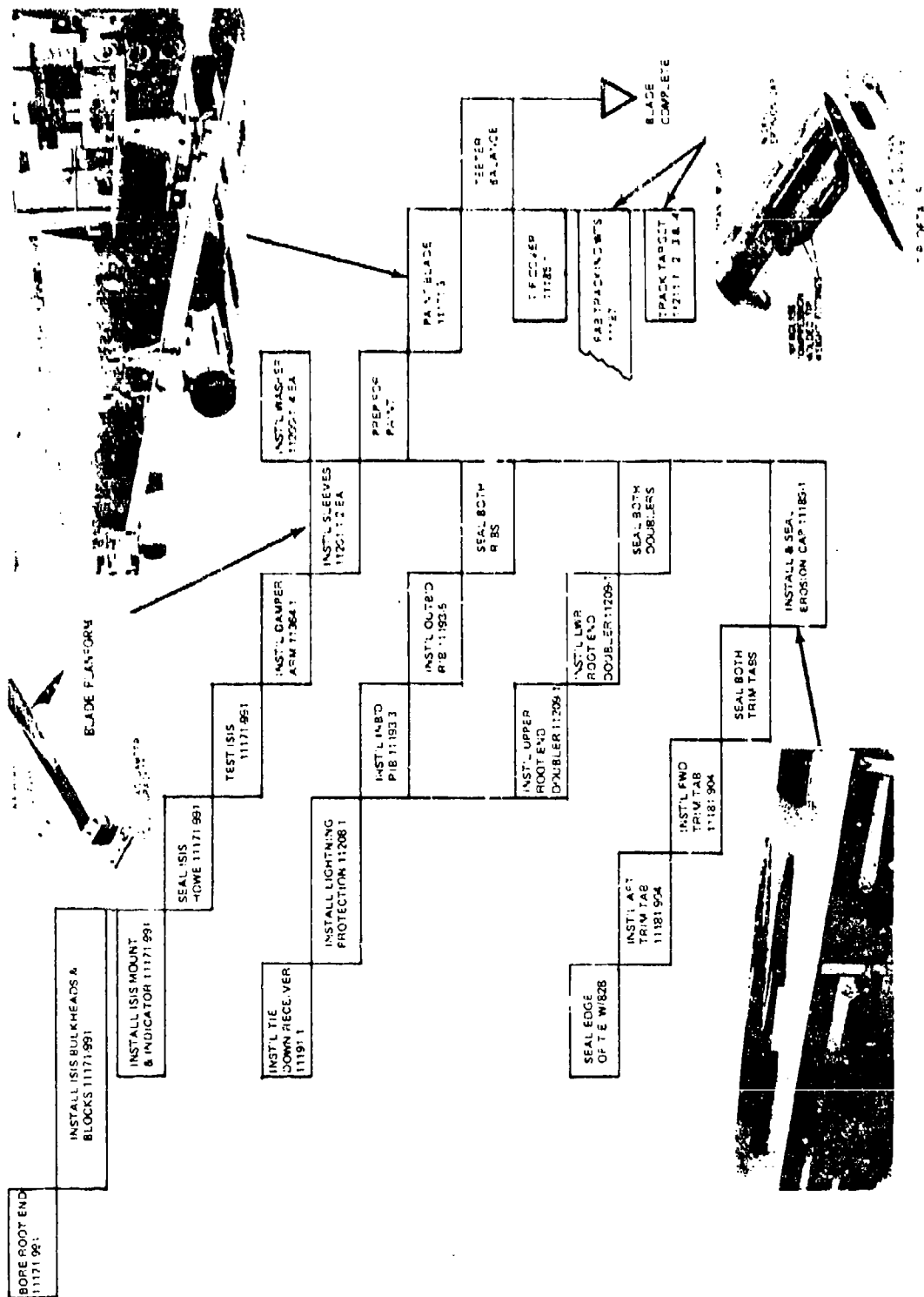


Figure 62. Final Assembly Flow Chart

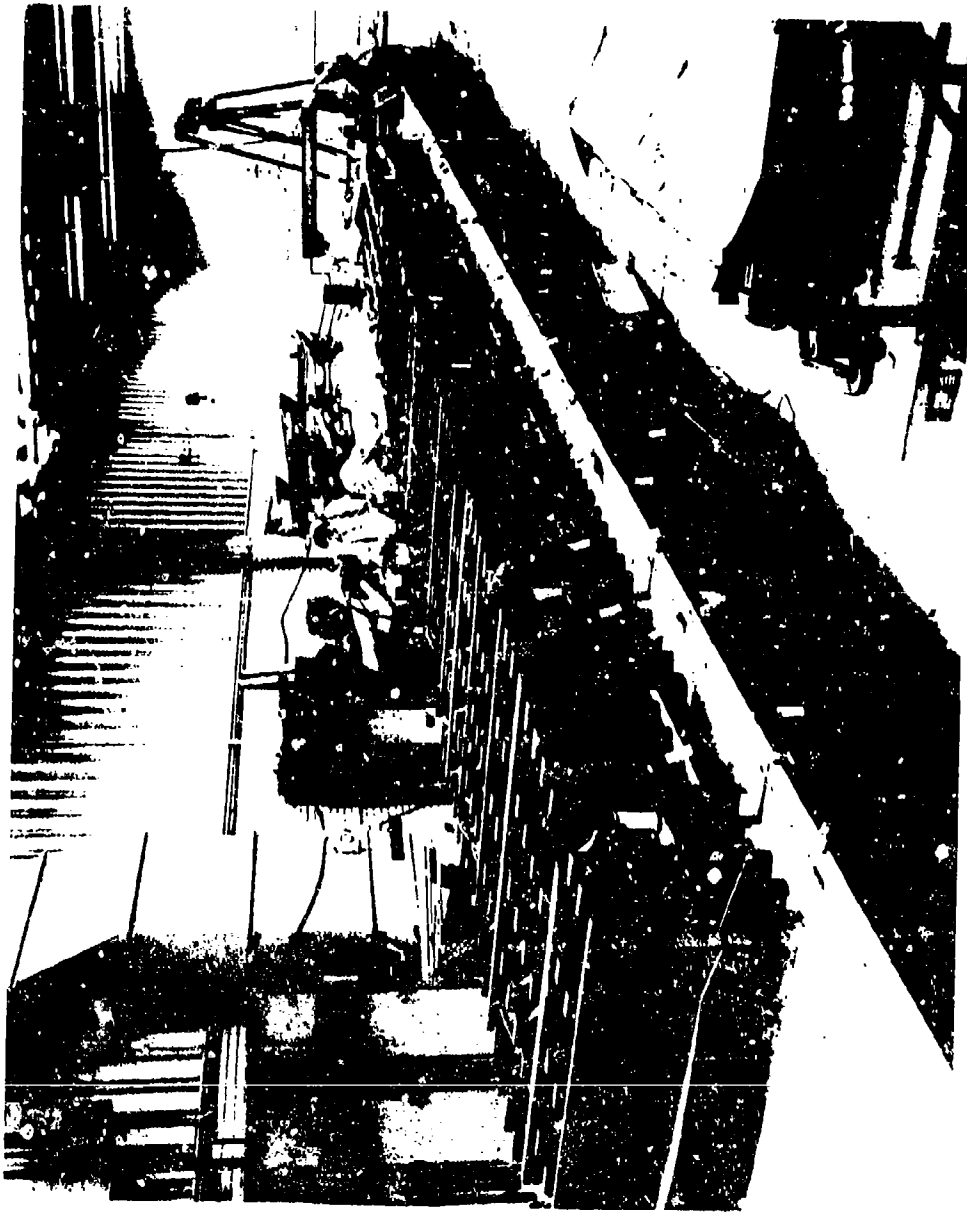


Figure 63. Main Bond Tool Being Closed

TABLE 10. COEFFICIENT OF THERMAL EXPANSION COMPARISONS

<u>Material</u>	<u>Coefficient of Thermal Expansion 10^{-6} In./In./°F</u>
Titanium	4.7
Glass/Epoxy Unidirectional	4.8
Glass/Epoxy Crossply	7.1
Mechanite H.S. (Tool Material)	5.9

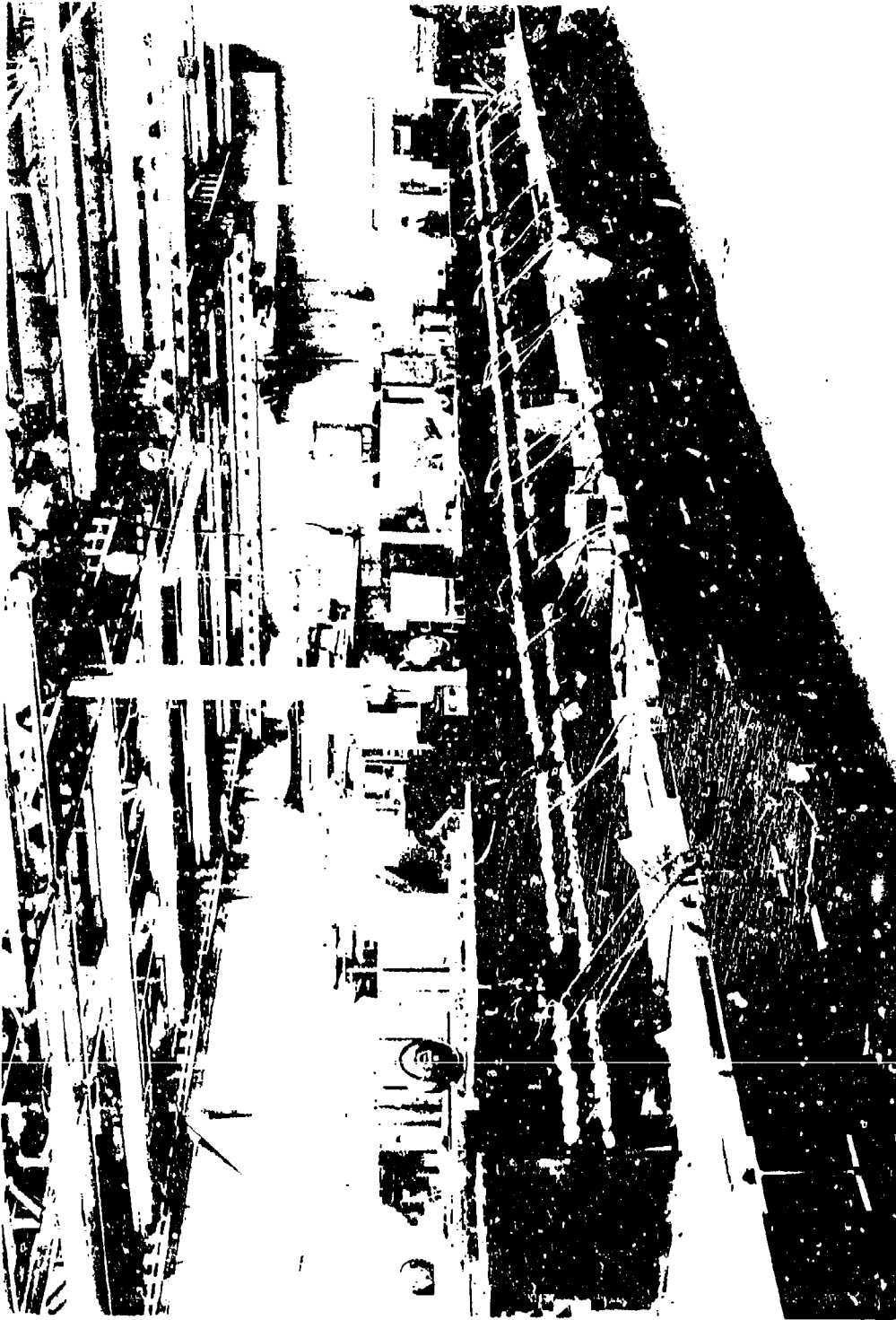


Figure 64. Spar Bonding Fixture Ready for Use

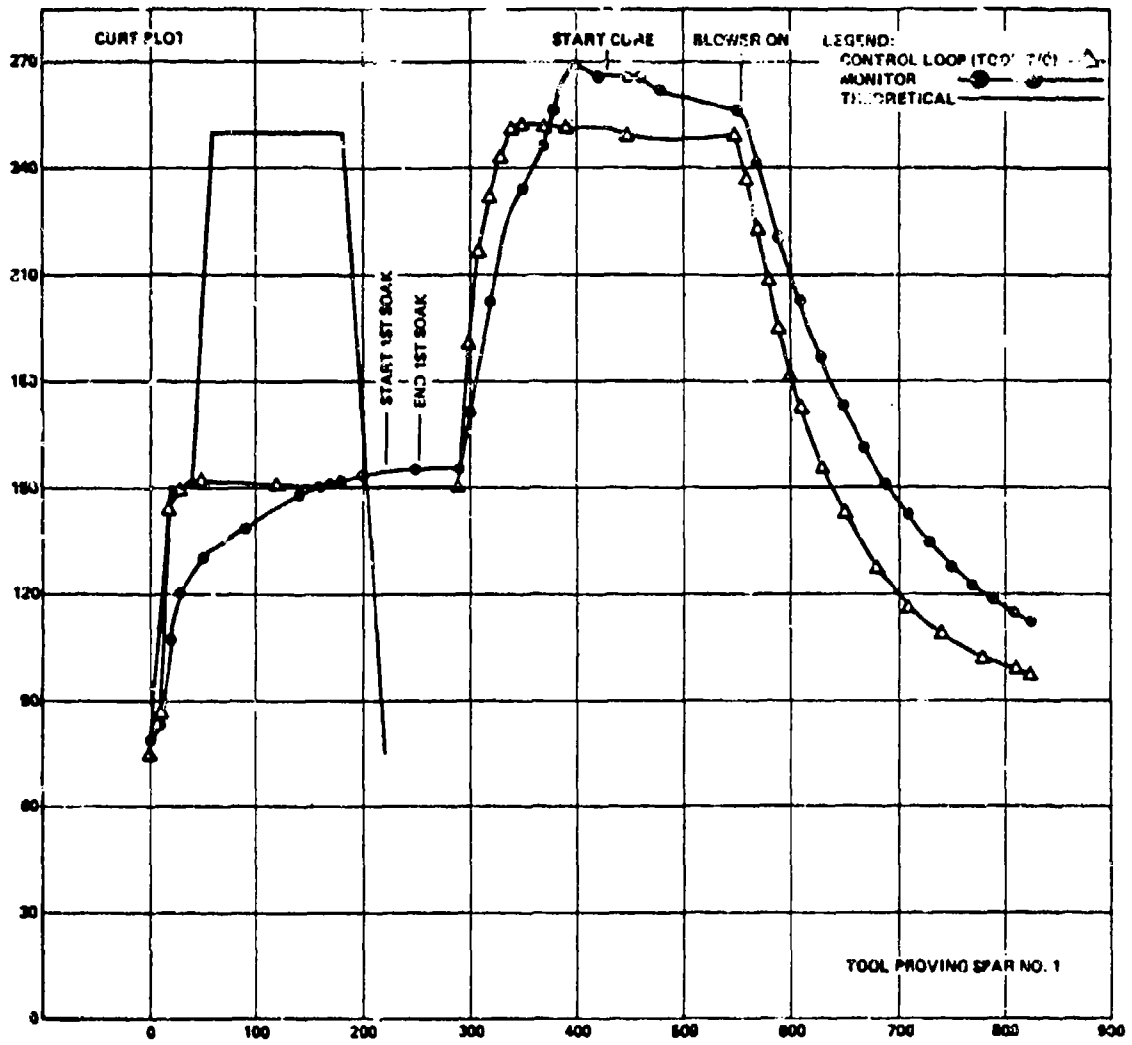


Figure 65. Spar Curing Operation Heating Cycle

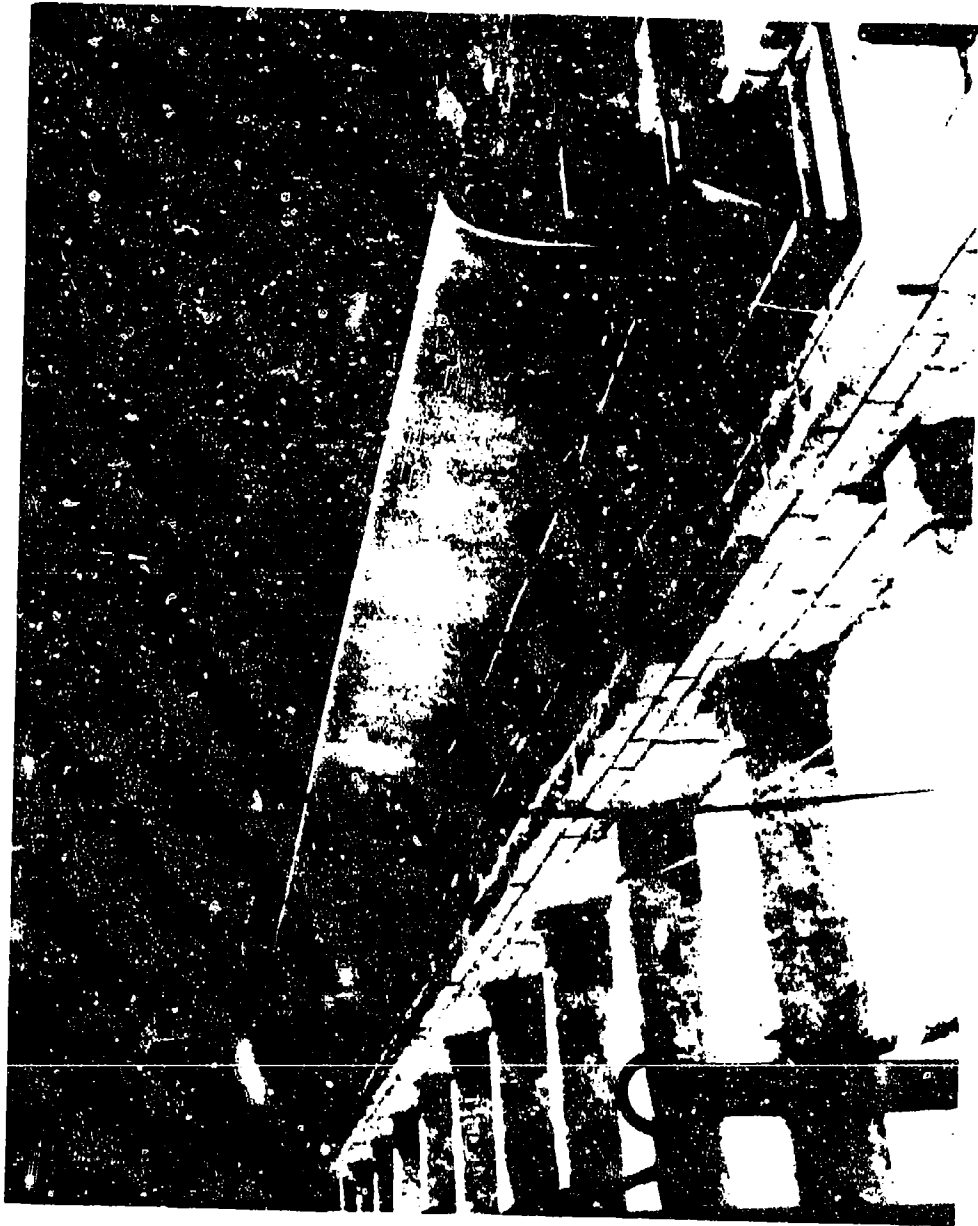


Figure 66. Titanium Cap Forming Tool

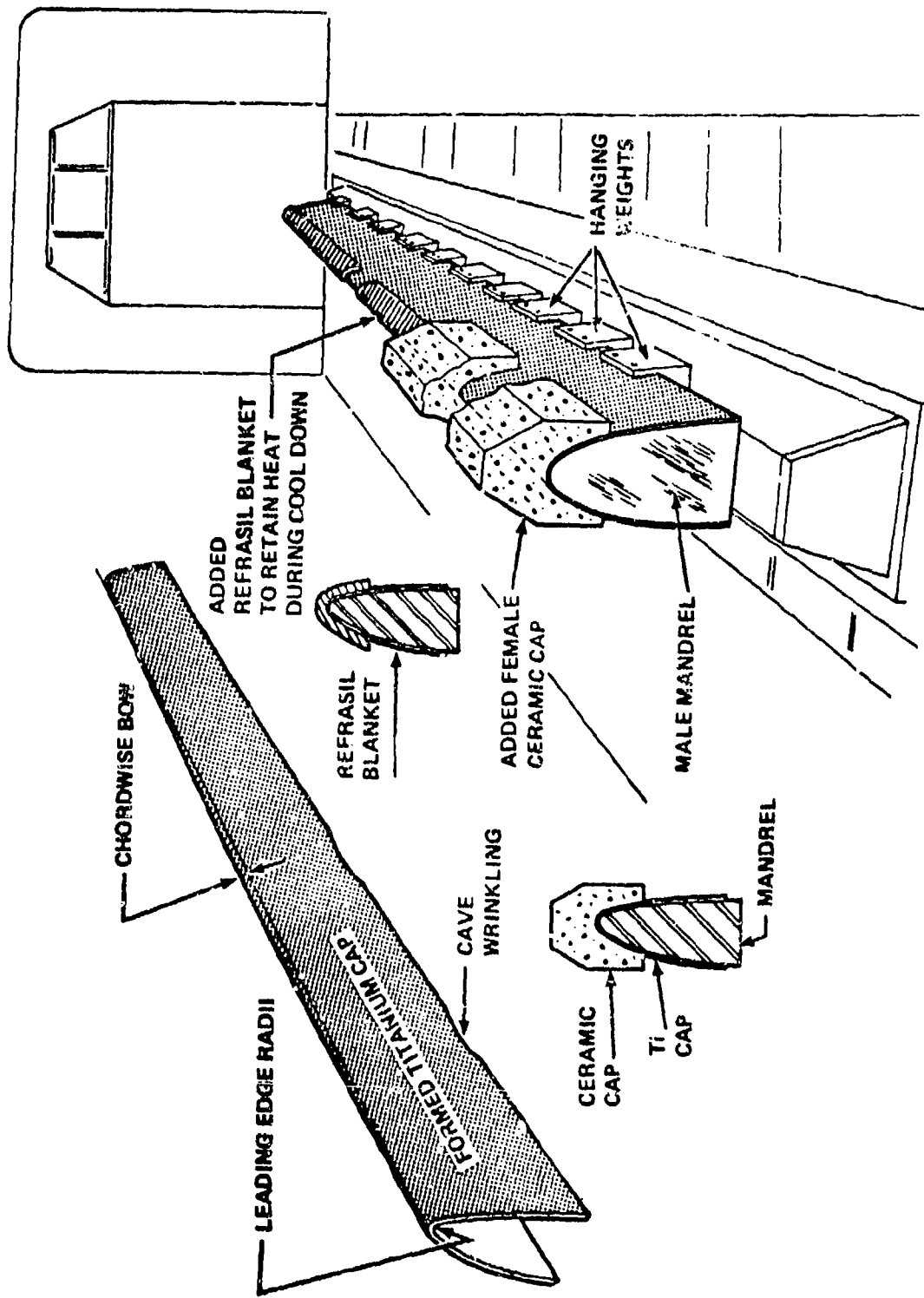


Figure 67. Tooling Improvements for Titanium Nose Cap

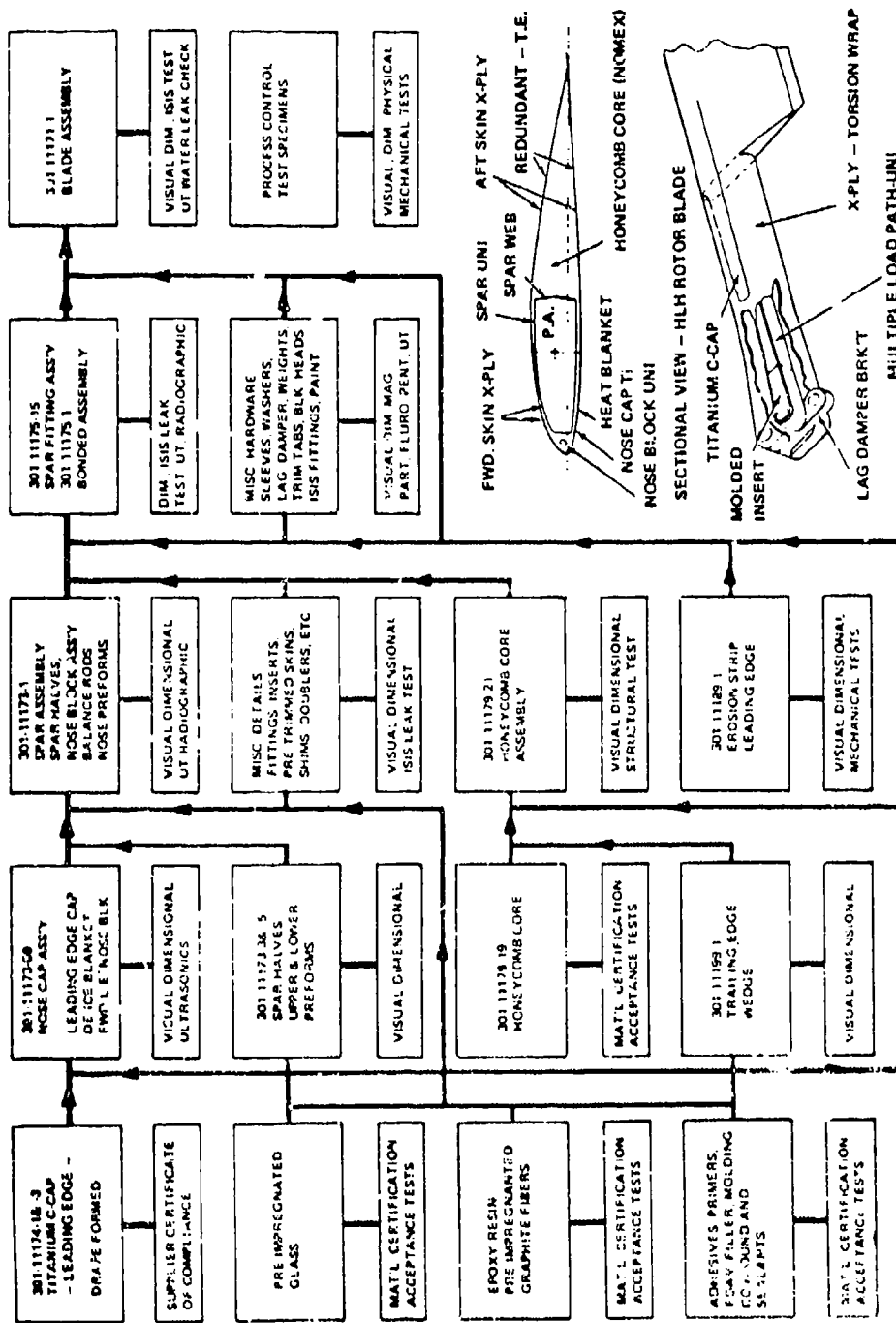


Figure 68. Quality Assurance Flow Chart

6.0 DEMONSTRATION TESTS

6.1 FULL-SCALE COMPONENT STRUCTURAL TESTS

This section reviews the results from a series of rotor blade structural demonstration tests. The structural test results, along with the design load predictions, structural analysis and rotor whirl demonstration, establish the flight worthiness of the HLH rotor blades. The primary objectives of these tests were to provide verification of the design limit and fatigue strengths of the HLH rotor blade full-scale components. The detailed descriptions of the tests are contained in Reference 17. The results of the design support root end test are contained in Reference 9. Maximum flight loads and special condition ground loads were applied to verify static strength. Fatigue loads were selected to establish endurance limits for use in the prediction of safe life hours for the rotor blade components. Failure mode, failure propagation, fail-safe characteristics, and the capability of the delta pressure integral spar inspection system (ISIS) were also investigated. Angular deflection measurements were recorded for verification of torsional stiffness in the root end and outboard torsion specimens.

The first set of test specimens were made to the specifications of the HLH/ATC rotor blade (Boeing Vertol Part No. 301-11171-1). Results from the initial structural substantiation tests were used to improve the HLH rotor blade design. These design improvements have been incorporated into the HLH Prototype rotor blade (Boeing Vertol Part No. 301-55101-1). Results from structural demonstration tests of the HLH Prototype rotor blade are included in this report.

The HLH rotor blade structural demonstration consisted of five separate tests. The test specimens represent portions of the rotor blade as shown in Figure 69.

Root End

These tests were conducted primarily to verify the static and fatigue strength of the root-end section of the HLH rotor blade.

- The root end static strength was demonstrated by successfully sustaining limit and ultimate loads.
- The 18,000-pound lug load fatigue endurance limit established by this test is sufficient to justify a safe life prediction of over 3600 hours (see Figure 70).
- A requirement for a revised anti-fretting system was identified during the initial fatigue testing. Fiber-glide was demonstrated to be a satisfactory solution for inhibiting fretting of the root end metal hardware.
- The design development root end test specimen could not retain ISIS vacuum due to leakage in the vicinity of the lag damper arm. During the structural demonstration test, a bulkhead, installed immediately outboard of the lag damper arm, was proven sufficient to retain the ISIS vacuum in the root end of the blade.
- A secondary objective of the root end test was to verify the torsional stiffness. This test indicated that the torsional stiffness of the root end is 1.34 times greater than theoretically predicted based on a comparison of predicted and measured torsional deflections between Stations 66 and 153.
- The fail-safe testing demonstrated that the root end is capable of sustaining at least 172 hours of high-speed level flight load with one attachment lug failed, and an additional 14 hours with a major failure simulated in this test by a 6' x 12" hole cut through the section at Station 104 (see Figure 71).

Outboard Torsion

These tests demonstrate the pitching moment static and fatigue strength of the HLH rotor blade.

- The torsion limit load capability was demonstrated on the outboard rotor blade specimen.
- A requirement for a precured heel to prevent premature fatigue failures caused by wrinkles was identified during the first torsion specimen fatigue test. The second torsion fatigue test specimen with its precured heel demonstrated an endurance limit of $\pm 80,000$ inch pounds. This endurance limit is sufficient to justify a 6131-hour safe fatigue life for the predicted flight loads. Except for the wrinkled spar heel, no failures occurred in either the titanium nose cap or the fiberglass spar during the torsion testing.
- Torsional stiffness and shear center location of the outboard section of the blade were verified by this test.
- The specimen sustained 107 hours of dynamic loading equal to or greater than V_H load with a simulated titanium failure. The simulated titanium crack did not propagate and the fiberglass did not fail.

Intermediate Bending

This test was conducted to establish the endurance limit of the rotor blade spar structure subjected to vibratory flapwise bending moment and static CF. Figure 72 shows a specimen in the test fixture.

- The fatigue strength of the titanium nose cap demonstrated by the intermediate bending tests is below the safe life design requirement. In the ATC specimen, this was due to shear cracks in the titanium created during the rolling process of the raw material. The material processing was changed for the nose cap used for the Prototype test specimen and no failures were experienced in the Prototype test due to shear cracks. In the Prototype specimen, fatigue cracks developed at molten titanium deposits on the nose cap. These deposits were created during the post-forming cleaning process. (Figure 73 shows a typical fatigue crack.)
- The 16,320 psi mean minus three sigma endurance limit established by these tests for the titanium nose cap is not sufficient to predict a 3600-hour life. The damaged caps have sufficient fatigue strength to provide a predicted life in excess of 1000 hours for the Prototype helicopter mission. Coupon tests show that elimination of defects in the titanium nose caps would result in a predicted safe life of 59,500 hours. (See Figure 74).
- 427 hours at level flight loads, and 109 hours at maneuver loads were demonstrated during fail-safe testing of the intermediate bending specimen with the titanium failed. The fiberglass maintained its structural integrity throughout the fatigue and fail-safe bending tests.
- Because of the demonstrated fail-safe characteristics of the composite rotor blade, cracking of the titanium nose cap is not considered to be a flight-safety issue for the Prototype flight test program. Therefore, Prototype blades fabricated with the same type nose caps as used in the Prototype test specimen are flyable on an "on-condition" basis.

Simulated Chordwise Airloads

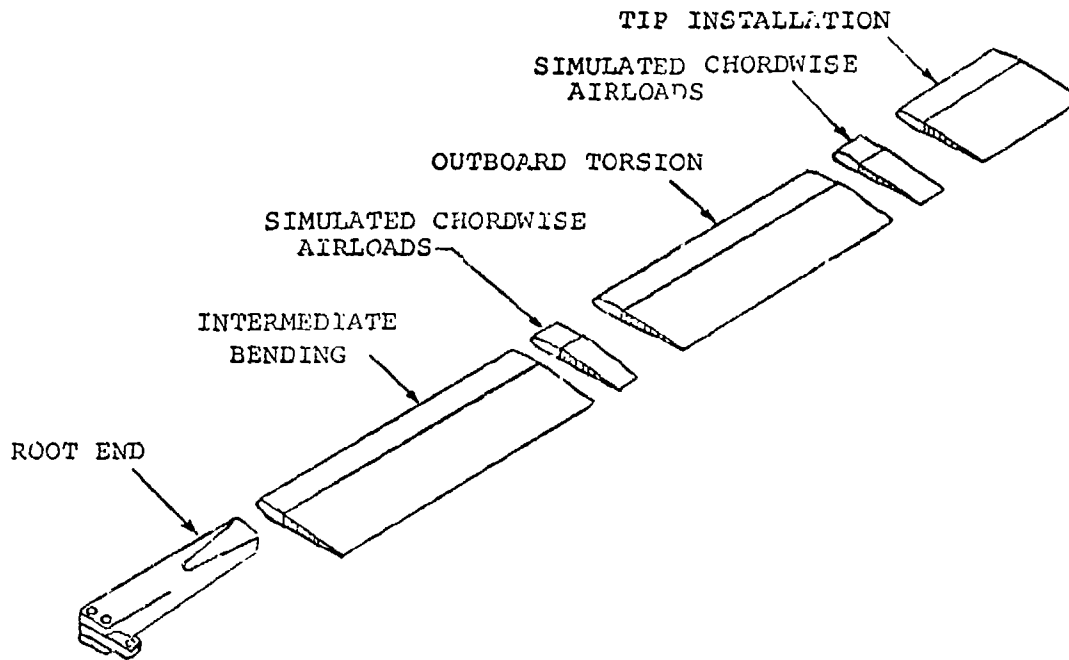
The simulated airloads test was conducted to demonstrate the fatigue capability of the Nomex honeycomb core and the bonded joint between the spar heel and the aft fairing. The test results are summarized in Figure 75.

- The fatigue strength of the Nomex core at the spar heel joint was found to be inadequate for the ATC design configuration. Premature failures occurred in the Nomex core due to core thickness and deflection in the spar heel. Neither effect was accounted for in the initial strength prediction.
- The rotor blade section was redesigned to reduce the spar heel deflection and to strengthen the core. The spar heel was stiffened using unidirectional graphite with the fibers oriented in the chordwise direction. The core density behind the heel was increased and a horizontal splice was introduced into the core. Fatigue testing of the redesigned chordwise airload specimens demonstrated an endurance limit for the Prototype rotor blade fairing that is adequate for predicting a safe life of over 3600 hours.
- No indications of failure occurred in the bond between the fairing skins and the spar heel indicating that this mode of failure is less critical for the HLM design.

Tip Section

Static and fatigue tests were conducted to verify the ultimate CF tension and vibratory flapwise bending moment capability of the structural elements concentrated at the tip of the HLM rotor blade. The tip structure retains the weights required for dynamic balance and rotor blade tracking.

- The vibratory loads applied to the tip specimen demonstrated a fatigue strength sufficient to establish a safe life prediction of over 3600 hours.
- The ultimate strengths of the tip retention hardware components were demonstrated by the successful application of tension loads equal or greater than 1.52 times the design ultimate loads.



TEST	SPECIMEN DESCRIPTION
Root End	#1 ATC Specimen #2 Redesigned Lag Damper Arm and Fiberglass Fretting Inhibitor
Outboard Torsion	#1 ATC Specimen #2 Prototype with Precured Spar Heel
Intermediate Bending	#1 ATC Specimen #2 Prototype with Precured Spar Heel
Simulated Chordwise Airloads	#1-#5 ATC Specimens #6-#11 Prototype Spar Heel and Fairing Core
Tip Installation	#1 ATC Specimen #2 Prototype Tip Fittings Cured with Spar

Figure 69. HLH Rotor Blade Structural Test Specimens

No Failures
 Specimens 1 and 2 ATC Configuration Reference D301-10239-2
 Specimen 3 Design Support Test

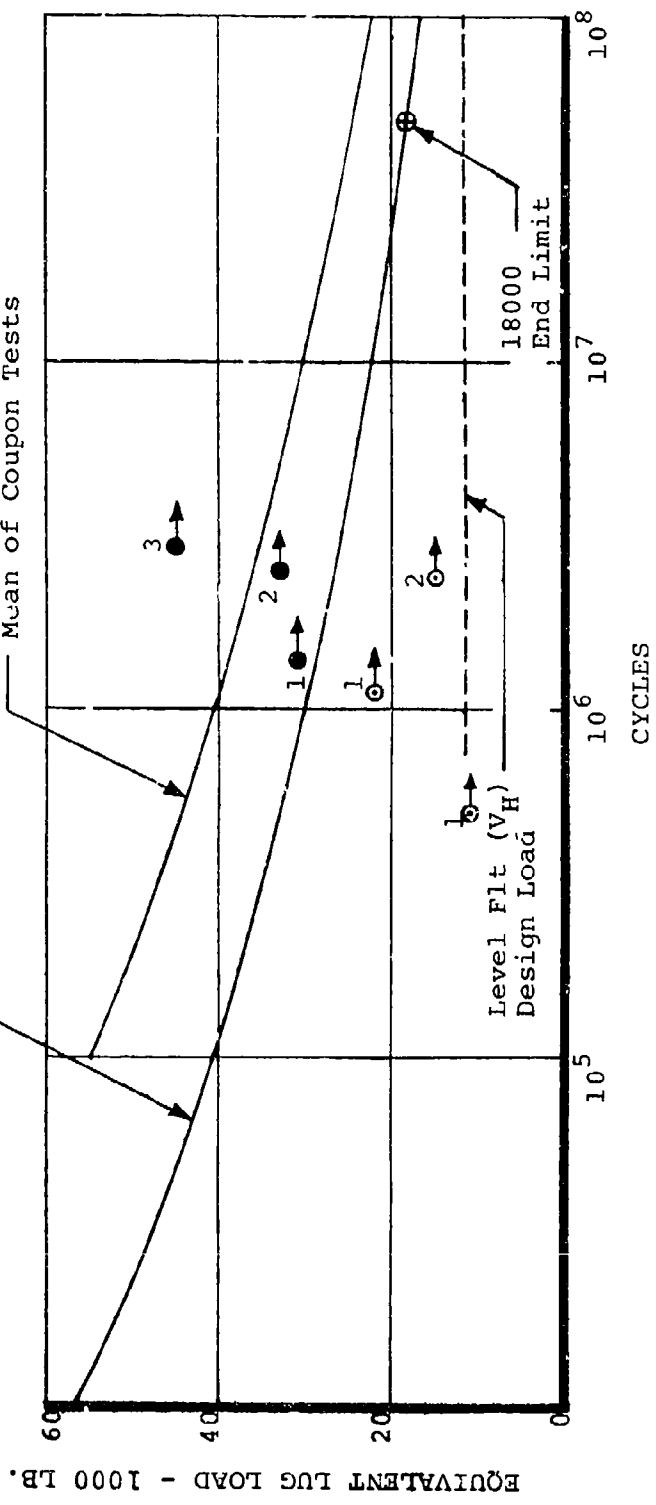


Figure 70. Full-Size Root End Tests Verified Design Allowables for Unidirectional Fiberglass



Figure 72. Intermediate Section Fatigue Test Fixture

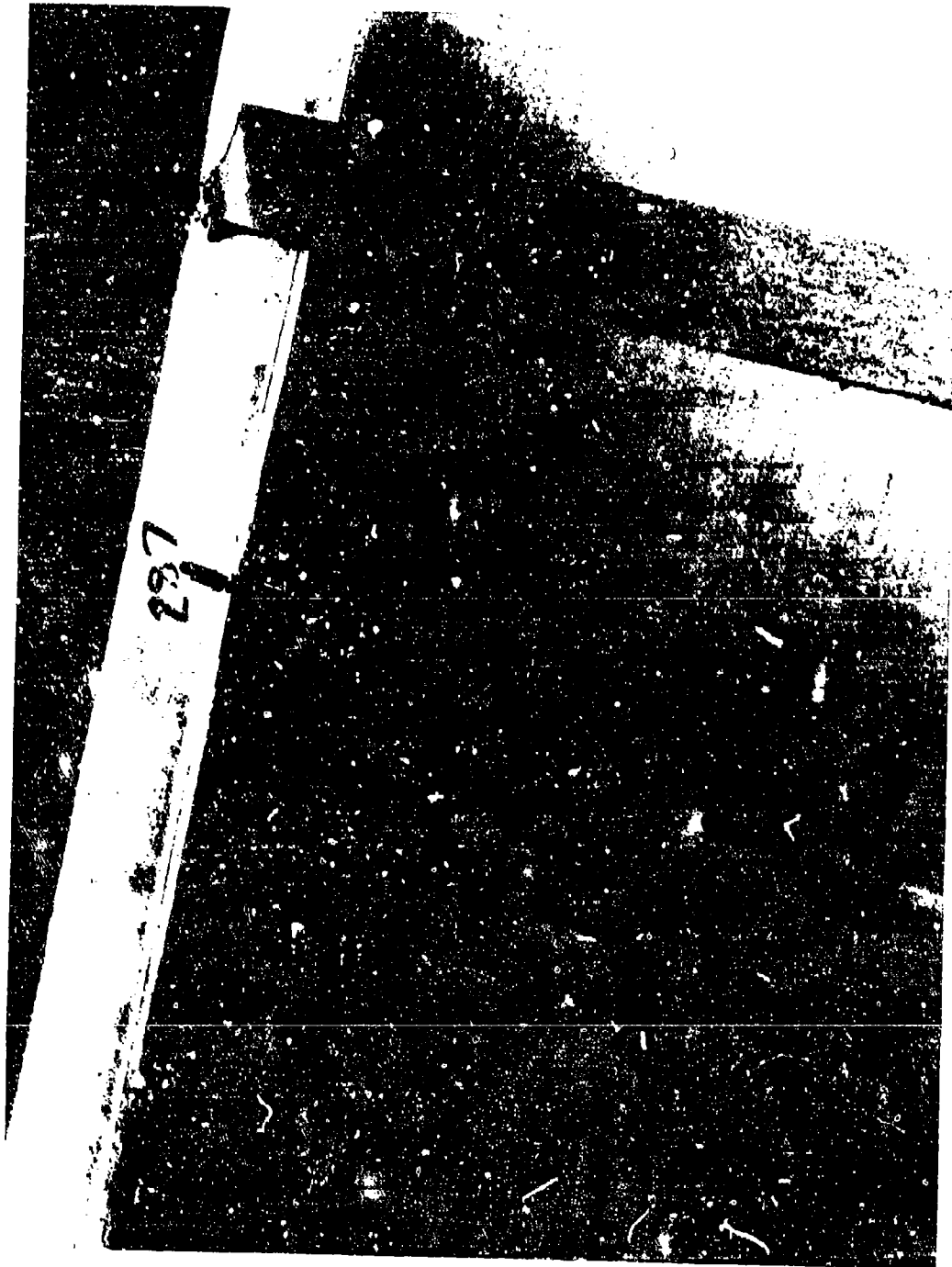


Figure 73. Titanium Nose Cap Fatigue Failure

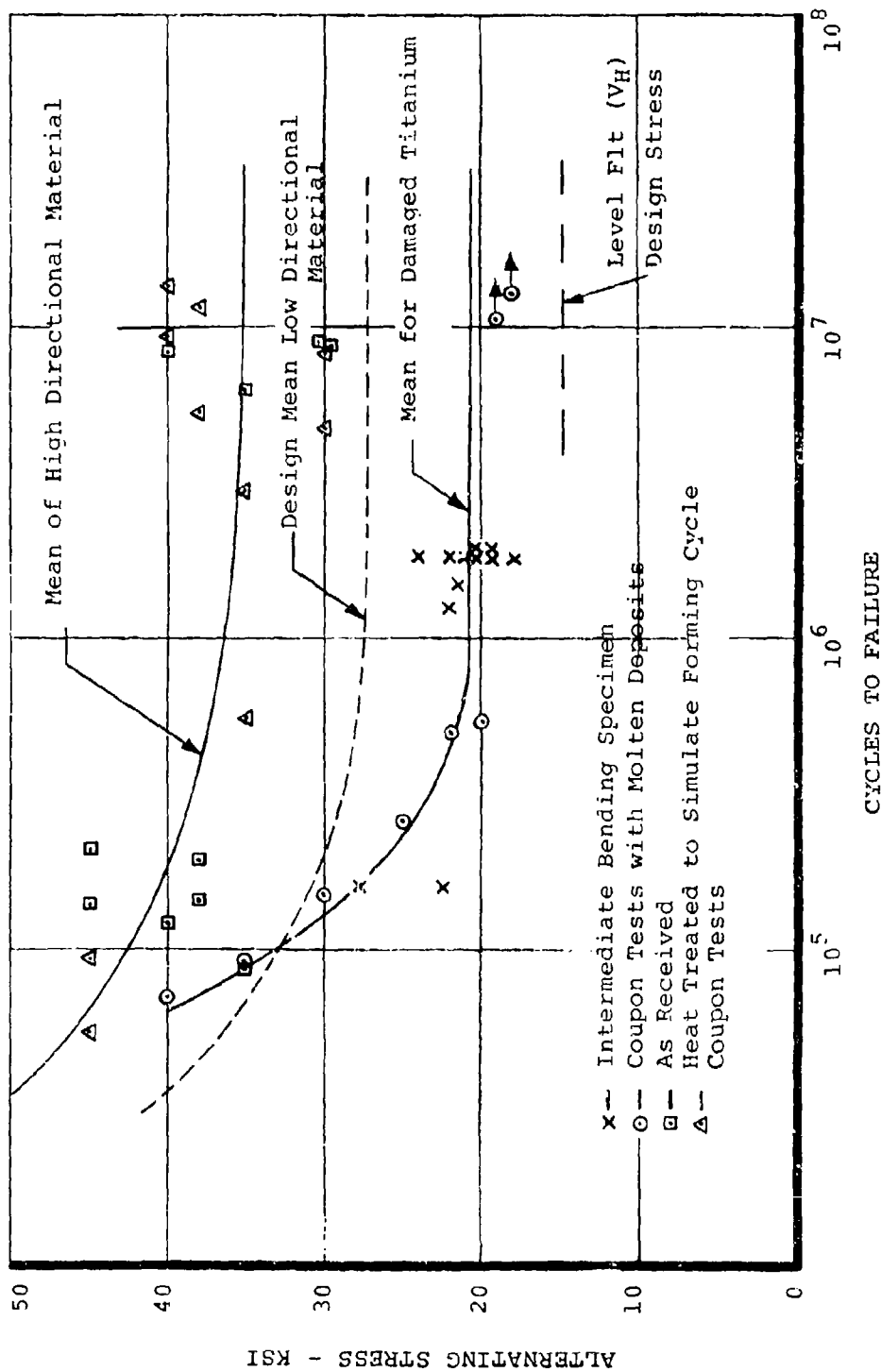
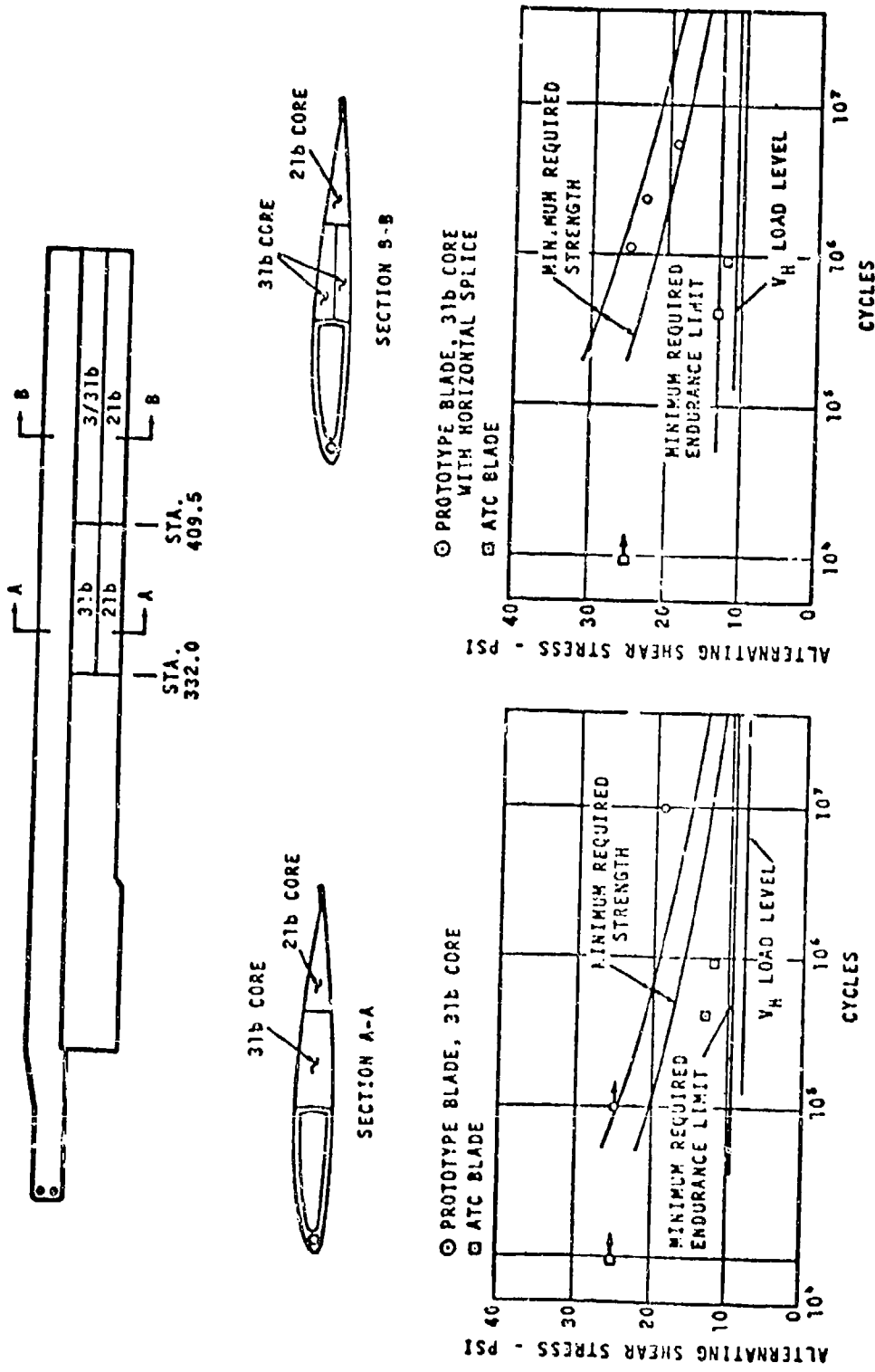


Figure 74. Fatigue Strength of Highly Directional 6AL4V Titanium Alloy Sheet With Effect of Molten Deposits



MODIFIED CONFIGURATION STRENGTH VERIFIED BY TEST

Figure 75. Nomex Honeycomb Prototype Configuration

6.2 NATURAL FREQUENCY AND STIFFNESS TEST

Static loads were applied to a full-scale HLH rotor blade to determine its flapwise and chordwise stiffnesses. These measured stiffnesses generally confirm the analytical predictions as shown in Figure 76.

A second objective of the full-scale blade test was to determine flapwise, chordwise and torsional natural frequencies and mode shapes at zero rotor speed. These natural frequencies and mode shapes were identified by varying the frequency of a driving force and observing the amplitude and phase relationship of the blade response. The test results are summarized in Figure 77.

The measured torsional natural frequency agreed closely with the theoretical frequency for the test configuration and confirms the predicted blade torsional stiffness/inertia properties.

The first and second flap bending frequencies compare acceptably with the analytical values. The third mode frequency is lower than calculated and further evaluation of this mode for in-flight rotating conditions is necessary.

Both the first and second chordwise bending frequencies are lower than calculated. The differences are attributed to the lower than predicted chordwise stiffness in the area of the fairing cut out. Based on the static results, the rotating frequency at normal rotor speed is expected to drop from a calculated value of 4.8 per rev to 4.5 per rev which is still considered acceptable.

The natural frequency and stiffness test results are reported in Reference 18. The proof load portion of this test program was never conducted because this blade was being held as a spare for the DSTR. It was planned that the proof load test be conducted following the completion of the DSTR test.

TABLE 11. COMPARISON OF THEORETICAL AND EXPERIMENTALLY DETERMINED BLADE BENDING STIFFNESS

STATION		FLEXURAL STIFFNESS $\cdot \text{EIX}10^6 \text{ lb in}^2$					
/R	INS	FLAPWISE			CHORDWISE		
		S/N 3	S/N 4	THEORY	S/N 3	S/N 4	THEORY
.13	72	1330	1280	1150	*	*	*
.158	87	*	*	*	1875	1850	1750
.218	120	838	808	790	1330	1410	1250
.29	160	501	*	496	5550	*	6100
.40	220	303	288	290	9250	*	9600
.60	330	231	244	235	7200	*	7900
.80	440	222	234	222	10350	*	9700

*No gages at these locations.

TABLE 12. COMPARISON OF THEORETICAL AND MEASURED NATURAL FREQUENCY

Mode	Test Results			Theoretical Natural Frequency	
	Support Station In.	Node Stations in.	Natural Frequency Hz	Test Setup Hz	On Hub Hz
1st Flap	420	422	2.35	2.41	2.44
2nd Flap	488	271, 488	7.5	7.98	8.07
3rd Flap	366	192, 366	15.	16.3	16.8
1st Torsion	549		10.77	10.6	11.4
2nd Torsion	549	382	29.71	29.6	31.8
1st Chord	407	410	9.23	10.4	10.5
2nd Chord	469	169, 462	23.1	27.8	28.7

6.3 LIGHTNING TOLERANCE EVALUATION

Laboratory testing demonstrated the effects of simulated lightning strikes (to 200 KA) to the HLH rotor blades. The results of these tests are contained in Reference 19.

Experience prior to these tests indicated a need to "ground" the titanium nose cap to prevent arcing across the root end of the spar to the rotor hub. Therefore, all tests were made with the titanium cap grounded.

The titanium cap and nickel erosion strip will take strikes in excess of 200 KA, with damage confined to pitting on the titanium outer "skin".

High voltage tests confirmed that lightning will strike the graphite in the blade's trailing edge, with a resulting decrease in strength of the graphite wedge, which does not constitute a safety-of-flight failure. Damage to the Nomex core results from charges arcing to the titanium cap from the trailing edge. It is concluded, therefore, to cover the trailing-edge graphite with wire mesh to isolate the graphite from a strike and to ground the mesh to the titanium cap. These measures will enable the blade to withstand lightning strikes in excess of 200 KA from any direction. During testing, the graphite in the spar did not attract any current.

For ATC HLH blades, the following lightning protection measures were taken:

1. The titanium cap was electrically grounded to the rotor hub through the lag damper bracket by a #6 wire brazed to a 1.00" x 20.00" copper plate which was bonded to the underside of the titanium cap. Current will arc to the copper plate around its perimeter.
2. Aluminum strips were placed at inboard and outboard ends of the blade to electrically ground the trailing edge graphite to the titanium cap.

For Prototype HLH blades, the following protection was incorporated:

1. A wire mesh covered the trailing-edge graphite, top and bottom, to form a "Faraday Cage" to prevent penetration of current.
2. Wire mesh was also used to electrically ground the trailing-edge cover to the titanium cap and to ground the titanium cap to the rotor hub.

These measures prevent lightning from penetrating the trailing-edge graphite, thus protecting the Nomex core from any arcing damage. Where the titanium cap is electrically grounded to the rotor hub, there is a minimum weight penalty and no aerodynamic compromise, and the blades will take repeated strikes with no repair to the mesh required.

6.4 WIND TUNNEL DEMONSTRATION TEST

A 14-foot-diameter HLH rotor demonstration model was tested in the Boeing V/STOL 20 ft x 20 ft wind tunnel. Testing was performed at full-scale tip speed of 750 ft/sec over a complete range of full-scale operating conditions which include the design hover condition ($C_{T/\sigma} = .082$) at a tip Mach number of .65 and forward flight trim conditions up to the maximum cruise speed of 150 KTAS ($\mu = .34$) and the high-speed dive condition at 200 KTAS ($\mu = .47$). The model rotor and supporting rotor test stand structure installed in the wind tunnel are illustrated in Figure 76.

The primary objectives of this rotor test (BVWT 115) were to demonstrate the performance capabilities of the HLH rotor system, to obtain rotor blade loads and to evaluate the concept of stall flutter damping. To accomplish the loads and damping objectives, both blades and control system were statically and dynamically scaled to the full-scale HLH rotor system including:

- Dynamically scaled blades (five natural modes)
- Dynamically scaled control system mass and inertia
- Scaled spherical elastomeric bearing retention system
- Variable swashplate support stiffness
- Variable swashplate damping
- Dynamic control load measurement capability

A detailed discussion of the test results is presented in the following paragraphs. The complete test results are contained in Reference 14.

Hover Figure of Merit

Hover performance for the HLH/ATC 14-foot-diameter rotor was measured out of ground effect. The resultant hover efficiency, or Figure of Merit (FM) is summarized in Figure 77, which presents FM as a function of rotor thrust coefficient ($C_{T/\sigma}$) at the design tip Mach number of .65. Correcting the 14-foot rotor test results for Reynolds number and blade instrumentation resulted in a FM of .751 at the design $C_{T/\sigma} = .0827$. Further correcting the FM for surface roughness to a "smooth" condition could yield an FM as high as .781. It is believed that the full-scale FM lies within this range (.751 - .781). The instrumentation and roughness corrections were determined from two-dimensional tests of a section of the model blade conducted at the University of Maryland Wind Tunnel (UMWT 667) in June 1973.

Cruise Efficiency

Lift to equivalent drag ratio (L/D_e) for the 14-foot-diameter HLH/ATC rotor system is presented in Figure 78 as a function of advance ratio, for model and full-scale Reynolds numbers. This chart presents the test results at conditions corresponding to the HLH forward rotor at 118,000 pounds, mid-center of gravity, with the external load ($f_e = 250 \text{ ft}^2$) at sea level, standard temperature; it compares these results to the adjusted 6-foot rotor data for the same conditions. At the design cruise speed of 130 KTAS ($\mu = .292$), the 14-foot rotor test results indicate an L/D_e of 8.10 (corrected to full-scale Reynolds number and blade instrumentation) compared to a goal of 7.31 and an L/D_e of 8.13 obtained by scaling up the 6-foot rotor test results. A further correction for surface roughness to a "smooth" condition could result in an L/D_e of 8.89.

Figure 78 relates the 14-foot rotor test results to the Boeing Vertol forward flight power required theory (A-79 Computer Program, see Reference 14).

Flying Qualities Boundary

The flying qualities boundary derived from the 14-foot-diameter rotor test is presented in Figure 79. The criteria for this boundary is based on a specified reduction in rotor lift curve slope with increased thrust. Comparison of the 14-foot rotor results with the 6-foot rotor boundary indicates an improvement with the larger scale (Reynolds No.) of the 14-foot rotor. The band of possible corrections to full-scale Reynolds Number includes the originally established goal for the advanced HLH rotor, which had been based on an 11% improvement over the 23010 airfoil.

Acoustics

Rotor noise data was obtained during hover (OGE) and forward flight (μ sweeps) test conditions. Rotational noise harmonic data was recorded to compare with the current prediction method used for the full-scale HLH. The modified Heron II prediction (HLH/ATC program - Ref. 7th Quarterly Report) provided good correlation with the recorded model data as shown in Figure 80.

Rotor Blade Loads

The wind tunnel test data confirms the theoretical load predictions and provides a basis for scaling to the full-scale HLH rotor. The measured flapwise bending moments are in agreement with the model rotor analytical predictions as shown in Figure 81. The chordwise bending moment correlation between theory and test indicates a conservatism in that the theory envelopes the test data as shown in Figure 81.

Figures 82 and 83 display a comparison of the measured pitch link load trends and a waveform comparison at $\mu = .344$ and $C_T/\sigma = .093$. The characteristic nose-down torsional moment is seen on the advancing side of the rotor; however, the magnitude is lower than predicted, and there is a nose-down perturbation around 230° azimuth that the theory does not predict.

Stall Flutter Damping

The addition of stall flutter damping in the nonrotating, fixed system controls generally reduces fixed system loads but has no effect on pitch link load peak to peak or on the stall flutter spike within the range of conditions tested. The Boeing Vertol analog analysis generally confirms the test results in that rotating system control loads for a blade having a torsional frequency near 5/rev are generally insensitive to fixed system damping, while fixed system loads are reduced.

One difference between the analog results and the test data is that the analog prediction shows a reduction in all three actuators, while the test data indicates a reduction in only two of the three actuators. However, a comparison of the maximum fixed system control load without damping to the maximum load with damping shows approximately a 50% load reduction with the addition of damping. See Figure 84. The 4/rev fixed system load was used as a basis for determining actuator loads since the loads are dominated by 4/rev.

Blade Torsion Load Growth

The load growth characteristics measured during this 14-foot model test are different between low μ and high μ . Below $\mu = .325$, the load growth is caused by the inception of stall flutter on the retreating blade; while above $\mu = .325$, the load break is caused by the torsion load growth on the advancing blade.

Figure 85 presents a blade torsion load limit envelope based on an alternating pitch link load of 4000 pounds (full scale). The test points shown for the 14-foot HLH rotor are compared with the line determined from the 6-foot-diameter rotor test of the CH-47C rotor (Reference 14). It is seen that the 14-foot HLH rotor exhibited results at least as good as the 6-foot CH-47C rotor. The rotor design condition of 150 knots at 118,000 pounds gross weight is below the 4000-pound limit established, indicating lower pitch link loads than the predicted value used for component design.

Aeroelastic Stability

The model rotor was "flown" out to 200 knots in a simulated dive ($M_{1,90} = .975$) to check for signs of aeroelastic instability. Figures 50 and 51 show the resultant pitch link load trends and a comparison of the predicted pitch link waveform versus the test waveform. No unusual load growth trends were encountered, and the correlation of the waveforms is excellent.



Figure 76. 14-Foot-Diameter Model HLH Rotor
Blade Installed in Wind Tunnel

OGE

$M_{TIP} = .65$

FULL SCALE REYNOLDS NUMBER

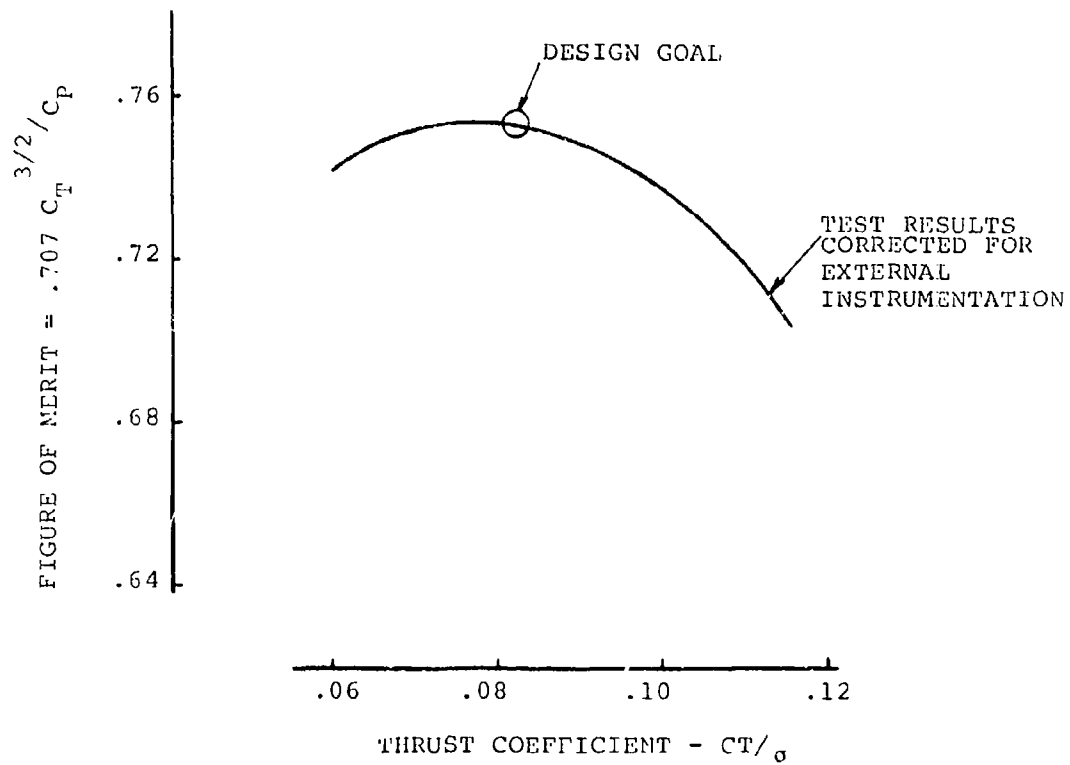


Figure 77. Hover Figure of Merit HLH/ATC
14-Foot-Diameter Rotor Wind
Tunnel Test

FULL SCALE CONDITIONS
 GW 118,000 LB.
 FWD ROTOR
 $f_e = 250 \text{ ft}^2$
 $V_{\text{TIP}} = 750 \text{ FPS}$
 SEA LEVEL/STD

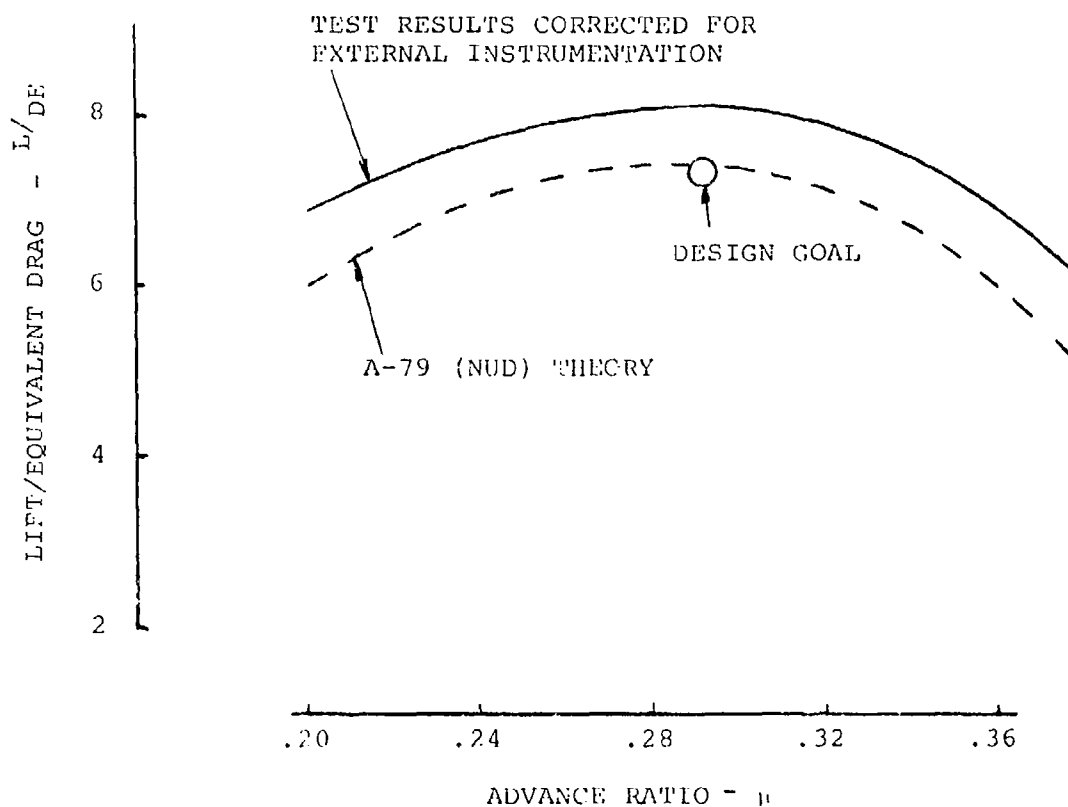


Figure 78. Cruise Efficiency HLH/ATC 14-Foot-Diameter Rotor Wind Tunnel Test

$V_{TIP} = 750 \text{ FPS}$
 $X/qd^2 \sigma = .20$

BAND OF TEST RESULTS
CORRECTED TO FULL SCALE

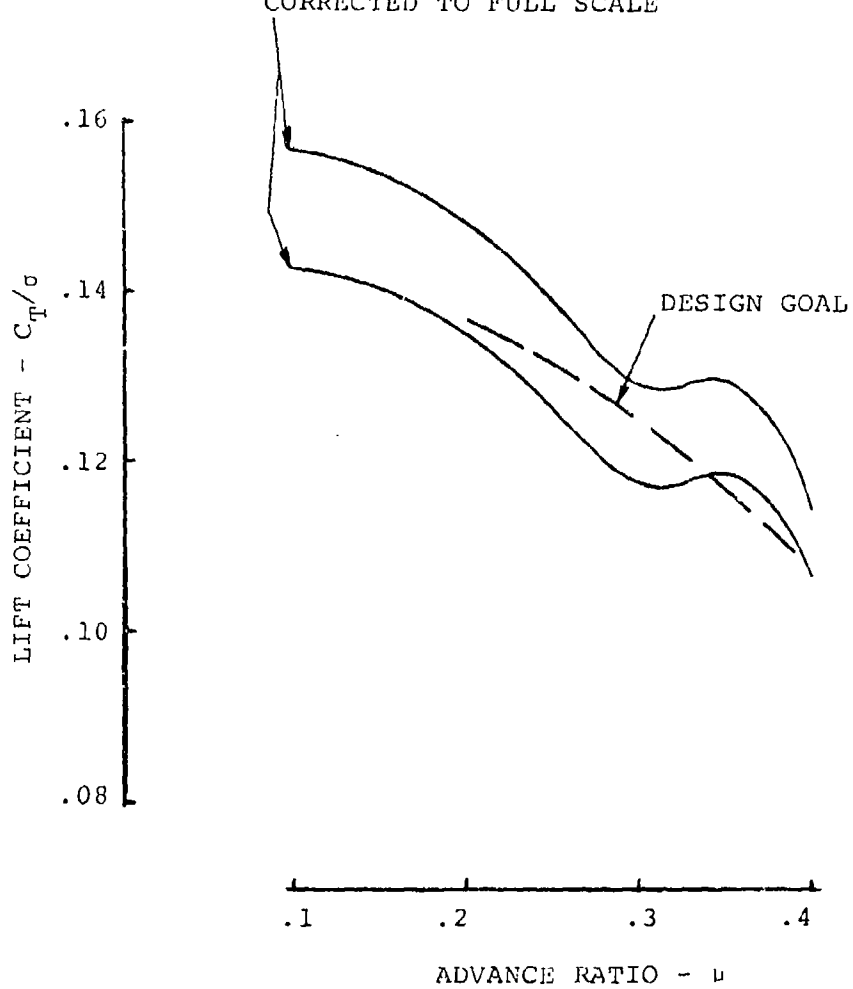


Figure 79. Flying Qualities Boundary HLH/ATC
14-Foot-Diameter Rotor Wind Tunnel
Test

$$CT/\sigma = .083$$

$$M_{TIP} = .65$$

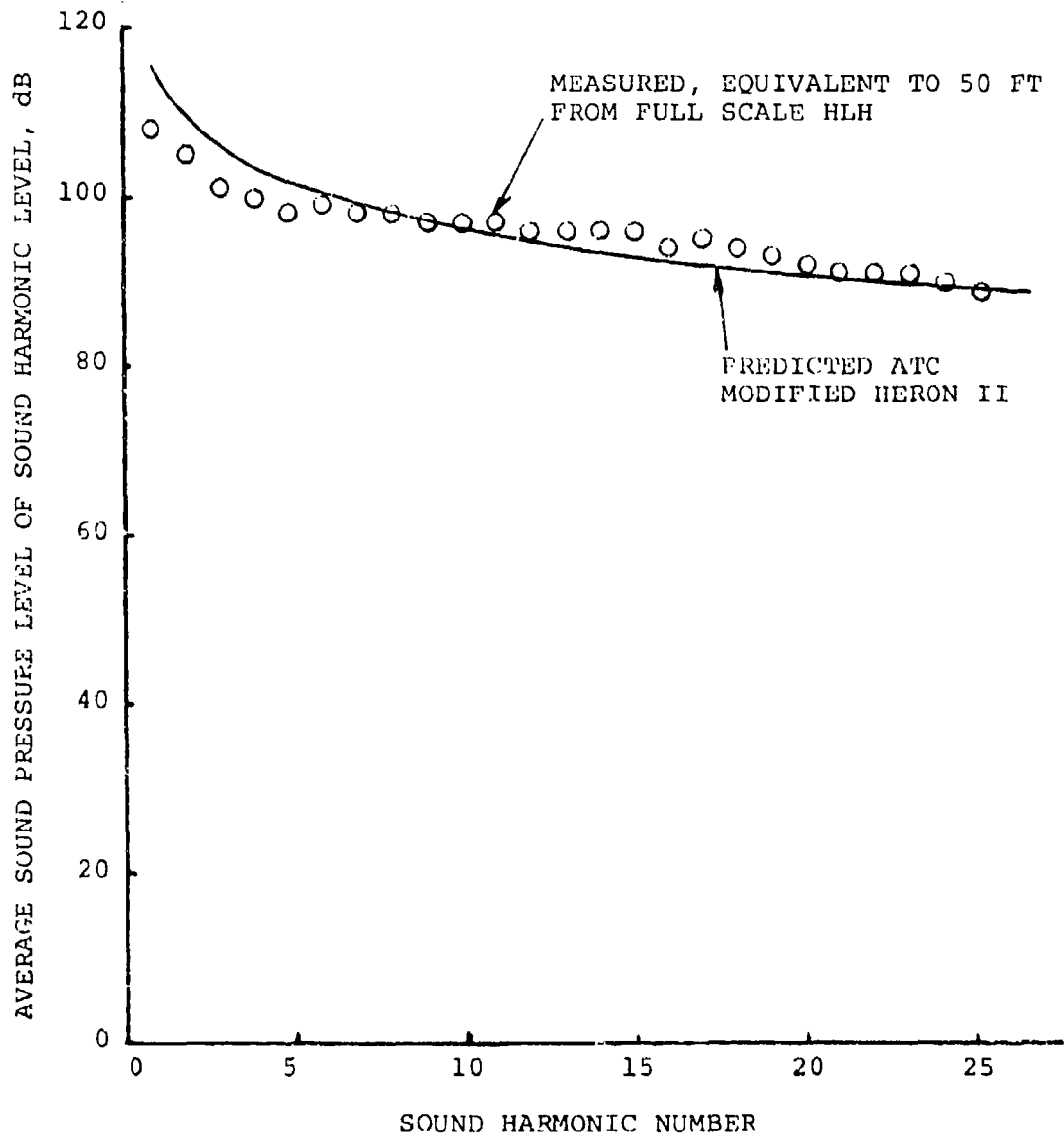


Figure 80. Rotational Noise of 14-Foot-Diameter Model Rotor

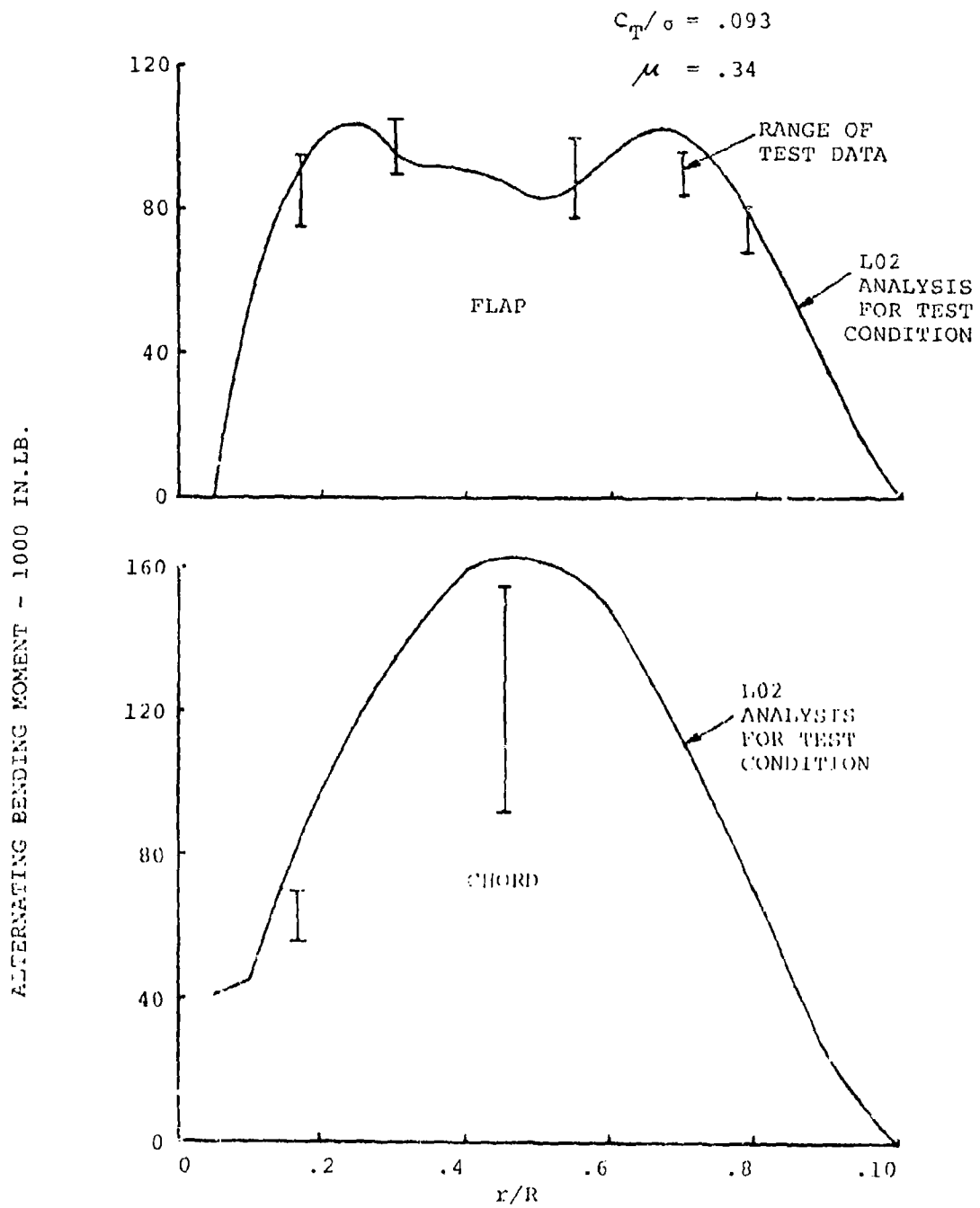


Figure 81. Comparison of Analytical Blade Bending Moments With Scaled 14-Foot-Diameter Rotor Wind Tunnel Test Data

SCALED WIND TUNNEL TEST DATA

$$C_{T1}/\sigma = .093$$

$$V_{TIP} = 750 \text{ FPS}$$

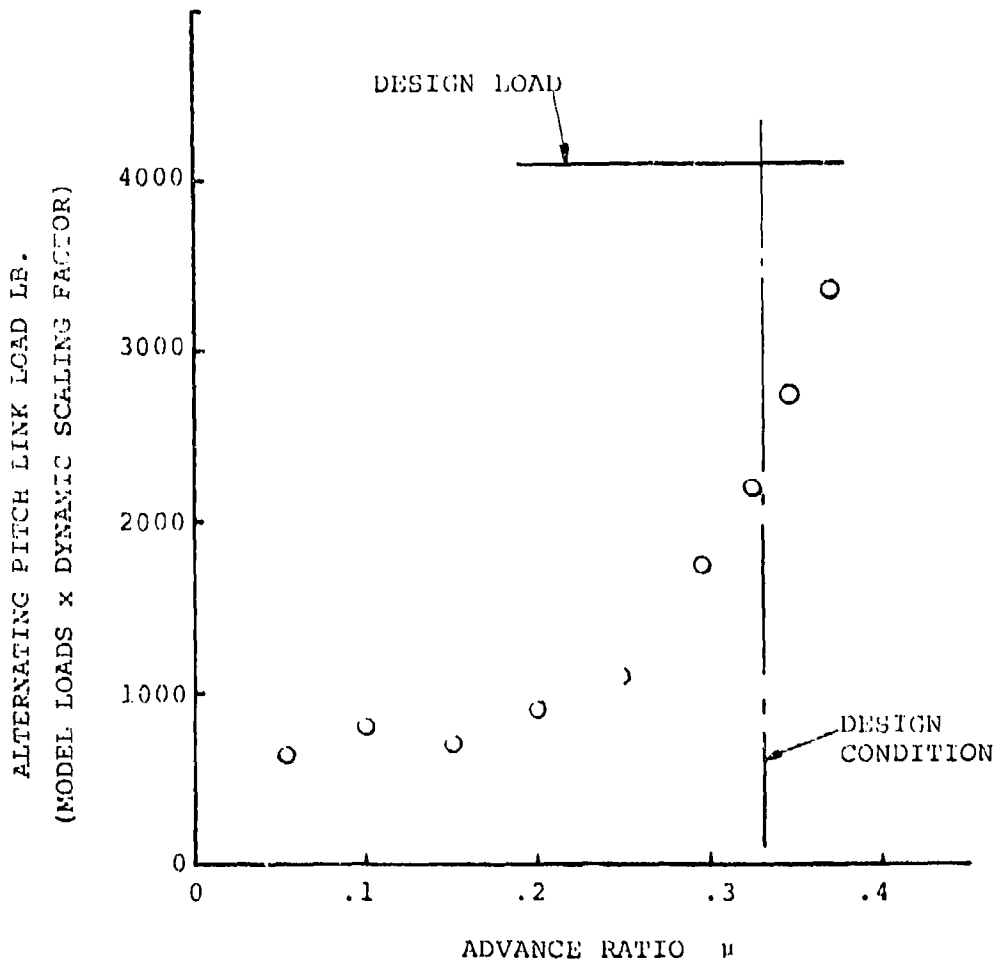


Figure 82. Comparison of Design Pitch Link Load With Scaled 14-Foot-Diameter Rotor Wind Tunnel Test Data

$$C_{T1}/\sigma = .093$$

$$\mu = .34$$

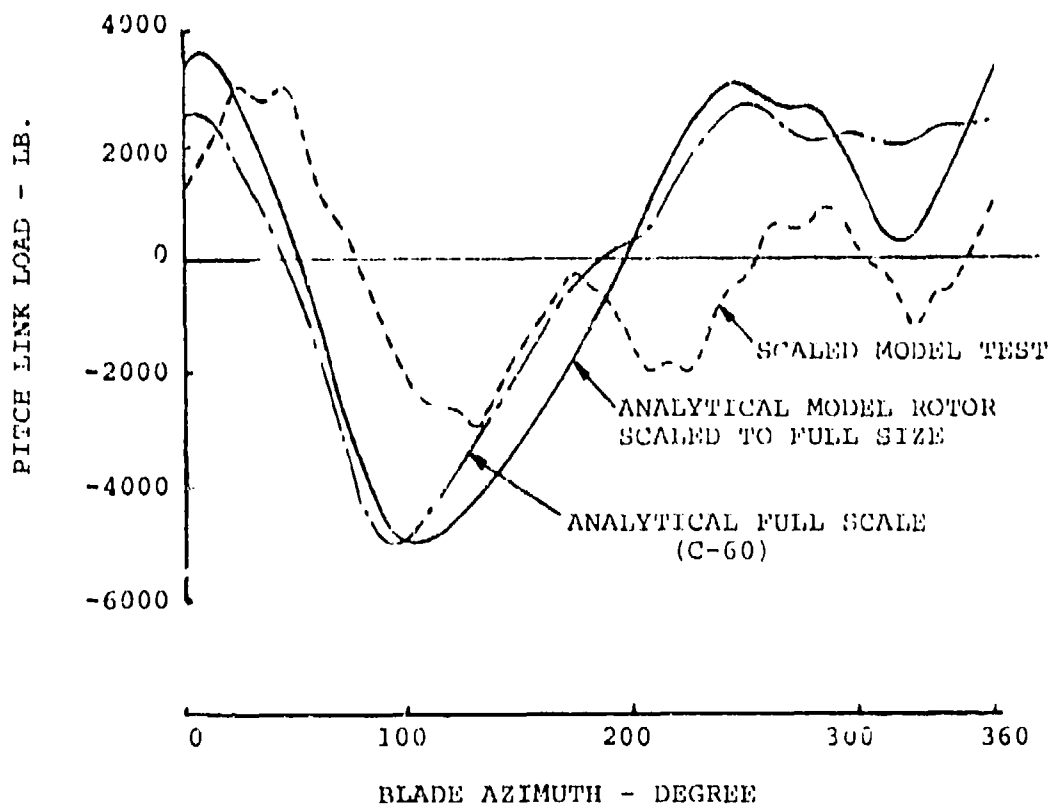


Figure 83. Comparison of Analytical Pitch Link Load With 14-Foot-Diameter Rotor Wind Tunnel Test Load for Level Flight Design Condition

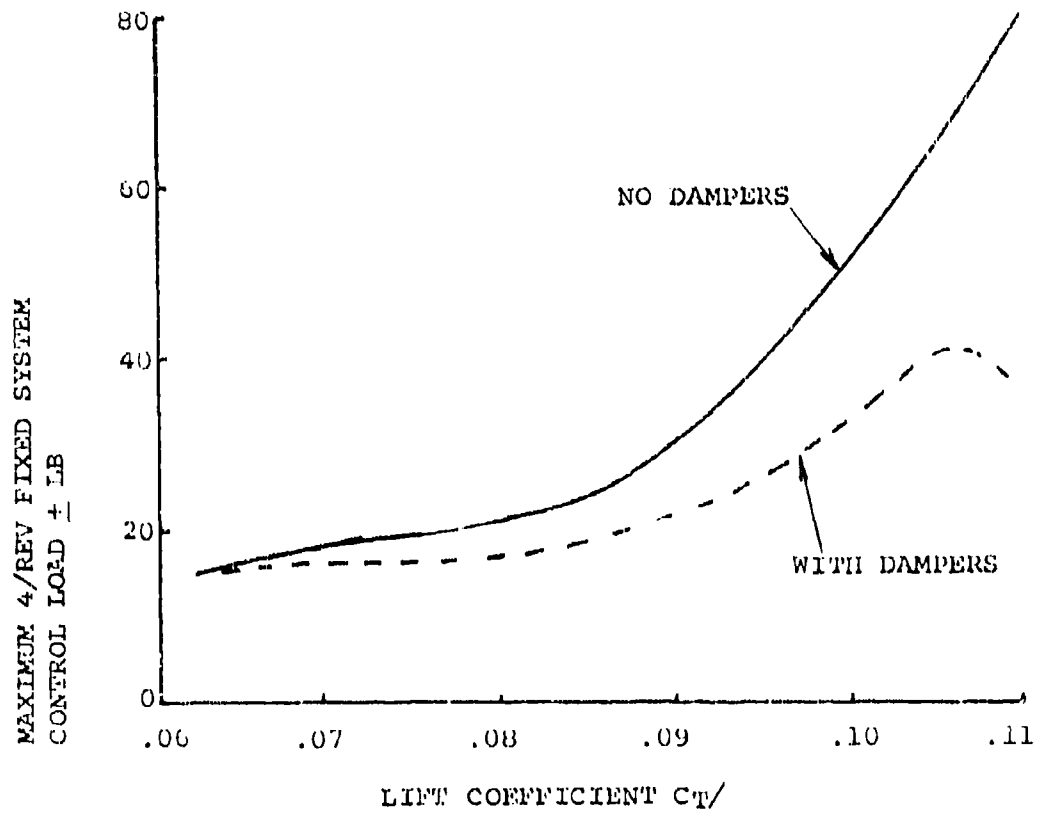


Figure 84. Fixed System Control Load Reduction With Damping, 14-Foot-Diameter Model Rotor Test

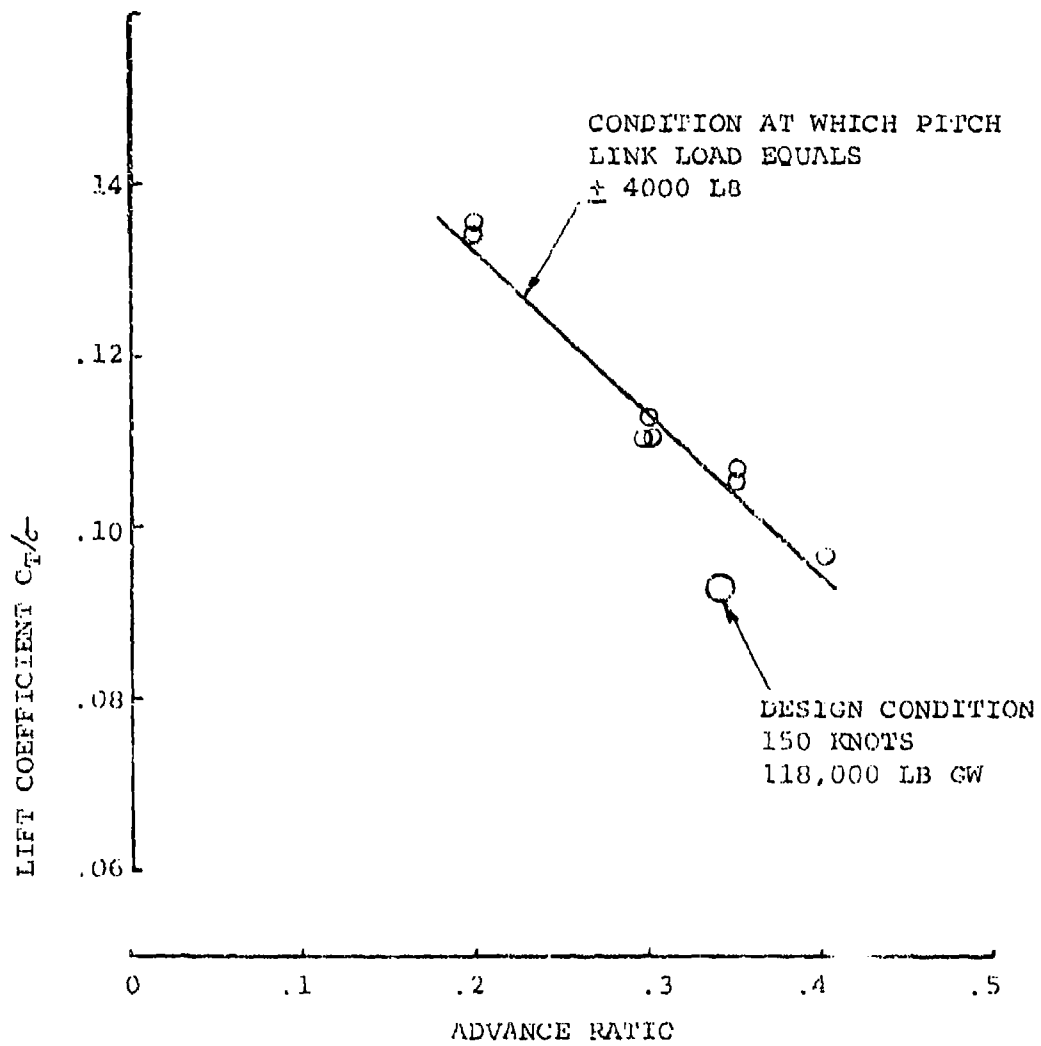


Figure 85. Blade Torsional Load Growth Fixed Load (a
 From 14-Foot-Diameter Model Rotor Test

6.5 ROTOR WHIRL DEMONSTRATION TESTS

Whirl Tower and DSTR tests of the full-scale HLH/ATC rotor system demonstrated the hover performance capability of the rotor and verified its functional and structural adequacy. Photographs of the Whirl Tower and DSTR facilities are shown in Figures 86 and 87. The results of these tests are contained in References 20 and 21.

The results from the whirl test that pertain to the rotor blade are summarized by the following statements:

1. The hover performance figure of merit objective of .751 was exceeded. Depending upon corrections for ground effect, the measured figure of merit lies between .767 and .795. Conservatively, taking the lower level of .767, the measured performance represents a 3,000-pound increase in payload capability for the HLH over the .751 figure of merit objective, (see Figure 89).
2. Stress and motion surveys indicate that the rotor performed as expected. Rotor blade frequencies closely matched predicted values (see Figures 89 and 90).
3. Rotor blade tracking was accomplished utilizing the inboard and outboard tabs to control the pitch link load range, as well as the blade track. Two methods of measuring blade track (which could be used in flight) were evaluated and provide comparable results within the limits of the tracking criteria.
4. Rotor over-speed tests up to 125% design rpm were conducted demonstrating the rotor structural adequacy.

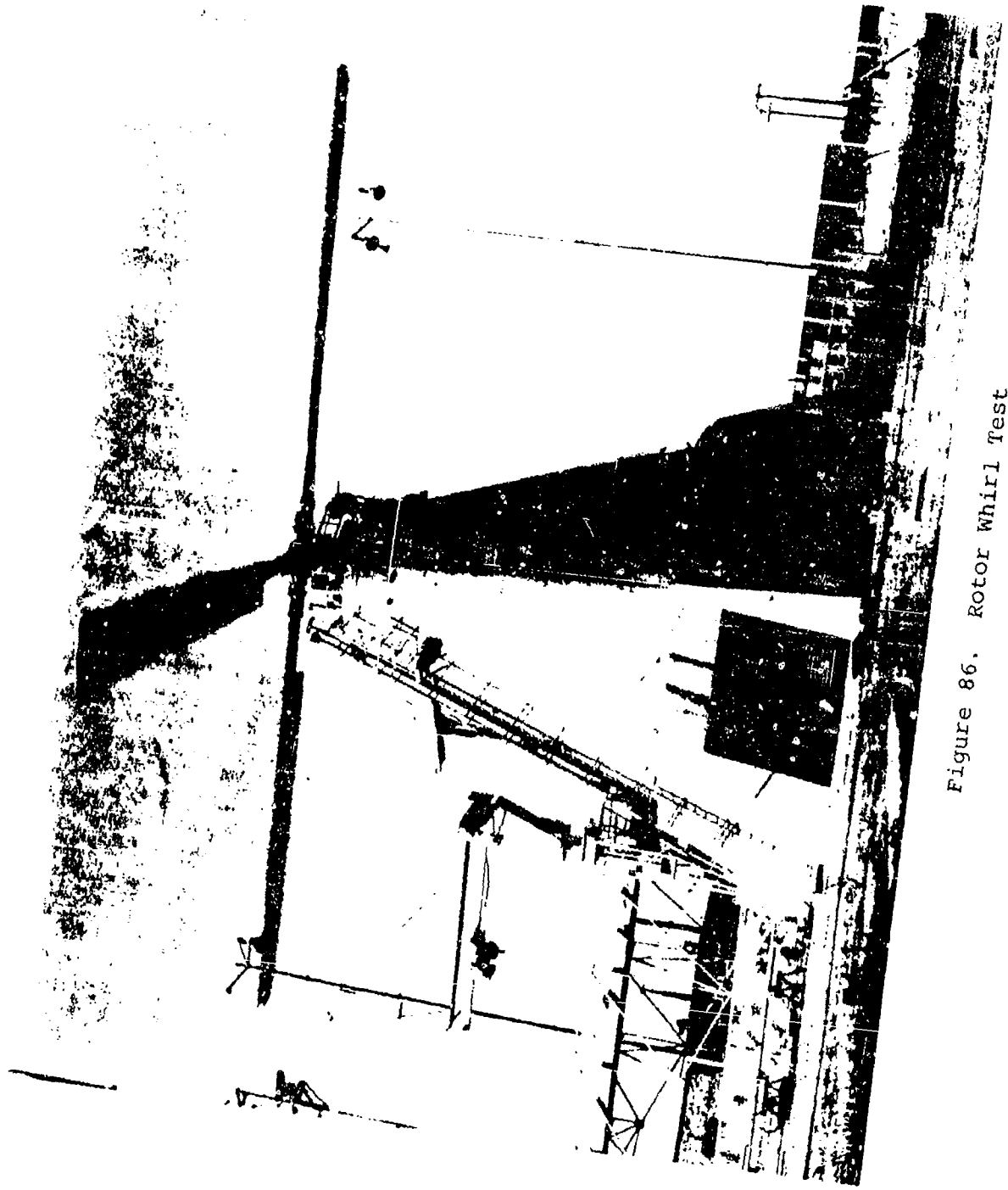


Figure 86. Rotor Whirl Test



Figure 87. Dynamic System Test Rig

$M_t = .65$

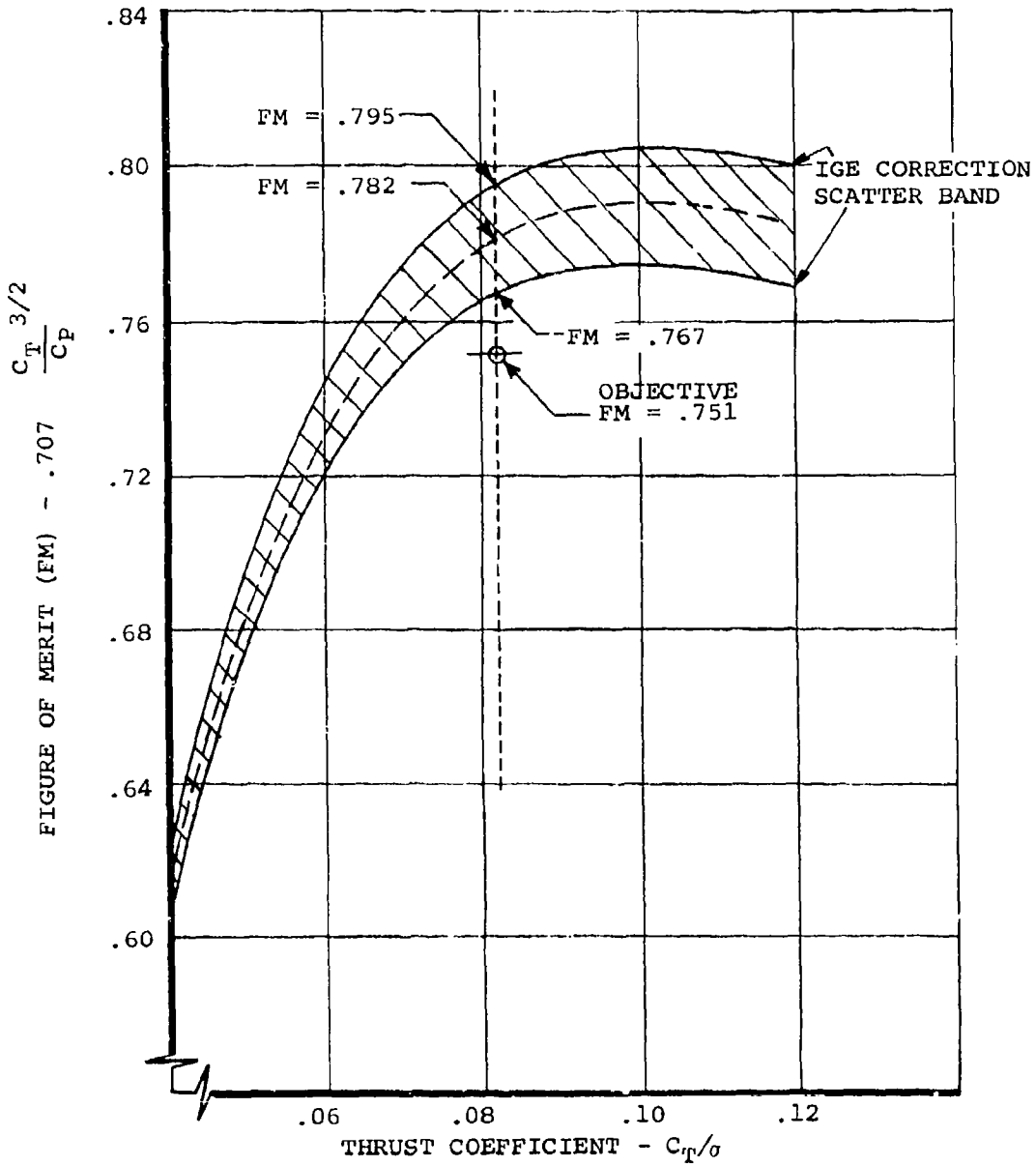


Figure 88. Rotor Hover Efficiency From Whirl Test

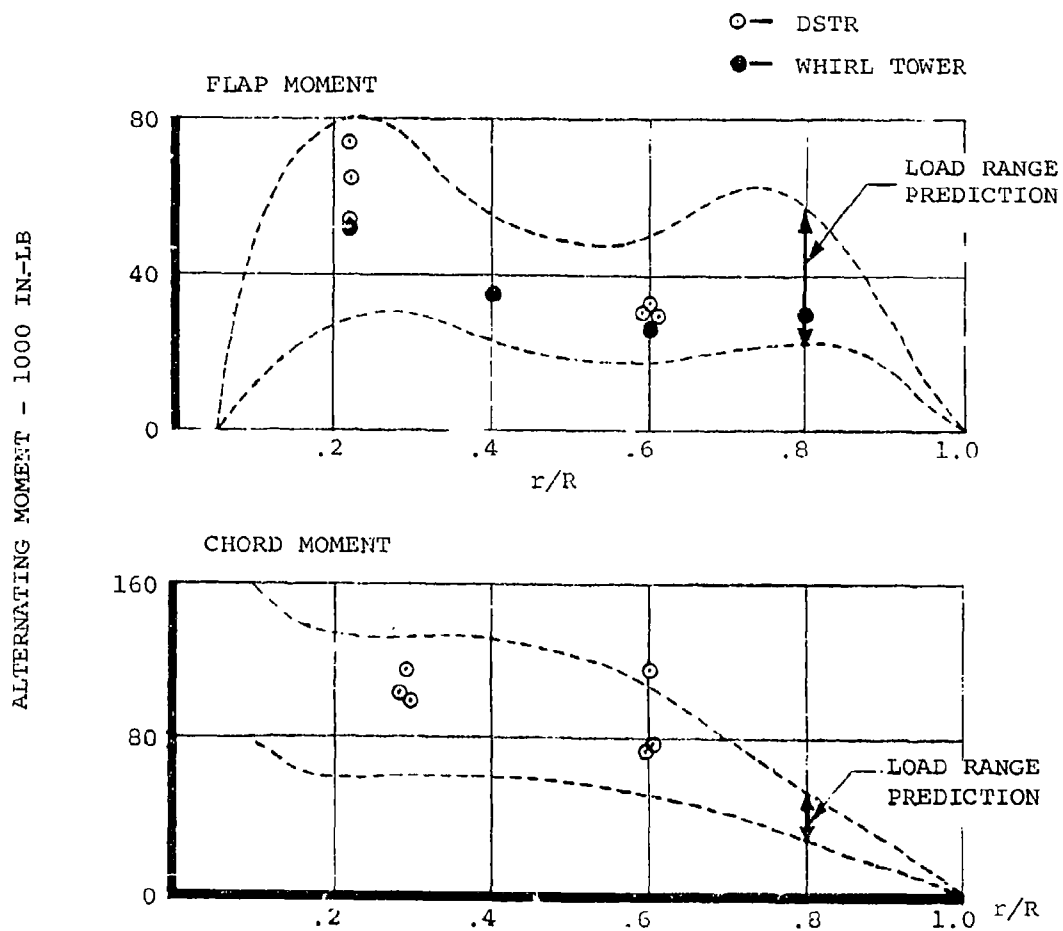


Figure 89. Blade Bending Moments From Whirl Tower and DSTR Tests

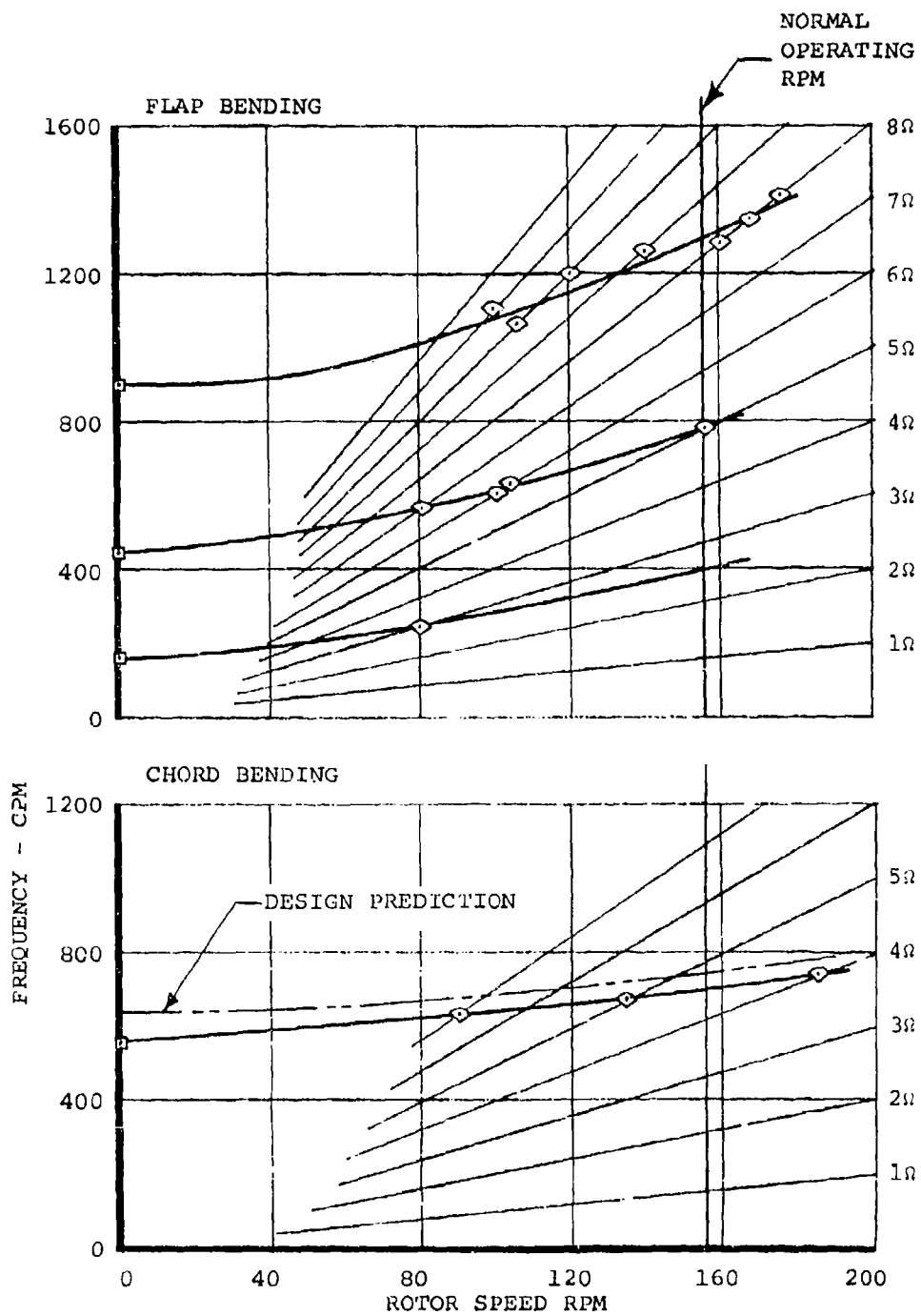


Figure 90. Blade Natural Frequencies Determined From Test

REFERENCES

1. D301-10062-1, HLH/ATC Rotor Blade Confirmation Trade Study, October 1971
2. D301-10100, HLH Quarterly Progress Reports
3. BMS 7-197, Boeing Material Specification for 6A14V Titanium Alloy Sheet
4. T301-10146-2, Test Results Report - HLH/ATC Rotor Blade Root End Design Support Test, October 1974
5. T301-10209-1, Test Results Report - HLH/ATC Core and Seal Development Tests (PE-511), June 1973
6. T301-10261-1, Test Results Report - HLH/ATC Rotor Blade Fatigue Test of Simulated Spar Section (PE-616), December 1973
7. T301-10234-1, Test Results Report, HLH/ATC Rotor Blade Pneumatic Failure Detection System Evaluation - Elliptical Tubes, August 1973
8. T301-10246-1, HLH/ATC Titanium Alloy (6A14V) Leading Edge Material - Effect of Crystallographic Texturing on Fatigue Strength, September 1973
9. D301-10239-2, Test Report - HLH/ATC Full-Scale Rotor Blade Fatigue and Static Tests (PE-629), January 1976
10. D301-10115-23, HLH Helicopter Main Rotor System Pendulum Absorber Prototype Flight Performance Demonstration Test Plan, September 1974
11. D301-10227-1, HLH/ATC Rotor System Structural Substantiation Report, Volume I, Rotor Blade Assembly, July 1973
12. AR-56 - Structural Design Requirements - Helicopters
13. S301-10000 Rev. E, Prime Item Description Document - Heavy Lift Helicopter

REFERENCES

14. T301-10229-1, Test Report - 14-Foot Diameter Model HLH Rotor Demonstration and Stall Flutter Damping Wind Tunnel Test, September 1973
15. "Pitch/Lag Instability of Helicopter Rotors", by Pei Chi Chou, Rotary Wing Aircraft Dynamics Session, IAS 26th Annual Meeting, January 1958
16. D301-10280, HLH Rotor Blade Manufacturing Technology Development Report, May 1974
17. D301-10239-1, Test Plan - HLH/ATC Full-Scale Blades (PE-628) October 1973
18. D301-10219-2, Test Results Report HLH-ATC Rotor Blade Bending Proof Load, Stiffness and Natural Frequency Test (PE-627) May 1974
19. D301-10240-2, Lightning Tolerance Evaluation of HLH Composite Rotor Blades
20. D301-10201-2, Test Report - HLH/ATC Rotor Whirl Demonstration Test (PE-294) July 1974
21. D301-10259-2, Test Report - HLH/ATC Dynamic System Test Rig
22. T301-10243-1, Test Results Report - HLH/ATC Rotor Blade Whirling Arm Rig Erosion Tests

LIST OF SYMBOLS

AGB	advanced geometry blade
ATC	advanced technology component
BIM	blade inspection method
c	rotor blade chord
cg	center of gravity
C_T/σ	thrust coefficient
DSTR	dynamic system test rig
f_e	equivalent drag area
FM	figure of merit (hover performance factor)
g	load factor
GW	gross weight
ISIS	integral spar inspection system
K_t	stress concentration factor
L/D_e	lift to equivalent drag ratio (fwd flight performance)
M.S.	margin of safety
OGE	out-of-ground effect
R	rotor blade radius measured from centerline of rotation
R	stress ratio
r	rotor blade station
RPM	rotor speed
TE	trailing edge
V_H	maximum forward level flight design speed
V_D	limit dive speed
x	blade chordwise distance from leading edge
α	coefficient
μ	advance ratio
μ	micro inches (10^{-6} inches)
ρ	density
σ	standard deviation
Ω	rotor speed

Reproduced From
Best Available Copy